Design, synthesis and applications of novel heterocycle for organic photovoltaic solar cells

A thesis submitted in fulfilment of the requirements for the degree of Doctor of Philosophy

Hemlata Patil

MSc Physics

School of Applied Sciences

College of Science Engineering and Health

RMIT University

October 2015

The price of success is hard work, dedication to the job at hand, and the determination that whether we win or lose, we have applied the best of ourselves to the task at hand.'

VINCE LOMBARDI

(American football player, coach, and executive)

DEDICATION

Confucius, Chinese teacher and philosopher has quoted, "Every piece of marble has a statue in it waiting to be released by a person of sufficient skill to chip away the unnecessary parts. Just as a sculptor to the marble so is education to the person."

Teacher's plays an important role in this process.

This thesis is dedicated to great teachers and supporters who lighten my life right from kindergarten to this post-graduate degree and keep encouraging me to continue my study. I am not certain; I would have determined this next phase of education without their encouragement.

I can't repay them. I can only ensure them to develop an ability to continue their work in future through guidance and enlighten few more lives.

Declaration

I certify that except where due acknowledgement has been made, the work is that of the author alone; the work has not been submitted previously, in whole or in part, to qualify for any other academic award; the content of the thesis/project is the result of work which has been carried out since the official commencement date of the approved research program; any editorial work, paid or unpaid, carried out by a third party is acknowledged; and, ethics procedures and guidelines have been followed.

Hemlata Patil

09/10/2015

Acknowledgements

It would not have been possible to write this doctoral thesis without the help and support of the kind people around me, to only some of whom it is possible to give particular mention here.

To begin with, this thesis was made possible through the help, support and patience of my principal supervisor, Dr. Sheshanath Bhosale, who undertook to act as my supervisor despite his many other academic and professional commitments. His wisdom, knowledge and commitment to the highest standards inspired and motivated me.

I express my appreciation to my second supervisor, Professor. Suresh Bhargava, for his continue support for the project.

I thankfully acknowledge the Professor Andrew T. Smith School of Applied sciences for financial support and also other academic and technical staff of RMIT University. The library and computer facilities of the university have also been requisite.

I also extend my thanks to the Lab manager, Mr Karl Lang and technical officers within School of Applied Science, Zahara

Homan and Nadia for their help in offering me the technical support and resources in running the project and also for their kindness, friendship and support. Mr Phil Francis, advice given by him has been a great help in using the microscopy in my research.

Amongst my fellow postgraduate students, the effort made by Anushree Rananavare, Sam Jackson, Melissa Kelson, Anuradha, Aron Raynor, Duong Duc La, and Postdocoral fellows Dr. Vinita Chaudhary, Dr. Deepa Dumbre, Dr. Selveakannan in endorsing an inspiring and welcoming academic and social environment will stand as an example to those who follow us and I thank each of them for their warm friendship, help and consideration.

Especially, I thank my husband, Mr. Prasad Patil for his personal support and great patience at all the times, without who this effort would have been worth nothing. Your love, support and constant patience have taught me so much about sacrifice, discipline and compromise. Very important to acknowledge my son (Mr. Aditya) who spent three years in child care to allow me to focus my study. I am so proud of you two and am deeply sorry for the time we spent apart.

My mother, father, sister and brother, who have always supported, stimulated and believed in me, in all my endeavours. To all my family members who have given me explicit support throughout, as always, for which my simple expression of thanks likewise does not serve.

I thank you God for giving me the strength to keep going when difficult situations aroused during this course.

Finally to quote Neil Armstrong "One step for a man and a giant leap for mankind" this small research step of mine gives a glimmering glimpse of what the future beholds for the industry.

Publications and presentations

Most of the work reported in this thesis has previously been presented in the following papers:

1) **Hemlata Patil,** Wang Xi Zu, Akhil Gupta, Ante Bilic, Prashant Sonar, Sidhanath V. Bhosale and Sheshanath V. Bhosale**.** A non-fullerene electron acceptor based on fluorene and diketopyrrolopyrrole building blocks for solution-processable organic solar cells with an impressive open-circuit voltage, ***Phys. Chem. Chem. Phys*.., 2014,** *16*, 23837-23842**.**
2) **Hemlata Patil**, Akhil Gupta, Ante Bilic, Sidhanath V. Bhosale, Sheshanath V. Bhosale **.** A solution processable electron acceptor based on diketopyrrolopyrrole and naphthalenediimide motifs for organic solar cells. ***Tetrahedron Letters,* 2014**, *55*, 4430-4432.
3) **Hemlata Patil**, Akhil Gupta, Ante Bilic, Sam Leslie Jackson, Kay Latham, Sheshanath V. Bhosale. Donor-acceptor-donor modular small organic molecules based on naphthalene diimide acceptor unit for solution processable photovoltaic devices**.** ***Journal of Electronics Material,* 2014**, *43*, 3243-3254.
4) **Hemlata Patil,** Akhil Gupta, Steven Priver, Ant Bilic, Prashant Sonar and Sheshanath V. Bhosale. Conjoint use of dibenzosilole and indan-1, 3-dione functionalities to prepare an efficient non-fullerene acceptor for solution-processable bulk-heterojunction devices, ***Asian J. Org. Chem***., **2015**, 10.1002/ajoc.201500207
5) **Hemlata Patil**, Wang Xi Zu, Akhil Gupta, Prashant Sonar, Ante Bilic, and Sheshanath V. Bhosale. Isoindigo-based small molecules with varied donor components for solution-rocessable organic field effective transistor devices, *Molecules* **2015**, *20*, 17362-17377.

Contribution to other publications:

1) Aaron M. Raynor, Akhil Gupta, **Hemlata Patil**, Ante Bilic, Sheshanath V.Bhosale Diketopyrrolopyrrole and benzothiadiazole based smallmolecule electron acceptor: Design, synthesis, characterization and photovoltaic properties. ***RSC Advances,*** 2014, *4*, 57635-57638.
2) Anushri Rananaware, Rajesh S. Bhosale, **Hemlata Patil**, Mohammad Al Kobaisi, Amanda Abraham, Ravi Shukla, Sidhanath V. Bhosale, Sheshanath V. Bhosale . Precise aggregation-induced emission enhancement *via* H^+ sensing and its use in ratiometric detection of intracellular pH values. ***RSC Advances,*** **2014**, *4*, 59078-59082.
3) Anushri Rananaware, Rajesh S. Bhosale, **Hemlata Patil**, Kei Ohkubo, Sam L. Jackson, Lathe S. Jones, Shunichi Fukuzumi, Sidhanath V. Bhosale, Sheshanath V. Bhosale "Tetraphenylethene-Based Star Shaped Porphyrins: Synthesis, Self-assembly, and Optical and Photophysical Study ***J.Org.Chem.*** **2015,** *80,* 3832-3840.
4) Akhil Gupta, Xizu Wang, Doli Srivani, Ben Alford, Vijila Chellappan, Ante Bilic, **Hemlata Patil**, Lathe A. Jones, Sidhanath V. Bhosale, Prashant Sonar and Sheshanath V. Bhosale.An electron accepting chromophore based on fluorene and naphthalenediimide blocks for solution-processable bulk heterojunction devices. ***Asian J. Org. Chem*****.,2015,** DOI: 10.1002

Abstract

Since the very first organic photovoltaic device was reported by the Tang group (1986), these devices have been subject of intensive investigation. From the late 1980s to early 90s, research started to gain momentum and two major classes of organic photovoltaic devices, namely polymeric and titanium dioxide film based solar cells, emerged. Later on in the mid-90s, polymeric solar cells came to be known as bulk–heterojunction (BHJ) solar cells and titanium dioxide film based solar cells came to be known as dye–sensitized solar cells (DSSCs). Both types of devices include organic materials and over time, a variety of materials have been used. Some examples include the use of polymeric entities, metal complexes and small molecular chromophores.

For the fabrication of both types of solar cells, organic materials and common organic solvents are used. The following material properties are vital for the optimal performance of organic solar cells:

- Light harvesting ability
- Narrow optical band-gap
- Solution processability of organic materials from common organic solvents such as chloroform, chlorobenzene and acetonitrile
- Stability of organic materials

For investigating the above mentioned material properties, a systematic study of newly designed BHJ materials, with tuned optoelectronics properties, has been carried out in this work. The investigated materials are based on a variety of structural modules, such as donor-acceptor-donor (D-A-D), acceptor-donor-acceptor (A-D-A) and A-A-A. The materials have been designed, synthesized, fully characterized and applied in organic BHJ devices.

A solution-processable non-fullerene electron acceptor (coded as **DPP1**, based on fluorene and diketopyrrolopyrrole building blocks) was designed, synthesized and fully characterized. **DPP1** revealed excellent solubility and high thermal stability, which are vital for easy processing. Upon using **DPP1** as an acceptor, along with the classical electron donor polymer poly (3-hexylthiophene), solution processable BHJ solar cells afforded a high open-circuit voltage of ~ 1.1 V. This is one of the highest values reported in the literature for a solution-processable BHJ device using a combination of fluorene and diketopyrrolopyrrole functionalities.

Similarly, a combination of naphthalene diimide (NDI) and diketopyrrolopyrrole (DPP) accepting units was employed to generate a non-fullerene electron acceptor (coded as **HP1**). NDI is a potential electron deficient fragment and has interesting physical and electronic properties. On the other hand, DPP also is an electron deficient unit and has proved to be an effective addition when placed at the

peripheries of a non-fullerene chromophore. These reasons encouraged the design of conjoint use of NDI and DPP functionalities, generating a target non-fullerene chromophore that will be highly soluble in common organic solvents, will exert excellent light harvesting properties and will be thermally stable. **HP1** was produced, where NDI was chosen as the central core with DPP as terminal units. **HP1** was synthesized in good yields and was applied in solution-processable BHJ devices, along with the classic electron donor poly (3-hexythiophene) (P3HT). **HP1** exhibited excellent thermal stability, broad absorption and appropriate energy levels matching with those of P3HT. **HP1** showed good BHJ performance and a high open circuit voltage of >1 V when tested in solution-processable devices.

Even though the advancement of non-fullerene acceptors is noteworthy, incentives remain to develop materials which will not only fill in the gap for fullerenes but will also have improved characteristics such as solubility and matching energy levels with donors. One strategy to design such materials is the conjoint use of donor and acceptor functionalities, which can be arranged in a meaningful manner to generate an elongated conjugate system. A novel, solution-processable non-fullerene electron acceptor, 2,2'-(((5,5-dioctyl-5*H*-dibenzo[*b*,*d*]silole-3,7-diyl)bis(thiophene-5,2-diyl))bis(methanylylidene))bis(1*H*-indene-1,3(2*H*)-dione) (coded as **N5**) comprised of dibenzosilole and 1,3-indanedione building blocks

was designed, synthesized and fully characterized. **N5** revealed excellent solubility in various organic solvents and high thermal stability, both of which are crucial for easy processing. **N5** had energy levels matching with those of standard donor poly(3-hexylthiophene). Solution-processable bulk-heterojunction cells were made using N5 and the conventional donor polymer poly(3-hexylthiophene). The target material **N5** showed very good BHJ performance when tested in solution-processable devices without any additional additives.

Design and development of new chromophores based on the D-A-D module was also carried out and the materials synthesised were tested as donors in the inverted BHJ device architecture. NDI was chosen as the central acceptor as it proved to exert good electronic properties while designing **HP1**. Moreover, an advantage of the NDI acceptor unit is its amenability to incorporate alkyl chains on the nitrogen atoms. Such lypophilic chains can enhance the solubility of target materials and can help in film formation without crystallization. To generate new push-pull chromophores, NDI was used in conjunction with two different donating units, triphenylamine (TPA) and benzothiophene (BT), and the performance of target materials was compared. New materials were coded as **S6** and **S7** and it was the first recorded attempt in which such donating units were used with NDI to generate target chromophores based on the D-A-D module. **S6** and **S7** were used in solution-processable inverted BHJ devices.

Furthermore, two novel solution processable small organic molecules based on the D-A-D module were successfully designed, synthesized and characterized. A common electron accepting moiety, isoindigo, along with different electron donating functionalities, triphenylamine and carbazole, was used in both the target materials, **S10** and **S11**. S10 and S11 were compared in terms of their optoelectronic properties. On comparing the carbazole analogue with the triphenylamine (TPA) analogue, TPA analogue gave an enhanced intramolecular charge transfer transition and reduction of optical band gap. Both of the target materials were designed as donors, exerted excellent solubility in common organic solvents, displayed good thermal stability and displayed promising optoelectronics properties. Such parameters allowed the measurement of their charge-carrier motilities using solution-processable organic field effective transistors. Both the target materials showed promising hole and electron mobilities.

Overall, this study provided an examination of the effect of changing the donor, π-bridge and acceptor part of the D-A-D and A-D-A modular materials for BHJ solar cells.

To my knowledge, the materials reported herein are the first examples in the literature where synchronous use of such building blocks is demonstrated, in order to design an efficient non-fullerene acceptor.

Table of contents **pages**

List of tables

List of figures

Abbreviations

APCE	Absorbed-photon-to-current generation efficiency
BHJ	Bulk-heterojunction
D-A/D-π-A	Donor-acceptor
DFT	Density functional theory
DSC	Dye-sensitized solar cell
ff	Fill factor
Fig.	Figure
GOT	Glossary of terms
HOMO	Highest occupied molecular orbital
IPCE	Incident photon to electron conversion efficiency
IR	Infra-red

ITO	Indium tinoxide
I-V	Current-voltage
J_{sc}	Short circuit current
LUMO	Lowest unoccupied molecular orbital
OPV	Organic photovoltaic
$PC_{61}BM$	Phenyl-C_{61}-butyric acid methyl ester
$PC_{71}BM$	Phenyl-C_{71}-butyric acid methyl ester
PCE	Power conversion efficiency
PEDOT:PSS	poly (3,4-ethylenedioxythiophene): poly(styrene sulfonate) (PEDOT:PSS)
P3HT	Poly (3-hexylthiophene)
PV	Photovoltaic
Ref/ref	Reference
UV-Vis	Ultraviolet-visible
V_{oc}	Open circuit voltage
η	Energy conversion efficiency

1. Introduction

1.1 Renewable energy and Usage

The conversion of solar into electrical energy is one of the most important areas of scientific research, driven by constantly growing human energy demands. Some of the most challenging targets for chemists are the design of efficient, viable, environmentally sustainable artificial photosynthetic systems that resemble the concepts of nature.

The energy usage is rapidly increasing in proportion to growing modern industries. The word energy in this context means consumable “energy resources”, the development of which has become a prerequisite for sustaining society. This increase in demand for energy resources has led to serious consequences, including deforestation and global warming. It is presumed that the planet will get warmer by 1 to 5 ^{o}C during the 21st century[1,2] and the estimated carbon dioxide (CO_2) concentration in the 22nd century would be sufficient enough for irreversible climate and nature changes[3,4]. Thus, there is an urgent need to explore new energy resources that are not reliant on the burning of fossil fuels.

Now days, the production and usage of fossil fuels such as coal, oil and gas give rise to a mass of environmental problems in addition to declining stocks. Approximately 80% of the energy supply worldwide is based on fossil fuels.[5] A major fossil fuel is coal and according to

the World Coal Institute, it only provides approximately one third of the global energy needs and 42% of the world's electricity.[6] At the current rate of consumption of coal, these non-renewable energy resources won't last for much longer. The second leading fuel, oil, will only last for another 52 years.[7] This means that the level of our usable energy resources is on the decline and there is a need to develop renewable energy sources.[8,9]

In recent years, global energy consumption has been increasing, and sustainable alternatives are being sought, such as geothermal power, wind power and tidal power. Renewable energy sources are one of the most important components of the global new strategy which is environmentally friendly and can be directly converted to electricity.[10,11] The 89 petawatts (1petawatt = 10^{15} watts) that falls on the planet's surface would provide enough energy every hour to supply mankind's energy demands for a year.[12,13] It is not possible to harness all, or even most of this solar radiation, but capturing less than 0.02% would be enough to meet the world's current energy needs. Solar power is therefore clearly the dominant solution in terms of humanity's energy needs. After 2030, it is expected that photovoltaic energy will become a significant part of the total energy generation and by 2050, it will supply 20 to 30% of the electrical demand.

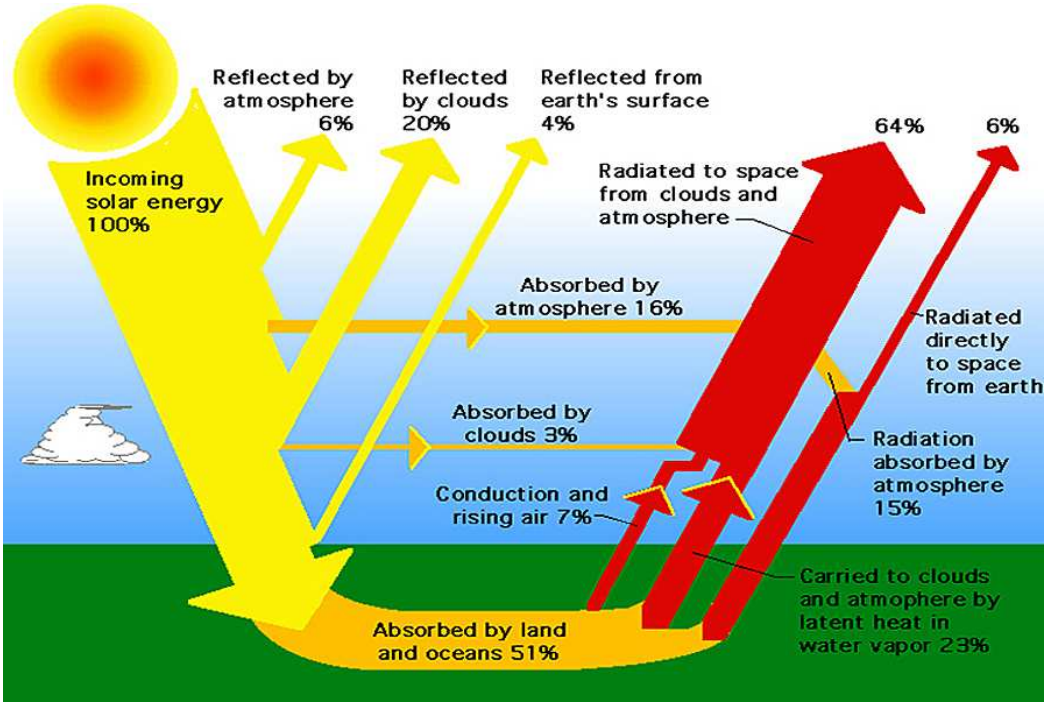

Figure 1.1. The model illustration of "Earth Radiation Budget Experiment" program.[14]

Gaining power from the sun is not only using photovoltaic (PV) cells to convert sunlight to electricity but also generating solar thermal systems, using mirrors to focus the Sun's heat to heat-up a working fluid that in turns drives a turbine. This solar technology includes the environmental and commercial advantages of noise and pollution free, non-toxic solar panels, no greenhouse gas emission, very little maintenance and grid independence. Also, the practical potential of solar electricity makes it attractive for large-scale utilization.

1.2 Photovoltaic solar cells

The photovoltaic (PV) effect is the creation of voltage or electric current in a material upon exposure to light. In 1839, French physicist Becquerel observed the photovoltaic effect while studying electrolytes.[15] Following in 1954, Chapin *et al*. reported the first photovoltaic with a high conversion efficiency of (approximately 6%).[16] These are considered to be the first generation PV solar cells. PV technology has gained momentum over time and is currently dominated by wafer-size single junction solar cells based on crystalline silicon that are assembled into a large module. Other semiconductor materials are under investigation for their low-cost. Inorganic semiconductor materials (thin films)[17,18] are more absorbing than crystalline silicon and can be processed directly onto large green area substrates, which are second-generation PV technologies, for example:

- Amorphous semiconductors such as cadmium sulphide (CdS) or cadmium telluride (CdTe).
- Chalcogenides such as copper indium selenide (CIS), or copper indium gallium selenide (CIGS).[19]

However, the second-generation PV cells remain a challenge in their controlled manufacturing and for their commercial applications.

In 1980, the Tang group developed the first single heterojunction organic PV cells and reported a power conversion efficiency of about

1%.[20] This work represents a major milestone for the development of organic based semiconductor PV devices. These cells are considered third generation PV technologies. To improve the power conversion efficiency, there is a need for further development

1.3 Organic Photovoltaic solar cells

Recently organic photovoltaic (OPV) solar cells merge into the research field, which is defined as those which include at least one organic material, such as small organic molecule or polymer during their fabrication. These can be further classified into two categories:

1. Bulk heterojunction solar cells
2. Dye sensitised solar cells

In the field of photovoltaics, organic solar cells have some fascinating features make them a unique alternative energy source. Organic solar cells in this form have the inherent advantages of being solution-processable, mechanically flexible and possessing versatility in their chemical structures, from advances in organic chemistry, which make them a promising substitute to conventional first-generation silicon-based solar cells.[21,22] Notably, the absorbance coefficients of organic materials are larger compared to the indirect band-gap of silicon. Furthermore, organic cells can be made on plastic substrates utilizing their mechanical flexibility and have the potential of making fully flexible electronic devices for real world applications in the future.

However, their commercial feasibility and production is a big challenge for researchers and industry. The major current disadvantage is their decreased stability and moderate efficiency compared to the conventional silicon- based solar cells. There are comprehensive efforts to solve these issues with the development of OPV solar cells and we can expect the commercialisation of OPV solar cells in the near future. The present work mainly focused on the synthesis and utilisation of donor-acceptor organic dyes for bulk-heterojunction solar cells.

1.4 Bulk Heterojunction Solar cells

A large degree of variation is possible within organic solar cell composition. In this section, bulk heterojunction (BHJ) organic solar cells are described in depth. BHJ solar cells are also referred to polymeric[23] or plastic solar cells.[24] One of the main components of this type of solar cell is a polymeric material that acts as an electron donor. There is current interest in the use small molecules as electron donors in BHJ applications, due to their ease of synthesis and purification, and are amenable to fabrication. Thus, my PhD thesis research work focused on the synthesis of small organic molecule based dyes for BHJ solar cells.

1.5 Working principle of bulk –heterojunction solar cells

The basic operational principle of a bilayer heterojunction and bulk-heterojunction solar cell is illustrated in the Figure 1.2 and detailed in the following subsections (**1.5.1-1.5.4**).

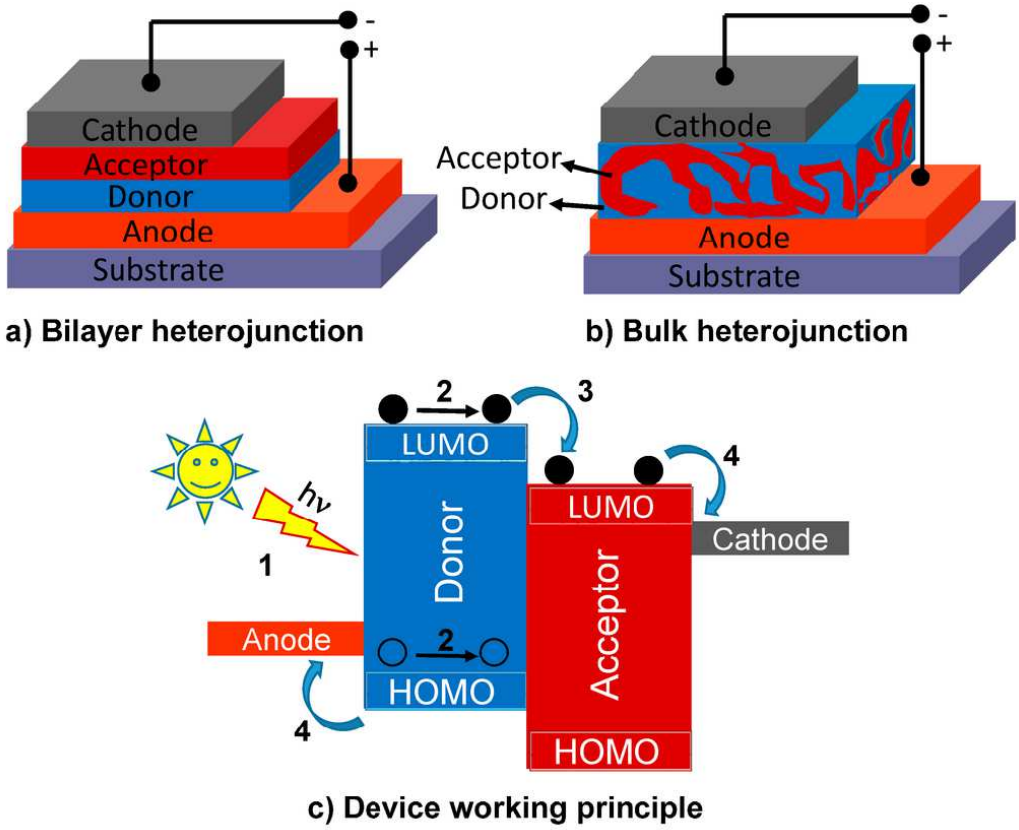

Figure 1.2. Illustrated basic operation principle of (a) bilayer heterojunction (b) BHJ and (c) device working principle from light absorption to charge collection.[25,26]

A BHJ in which one of the electrodes must be semi-transparent (typically glass coated with conducting material indium tin oxide (ITO)), but a thin organic material layer can also be used as shown in

Figure 1.2a. The most common electron acceptor (typically C_{60} or its derivative) which layered on the substrate followed by photo-absorbing layer of the poly(3-hexylthiophene) (P3HT) on the top. This is the simplest device that promotes the exciton separation and is a planar heterojunction sandwiched between two different electrodes, such as tin indium oxide (ITO), coated with PEDOT:PSS or fluorinated tin oxide (FTO) and a reflecting metal, which is usually aluminium, calcium or silver.

On the other hand, in BHJ device architecture the active layers are an intimate mixture of donor and acceptor materials, and can therefore notably increase the interface between donor and acceptor (Figure 1.2b). This is very commonly used for the successful architecture of polymeric solar cells. In which is the most successful device architecture for polymeric photovoltaic solar cells are the BHJ cells. In this device architecture, donor and acceptor materials form a continuous interpenetrating network. These types of devices include an active layer, which is spin casted from a solution of donor and acceptor materials. For fabrication of these devices, common organic solvents such as chlorobenzene, dichloromethane, chloroform and toluene are used to deposit active layer of donor and acceptor molecules on to surface of the conducting metal oxide.

A BHJ solar cell consists of a four step working mechanism, in which first is exciton creation, followed by exciton diffusion then charge

carrier dissociation and finally charge collection as illustrated in Figure 1.2c.[25,26] The following four subsections (**1.5.1-1.5.4**) describe the mechanism in detail (Figure 1.2a-c).

1.5.1 Exciton creation: At the maximum of the absorption spectrum, the conjugate polymer absorbs light very efficiently due to its high absorption coefficient (10^5 cm^{-1}). Hence only a few nanometers of the photoactive layer are required to absorb all the light at the absorption maximum. An electron is excited from the ground state to the excited state, leaving a hole with the opposite electric charge, forming an electron-hole pair which it is attracted by Coulombic force, also called exciton.

1.5.2 Exciton Diffusion: Within the conjugated polymer, the exciton has a relatively high binding energy (0.2-0.4V), because of the low relative di-electric constant. In organic solar cells, an efficient electron acceptor is used to dissociate the strongly bounded exciton into free charge carriers. The interface of acceptor and donor exciton has to diffuse before it gets decomposed. In a conjugate polymer, the exciton diffusion length is only 5-10 nm. Photons can be absorbed within this exciton diffusion range at the interface, contributing to the device power conversion efficiency (PCE).

1.5.3 Charge carrier dissociation: To separate electron and hole pair at the donor/acceptor interface, the HOMO (Highest Occupied

Molecular Orbital) and LUMO (Lowest Unoccupied Molecular Orbital) levels of an acceptor have to be higher than those in the donor to be energetically suitable. Electrons jump from the HOMO level of donor to the LUMO level of acceptor, with holes remaining at the HOMO level of donor. The advisable HOMO-LUMO energy difference is not too much.

1.5.4 Charge Collection: A free charge carrier is generated at the D/A interface, electrons and holes are transferred *via* acceptor and donor materials, which require high charge–carrier mobility. Positive charges are collected by the anode and the negative charges are withdrawn by cathode, hence, a photocurrent is generated in the external circuit.

1.6 Characterisation of organic solar cells

A number of following parameters can be derived from the light current curve which is shown in Figure 1.3 and followed by a detailed description in subsection (**1.6.1-1.6.4**).

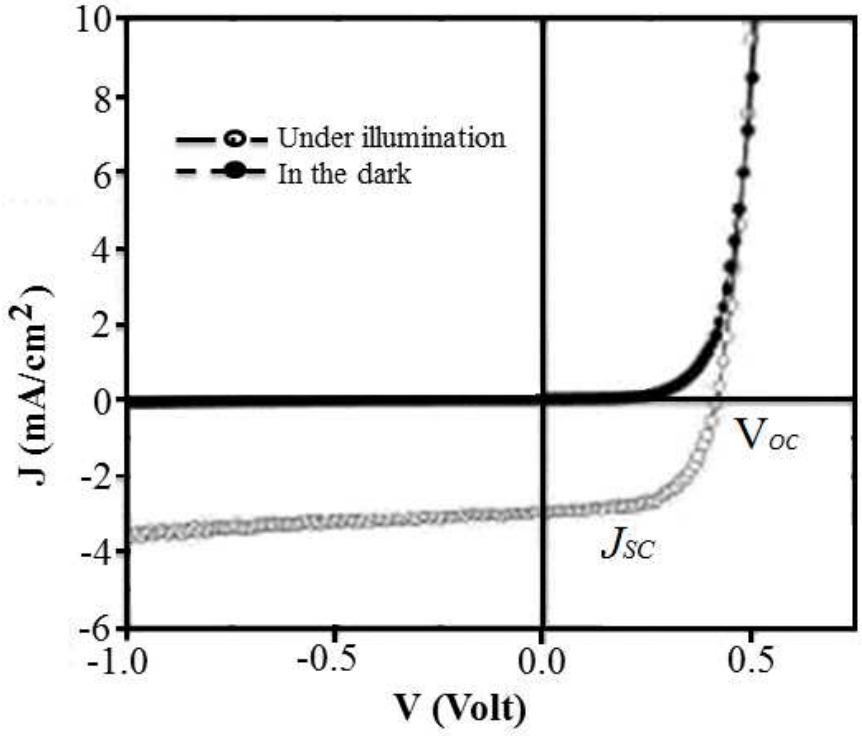

Figure 1.3. The model characterisation technique for organic solar cells.

1.6.1 Open circuit voltage (V_{oc}): The *Voc* represents the maximum voltage (photon) that can be obtain from a solar cell, and is dependent on the organic material in its construction, which dictates the energy difference between the HUMO level of the electron donor layer and the LUMO level of the electron acceptor. A charge recombination process can also influence *Voc*, resulting in a lower maximum *Voc*.

1.6.2 Short Circuit current (J_{sc}): This depends on the number of absorbed photons and can be capitalized by the solar cell only if saturation did not occur. *Jsc* also depends on the:

- Surface area of photoactive layer
- Overlap between the absorption spectrum of the solar cell and solar spectrum
- Device thickness
- Charge collection efficiency

$$I_{sc} \alpha \eta_{abs} \cdot \eta_{diss} \cdot \eta_{out}$$

1.6.3 Fill factor (FF): The FF factor is depends on the competition between charge carrier recombination and transport process. Power conversion efficiency is the ratio of maximum delivered electrical power to the incident light power (p_0) and requires the calculation of the fill factor (FF) then incident light power (p_0):

$$FF = \frac{J_m V_m}{J_{sc} V_{oc}}$$

Where J_m and V_m represent the current density and voltage at the maximum deliverable power point, respectively.

1.6.4 Power Conversion efficiency (η_p): is the ratio of maximum delivered electrical power to the incident light power (p_0) and is calculated by:

$$\eta_p = \frac{J_m V_m}{P_0} = \frac{J_{sc} V_{oc} FF}{P_0}$$

1.7 Literature review of the organic molecules used for BHJ solar cells

Research into organic based BHJ solar cells[27,28] has gained huge momentum over the past two decades because of their potential to replace traditional inorganic photovoltaic devices. This is due to the improvement in their conversion efficiencies. Also organic molecules made up of C, N and O, which are naturally degradable. Most research is focused on the donor materials, which are referred to as *p*-type materials and are used to make an active layer with acceptor or *n*-type semiconducting material.

Within the scope of this thesis, the literature review is focused on the different classes of organic materials that have specifically been used as donor materials for solution processable BHJ solar cell devices, as shown in Figure 1.4.

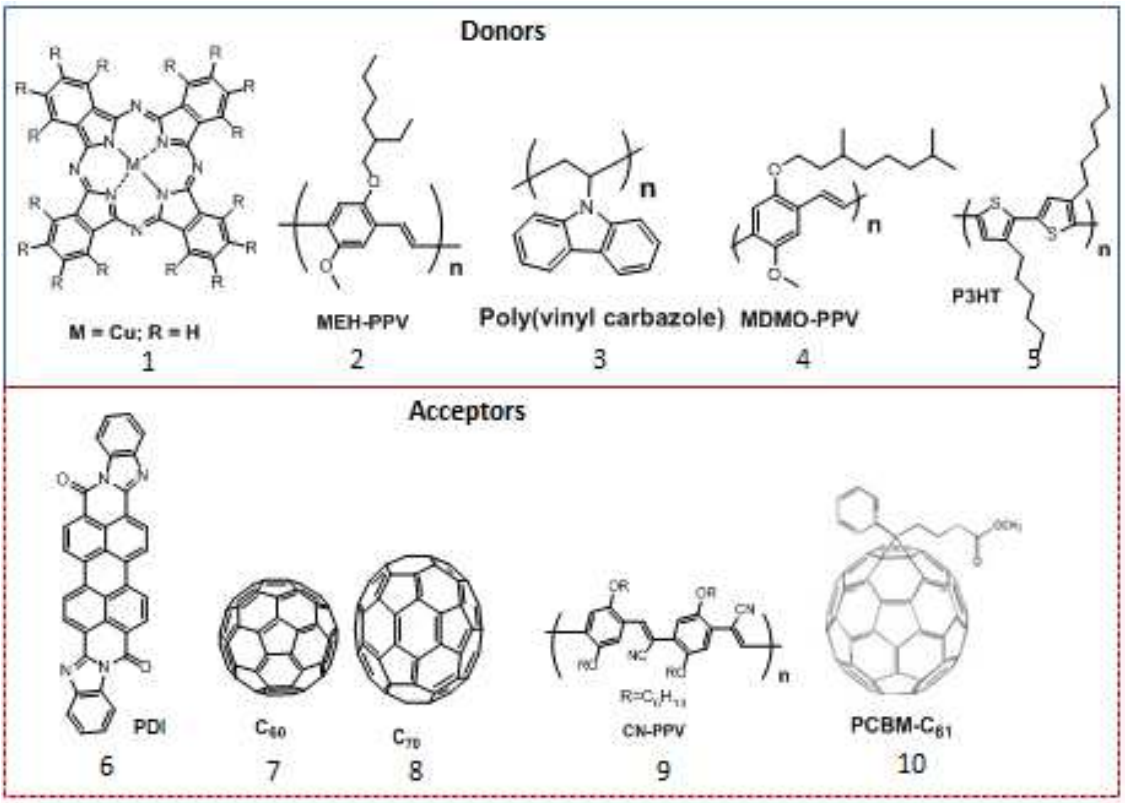

Figure 1.4. Literature electron donor and acceptor molecules used for BHJ solar cells.

The first report by Tang and co-workers reported their work on a bilayer heterojunction organic solar cell where copper phthalocyanine (CuPc) acts as a redox mediator coupled with a perylene-based small molecule as an acceptor (Fig. 1.4, example 1 & 6). Their findings on the bilayer device provided a PCE of 0.95% with a relatively high fill factor of 0.65.[20] Over the following decade, OPV solar cells were studied with limited success, most investigations focussing on the use of conjugated polymers as donor materials and a fullerene as acceptor materials. For example, the use of poly [2-methoxy-5-(2'-ethylhexyloxy)-p-phenylenevinylene] (MEH: PPV) as a donor material and C_{60} as an acceptor material[29] in the bilayer heterojunction

solar cell (Fig. 1.4, example 2 & 7). They have shown that a significant photoinduced electron transfer (PET) occurs from the conjugated polymer to the fullerene acceptors. At the same time, Wang and co-workers reported a study of the photoconducting films of polyvinylcarbazole doped with fullerenes (mixtures of C_{60} and C_{70}),[30] which indicated that the use of higher fullerene, such as C_{70}, or its derivatives can also be used as acceptor materials for OPV applications (Fig. 1.4, example 3, 7 & 8). It was realised that there exists an interpenetrating network of polymers in active layers and photon absorption creates excitons, which must be dissociated at an interface.

Halls *et al.* reported the use of MEH-PPV along with cyano-poly (p-phenylenevinylenes: CN-PPVs) (Fig. 1.4, example 4 & 9) as a polymeric network for efficient photodiodes, in 1995.[31] This work involved the use of an active spin-cast, thin-film layer from a common solution of donor and acceptor polymers onto an ITO-coated glass substrate. The use of such polymeric network and thin film deposition on the conducting metal oxide was likely a requirement for solar energy conversion. Yu, Heeger group reported the use of same donor (MEH-PPV) along with C_{60} or its solubilised derivative (PCBM) as an acceptor (Fig. 1.4, example 2 & 10) further indicated the photoinduced electron transfer from MEH-PPV to PCBM took place with a good energy conversion efficiency.[32] In another report, Shaheen *et al.* explored the use of MDMO-PPV (poly [2-methoxy-5

(3′, 7′-dimethyloctyloxy)-1,4-phenylenevinylene]) as a donor and PCBM as an acceptor material (Fig. 1.4, example 4 & 10) achieving 2.5% PCE solar cells, which was great achievement.[33]

Although, the use of conjugated polymers has been a major focus in the field of OPVs, they have a limited light absorbance in the visible region (400 nm–700 nm) and lower values of absorption maxima (λ_{max}) which would suggest they are high-energy band gap materials. Moreover, because of low charge carrier mobilities of these PPV polymers, efficiencies did not exceed 3% at their best[34,35] and the general interest in this class of materials has faded.

Thereafter, research efforts were focused on poly(alkylthiophenes), perticularly poly(3-hexylthiophene) (P3HT), as the donor class of polymeric materials. An encouraging report by Brabec and co-workers emanated in 2002 using the combination of P3HT: PCBM solar cells with a weight ratio of donor:acceptor in 1:3 ratio.[36] This paper appeared to be the starting point for the rapid development of P3HT:PCBM blends and also for improved understanding the device physics followed by the first explicit report on efficiency enhancement by thermal annealing[37].

In similar class of molecules, Brabec's device obtained PCE of 4.4%, (Fig. 1.4, example 5&10)[38] which was the most efficient device, published at the time in which the dye was completely solution

processable without any special treatment. An efficiency of ~5% was claimed to be formed from the same cell when it underwent thermal annealing at 150 °C, and it was highly stable after this treatment.[39] Following the success of the P3HT/PCBM combination, Brabec and co-workers suggested that the BHJ solar cells have the potential to reach an energy conversion efficiency of up to 10%.[40] Consequently, research surged in the search of new donor polymeric materials that would exhibit better photophysical properties, such as broader spectral response, improved hole transport and favourably tuned HOMO/LUMO energy levels that match well with that of existing acceptors.[41,42]

Since 2007, various research groups have focused on generating novel conjugated polymers as donor materials and fabricating them into OPV devices, with PCBM as an acceptor. The idea of using conjugated polymers has expanded to include different classes of organic materials possessing a range of electronic behaviours, such as being electron rich (donor) or electron poor (acceptor), which can be used to generate a polymeric backbone within BHJ devices.

1.8 Key Conjugated Polymers

Within the scope of this thesis, Figure 1.5 describes the development of a major classes of small molecular donors that have specifically been reported for solution processable organic photovoltaic devices.

Slooff *et al*. reported the use of dialkylfluorenes as donors and benzothiadiazole as an acceptor for the fabrication of BHJ solar cells, affording 4.2% efficiency (Figure 1.5, example 11 & 10).[43] The use of dialkylfluorene gathered much attention due to its good charge transport and stability properties. Heeger and co-workers were able to enhance the device performance by the addition of alkanedithiols during the formation of the blend solution (Figure 1.5, example 12).[44] It was reported that the efficiency was enhanced from 2.8% to 5.2% by altering the bulk-heterojunction morphology. This paper has been cited 1122 times and sets as an example of using cyclopentanedithiophene as an efficient donor block (Figure 1.5, example 13)[45]. In another example, a semiconducting copolymer (Figure 1.5, example 14)[46] containing dithienothiophene as a donor and DPP as an acceptor has been reported the highest hole mobility of around 2 $cm^2V^{-1}s^{-1,}$ and when incorporated into devices, afforded a power conversion efficiency of 5.4%. The high efficiency of the polymer was ascribed to copolymerisation of the thiophene groups. Moulé *et al*. further explored this donor block in a series of polymers (Figure 1.5, example 15)[45], where benzothiadiazole and quinoxaline were used as acceptor functionalities. The benzothiadiazole performed moderately compared to quinoxaline-based polymers, which failed to produce efficient solar cells. It was concluded that the use of the acceptor fragment plays just as an important role in the design and development of novel polymers as the donor fragment.

DPP and benzodithiophene (BDP) have been shown to be among the best functionalities for acceptor and donor components respectively. However, by substituting benzodithiophene with naphthodithiophene, Peng *et al.,* showed the device performance could be improved further. In their work they used PNDTDPP polymer (Figure 1.5, example 16), which is enhanced photovoltaic performance up to a PCE of 5.37%, compared to benzodithiophene-based copolymer PBDDPP, which was 2.91% PCE in conventional device structures.[47] The Heeney group has reported a dithienogermole-benzothiadiazole copolymer (Figure 1.5, example 17) with a PCE of 4.5% and high charge carrier mobility. They found that the dithienogermole functionality is stable under basic conditions to allow Suzuki polycondensation when associated with analogous dithienosilole.[48] The Franky group reported the same polymer, dithienogermole-*N*-alkylthienopyrrole-4, 6-dione (Figure 1.5, example 18), with inverted device structure and a PCE of 7.4% was confirmed.[49] It was claimed that the polymer solar cells with an inverted device structure are compatible with roll-to-roll fabrication processing.

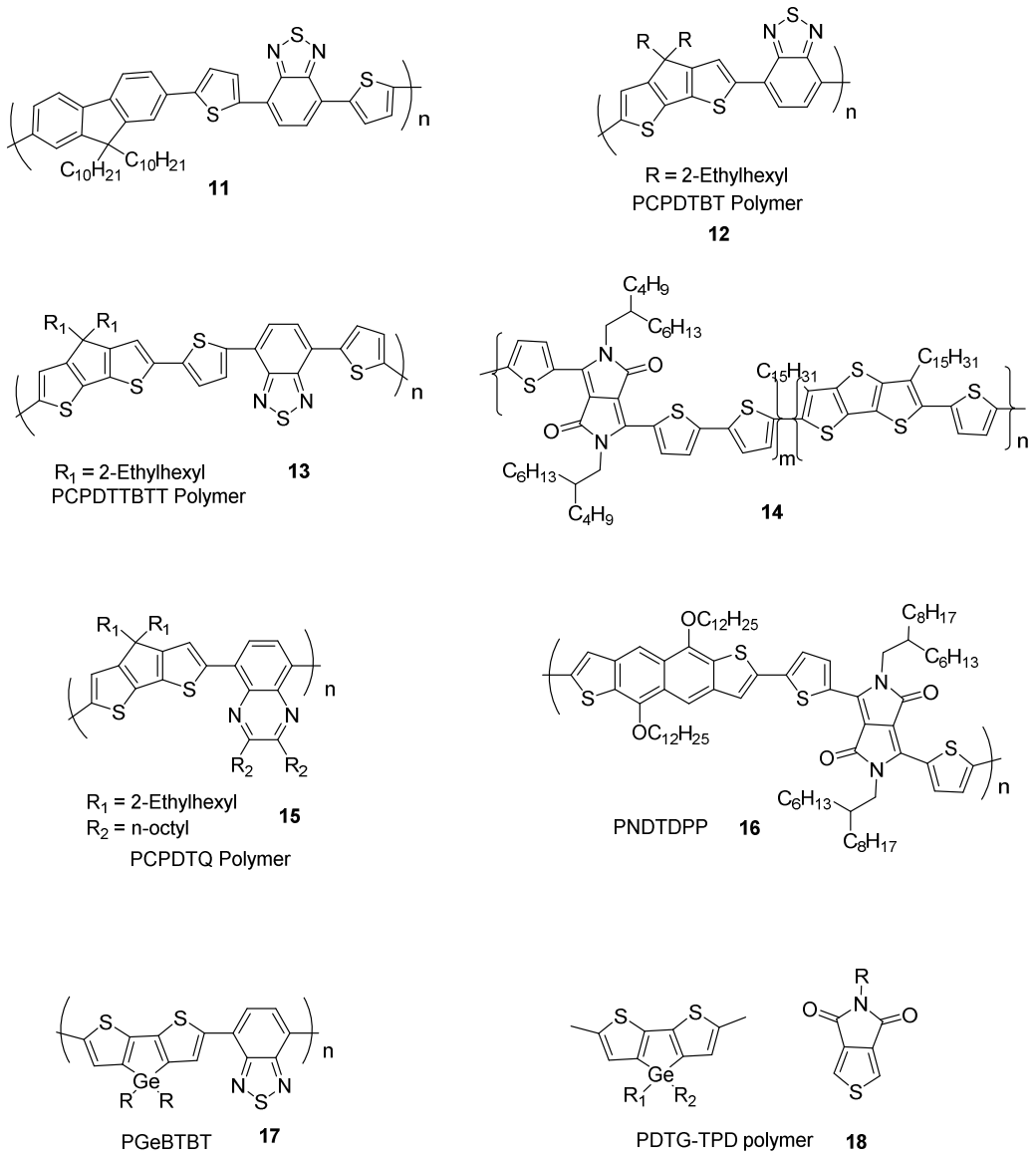

Figure 1.5. Literature reported donor polymeric entities used in solution processable BHJ solar cell devices, in combination with PCBM as an acceptor.

Many review articles[50-58] have been published in the past on the use of conjugated polymers and on the device physics of organic photovoltaic devices, which further helps us to understand the working mechanisms, but are out of the scope of this study.

So far most of the research in the field of organic BHJ solar cells has been focused on the use of fullerene-based acceptors and *p*-type conducting polymers as donors. Current research in the field of small organic molecules has demonstrated the feasibility of solution-processed BHJ devices composed entirely of these molecular solids. The development of small organic molecules offers potential advantages over conjugated polymer systems in terms of simplicity of purification, batch-to-batch reproducibility and flexibility to scale-up.

Following is the list of the common synthons that have been used for the development of conjugated polymers as well as small organic molecules in the BHJ field of research (Table 1.1).

The first small molecular BHJ devices were reported in 2000 and 2001. These reports included solution processable phthalocyanine or hexabenzocoronene in combination with perylene blends[59] (Table 1.1, example 19 & 20).[60] However these devices exhibited poor device performance compared to the polymeric systems. The disappointing results of this pioneering report failed to generate interest in the field of small molecule BHJ devices until 2005, when Roncalli and Lloyd reported the use of fused aromatics, such as pentacene and oligothiophenes. The solution processable BHJ devices of these aromatics gave a 0.5% PCE (Table 1.1, example **21** & 22).[61,62] At around the same time, Sun *et al.* reported the use of X-shaped oligothiophenes with different conjugation lengths for solution processable BHJ devices with PCE up to 0.8% (Table 1.1, example

23).[63] These studies indicate that the photovoltaic effect is mainly dependent on structural characteristics. In another report, Roncalli group used oligothiophenes in conjugation with triphenylamine as an electron donor and indanedione or dicyanovinyl groups as electron acceptor, in their extended work. A PCE of ~1.20% (Table 1.1, example 24) was reported for the star-shaped donor-acceptor small molecule by Roquet *et al.* They found that the introduction of acceptor groups induced an intramolecular charge transfer that resulted in longer wavelengths and narrow band gaps.[64] Further improvements in donor-acceptor system were reported by the Meerholz group, using merocyanine colorants with a variety of donor and acceptor functionalities, to give a PCE of ~1.74% (Table 1.1, example 25).[65]

Upon the successful strategy development of donor-acceptor small molecular designs, other modular designs such as donor-acceptor-donor (D-A-D), acceptor-donor-acceptor-donor-acceptor (A-D-A-D-A), acceptor-donor-acceptor (A-D-A) or donor-acceptor-donor-acceptor-donor (D-A-D-A-D) were also investigated. The first report of this was by the Nguyen group, who used a donor-acceptor-donor module, in which thiophenes and benzofuran were used as donors and diketopyrrolopyrrole as an acceptor (Table 1.1, example 26 & 27). The new reported materials were solution processable and displayed good film characteristics from their blend solutions, in combination

with a fullerene acceptor. A PCE of up to 4.4% was reported, with thermal annealing of the devices for effective BHJ morphologies.[66,67]

Table 1.1: Literature reported small organic molecules as donor materials for solution processable organic solar cells

Entry	Donor materials	Acceptor	Ref.	Remarks
19	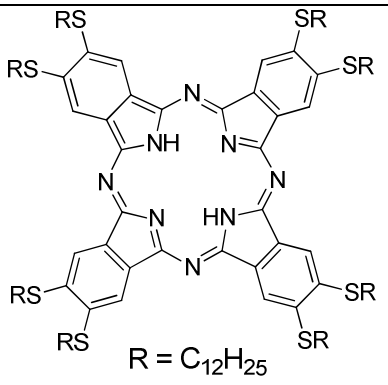 HPc 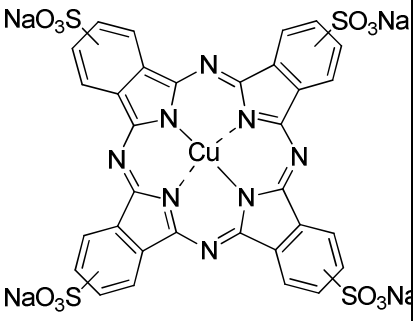 CuPc	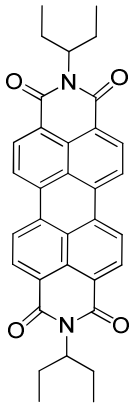 Perylene	59	Phthalocyanine/perylene blends Published: 2000 PCE: 0.3% to 1.0%
20			60	First use of hexabenzocoronene/perylene blends Published: 2001

	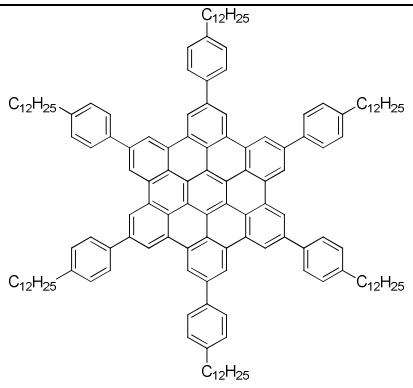 HBC-PhC$_{12}$	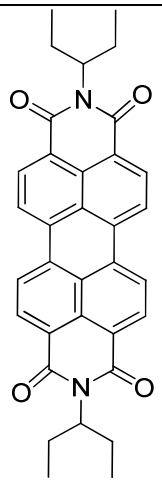 Perylene		
21	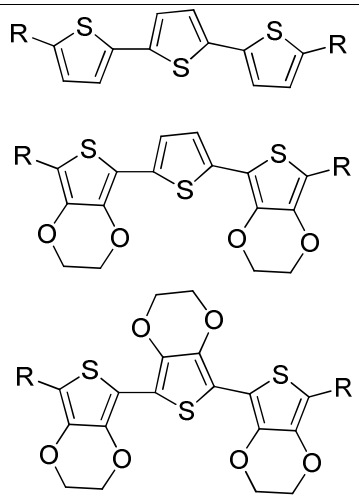 R = n-Hexyl	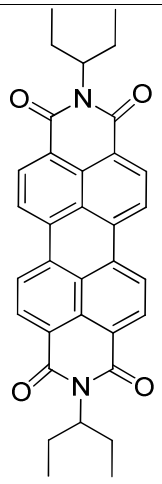 DP13	61	π-conjugated oligothiophenes/perylene blends Published: 2006 PCE: 0.3%
22	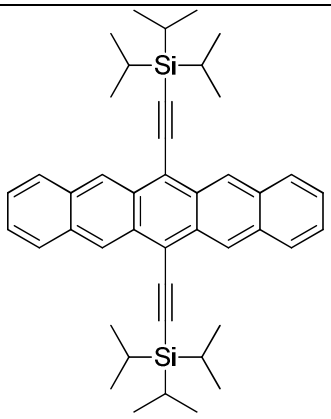 TIPC-Pentacene	Fullerene C_{60}	62	TIPS-pentacene/C_{60} blends Published: 2006 PCE: 0.52%
23		PCBM-C_{61}	63	X-shaped oligothiophenes/P

	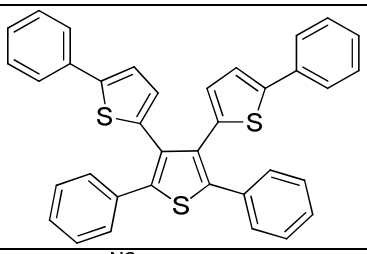			CBM-C_{61} blend Published: 2006 PCE: up to 0.8%
24	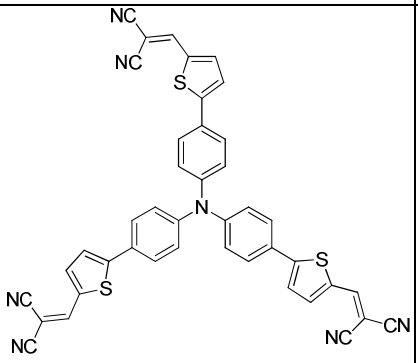	C_{60} Derivative	64	Donor-acceptor star shaped molecules Published: 2006 PCE: ~1.2%
25	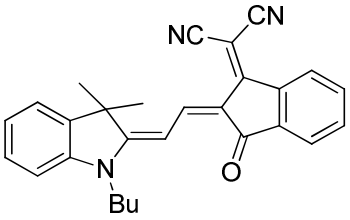	PCBM-C_{60}	65	Donor-acceptor merocyanine colorants Published: 2008 PCE: 1.74%; Highest PCE until 2008
26	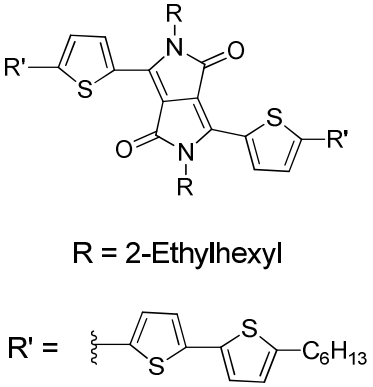	PCBM-C_{71}	66	D-A-D modular small organic molecule Published: 2009 PCE: 3.0%
27	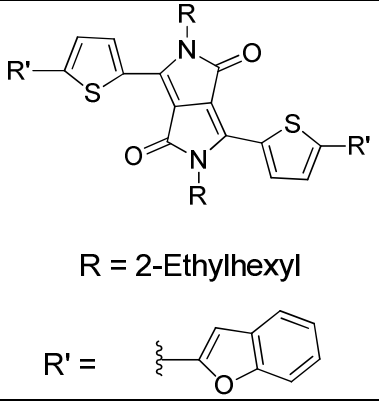	PCBM-C_{71}	67	D-A-D modular small organic molecule Published: 2009 PCE: 4.4%; Highest PCE in 2009 Cites: 221

28	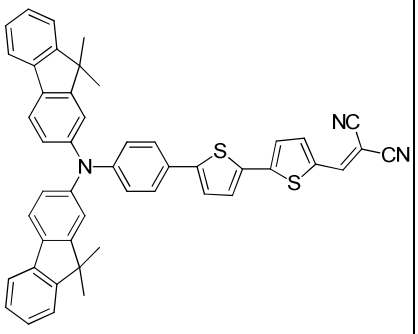	PCBM-C_{71}	68	D–A modular small organic molecules Published: 2011 PCE = 2.46% (no additive) PCE = 3.66% (with 3% chloronaphthalene additive)
29	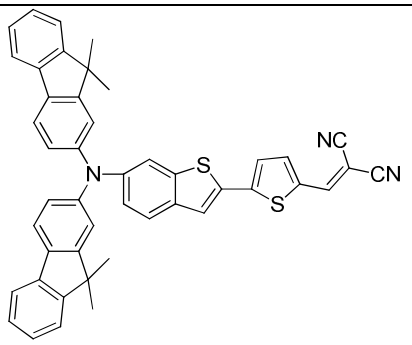	PCBM-C_{71}	69	D-A modular small organic molecules containing bisdimethylfluorenyl amino benzothiophene functionality Published: 2012 PCE: 4.01% High V_{oc}: 0.95V
30	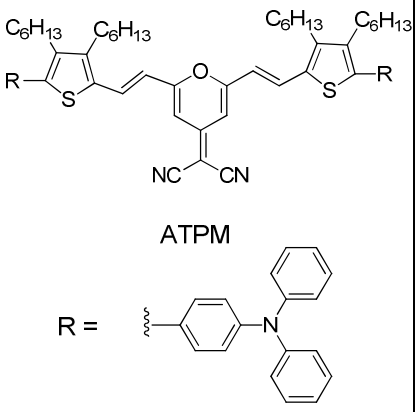	PCBM-C_{61}	70	D-A-D modular small organic molecules Published: 2011 PCE: 1.31% High V_{oc}: 1.0V Highest ever reported V_{oc} for small molecular solids
32	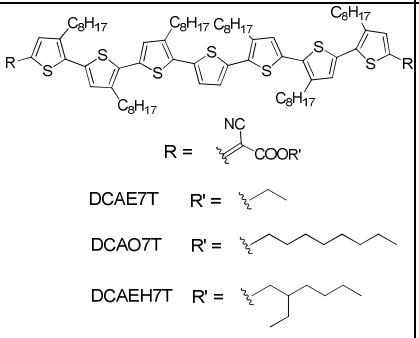	PCBM-C_{61}	72	A-D-A modular donor materials based on oligothiophenes Published: 2011 PCE: 5.08%
33		PCBM-	73	Donor:

	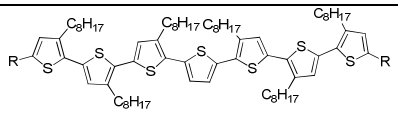 DERHD7T 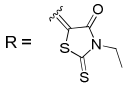	C_{61}		oligothiophenes Acceptor: *N*-ethylrhodanine Published: 2012 PCE: 6.1%
34	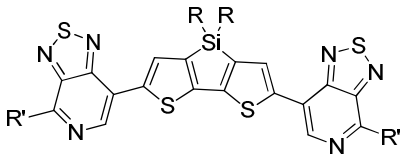 R = 2-Ethylhexyl R' = 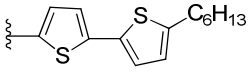	PCBM-C_{71}	74	D-A-D-A-D modular donors based on central dithienosilole and thiadiazolopyridine acceptor Published: 2011 PCE: 3.0%
35	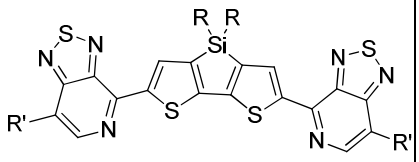 R = 2-Ethylhexyl R' = 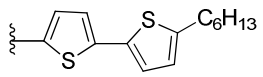	PCBM-C_{71}	75	D-A-D-A-D modular design Donor: dithienosilole Acceptor: thiadiazolopyridine Use of metal oxide in device design Published: 2012 PCE: 6.7%
36	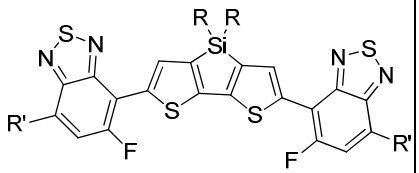 R = 2-Ethylhexyl R' = 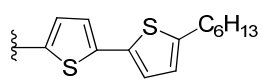	PCBM-C_{71}	76	D-A-D-A-D modular donors based on central dithienosilole and fluorobenzothiadiazole acceptor Published: 2012 PCE: 7.0% with 0.4% *v/v* addition of 1,8-diiodooctane as

				an additive
37	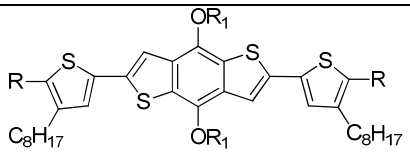 R_1 = 2-Ethylhexyl R = 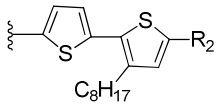 R_2 = 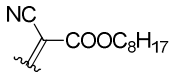 , 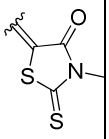	PCBM-C_{61} and PCBM-C_{71}	77	A-D-A modular donor materials based on central benzodithiophene and *N*-ethylrhodanine terminals Published: Sept. 2012; PCE: 7.38% (certified 7.10%); Highest reported efficiency for small molecular solution processable organic photovoltaic device
38	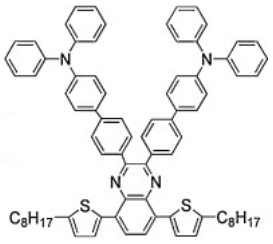 TPA-PQ-T 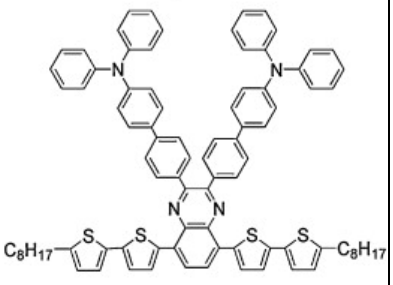 TPA-PQ-2T	PCBM-C_{61}	78	Published 2015. PCE: 1.28%.

39	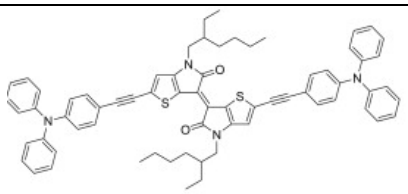 TII-TPA 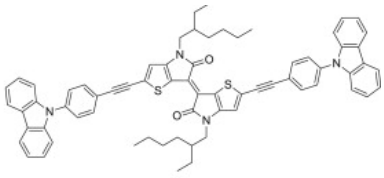 TII-PCz	PCBM-C_{61}	79	D-A-D module. Pi-conjugated molecule. PCE: 2.23%
40	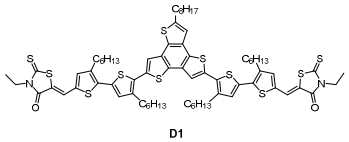 D1 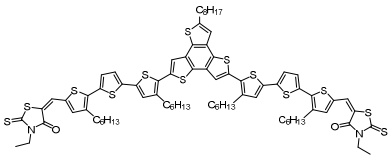 D2	PCBM-C_{61}	80	A-D-A module. PCE: 2.10%
41	**MEH-PPV**	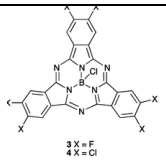 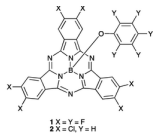	81	PCE: 3.5%
42	P3HT	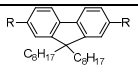 PMI-F-PMI R = 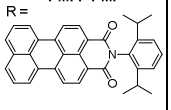	82	Published: 2015. PCE: 2.30%

43	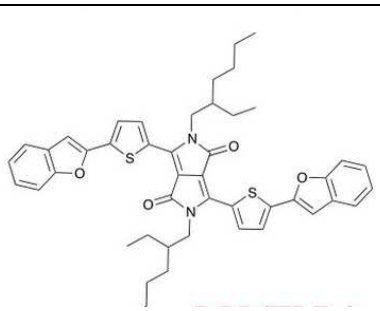	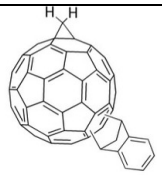	83	Published: 2015. PCE: 5.1%

The Ko group explored D-A systems bearing bis-dimethylfluorenylamino derivatives as donors, thiophenes as central π-spacers and dicyanovinylidene as an electron acceptor (Table 1.1, example 28 & 29). Their finding revealed that the use of the benzothiophene moiety in the donor part helped to achieve a higher open circuit voltage when compared with its phenyl counterpart. The device exhibited a high PCE of 4.01% with a high open circuit voltage of 0.95 V.[68,69]

A series of materials based on the D-A-D design were further explored by Li *et al.* using 2-pyran-4-ylidenemalononitrile as an electron-accepting moiety and triphenylamine as an electron-donating moiety, linked by different electron-donating moieties and PCBM-C61 as an acceptor (Table 1.1, example 30). A PCE of 1.31% was among the best with a high open circuit voltage of 1V shown for the first time.[70] Similarly, Shi *et al.* reported the use of a triphenylamine donor and the new electron-withdrawing building block thiazolothiazole (Table 1.1, example 31). Solution processed solar cells based on blends of donor and PCBM-C_{71} afforded a PCE of

3.73%, after thermal annealing.[71] A-D-A design has been developed by Liu *et al.* In their design, they have used oligothiophenes as the central moiety with end-capped bis-alkyl-cyanoacetate acceptor groups (with different alkyl substitutions). These A-D-A dyes were used to achieve series of materials (Table 1.1, example 32). They found that the use of end-capped alkyl-chains not only enhanced the solubility, but also improved the packing structure and miscibility with PCBM. A solution processable BHJ device afforded a PCE of 5.08% with the use of an octyl-substituted cyanoacetate acceptor.[72] In similar fashion, Li *et al.* prepared solution processable, *N*-ethylrhodanine-based, small molecule, organic photovoltaic cells which exhibited a PCE of 6.1% and derivatives show very high mobility (Table 1.1, example 33).[73]

The Bazan group developed another modular framework based on the A-D-A arrangement, where dithienosilole was the central donor and thiadiazolopyridine was an acceptor, with donor end-capping units (Table 1.1, example 34). This design achieved strong charge transfer characteristics, with broad optical absorption spectra and achieved a PCE > 3%.[74] Using the same material with slight changes to the device architecture, an impressive PCE of 6.7% was achieved. This device used a 7:3 ratio of donor:$PC_{71}BM$ and a small percentage of solvent additive (0.25% *v/v* of 1,8-diiodooctane) during the film-formation process (table 1.1, example 35).[75] Using a similar principle, they have also designed another molecule bearing

fluorobenzothiadiazole as the central donor (Table 1.1, example 36) and the use of fluorine provided an electron-withdrawing functionality with no lone pairs of electrons that may be prone to participate in acid/base reactions. In OPV devices, the best improvement was observed by heating the device to 130 °C, yielding a PCE of 5.8%. Furthermore, the use of solvent additives such as 1,8-diiodooctane (0.40% *v/v*) improved the PCE to 7.0%, with relatively high fill factor of 0.68.[76]

In 2012, the Chen group used benzodithiophene in their A-D-A to design two new small molecules (Table 1.1, example 37). The use of a 3-ethylrhodanine terminal in the A-D-A design helped to improve the solar light absorption and the solar cell devices based on the corresponding compound afforded a PCE of 7.38%. This is the highest reported efficiency for a small molecule based solution processable organic solar cell.[77]

Recently, Liu group designed and synthesized two star shape D-A type small molecules of triphenalamine (TPA)-phenylquinoxiline (PQ)- thiophene (T) and TPA-PQ-2T (Table 1.1, example 38). Where PQ was used as central core and acceptor unit, TPA used as hole-transporting moieties and T and 2T were used as arms and donor units. In this solution –processed, TPA-PQ-T based solar cell,the PCE obtained was 1.28%.[78]

Two acetylene-bridged D-A-D type, small, π-conjugated molecules involving triphenylamine or *N*-phenylcarbazole as donor blocks (D) and thienoisoindigo as the acceptor unit (A) were synthesized and characterized by Oleh Vybornyi *et al.* The triphenylamine end-capped derivative reported the highest PCE value of ~2.20% (Table 1.1, example 39).[79]

Meng *et al*. (Table 1.1, example 40) designed and synthesized two novel A–D–A small molecules containing benzo[1,2-*b*:3,4-*b′*:5,6-*b″*]trithiophene as the central electron-donating unit, 3-ethylrhodanine as end-capped electron-withdrawing units, and two or three thiophene molecules as conjugated π-bridges. The effects of the conjugated π-bridges on the photophysical, electrochemical and photovoltaic properties, as well as the aggregated structure, were fully investigated. This led to a device with improved photovoltaic performance, a PCE of 2.10% and an amazingly high V_{oc} of 1.10 V.[80]

The Ebenhoch group reported the fabrication of solution-processed BHJ devices from subphthalocyanine (SubPc) units as the acceptor component and conventional polymeric donor materials (such as MEH-PPV, P3HT and PTB7). The high solubility of the SubPc derivatives the formation of efficient donor/acceptor networks were prepared which exhibited a PCE of 0.4% with MEH-PPV, 1.1% with P3HT and 3.5% with PTB7 (Table 1.1, example 41).[81]

A fluorene-centered, perylene monoimide dimer (PMI-F-PMI) with a partly non-coplanar configuration has been developed by the Zhang group. Optimum power conversion efficiency of the OSC based on PMI-F-PMI as an acceptor, and poly (3-hexyl thiophene) (P3HT) as a donor, of up to 2.30% were obtained (Table 1.1, example 42) after annealing at 150 °C. Because of the relatively balanced electron–hole transportation and the smooth morphology, PMI-F-PMI is superior to its sister (PMI-F) and parent (PMI) compounds as an acceptor in BHJ solar cells.[82]

Ryan & Matsuo reported (Table 1.1, example 43) methano indene fullerene (MIF) dye i.e. a bis-functionalised C_{60} fullerene as an acceptor that has a LUMO level 140 mV higher than PCBM, in solution processed SMOSCs with a well-known small molecule donor, DPP $(TBFu)_2$. MIF-based devices show an enhanced V_{OC} of 140 mV over that from $PC_{61}BM$ and only a small decrease in the J_{SC}, with the PCE increasing to 5.1% (*vs.* 4.5% for $PC_{61}BM$).[83]

Recent development in OPV field have been intensely reviewed on the use of small molecular solids further helps to deepen our knowledge on device physics and mechanism.[84-85] These reviews highlight that most of the small molecular solids have been used with either vapour deposited or solution processable organic solar cells. Examples of commonly used synthons, for the development of polymeric and small molecular materials, are illustrated in Table 1.2.

Table 1.2: Commonly used synthons for the development of polymeric and small molecular materials for solution processable BHJ devices.

NO.	Structural motif	Donor	Acceptor	References
44	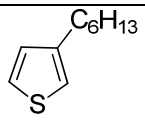 3-Hexylthiophene	Yes	No	39, 86
45	 Thiophene	Yes	No	66, 87
46	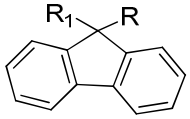 Fluorene	Yes	No	43, 68
47	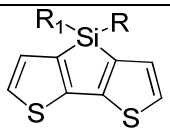 Dithienosilole	Yes	No	88, 89
48	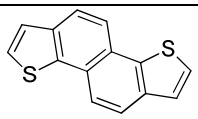 Naphthodithiophene	Yes	No	90, 91
49	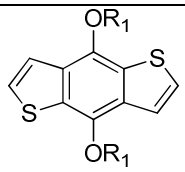 Benzodithiophene	Yes	No	77

50	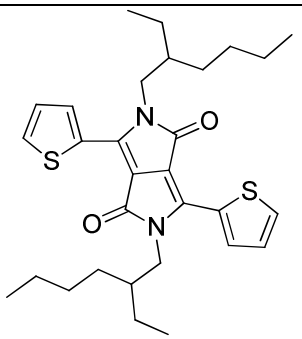 Diketopyrrolopyrrole	No	Yes	67
51	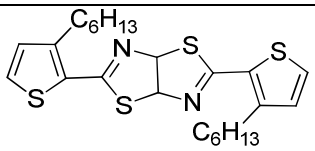 Dithienylthiazolothiazole	No	Yes	71
52	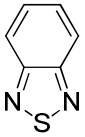 Benzothiadiazole	No	Yes	90

1.9 Literature limitations and project aims

Within the scope of this thesis, the literature review presented here signifies a variety of organic materials that have been used for the fabrication of solution-processable BHJ solar cells. Small organic molecules as well as polymeric entities have been used as BHJ materials. Most of the organic materials have been developed on the basis of various structural modules such as D-A, A-D-A and D-A-D to name a few. Most of the materials have been designed randomly and the reported literature fails to provide any correlation between the various fragments of a particular molecule, and how the optoelectronic and photovoltaic properties are affected with the structural changes. Moreover, there is no material development program based on a common structural ground. Furthermore, the reported literature lacks in an A-B comparison of structural change *vs* the photovoltaic behaviour, which is an essential feature for the design and development of new BHJ materials.

Apart from the above mentioned problems the literature reported strategies provide limited solutions to some of the important features that are essential for a BHJ material.

Few main features that are of utmost importance are depicted below:

- Stability of organic materials and hence an overall stability of the BHJ device

- Solubility of organic materials as the materials are processed using common organic solvents such as chloroform, dichlorobenzene and toluene
- Flexibility of organic materials
- Broad absorption over the visible range, and possibly to near IR, for an efficient ICT
- Comparative modular designs examination for the generation of new materials with tuneable photo-physical properties so that the materials can perform better than their previous analogues.

1.9.1 Overcoming the literature issues: Diverse entities of small aromatic π-conjugated functional molecules have attracted enormous research interest in light of their applications in optoelectronics. Weak molecular non-covalent forces such as π–π interactions, Vander Waals and electrostatic interaction play crucial role in the device fabrication strategy. In this regard, we plan to use newer small target molecules that include functionalities such as NDI and DPP in conjugation with other donor and/or acceptor moieties for further development of the material design in the emerging field of BHJ devices. The use of NDI and DPP functionalities for the development of targets will satisfy most of the features mentioned above in the section 1.9.

Amongst aromatic molecules that have found utility, especially in the design of conducting materials, NDIs have attracted much attention

due to their tendency to form n-type semiconductor materials.[92] Naphthalenediimides (NDIs) have been used for decades as electron acceptors in covalent and non-covalent systems such as dyads and triads as well as sophisticated architectures in catenanes and rotaxanes.[93] However, their optical properties are discreetly limiting their utility. In 2002, the Würthner group discovered that a slight modification to the core substitution (Figure 1.6) by one or up to four electron-donating groups on the NDI ring introduces a new electronic transition with charge transfer character located in the visible region.[94,95] Consequently, cNDIs have opened this class for further investigation, by combining optical and structural changes at the supramolecular[96] and molecular level.[97] Applications of cNDI derivatives have not yet been extensively studied in solar cell applications, with only a few controlled nanostructures being reported.[92-96]

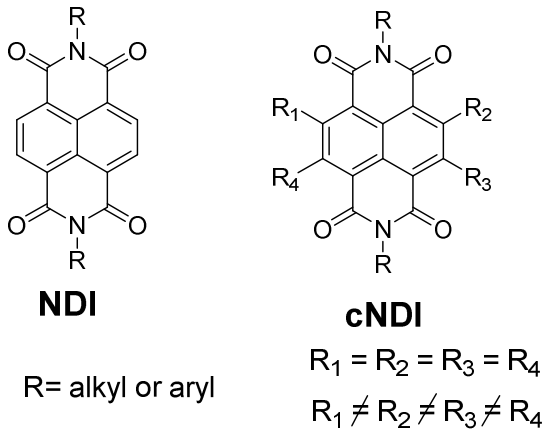

Figure 1.6. Napthelene diimide (NDI) and core-substituted naphthalene diimide (cNDI) structures.

On the other hand, organic dyes based on diketopyrrolopyrrole (DPP) functionality[98] have been widely studied as organic pigments in industrial applications such as paints, plastics and inks (Figure 1.7).

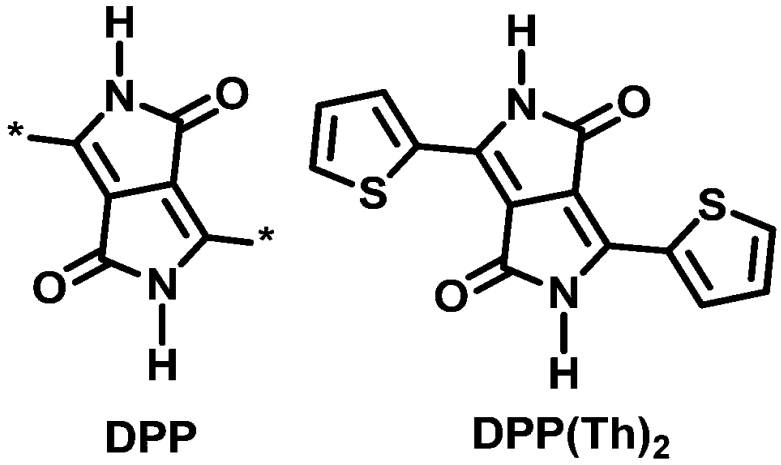

Figure 1.7. Structures of diketopyrrolopyrrole and thiopehne substituted diketopyrrolopyrrole.

DPP building blocks are reported to be potential planer conjugated structures, containing an electron deficient fragment and electron accepting amide group. An advantage of DPP accepting functionality is the possibility to incorporate alkyl chains on the nitrogen atoms that helps to improve the solubility of target materials and also helps with excellent film formation without crystallization. DPP unit can also be used to construct low-band gap materials. The assimilation of a DPP unit into a conjugated backbone can modify the optical energy levels and fine tune the absorption pattern.

1.9.2 Typical aims of this PhD project

Based on the literature survey and importance of cNDI and DPP functionalities, this PhD project will aim to design and develop novel target materials that will incorporate NDI and DPP blocks and will be based on the structural modules such as D-A-D, A-A-A, A-D-A.

The main focus of my PhD work will be the design of novel materials in such a way that they fulfil most of the basic structural requirements, such as solubility, stability, low band-gap and broad absorption. The materials will be designed using a variety of donors and/or acceptors functionalities along with NDI and DPP. It is important to mention that we'll take account of design prerequisites that will help us to generate a target depicting (1) strong and broad absorption, (2) adequate solubility, (3) high charge carrier mobility, (4) low band gap and (5) appropriately tuned HOMO and LUMO energy levels.

1.10 Project approach

For achieving the results based on the above mentioned research aims, we can define the project approach in the form of a flow chart that will help to understand the various steps for the set research goals. The flow chart is followed by **Table 1.3**, which will show the involvement of various people working on this project as part of my Ph. D.

Please note that the flow chart and **Table 1.3** are related with each other.

The flow diagram can be represented as follows:

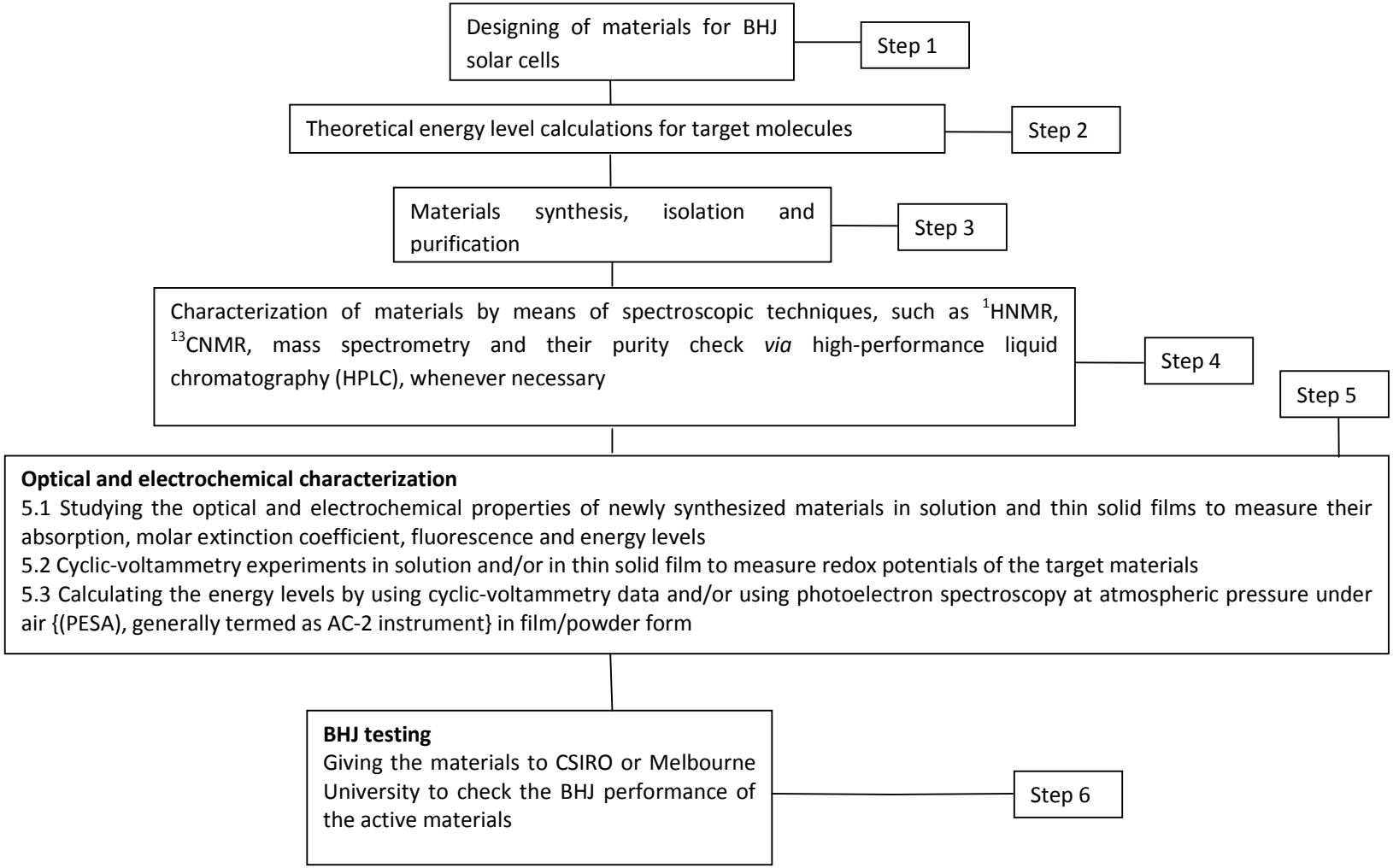
Designing of materials for BHJ solar cells
Step 1
Theoretical energy level calculations for target molecules
Step 2
Materials synthesis, isolation and purification
Step 3
Characterization of materials by means of spectroscopic techniques, such as ^{1}HNMR, ^{13}CNMR, mass spectrometry and their purity check *via* high-performance liquid chromatography (HPLC), whenever necessary
Step 4
Step 5
Optical and electrochemical characterization
5.1 Studying the optical and electrochemical properties of newly synthesized materials in solution and thin solid films to measure their absorption, molar extinction coefficient, fluorescence and energy levels
5.2 Cyclic-voltammetry experiments in solution and/or in thin solid film to measure redox potentials of the target materials
5.3 Calculating the energy levels by using cyclic-voltammetry data and/or using photoelectron spectroscopy at atmospheric pressure under air {(PESA), generally termed as AC-2 instrument} in film/powder form
BHJ testing
Giving the materials to CSIRO or Melbourne University to check the BHJ performance of the active materials
Step 6

Table 1.3: Involvement of various people in my Ph. D. project

Steps	**People involved**	**Facility**	**Remarks**
1	Hemlata Patil Akhil Gupta	RMIT and CSIRO	
2	Ante Bilic	CSIRO	CSIRO Virtual Nanoscience Laboratory
3	Hemlata Patil	RMIT	RMIT School of Applied Sciences
4	Hemlata Patil	RMIT	RMIT School of Applied Sciences
5.1	Hemlata Patil	RMIT	RMIT School of Applied Sciences
5.2	Hemlata Patil	RMIT	RMIT School of Applied Sciences
5.3	Hemlata Patil, Akhil Gupta	RMIT and CSIRO	RMIT School of Applied Sciences

6	Akhil Gupta and Prashant Sonar	CSIRO and Queensland University	BHJ device fabrication facility

NOTE

- Hemlata Patil conducted synthesis, purification and characterization of all the materials at the RMIT facilities.
- Materials reported for BHJ solar cells were tested by Drs Akhil Gupta and Dr. Prashant Sonar at Queensland University of Technology, Brisbane.
- DFT calculations on all the materials were performed by Dr Ante Bilic at the CSIRO Virtual Nanoscience Laboratory, Parkville VIC 3052
- Analytical measurements such as CV, AFM and TGA were conducted at the RMIT facilities.
- PESA measurements were conducted at the CSIRO facility by Akhil Gupta.

1.11 Appendix of terms

A) Heterojunction

A heterojunction is the interface that occurs between two layers or regions of dissimilar semiconductors. These semiconducting materials generally have unequal band gaps.

B) Exciton

An exciton is said to be a bound state of an electron and an imaginary particle called hole. As such it is an electron-hole pair has no net charge.

C) PEDOT:PSS

PEDOT:PSS or poly (3, 4-ethylenedioxythiophene) poly (styrenesulfonate) is a polymer mixture of two ionomers (An ionomer is a polymer that comprises repeat units of both electrically neutral repeating units and ionized repeating units).

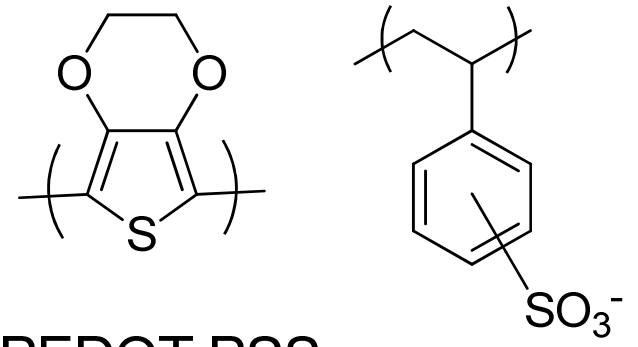

PEDOT:PSS
polymeric mixture structure

One component in this mixture is made up of sodium polystyrene sulfonate. Some of the sulfonyl groups are deprotonated and carry a negative charge. The other component, poly (3, 4-ethylenedioxythiophene) or PEDOT, is a conjugated polymer which carries positive charges and is based on polythiophene. Together the charged macromolecules form a macromolecular salt.

D) Annealing

Annealing, in materials science, is a heat treatment wherein a material is altered through increased temperatures, causing changes in its properties such as strength and hardness. It involves heating the material to above the re-crystallization temperature, maintaining a suitable temperature, and then cooling. Annealing is used to induce ductility, soften material, relieve internal stresses, and refine the structure, by making it homogeneous.

E) Fermi level

The Fermi Level is the energy level which is occupied by the electron orbital at absolute zero (0 Kelvin) temperature. The level of occupancy determines the conductivity of different materials.

1.12 References

1. Cubasch U.; Meehl G. A. Climate Change 2001: The Scientific Basis, Eds J. T. Houghton *et al*., Cambridge Univ. Press, Cambridge, **2001**, Chapter 9: Projections of future climate change, pp. 525–582.
2. Wigley T. M. L.; Raper S. C. B. Interpretation of high projections for global-mean warming, *Science*, **2001**, *293*, 451–454.
3. Orr J. C. *et al*. Anthropogenic ocean acidification over the twenty-first century and its impact on calcifying organisms, *Nature*, **2005**, *437*, 681–686.
4. Karl T. R.; Trenberth K. E. Modern global climate change, *Science*, **2003**, *302*, 1719–1723
5. **2012** Key World Energy Statistics, International Energy Agency,ParisFrance;http://www.iea.org/publications/freepublications/publication/kwes.pdf
6. http://www.worldcoal.org/resources/coal-statistics/
7. BP Statistical Review of World Energy, June **2012**; bp.com/statistical review
8. Meng Q. Y.; Bentley R. W. Global oil peaking: Responding to the case for abundant supplies of oil, *Energy*, **2008**, *33*, 1179–1184.
9. Bentley R. W. Global oil & gas depletion: an overview, *Energy Policy*, **2002**, *30*, 189–205.

10. Energy Technology Perspective **2008**: An International EnergyAgency(IEA)factsheetrenewables,pp7;http://www.iea .org/techno/etp/fact_sheet_ETP2008.pdf.
11. World Energy Council-**2010** survey of energy resources; http://www.worldenergy.org/documents/ser2010exsumsept8. pdf.
12. Schiermeier Q.; Tollefson J.; Scully T.; Witze A.; Morton O. Energy alternatives: Electricity without carbon, *Nature*, **2008**, *454*, 816–823.
13. Tester J. W. *et al.* Sustainable Energy: Choosing among options, **2005** The MIT Press, ISBN 0-262-20153-4.
14. Kiehl J.T.; Trenberth K. E. Earth's annual global mean energy budget, *Bull. Amer. Meteor. Soc.*, **1997**, *78*,197-208.
15. Becquerel E. Observations of photovoltaic effects,*C. R. Acad. Sci.*, **1839**, *9*, 561–567.
16. Chapin D. M.; Fuller C. S.; Pearson G. L. A new silicon p-n junction photocell for converting solar radiation into electric power, *J. Appl. Phys.*, **1954**, *25*, 676–677.
17. Hegedus S. Thin film solar modules: The low cost, high throughput and versatile alternative to Si wafers, *Prog. Photovolt: Res. Appl.*, **2006**, *14*, 393–411.
18. Butler D. Thin films: ready for their close-up? *Nature*, **2008**, *454*, 558–559.
19. Slaoui A.; Collins R. T. Advanced Inorganic Materials for Photovoltaic, *MRS Bull.*, **2007**, *32*, 211–218.

20. Tang C. W. Two layer organic photovoltaic cell, *Appl. Phys. Lett.*, **1986**, *48*, 183–185.
21. Brabec C. J. Organic Photovoltaics: Technology and market, *Solar Energy Mater Solar Cells*, **2004**, *83*, 273–292.
22. Coakley K. M.; McGehee M. D. Conjugated polymer photovoltaic cells, *Chem. Mater*, **2004**, *16*, 4533–4542.
23. Mayer A. C.; Scully S. R.; Hardin B. E.; Rowell M. W.; McGhee M. D. Polymer-based solar cells, *Materials Today*, **2007**, *10*, 28–33.
24. Brabec C. J.; Sariciftci N. S.; Hummelen J. C. Plastic solar cells, *Adv. Funct. Mater*, **2001**, *11*, 15–26.
25. Prabhakaran K.; Sureshraju V.; Yamuna E.; Shueh L.Y.; Choongik K.; Ming C.C.; Fused-thiophene based materials for organic photovoltaic and dye-sensitized solar cells, *Polymers*, **2014**, *6*, 2645–2669.
26. Fonash S. J.; Solar cell device physics (book) 2nd edition, **2010.**
27. Günes S.; Neugebauer H.; Sariciftci N. S. Conjugated polymer-based organic solar cells, *Chem. Rev.*, **2007**, *107*, 1324–1338.
28. Thompson B. C.; Frechet J. M. J. Polymer-fullerene composite solar cells, *Angew. Chem. Int. Ed.*, **2008**, *47*, 58–77.

29. Saraciftci N. S.; Smilowitz L.; Heeger A. J.; Wudl F. Photoinduced electron transfer from a conducting polymer to buckminsterfullerene, *Science*, **1992**, *258*, 1474–1476.
30. Wang Y. Photoconductivity of fullerene-doped polymers, *Nature*, **1992**, *356*, 585–587.
31. Halls J. J. M.; Walsh C. A.; Greenham N. C.; Marseglia E. A.; Friend R. H.; Moratti S. C.; Holmes A. B. Efficient photodiodes from interpenetrating polymer networks, *Nature*, **1995**, *376*, 498–500.
32. Yu G.; Gao J.; Hummelen J. C.; Wudl F.; Heeger A. J. Polymer photovoltaic cells: Enhanced efficiencies *via* a network of internal donor-acceptor heterojunctions, *Science*, **1995**, *270*, 1789–1791.
33. Shaheen S. E.; Brabec C. J.; Sariciftci N. S.; Padinger F.; Fromherz T.; Hummelen J. C. 2.5% efficient organic plastic solar cells, *Appl. Phys. Lett*, **2001**, *78*, 841–843.
34. Brabec C. J.; Shaheen S. E.; Winder C.; Sariciftci N. S.; Denk P. Effect of LiF/metal electrodes on the performance of plastic solar cells, *Appl. Phys.Lett*, **2002**, *80*, 1288–1290.
35. Mihailetchi V. D. *et al*. Compositional dependence of the perormance of poly(*p*-phenylenevinylene):Methanofullerene bulk-heterojunction solar cells, *Adv. Funct. Mater.*, **2005**, *15*, 795–801.

36. Schilinsky P.; Waldauf C.; Brabec C. J. Recombination and loss analysis in polythiophene based bulk-heterojunction photodetectors, *Appl. Phys. Lett.*, **2002**, *81*, 3885–3887.
37. Padinger F.; Rittberger R. S.; Sariciftci N. S. Effects of postproduction treatment on plastic solar cells, *Adv. Funct. Mater*, **2003**, *13*, 85–88.
38. Li G.; Shrotriya V.; Huang J.; Yao Y.; Moriaty T.; Emery K.; Yang Y. High-efficiency solution processable polymer photovoltaic cells by self-organization of polymer blends, *Nat. Mater*, **2005**, *4*, 864–868.
39. Ma W.; Yang C.; Gong X.; Lee K.; Heeger A. J. Thermally stable, efficient polymer solar cells with nanoscale control of the interpenetrating network morphology, *Adv. Funct. Mater*, **2005**, *15*, 1617–1622.
40. Scharber M. C.; Muhlbacher D.; Koppe M.; Denk P.; Waldauf C.; Heeger A. J.; Brabec C. J. Design rules for donors in bulk-heterojunction solar cells towards 10% energy-conversion efficiency, *Adv. Mater*, **2006**, *18*, 789–794.
41. Cheng Y. J.; Yang S. H.; Hsu C. S. Synthesis of conjugated polymers for organic solar cell applications, *Chem. Rev.*, **2009**, *109*, 5868–5923.
42. Liang Y.; Yu L. A new class of semiconducting polymers for bulk heterojunction solar cells with exceptionally high performance, *Acc. Chem. Res.*, **2010**, *43*, 1227–1236.

43. Slooff L. H. *et al.* Determining the internal quantum efficiency of highly efficient polymer solar cells through optical modelling, *Appl. Phys. Lett*, **2007**, *90*, 1–3.
44. Peet J.; Kim J. Y.; Coates N. E.; Ma W. L.; Moses D.; Heeger A. J.; Bazan G. C. Efficiency enhancement in low-bandgap polymer solar cells by processing with alkanedithiols, *Nat. Mater*, **2007**, *6*, 497–500.
45. Moule A. J. *et al*. Two novel cyclopentadithiophene-based alternating copolymers as potential donor components for high-efficiency bulk-heterojunction-type solar cells, *Chem. Mater*, **2008**, *20*, 4045–4050.
46. Li. J.; Ong .K. H.; Lim. S.L.; Ng. G. M.; Tan. H. S.; Chen. Z. K. A random copolymer based on dithienothiophene and diketopyrrolopyrrole units for high performance organic solar cells, *Chem. Commun*, **2011**, *47*, 9480–9482.
47. Peng Q.; Huang Q.; Hou X.; Chang P.; Xu J.; Deng S. Enhanced solar cell performance by replacing benzodithiophene with naphthodithiophene in diketopyrrolopyrrole-based copolymers, *Chem. Commun.*, **2012**, *48*, 11452–11454.
48. Fei Z. *et al.* A low band gap co-polymer of dithienogermole and 2,1,3-benzothiadiazole by Suzuki polycondensation and its application in transistor and photovoltaic cells, *J. Mater. Chem.*, **2011**, *21*, 16257–16263.

49. Small C. E. *et al*. High-efficiency inverted dithienogermole–thienopyrrolodione-based polymer solar cells, *Nature Photonics*, **2012**, *6*, 115–120.
50. Brabec C. J.; Gowrisanker S.; Halls J. J. M.; Laird D.; Jia S.; Williams S. P. Polymer–fullerene bulk-heterojunction solar cells, *Adv. Mater*, **2010**, *22*, 3839–3856.
51. Helgesen M.; Sondergaard R.; Krebs F. C. Feature Article: Advanced materials and processes for polymer solar cell devices, *J. Mater. Chem.*, **2010**, *20*, 36–60.
52. Gendron D.; Leclerc M. Perspective: New conjugated polymers for plastic solar cells, *Energy Environ. Sci.*, **2011**, *4*, 1225–1237.
53. Son H. J.; He F.; Carsten B.; Yu L. Feature Article: Are we there yet? Design of better-conjugated polymers for polymer solar cells, *J. Mater. Chem.*, **2011**, *21*, 18934–18945.
54. Qu S.; Tian H. Feature Article: Diketopyrrolopyrrole-based materials for organic photovoltaics, *Chem. Commun*, **2012**, *48*, 3039–3051.
55. Sista S.; Hong Z.; Chenx L.M.; Yang Y. Tandem polymer photovoltaic cells current status, challenges and future outlook, *Energy Environ. Sci.*, **2011**, *4*, 1606.
56. Jen A.K.Y. Recent advances in solution-processed interfacial materials for efficient and stable polymer solar cells, *Energy Environ. Sci.*, **2012**, *5*, 5994–6011.

57. Li G.; Zhu R.; Yang Y. Polymer solar cells, *Nature Photonics*, **2012**, *6*, 153–161
58. Boudreault P. L. T.; Najari A.; Leclerc M. Processable low-bandgap polymers for photovoltaic applications, *Chem. Mater*, **2011**, *23*, 456–469.
59. Petritsch K.; Dittmer J. J.; Marseglia E. A.; Friend R. H.; Lux A.; Rozenberg G. G.; Moratti S. C.; Holmes A. B. Dye-based donor/acceptor solar cells, *Solar Energy Materials & Solar Cells*, **2000**, *61*, 63–72.
60. Schmidt-Mende L.; Fechtenkötter A.; Müllen K.; Moons E.; Friend R. H.; MacKenzie J. D. Self-organized discotic liquid crystals for high-efficiency organic photovoltaic, *Science*, **2001**, *293*, 1119–1122.
61. Roncali J.; Frére P.; Blanchard P.; Bettignies R.; Turbiez M.; Roquet S.; Leriche P.; Nicolas Y. Molecular and supramolecular engineering of π-conjugated systems for photovoltaic conversion, *Thin Solid Films*, **2006**, *511*, 567-575.
62. Lloyd M. T.; Mayer A. C.; Tayi A. S.; Bowen A. M.; Kasen T. G.; Herman D. J.; Mourey D. A.: Anthony J. E.; Malliaras G. G. Photovoltaic cells from a soluble pentacene derivative, *Organic Electronics*, **2006**, *7*, 243–248.
63. Sun X. *et al*. X-shaped oligothiophenes as a new class of electron donors for bulk-heterojunction solar cells, *J. Phys. Chem. B*, **2006**, *110*, 7702–7707.

64. Roquet S.; Cravino A.; Leriche P.; Alévéque O.; Frére P.; Roncali J. Triphenylamine-Thienylenevinylene hybrid systems with internal charge transfer as donor materials for heterojunction solar cells, *J. Am. Chem. Soc.*, **2006**, *128*, 3459–3466.
65. Kronenberg N. M.; Deppisch M.; Würthner F.; Lademann H. W. A.; Deing K.; Meerholz K. Bulk heterojunction organic solar cells based on merocyanine colorants, *Chem. Commun.*, **2008**, 6489–6491.
66. Tamayo A. B.; Dang X.D.; Walker B.; Seo J.; Kent T.; Nguyen T.Q. A low band gap, solution processable oligothiophene with a dialkylated diketopyrrolopyrrole chromophore for use in bulk heterojunction solar cells, *Applied Physics Letters*, **2009**, *94*, 103301–3.
67. Walker B. *et al.* Nanoscale phase separation and high photovoltaic efficiency in solution-processed, small-molecule bulk heterojunction solar cells, *Adv. Funct. Mater.*, **2009**, *19*, 3063–3069.
68. Ko H. M.; Choi H.; Paek S.; Kim K.; Song K.; Lee J. K.; Ko J. Molecular engineering of push-pull chromophore for efficient bulk-heterojunction morphology in solution processed small molecule organic photovoltaics, *J. Mater. Chem.*, **2011**, *21*, 7248–7253.
69. Kim J.; Ko H. M.; Cho N.; Paek S.; Lee J. K.; Ko J. Efficient small molecule organic semiconductor containing

bisdimethylfluorenyl amino benzo[b]thiophene for high open circuit voltage in high efficiency solution processed organic solar cell, *RSC Adv.*, **2012**, *2*, 2692–2695.

70. Li Z. *et al*. Design and synthesis of solution processable small molecules towards high photovoltaic performance, *J. Mater. Chem.*, **2011**, *21*, 2159–2168.
71. Shi Q.; Cheng P.; Li Y.; Zhan X. A solution processable D-A-D molecule based on Thiazolothiazole for high performance organic solar cells, *Adv. Energy Mater.*, **2012**, *2*, 63–67.
72. Liu Y.; Wan X.; Wang F.; Zhou J.; Long G.; Tian J.; You J.; Yang Y.; Chen Y. Spin-coated small molecules for high performance solar cells, *Adv. Energy Mater.*, **2011**, *1*, 771–775.
73. Li Z.; He G.; Wan X.; Liu Y.; Zhou J.; Long G.; Zuo Y.; Zhang M.; Chen Y. Solution processable rhodanine-based small molecule organic photovoltaic cells with a power conversion efficiency of 6.1%, *Adv. Energy Mater.*, **2012**, *2*, 74–77.
74. Welch G. C. *et al*. A modular molecular framework for utility in small-molecule solution-processed organic photovoltaic devices, *J. Mater. Chem.*, **2011**, *21*, 12700–12709.

75. Sun Y.; Welch G. C.; Leong W. L.; Takacs C. J.; Bazan G. C.; Heeger A. J. Solution-processed small-molecule solar cells with 6.7% efficiency, *Nat. Mater.*, **2012**, *11*, 44–48.
76. Van der Poll S. T.; Love J. A.; Nguyen T. –Q.; Bazan G. C. Non-basic high-performance molecules for solution-processed organic solar cells, *Adv. Mater.*, **2012**, *24*, 3646–3649.
77. Zhou J. *et al*. Small molecules based on Benzo[1,2-b:4,5-b′]dithiophene unit for high-performance solution-processed organic solar cells, *J. Am. Chem. Soc.*, **2012**, *134*, 16345−16351.
78. Fan, Q.; Cui, J.; Liu, Y.; Su, W.; Wang, Y.; Tan, H.; Yu, D.; Gao, H.; Deng, X.; Zhu, W. Synthesis and photovoltaic properties of two star-shaped molecules involving phenylquinoxaline as core and triphenylamine and thiophene units as arms. *Syn. Met.*, **2015**, *204*, 25–31.
79. Vybornyi O.; Jiang Y.; Baert F.; Demeter D.; Roncali J.; Blanchard P.; Cabanetos C. Solution-processable thienoisoindigo-based molecular donors for organic solar cells with high open-circuit voltage. *Dyes and Pigments*, **2014**, *114*, 17–22.
80. Meng W.; Hailu L.; Bin Z.; Jian Z.; Juan Z.; Yong P.; Huajie C.; and Songting T.Novel solution-processible small molecules based on benzo [1,2-*b*: 3,4-*b*′: 5,6-*b*′′]

trithiophene for effective organic photovoltaics with high open-circuit voltage. *RSC Adv.*, **2015**, *5*, 14540–14546.

81. Bernd E.; Nor P.; Vincent R.; Graeme C.; Ifor S.; Solution-processed boron subphthalocyanine derivatives as acceptors for organic bulk-heterojunction solar cells. *Journal of Material Chemistry,* **2015**, *3*, 7345–7352.
82. Youdi Z.; Yi X.; Yuanpeng X.; Linlin Z.; Dequan S.; Chaunhui C. Fluorene-centered perylene monoimides as potential non-fullerene acceptor in organic solar cells. *Journal of Organic Electronics*, **2015**, *21*,184–191.
83. James R.; & Yutaka M**.** Increased Efficiency in Small Molecule Organic Solar Cells through the Use of a 56-π Electron Acceptor–Methano Indene Fullerene, *Sci. Rep.*, **2015**, *5*, article number: 8319 doi:10.1038/srep08319.
85. Walker B.; Kim C.; Nguyen T. Small molecule solution-processed bulk heterojunction solar cells, *Chem. Mater.* **2011**, *23*, 470–482.
86. Mishra A.; Bäuerle P. Small molecule organic semiconductors on the move: Promises for future solar energy technology, *Angew. Chem. Int. Ed.*, **2012**, *51*, 2020–2067.
87. Zhang J. *et al*. Solution-processable star-shaped molecules with Triphenylamine core and Dicyanovinyl end groups for organic solar cells, *Chem. Mater.*, **2011**, *23*, 817–822.

88. Blouin N.; Michaud A.; Leclerc M. A low band-gap poly (2,7-carbazole) derivative for use in high-performance solar cells, *Adv. Mater.*, **2007**, *19*, 2295–2300.
89. Zhang Z. G.; Min J.; Zhang S.; Zhang J.; Zhang M.; Li Y. Alkyl chain engineering on a dithieno[3,2-b:20,30-d]silole-altdithienylthiazolo[5,4-d]thiazole copolymer toward high performance bulk heterojunction solar cells, *Chem. Comun.*, **2011**, *47*,9474–9476.
90. Zhou J.; Wan X.; Liu Y.; Long G.; Wang F.; Li Z.; Zuo Y.; Li C.; Chen Y. A planar small molecule with dithienosilole core for high efficiency solution-processed organic photovoltaic cells, *Chem. Mater.*, **2011**, *23*, 4666–4668.
91. Dutta P. *et al*. Development of naphtha [1,2-b: 5,6-b0] dithiophene based novel small molecules for efficient bulk-heterojunction organic solar cells, *Chem. Commun.*, **2012**, *48*, 573–575.
92. Dutta P. *et al*. Naphtho [1,2-b: 5, 6-b0] dithiophene-based conjugated polymer as a new electron donor for bulk heterojunction organic solar cells, *Polym. Chem.*, **2012**, *3*, 601–604.
93. Katz H.E.; Lovinger A.J.; Kloc C.; Siegrist T.; Li W.; Lin Y.Y.; A. Dodabalapur A. A soluble and air-stable organic semiconductor with high electron mobility. *Nature*, **2000**, *404*, 478–481.

94. Bhosale S. V.; Jani C.H.; and Langford S.J. Chemistry of naphthalene diimides, *Chem. Soc. Rev*., **2008**, *37(2)*, 331–42.
95. Würthner F.; Ahmed S.; Thalacker C.; Debaerdemaeker T. Core substitute naphthalene bisimides: new fluorophers with tuneable emission wavelength of for FRET studies, *Chem. Eur. J.*, **2002**, *8*, 4742–4750.
96. Bhosale S. V.; Jani C.; Lalander C. H.; Langford S. J. Solvophobic control of core- substituted naphthalene diimide nanostructures, *Chem. Commun*., **2010**, *46*, 973–975.
97. Bhosale, S.; Sisson, A. L.; Talukdar, P.; Fürstenberg, A.; Banerji, N.; Vauthey, E.; Bollot, G.; Mareda, J.; Röger, C.; Würthner, F.; Sakai, N.; Matile, S. Photoproduction of Proton Gradients with π-Stacked Fluorophore Scaffolds in Lipid Bilayers, *Science*, **2006,** *313*, 84–86.
98. Lin, Y.; Li, Y.; Zhan, X. Small molecule semiconductors for high-efficiency organic photovoltaics, *Chem. Soc. Rev*., **2012**, *41*, 4245–4272.

Chapter 2

A non-fullerene electron acceptor based on fluorine and diketopyrrolopyrrole building blocks for solution-processable organic solar cells with an impressive open-circuit voltage

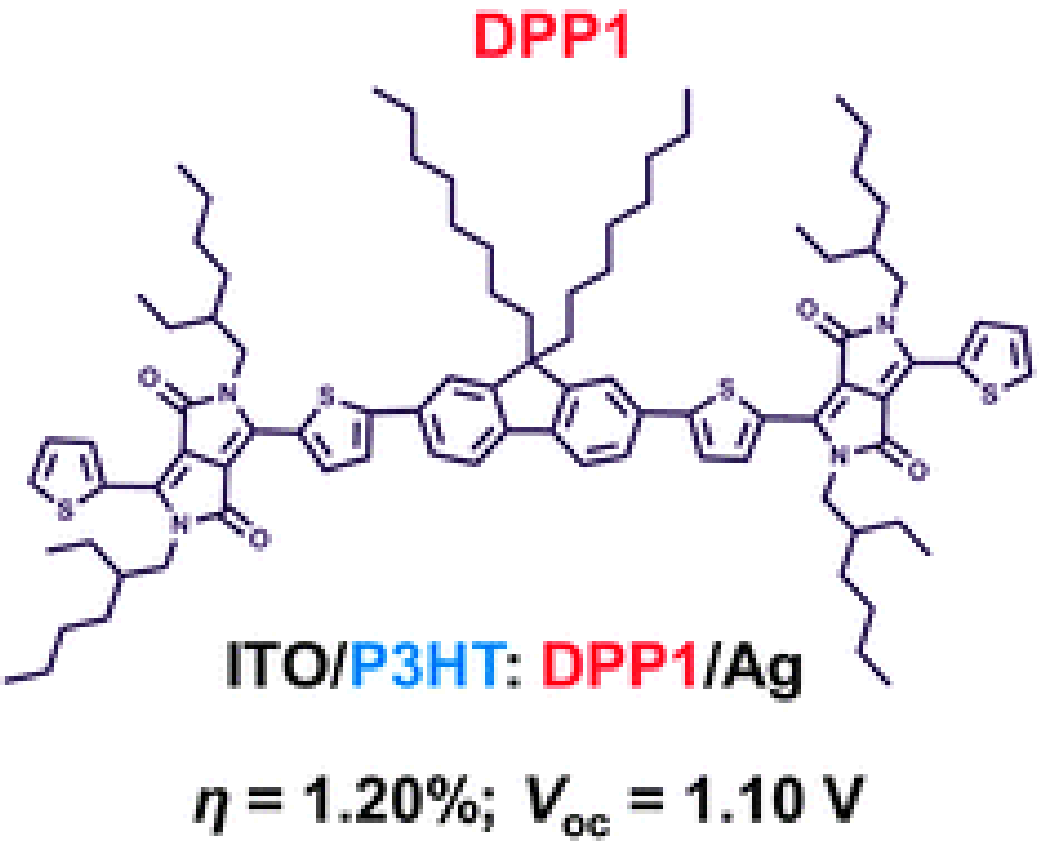

Journal article published in *Physical Chemistry Chemical Physics* presented as **Chapter 2**.

PCCP

PAPER

View Article Online
View Journal | View Issue

Cite this: *Phys. Chem. Chem. Phys.*, 2014, **16**, 23837

A non-fullerene electron acceptor based on fluorene and diketopyrrolopyrrole building blocks for solution-processable organic solar cells with an impressive open-circuit voltage†

Hemlata Patil,[a] Wang Xi Zu,[b] Akhil Gupta,*[ac] Vijila Chellappan,[b] Ante Bilic,[d] Prashant Sonar,‡*[b] Anushri Rananaware,[a] Sidhanath V. Bhosale[e] and Sheshanath V. Bhosale*[a]

Received 20th August 2014,
Accepted 25th September 2014

DOI: 10.1039/c4cp03727h

www.rsc.org/pccp

A novel solution-processable non-fullerene electron acceptor 6,6′-(5,5′-(9,9-dioctyl-9*H*-fluorene-2,7-diyl)bis(thiophene-5,2-diyl))bis(2,5-bis(2-ethylhexyl)-3-(thiophen-2-yl)pyrrolo[3,4-c]pyrrole-1,4(2*H*,5*H*)-dione) (DPP1) based on fluorene and diketopyrrolopyrrole conjugated moieties was designed, synthesized and fully characterized. DPP1 exhibited excellent solubility and high thermal stability which are essential for easy processing. Upon using DPP1 as an acceptor with the classical electron donor poly(3-hexylthiophene), solution processable bulk-heterojunction solar cells afforded a power conversion efficiency of 1.2% with a high open-circuit voltage (1.1 V). As per our knowledge, this value of open circuit voltage is one of the highest values reported so far for a bulk-heterojunction device using DPP1 as a non-fullerene acceptor.

In academic and industry sectors, organic bulk-heterojunction (BHJ) solar cell research has gained momentum in view of their potential for the fabrication of low-cost, light weight and flexible photovoltaic devices.[1] Power conversion efficiencies (PCEs) over 9% for polymer- and small molecule-based BHJ devices have been achieved.[2] Donor functionalities such as conventional semiconducting polymers [poly(3-hexylthiophene) (P3HT)] and other donor–acceptor semiconducting polymers and small organic molecules have been examined in conjunction with soluble fullerene derivatives such as [6,6]-phenyl-C_{61}-butyric acid methyl ester ($PC_{61}BM$) as an electron acceptor material for achieving higher performance.[3] Much attention has been given to the design and development of donor materials whereas there is not much work that has been done so far on the electron accepting materials.[4] With regard to electron acceptor materials, fullerenes and their derivatives, such as $PC_{61}BM$ and $PC_{71}BM$, are the most common acceptors of choice mainly due to their superior electron affinity and good electron mobility.[5] However, fullerenes suffer from a number of disadvantages, such as high cost, weak absorption in the visible spectrum, restricted electronic tuning *via* synthesis and cumbersome purification. Also, a large electron affinity of fullerene derivatives can yield a low open-circuit voltage (V_{oc}) of the photovoltaic devices.[6] The above addressed issues with fullerenes provide a strong incentive to explore novel, easily processable and cheap non-fullerene electron acceptors. In order to design the new acceptor structures, we have to take into account some of the important features such as strong and broad absorption, adequate solubility, high charge carrier mobility and appropriate energy levels.

Recently, non-fullerene electron acceptors have been developed[7] and PCEs exceeding 2% and 4% have been achieved using archetypal P3HT and non-P3HT donors, respectively.[8] Even though this progress is encouraging, considerable scope still exists to develop new non-fullerene acceptors which possess strong optical absorption and good photochemical stability. Recently, fluorene (FL) has been used as one of the promising building blocks for synthesizing potential electron-deficient non-fullerene electron acceptors.[8c] Amongst various electron deficient building blocks, a fused aromatic electron withdrawing diketopyrrolopyrrole (DPP) functionality has been proved to be

[a] *School of Applied Sciences, RMIT University, GPO Box 2476V, Melbourne Victoria 3001, Australia. E-mail: sheshanath.bhosale@rmit.edu.au; Tel: +61 3 99252680*
[b] *Institute of Materials Research and Engineering (IMRE), 3, Research Link, Singapore 117602*
[c] *Medicinal Chemistry, Monash Institute of Pharmaceutical Sciences, Monash University, Parkville Victoria 3052, Australia. E-mail: akhil.gupta@monash.edu; Tel: +61 3 99039599*
[d] *CSIRO Computational Informatics, Private Bag 33, Clayton South Victoria 3169, Australia*
[e] *Polymers and Functional Material Division, CSIR-Indian Institute of Chemical Technology, Hyderabad 50060, AP, India*

† Electronic supplementary information (ESI) available: Synthetic details, experimental procedures, DFT calculations, PESA diagram, TGA and DSC curves. See DOI: 10.1039/c4cp03727h

‡ Current address: School of Chemistry, Physics and Mechanical Engineering, Queensland University of Technology (QUT), GPO Box 2434, Brisbane, QLD 4001, Australia. E-mail: sonar.prashant@qut.edu.au.

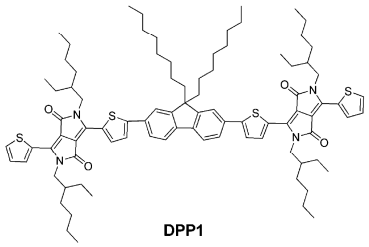

Fig. 1 Molecular structure of the investigated non-fullerene electron acceptor chromophore **DPP1**.

one of the most promising moiety for synthesizing donor–acceptor based small molecular electron acceptors for BHJ devices.[7] It was envisaged that the combination of FL as a donor and the DPP unit as an acceptor could provide highly conjugated donor–acceptor chromophores with good planarity, high thermal stability, better electron affinity and enhanced solubility *via* attachment of preferred alkyl substituents. Our group has already developed promising p-type photoactive materials for solution-processable organic photovoltaic devices.[9]

Herein, we report the synthesis of a novel non-fullerene electron acceptor 6,6′-(5,5′-(9,9-dioctyl-9*H*-fluorene-2,7-diyl)bis(thiophene-5,2-diyl))bis(2,5-bis(2-ethylhexyl)-3-(thiophen-2-yl)pyrrolo[3,4-*c*]pyrrole-1,4(2*H*,5*H*)-dione) based on FL as a central core with DPP substituents (**DPP1**; as shown in Fig. 1) end capped at both the ends.

DPP1 has been used as an electron acceptor along with a classical electron donor P3HT for solution-processable BHJ devices. Compound **DPP1** was synthesized in a straightforward manner with high yield *via* a Suzuki coupling reaction between commercially available (9,9-dioctyl-9*H*-fluorene-2,7-diyl)diboronic acid (**1**) and 3-(5-bromothiophen-2-yl)-2,5-bis(2-ethylhexyl)-6-(thiophen-2-yl)pyrrolo[3,4-*c*]pyrrole-1,4(2*H*,5*H*)-dione (**2**). The reaction was conducted in a dioxane:2 M potassium carbonate (K_2CO_3) solvent mixture at 90 °C for 48 hours using tetrakis(triphenylphosphine)-palladium(0) [$Pd(PPh_3)_4$] as a catalyst (Scheme 1). **DPP1** was worked up using a conventional method and purified by simple column chromatography. The purity of the compound was confirmed by mass spectrometry (MS), ^{1}H and ^{13}C NMR spectroscopy techniques (for synthetic details, see ESI†). **DPP1** was found to be highly soluble in a variety of organic solvents such as chloroform, dichlorobenzene and toluene (for instance, 30 mg mL^{-1} in *o*-dichlorobenzene). High solubility is absolutely required for the fabrication of solution-processable roll to roll BHJ devices and **DPP1** fulfils this criterion.

The normalized optical absorption spectra of **DPP1** in chloroform solution (8.7×10^{-7} M) and as a thin solid film are shown in Fig. 2.

In solution, **DPP1** exhibits strong absorption with a maximum extinction coefficient of 13.4×10^4 M^{-1} cm^{-1} at 599 nm. As a thin film, **DPP1** shows a broad absorption peak throughout the visible region (400–700 nm) which is red-shifted by around 20 nm compared to its solution spectrum. Such a red shift is attributed with the solid state ordering of the molecule.

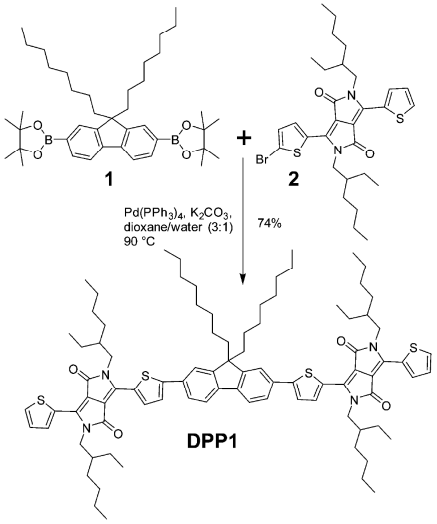

Scheme 1 Reaction strategy for the synthesis of **DPP1**.

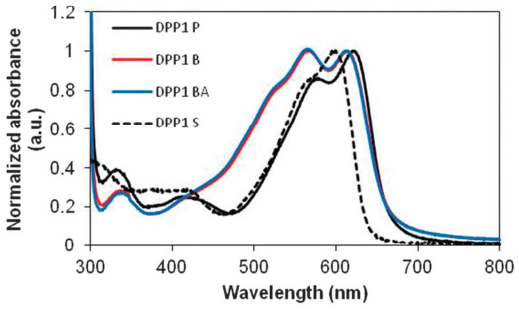

Fig. 2 UV-vis absorption spectra of a pristine film (**DPP1 P**; solid black curve), in chloroform solution (**DPP1 S**; dotted black curve), a 1 : 1 P3HT : **DPP1** blend film (**DPP1 B**; red curve) and a post-annealed (150 °C for 5 min) blend film (**DPP1 BA**; blue curve).

The optical band gap was calculated from the tangent of the edge of longest wavelength (absorption cut-off) in thin solid films. This value was found to be 1.80 eV. We also measured the optical data for the P3HT : **DPP1** blend (in a ratio of 1 : 1 w/w and spin coated on a glass) as a thin film at room temperature and post-annealed at 150 °C (see Fig. 2). Thin films of blends of P3HT and **DPP1** show quenching of the photoluminescence (see Fig. S1 in ESI†).

Theoretical density functional theory (DFT) calculations using the Gaussian 09 suite of programs[10] and the B3LYP/6-311+G(d,p)//B3LYP/6-31G(d) level of theory indicated that orbital densities are evenly distributed over the whole molecular backbone of **DPP1** (see Fig. S2 in ESI†). This finding is consistent with the earlier reported best performing non-fullerene acceptor where the FL moiety was also used as one of the building blocks.[8c]

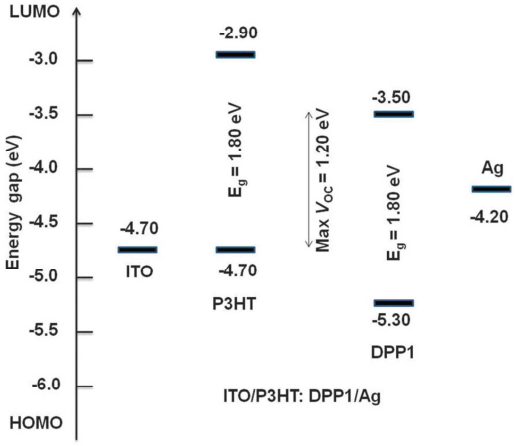

Fig. 3 Energy level diagram showing alignments of different components of BHJ device architecture.

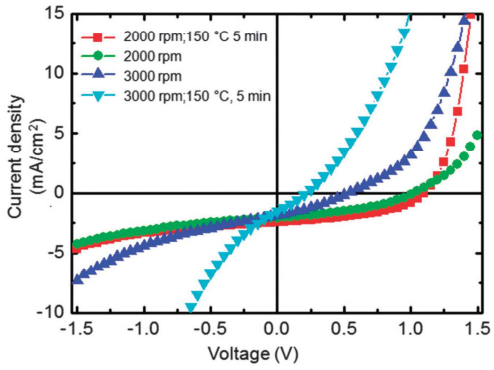

Fig. 4 Current–voltage (*J–V*) curves for devices based on **DPP1** in blends with P3HT (1 : 1 wt) under simulated sunlight (AM 1.5, 1000 W m^{-2}). Device structure is: ITO/PEDOT:PSS (35 nm)/active layer/Ca (15 nm)/Ag (100 nm).

Table 1 Photovoltaic properties of small area single cell modules based on blend layers of P3HT:**DPP1** with different processing conditions

Sample (spin rate)	PCE (%)	V_{oc} (V)	J_{sc} (mA cm^{-2})	FF (%)
3000 rpm	0.32	0.53	1.85	32
3000 rpm 150 °C 5 min[a]	0.09	0.22	1.52	28
2000 rpm	0.81	1.03	2.04	39
2000 rpm 150 °C 5 min[a]	1.20	1.10	2.42	45

[a] Active layer annealing before depositing the cathode.

The highest occupied molecular orbital (HOMO) energy of **DPP1** was measured using the photo electron spectroscopy in air (PESA) technique using the spin coated thin film of **DPP1** (Fig. S3 in ESI†). The lowest unoccupied molecular orbital (LUMO) energy was calculated by taking the difference between optical bandgap and the HOMO value. The measured HOMO and LUMO energies were found to be −5.30 eV and −3.50 eV respectively. The difference between the LUMO of **DPP1** (−3.50 eV) and the HOMO of P3HT (−4.70 eV from PESA) is as large as 1.20 eV (theoretical open circuit voltage V_{oc}), which is promising for achieving a high V_{oc} in solar cells (see Fig. 3 for the energy level diagram).

It was further realized that despite the presence of interesting and lucrative optoelectronic properties, organic semiconducting materials must possess thermal stability so that they can endure rigid device fabricating conditions, such as device annealing at a higher temperature. In-line with this requirement, we conducted thermogravimetric analysis (TGA). TGA analysis established that **DPP1** exhibits excellent thermal stability and is stable up to 350 °C (Fig. S4 in ESI†), a finding that supports high temperature annealing of P3HT:**DPP1** devices. In addition to TGA, we also conducted differential scanning calorimetry (DSC) analysis of **DPP1** to examine thermal transitions. The DSC thermogram of **DPP1** indicates melting transition at around 259 °C (Fig. S5 in ESI†). Initially, the newly synthesized **DPP1** was used as a non-fullerene acceptor (n-type) with classical donor polymer P3HT (p-type) for solution-processed BHJ OPV devices to test its performance. BHJ architectures typically deliver higher power conversion efficiencies (PCEs) by maximising the surface area of the interface between the p- and n-type materials in the active layer. The BHJ device structure used in this study was ITO/PEDOT:PSS (35 nm)/active layer/Ca (15 nm)/Ag (100 nm) where the active layer was a solution-processed blend of P3HT and **DPP1**. An initial screen of the efficacy of the target compound, **DPP1**, as a non-fullerene acceptor exhibits promising performance.

The *J–V* characteristics are shown in Fig. 4 and the device performance is summarized in Table 1. Table 1 summarizes the photovoltaic cell parameters [short circuit voltage (V_{oc}), current density (J_{sc}), fill factor (FF), and PCE] for P3HT:**DPP1** blends.

Thermal annealing of devices at 150 °C showed an improvement in PCEs of about 50% when compared with as-casted devices. Overall, BHJ devices show significantly improved performance; V_{oc}, J_{sc}, FF and PCE reached 1.10 V, 2.42 mA cm^{-2}, 0.45 and 1.20%, respectively, when annealed at 150 °C for 2000 rpm spin coated blend film. These BHJ devices yielded very high V_{oc} as we expected, and it is notable that the V_{oc} of 1.1 V is among the highest values reported so far for a single BHJ device,[8,11] and can be attributed to a very large energy-gap (1.20 eV) between the LUMO of **DPP1** and the HOMO of P3HT. The thickness of active layer affects the J_{sc}, FF and V_{oc}. The FF and V_{oc} decrease rapidly when we increased the thickness of the active layer by increasing the concentration of the donor–acceptor blend and decreasing the spin speed. This is due to the deposition of a very thick layer that can hamper the charge carrier mobility and the charge collection at the respective electrodes can slow down. In addition, the film morphology and uniformity of the film was not good enough to fabricate OPV devices using lower spin speed. Lower spin speeds can generate thicker films and such kind of morphology is not favourable for higher performance. After optimizing device fabrication at 2000 rpm, 3000 rpm and 4000 rpm spin speeds, we got the best devices for blend films spun at 2000 rpm and 3000 rpm.

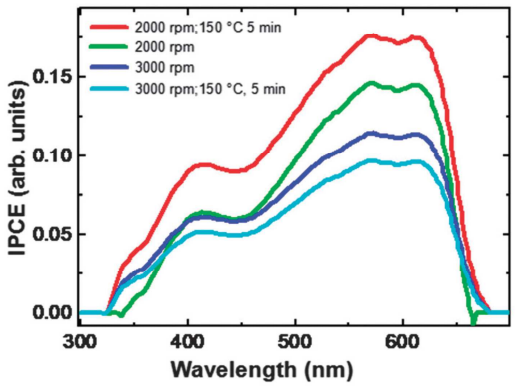

Fig. 5 IPCE spectra measured for P3HT:**DPP1** based OPV devices under various processing conditions.

Incident photon-to-current-conversion efficiency (IPCE) spectra of the devices (see Fig. 5) are consistent with the P3HT:**DPP1** blend film absorption and show broad IPCE from 300 to 700 nm with an IPCE maximum of ~17% at 580 and 620 nm. The lower J_{sc} of the P3HT:**DPP1** blend system is also attributed with an overlay of **DPP1** and P3HT spectra. Higher J_{sc} is desirable if there is offset in absorption for p- and n-type materials. We believe that with other low band gap conjugated donor materials over a broad range of wavelengths, higher PCE can be achieved.

We also investigated the surface microstructure of the P3HT:**DPP1** blend thin film using atomic force microscopy (AFM) in its tapping mode (see Fig. 6).This study indicated the presence of microcrystalline domains in the blend after annealing at 150 °C for 5 min. The crystalline grains grew larger at 150 °C and appeared clearly in the AFM image. This ordering is affiliated with the self-organization of P3HT polymeric chains which is beneficial for effective charge transport. The root mean square (RMS) roughness values were measured and were found to be 8.2 nm and 2.1 nm, respectively, before and after annealing the blend film.

For the annealed film, the active layer becomes smoother which is primarily due to the removal of solvent and rearrangement of the film during the annealing process. These changes in morphology due to annealing of the blend film reflect the improved device performance. Additionally, the tuning of the morphological pattern at 150 °C is also consistent with the glass transition temperature of P3HT which is around 140 °C.[12] In an attempt to measure the charge carrier mobility of **DPP1**, a thin film of pristine **DPP1** was spin coated on self-assembled monolayer (SAM) treated Si/SiO_2 substrates and the mobility was measured using top contact bottom gate transistor geometry (see experimental for details in the ESI†). No electron mobility was observed for the pristine **DPP1**, however, the hole mobility was measured to be 10^{-4} cm^2 V^{-1} s^{-1} (see the transfer and output characteristics of OFETs in Fig. S6 in the ESI†). The lack of electron mobility in the pristine film might be related to the higher LUMO value of **DPP1** with respect to vacuum, electron traps at the dielectric-**DPP1** interface and lower electron affinity. We also probed the electron mobility of **DPP1** by the time of flight photoconductivity (TOF-PC) method. The electron mobility was directly obtained from the integrated measurement on a simple diode structure of ITO/**DPP1** (400 nm)/Al. The film was excited using a pulsed laser of wavelength 620 nm (pulse width <5 ns, 1Hz repetition rate). A negative voltage bias was applied across the device in order to measure the electron mobility. The TOF transients due to electrons are measured using an oscilloscope by varying the bias voltage. The details of the TOF experimental set-up are elaborated elsewhere.[13,14] The TOF measurements were carried out using integrated mode as the film thickness used in this measurement was 400 nm. The variation of total charge accumulated at the collecting electrode with respect to time is measured in the integrated TOF-PC method. The time taken to collect the maximum charge (t_m) is estimated from the transient and the charge mobility (μ) was measured using the relation $\mu = d^2/t_m V$, where d is the film thickness and V is the applied voltage. The advantage of the TOF-PC method is that the charge mobility is independent of contacts and it allows the measurement of charge mobility in dispersive samples as well as in thin film samples. The details of the integrated TOF-PC technique is elaborated in literature.[15] The TOF-PC transients measured are shown in the inset of Fig. 7. The t_m was obtained from the transients and the calculated

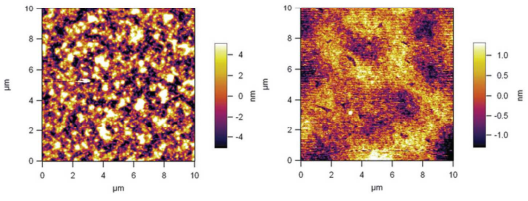

Fig. 6 AFM images for a thin film of P3HT:**DPP1** blend (left) and as-casted **DPP1** (right) annealed at 150 °C for 5 min (1:1 blend in 1 mL *o*-DCB, 2000 rpm s^{-1} for 1 min).

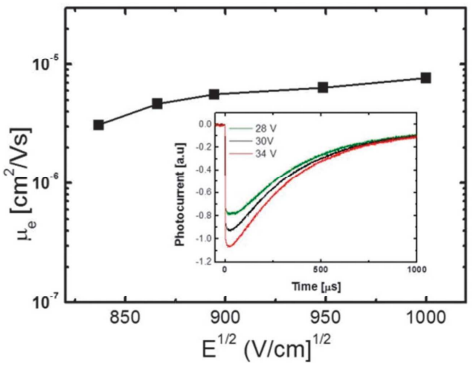

Fig. 7 Variation of electron mobility with applied electric field. Inset: current integrated TOF-PC transients for electrons measured for different applied voltages.

electron mobility for different electric fields is shown in Fig. 7. The obtained electron mobility is in the range of 8×10^{-6} cm^2 V^{-1} s^{-1} at an applied electric field of 1 MV cm^{-1}.

Although the material reported in this study achieved very high V_{oc} with promising power conversion efficiency in OPV devices, the discovery of such materials exhibiting promising optoelectronic properties opens up the way to develop such motifs (based on the central FL functionality) and paves the way for such materials to be used for other organic electronic applications such as organic light-emitting diodes and organic field-effective transistors.

Conclusions

In summary, we have designed, synthesized and successfully developed a novel non-fullerene electron acceptor 6,6′-(5,5′-(9,9-dioctyl-9*H*-fluorene-2,7-diyl)bis(thiophene-5,2-diyl))-bis(2,5-bis(2-ethylhexyl)-3-(thiophen-2-yl)pyrrolo[3,4-*c*]pyrrole 1,4(2*H*,5*H*)-dione) (**DPP1**) with fluorene (FL) as a central core and diketopyrrolopyrrole (DPP) units as the terminal substituents. **DPP1** was synthesized in one-pot *via* Suzuki coupling; it has excellent solubility and thermal stability, strong and broad absorption and matching energy levels with P3HT. The BHJ devices based on a P3HT : **DPP1** blend (1 : 1) after annealing at 150 °C for 5 min yielded a notable PCE of 1.20% and a very high V_{oc} of 1.10 V. The electron mobility of DPP1 was also measured 8×10^{-6} cm^2 V^{-1} s^{-1} using the time of flight photoconductivity (TOF-PC) method. Our results strongly support the excellent prospects of simple non-fullerene electron acceptors such as **DPP1**, and their future derived analogues, for applications in solution-processable OPV devices.

Acknowledgements

Sh. V. B. acknowledges financial support from the Australian Research Council under a Future Fellowship Scheme (FT110100152) and the School of Applied Sciences (RMIT University) for the facilities. The CSIRO Material Science and Engineering (CMSE) is acknowledged for providing support through a visiting fellow position (A. G.). A. B. thanks CSIRO for support through the Julius Career Award. The use of the NCI National Facility supercomputers at the ANU is gratefully acknowledged. W. X and P. S. thank the Institute of Materials Research and Engineering (IMRE), the Agency for Science, Technology and Research (A*STAR), and the "Printable high performance semiconducting materials for OPVs and OTFTs" for financial support.

Notes and references

1 (*a*) S. Günes, H. Neugebauer and N. S. Sariciftci, *Chem. Rev.*, 2007, **107**, 1324; (*b*) B. C. Thompson and J. M. J. Frechet, *Angew. Chem., Int. Ed.*, 2008, **47**, 58.

2 (*a*) Z. He, C. Zhong, S. Su, M. Xu, H. Wu and Y. Cao, *Nat. Photonics*, 2012, **6**, 593; (*b*) J. Zhou, Y. Zuo, X. Wan, G. Long, Q. Zhang, W. Ni, Y. Liu, Z. Li, G. He, C. Li, B. Kan, M. Li and Y. Chen, *J. Am. Chem. Soc.*, 2013, **135**, 8484; (*c*) V. Gupta, A. K. K. Kyaw, D. H. Wang, S. Chand, G. C. Bazan and A. J. Heeger, *Sci. Rep.*, 2013, **3**, 1965.

3 (*a*) Y. Lin, Y. Li and X. Zhan, *Chem. Soc. Rev.*, 2012, **41**, 4245; (*b*) Y. Li, *Acc. Chem. Res.*, 2012, **45**, 723; (*c*) J. Roncali, *Acc. Chem. Res.*, 2009, **42**, 1719.

4 (*a*) P.-L. T. Boudreault, A. Najari and M. Leclerc, *Chem. Mater.*, 2011, **23**, 456; (*b*) A. Gupta, S. E. Watkins, A. D. Scully, Th. B. Singh, G. J. Wilson, L. J. Rozanski and R. A. Evans, *Synth. Met.*, 2011, **161**, 856; (*c*) C. J. Brabec, S. Gowrisanker, J. J. M. Halls, D. Laird, S. Jia and S. P. Williams, *Adv. Mater.*, 2010, **22**, 3839; (*d*) B. Walker, C. Kim and T.-Q. Nguyen, *Chem. Mater.*, 2011, **23**, 470; (*e*) Y. Li, Q. Guo, Z. Li, J. Pei and W. Tian, *Energy Environ. Sci.*, 2010, **3**, 1427; (*f*) A. Mishra and P. Bäuerle, *Angew. Chem., Int. Ed.*, 2012, **51**, 2020.

5 (*a*) F. G. Brunetti, X. Gong, M. Tong, A. J. Heeger and F. Wudl, *Angew. Chem., Int. Ed.*, 2010, **49**, 532; (*b*) F. G. Brunetti, R. Kumar and F. Wudl, *J. Mater. Chem.*, 2010, **20**, 2934.

6 R. Y. C. Shin, P. Sonar, P. S. Siew, Z. K. Chen and A. Sellinger, *J. Org. Chem.*, 2009, **74**, 3293.

7 (*a*) J. E. Anthony, *Chem. Mater.*, 2011, **23**, 583; (*b*) P. Sonar, J. P. Fong Lim and K. L. Chan, *Energy Environ. Sci.*, 2011, **4**, 1558; (*c*) P. Sonar, G. M. Ng, T. T. Lin, A. Dodabalapur and Z. K. Chen, *J. Mater. Chem.*, 2010, **20**, 3626; (*d*) Y. Li, P. Sonar, L. Murphy and W. Hong, *Energy Environ. Sci.*, 2013, **6**, 1684; (*e*) C. B. Nielsen, M. Turbiez and I. McCulloch, *Adv. Mater.*, 2013, **25**, 1859; (*f*) J. D. Yuen and F. Wudl, *Energy Environ. Sci.*, 2013, **6**, 392; (*g*) B. P. Karsten, J. C. Bijleveld and R. A. J. Janssen, *Macromol. Rapid Commun.*, 2010, **31**, 1554; (*h*) Y. Lin and X. Zhan, *Mater. Horiz.*, 2014, **1**, 470–488; (*i*) Y. Lin, Y. Li and X. Zhan, *Adv. Energy Mater.*, 2013, **3**, 724; (*j*) Y. Lin, P. Cheng, Y. Li and X. Zhan, *Chem. Commun.*, 2012, **48**, 4773; (*k*) A. F. Eftaiha, J. P. Sun, I. G. Hill and G. C. Welch, *J. Mater. Chem. A*, 2014, **2**, 1201; (*l*) Y. Lin, Y. Wang, J. Wang, J. Hou, Y. Li, D. Zhu and X. Zhan, *Adv. Mater.*, 2014, **26**, 5137–5142; (*m*) Y. Lin, J. Wang, S. Dai, Y. Li, D. Zhu and X. Zhan, *Adv. Energy Mater.*, 2014, DOI: 10.1002/aenm.201400420.

8 (*a*) J. T. Bloking, X. Han, A. T. Higgs, J. P. Kastrop, L. Pandey, J. E. Norton, C. Risko, C. E. Chen, J.-L. Brédas, M. D. McGehee and A. Sellinger, *Chem. Mater.*, 2011, **23**, 5484; (*b*) Y. Lin, Y. Li and X. Zhan, *Adv. Energy Mater.*, 2013, **3**, 724; (*c*) K. N. Winzenberg, P. Kemppinen, F. H. Scholes, G. E. Collis, Y. Shu, T. B. Singh, A. Bilic, C. M. Forsyth and S. E. Watkins, *Chem. Commun.*, 2013, **49**, 6307; (*d*) C. H. Woo, T. W. Holcombe, D. A. Unruh, A. Sellinger and J. M. J. Fréchet, *Chem. Mater.*, 2010, **22**, 1673; (*e*) Y. Zhou, L. Ding, K. Shi, Y.-Z. Dai, N. Ai, J. Wang and J. Pei, *Adv. Mater.*, 2012, **24**, 957; (*f*) T. Zhou, T. Jia, B. Kang, F. Li, M. Fahlman and Y. Wang, *Adv. Energy Mater.*, 2011, **1**, 431; (*g*) X. Zhang, Z. Lu, L. Ye, C. Zhan, J. Hou, S. Zhang, B. Jiang, Y. Zhao, J. Huang, S. Zhang, Y. Liu, Q. Shi, Y. Liu and J. Yao, *Adv. Mater.*, 2013, **25**, 5791.

9 (*a*) A. Gupta, A. Ali, A. Bilic, M. Gao, K. Hegedus, B. Singh, S. E. Watkins, G. J. Wilson, U. Bach and R. A. Evans, *Chem. Commun.*, 2012, **48**, 1889; (*b*) A. Gupta, V. Armel, W. Xiang, G. Fanchini, S. E. Watkins, D. R. MacFarlane, U. Bach and R. A. Evans, *Tetrahedron*, 2013, **69**, 3584; (*c*) R. J. Kumar, Q. I. Churches, J. Subbiah, A. Gupta, A. Ali, R. A. Evans and A. B. Holmes, *Chem. Commun.*, 2013, **49**, 6552; (*d*) A. Gupta, A. Ali, T. B. Singh, A. Bilic, U. Bach and R. A. Evans, *Tetrahedron*, 2012, **68**, 9440.

10 M. J. Frisch, *et al.*, Gaussian 09 revision D.01, Gaussian Inc. Wallingford CT, 2013.

11 Y. Lin, P. Cheng, Y. Li and X. Zhan, *Chem. Commun.*, 2012, **48**, 4773.

12 G. Li, V. Shrotriya, J. Huang, Y. Yao, T. Moriarty, K. Emery and Y. Yang, *Nat. Mater.*, 2005, **4**, 864.

13 M. J. Tan, W. P. Goh, L. Jun, G. Pundir, C. Vijila and C. Z. Kuan, *ACS Appl. Mater. Interfaces*, 2010, **2**, 1414.

14 C. Vijila, N. G. Meng, C. Z. Kuan, Z. Furong and C. S. Jin, *J. Polym. Sci., Part B: Polym. Phys.*, 2008, **46**, 1159.

15 J. Campbell, D. D. C. Bradley and H. Antoniadis, *Appl. Phys. Lett.*, 2001, **79**, 2133.

Experimental Part

Section 1: Synthetic Details

DPP1 was synthesized as per the reaction scheme 1 depicted in the main text.

*1.1 6,6'-((9,9-dioctyl-9H-fluorene-2,7-diyl)bis(thiophene-5,2-diyl))bis(2,5-bis(2-ethylhexyl) -3-(thiophen-2-yl)-2,5-dihydropyrrolo[3,4-c]pyrrole-1,4-dione) (**DPP1**)*

Compounds 2,2'-(9,9-dioctyl-9H-fluorene-2,7-diyl)bis(4,4,5,5-tetramethyl-1,3,2-dioxaborolane (**1**) (150 mg, 0.23 mmol) and 3-(5-bromothiophen-2-yl)-2,5-bis(2-ethylhexyl)-6-(thiophen-2-yl)-2,5-dihydropyrrolo[3,4-c]pyrrole-1,4-dione (**2**) (308 mg, 0.51 mmol) were mixed in 15.0 mL of dioxane in a 50.0 mL round bottom flask at room temperature. The reaction mixture was stirred for 15 minutes followed by the addition of aqueous 2 M K_2CO_3 (5.00 mL). The resulting suspension was degassed for 10 minutes by purging argon, and tetrakis(triphenylphosphine)palladium(0) [$Pd(PPh_3)_4$] catalyst (115 mg, 0.10 mmol) was added to the reaction mixture. The reaction mixture was heated at 90 °C in an oil bath for 24 hrs in the absence of light and the reaction progress was followed by thin-layer chromatography (TLC), which indicated the consumption of starting 1. The reaction mixture was cooled to room temperature, extracted with chloroform (25 mL) and the organic layer was separated. The organic layer was washed with water (2 × 100 mL) followed by brine (50 mL), dried over anhydrous $MgSO_4$ and recovered to get a crude solid which was purified through column chromatography on silica gel (chloroform/hexane = 1 : 1 as eluent) to afford **DPP1** (250 mg) as a black powder. Yield: 74%. M.p.: 130–132 °C. FT-IR (thin solid film, cm^{-1}): 3080, 2955, 2925, 2855, 1661, 1555, 1443, 1419, 1401, 1316, 1231, 1100, 857, 812, 735. ^1H NMR (CD_2Cl_2, 400 MHz, δ/ppm): 9.07–9.06 (m, 2H), 8.91–8.90 (m, 2H), 7.85–7.83 (m, 2H), 7.79–7.77 (m, 2H), 7.74–7.71 (m, 4H), 7.65–7.64 (m, 2H), 7.36–7.32 (m, 2H), 4.19–4.03 (m, 8H), 2.16–2.12 (m, 4H), 2.07–1.96 (m, 2H), 1.95–1.83 (m, 2H), 1.51–1.28 (m, 32H), 1.22–1.04 (m, 24H), 1.00–0.89 (m, 24H), 0.83–0.80 (m, 6H). ^{13}C NMR (CD_2Cl_2, 400 MHz, δ/ppm): 161.83, 161.64, 152.39, 150.47, 141.46, 140.22, 139.78, 136.97, 134.93, 132.57, 130.63, 130.22, 128.84, 128.37, 125.47, 124.45, 120.78, 120.47, 108.33, 108.16, 77.68, 45.85, 39.50, 39.29, 31.89, 30.51, 30.32, 30.05, 29.32, 28.72, 28.52, 23.99, 23.80, 23.66, 23.21, 22.72, 14.03, 13.94, 10.50, 10.39; HRMS (APCI): $[M]^+$, found 1434.8021. $C_{89}H_{118}N_4O_4{}^{32}S_4$ requires 1434.8030.

Section 2. Spectroscopic characterization of **DPP1**

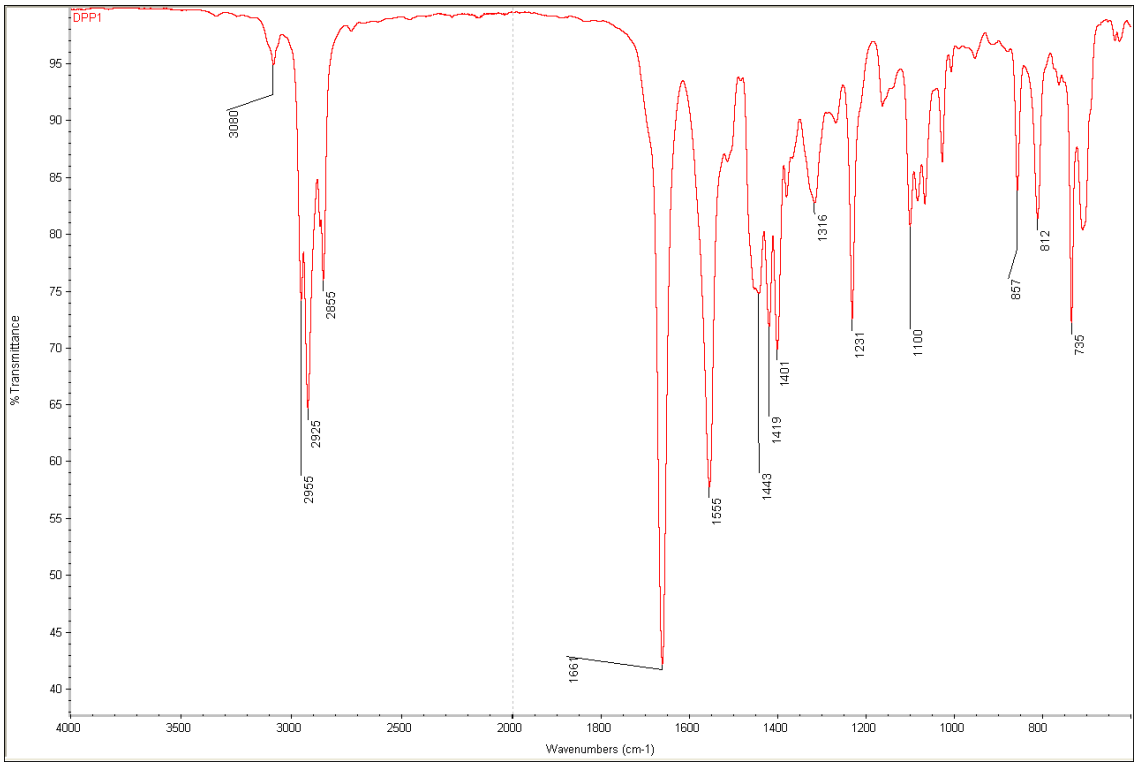

Fig. S2.1 FTIR Spectrum of **DPP1**

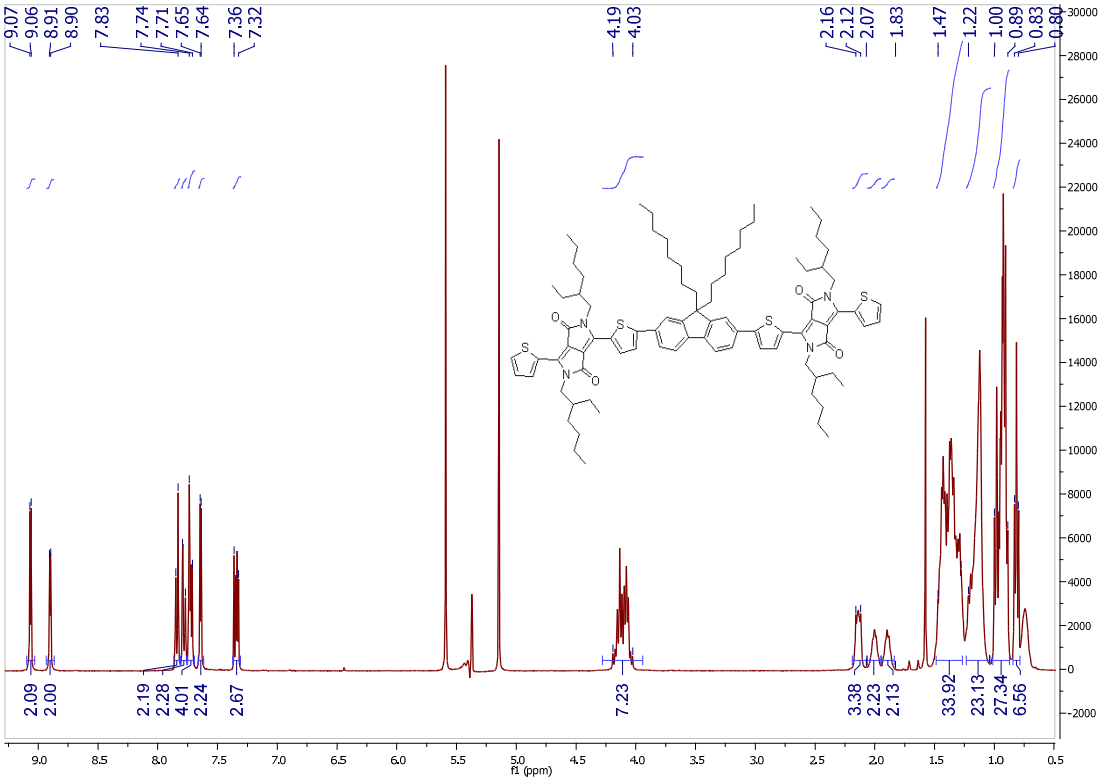

Fig. S2.2 ^{1}H NMR Spectrum of **DPP1** in ($CDCl_3$)

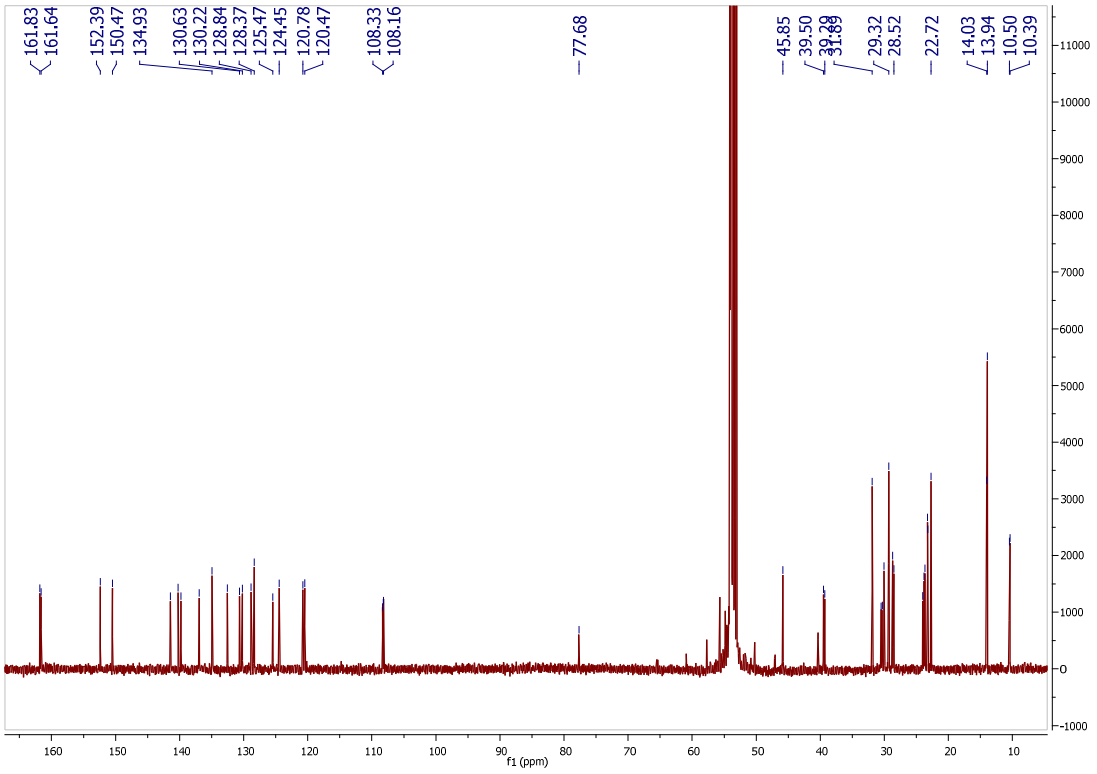

Fig. S2.3 ^{13}C NMR Spectrum of **DPP1** in ($CDCl_3$)

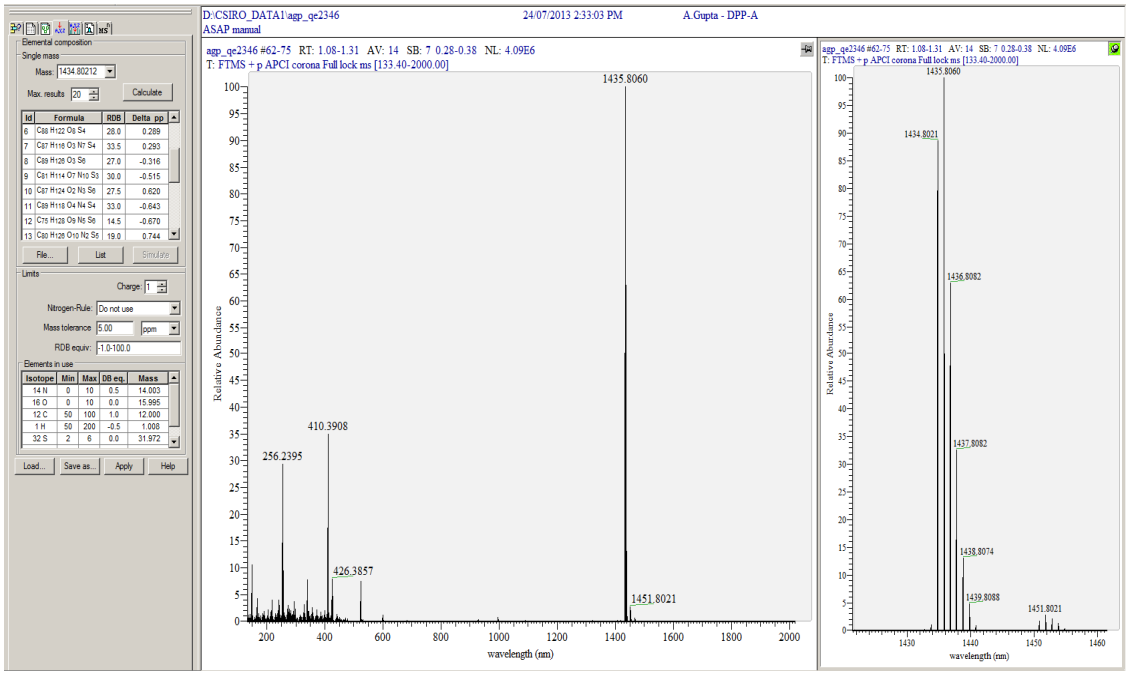

Fig. S2.4 HRMS Spectrum of **DPP1**

$[M]^+$

m/z	Theo. Mass	Delta (ppm)	Composition
1434.8021	1434.8022	-0.04	C88 H114 O9 N4 S2
	1434.8024	-0.16	C95 H112 O N5 S3
	1434.8019	0.17	C95 H120 N S5
	1434.8024	-0.19	C81 H122 O6 N6 S5
	1434.8017	0.27	C73 H126 O8 N8 S6
	1434.8017	0.29	C88 H122 O8 S4
	1434.8017	0.29	C87 H116 O3 N7 S4
	1434.8026	-0.32	C89 H126 O3 S6
	1434.8029	-0.52	C81 H114 O7 N10 S3
	1434.8012	0.62	C87 H124 O2 N3 S6
	1434.8030	**-0.64**	**C89 H118 O4 N4 S4**
	1434.8031	-0.67	C75 H128 O9 N5 S6
	1434.8011	0.74	C80 H126 O10 N2 S5
	1434.8010	0.75	C79 H120 O5 N9 S5
	1434.8010	0.77	C94 H116 O5 N S3
	1434.8010	0.77	C93 H110 N8 S3
	1434.8008	0.90	C86 H112 O8 N7 S2
	1434.8035	-0.97	C89 H110 O5 N8 S2
	1434.8035	-0.97	C90 H116 O10 N S2
	1434.8036	-1.00	C75 H120 O10 N9 S4

Section 3 Experimental part of optical electronic properties and device fabrication

3.1. Materials

All the reagents and chemicals used, unless otherwise specified, were purchased from Sigma-Aldrich Co. The solvents used for reactions were obtained from Merck Speciality Chemicals (Sydney, Australia) and were used as such. 3-(5-bromothiophen-2-yl)-2,5-bis(2-ethylhexyl)-6-(thiophen-2-yl)-2,5-dihydropyrrolo[3,4-c]pyrrole-1,4-dione was purchased from Luminescence Technology Corporation, Taiwan and was used as such.

3.2. Instruments and characterization

Unless otherwise specified, all ^{1}H and ^{13}C NMR spectra were recorded using a Bruker AV400 spectrometer at 400 MHz and 100.6 MHz, respectively, or a Bruker AV200 spectrometer at 200 MHz and 50 MHz, respectively. Chemical shifts (δ) are measured in parts per million. Thin Layer Chromatography (TLC) was performed using 0.25 mm thick plates precoated with Merck Kieselgel 60 F_{254} silica gel, and visualised using ultraviolet (UV) light (254 nm and 365 nm). Melting points were measured using a Gallenkamp MPD350 digital melting point apparatus and are uncorrected. High resolution mass spectra (atmospheric-pressure chemical ionization (APCI)) experiments were carried out on a Thermo Scientific Q-Exactive FTMS, ionizing by APCI from an ASAP probe [S1].

All ultraviolet-visible (UV-vis) absorption spectra were recorded on a Hewlett Packard HP 8453 Diode array UV-visible spectrophotometer. Thin films were spin-coated from *o*-chlorobenzene (*o*-DCB) at a spin speed of 2000 rpm for 1 min onto cleaned glass slides. **DPP1** was spin-coated from solutions at a concentration of 30 mg/mL. P3HT: **DPP1** blend solutions were prepared in the same manner as for devices, i.e. P3HT (15 mg) and **DPP1** (15 mg) in a total volume of 1 mL. Where specified, films were annealed at 150 ℃ for 5 min. Fluorescence spectra were recorded using a Perkin-Elmer LS50B fluorimeter. Photoelectron Spectroscopy in Air (PESA) measurements were recorded using a Riken Keiki AC-2 PESA spectrometer with a power setting of 5 nW and a power number of 0.5. Samples for PESA were prepared on clean glass substrates. The thermal stability of **DPP1** was investigated by thermogravimetric analysis (TGA). TGA was run at a heating rate of 10 °C/min, from room temperature to 800 °C.

3.3. Device fabrication and characterization of photovoltaic devices

Indium tin oxide (ITO)-coated glass (10Ω/□) was cleaned by standing in a stirred solution of 5% (v/v) Deconex 12PA detergent at 90 °C for 20 min. The ITO-coated glass was then successively sonicated for 10 min each in distilled water, acetone, and isopropanol. The substrates were then exposed to a UV-ozone clean at room temperature for 10 min. UV/ozone cleaning of glass substrates was performed using a Novascan PDS-UVT, UV/ozone cleaner with the platform set to maximum height. The intensity of the lamp was greater than 36 mW/cm^2 at a distance of 10 cm. At ambient conditions, the ozone output of the UV cleaner is greater than 50 ppm. Aqueous solutions of PEDOT/PSS (HC Starck, Baytron P AI 4083) were filtered (0.45 µm PVDF filter) and deposited onto glass substrates in air by spin coating (Laurell WS-400B-6NPP lite single wafer spin processor) at 4000 rpm for 60 s to give a layer having a thickness of 35 ± 5 nm. The PEDOT/PSS layer was then annealed on a hotplate in a glove box at 120 °C for 10 min. For OPV devices, the newly synthesized organic n-type material (**DPP1**) and P3HT (Nano-C) were separately dissolved in individual vials by magnetic stirring. Blend ratios and solution concentrations were varied to optimize device performance. The solutions were then combined, filtered (0.45 µm PTFE filter), and deposited by spin coating (SCS G3P spin coater) onto the ITO-coated glass substrates inside a glove box (with H_2O and O_2 levels both <1 ppm). Film thicknesses were determined on identical samples using a Dektak 6M Profilometer. The coated substrates were then transferred (without exposure to air) to a vacuum evaporator inside an adjacent nitrogen-filled glove box. Samples were placed on a shadow mask in a tray. The area defined by the shadow mask gave device areas of exactly 0.09 cm^2. Deposition rates and film thicknesses were monitored using a calibrated quartz thickness monitor inside the vacuum chamber. Layers of calcium (Ca) (Aldrich), from an open tungsten boat, and aluminum (Al) (3 pellets of 99.999%, KJ Lesker), from an alumina-coated graphite boat, having thicknesses of 15 nm and 100 nm, respectively, were evaporated onto the active layer by thermal evaporation at pressures less than 2×10^{-6} mbar Current density–voltage

(J–V) characteristics of OSCs were measured under AM1.5G illumination at 100 mW/cm^2 (SAN-EI Electric XEC-301S solar simulator). Light intensity of the solar simulator

was calibrated using a monosilicon detector (with KG-5 visible color filter) to minimize the spectral mismatch.

For incident photon conversion efficiency (IPCE) measurements, the devices were in suit tested in glove-box. IPCE data were collected using an Oriel 150W lamp coupled to a monochromator and an optical fibre. The output of the optical fibre was focused to give a beam that was contained within the area of the device. IPCE data were calibrated with a standard, unfiltered Si cell.

AFM topographic maps were performed directly on the active layer of the P3HT: **DPP1** blends using an Asylum Research MFP-3D-SA instrument. The AFM was run in intermittent contact mode (tapping mode) using MicroMasch NSC18 tips (typical resonant frequency ~100 kHz, typical probe radius ~10 nm and typical aspect ratio 3:1).

3.4. Device preparation for thin film transistors

We used thin film transistor (TFT) substrates Gen. 5: "end-of-line test substrates for customized semiconductor" purchased from Fraunhofer IMPS. Gate dielectric layers were thermally oxidized 230 ±10 nm SiO_2. Test chip sizes were 15 × 15 mm^2. Via Gate contact pads were 0.5 × 0.5 mm^2 structured by lift off technique.

The SiO_2 layer was cleaned with acetone followed by 2-propanol, and then treated with UV ozone. Bottom contact TFTs with prepatterned source drain electrodes having a fixed channel width of 2000 μm and varying channel lengths of 2.5, 5, 10, 20 μm, with a total of 16 devices in one test chip were employed. Gate via, source drain contacts were 30 nm of Au with 10 nm high work function adhesion layer (ITO) (structured by lift off techniques). HMDS and OTS were applied as a passivation layer prior to the deposition of active layer. Device fabrication was completed by deposition of **DPP1 (dissolved in CHCl3)** by spin coating at 3000 rpm for 1 minute. Measurements of the transistor characteristics were done using an Agilent parameter analyser B1500A. Estimation of the carrier mobility was done using the standard transistor equation (1) in saturation mode:

$$\mu = \frac{2L}{WC_i}\left(\frac{\delta\sqrt{I_D}}{\delta V_G}\right)^2 \qquad (1)$$

where μ is the two probe field effect mobility, L= channel length, C_i is the gate insulator capacitance.

Table 1.1 TA- thermal annealing, OTS-octyl trichlorosilane, HMDS-hexamethyldisilazane, V_T-threshold voltage.

	Solvent	Surface treatment	TA	hole		
				$\mu[cm^2V^{-1}s^{-1}]$	V_T [V]	On/off
DPP1	$CHCl_3$	OTS	Xa	4.8×10^{-4}	-6	1.8×10^{5}
	$CHCl_3$	OTS	A80	5.2×10^{-4}	-10	1.3×10^{4}
	$CHCl_3$	HMDS	Xa	1.2×10^{-4}	-19	6.7×10^{3}
	$CHCl_3$	HMDS	A80	1.1×10^{-5}	-15	1.6×10^{3}

Section 4. Figures of material characterisation

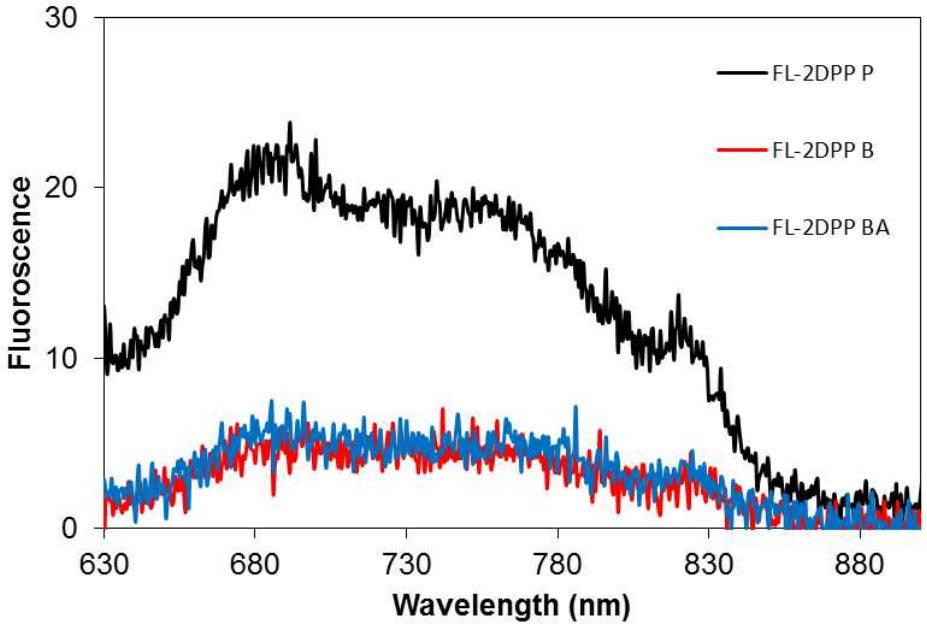

Fig. S1 Fluorescence spectra of pristine film of **DPP1** (black curve; **DPP1 P**) along with its blend with P3HT [as-cast (red curve; **DPP1 B**) and annealed blend at 150 °C for 5 min (blue curve; **DPP1 BA**)], spin-coated from *o*-dichlorobenzene (λ_{ex} = 600 nm).

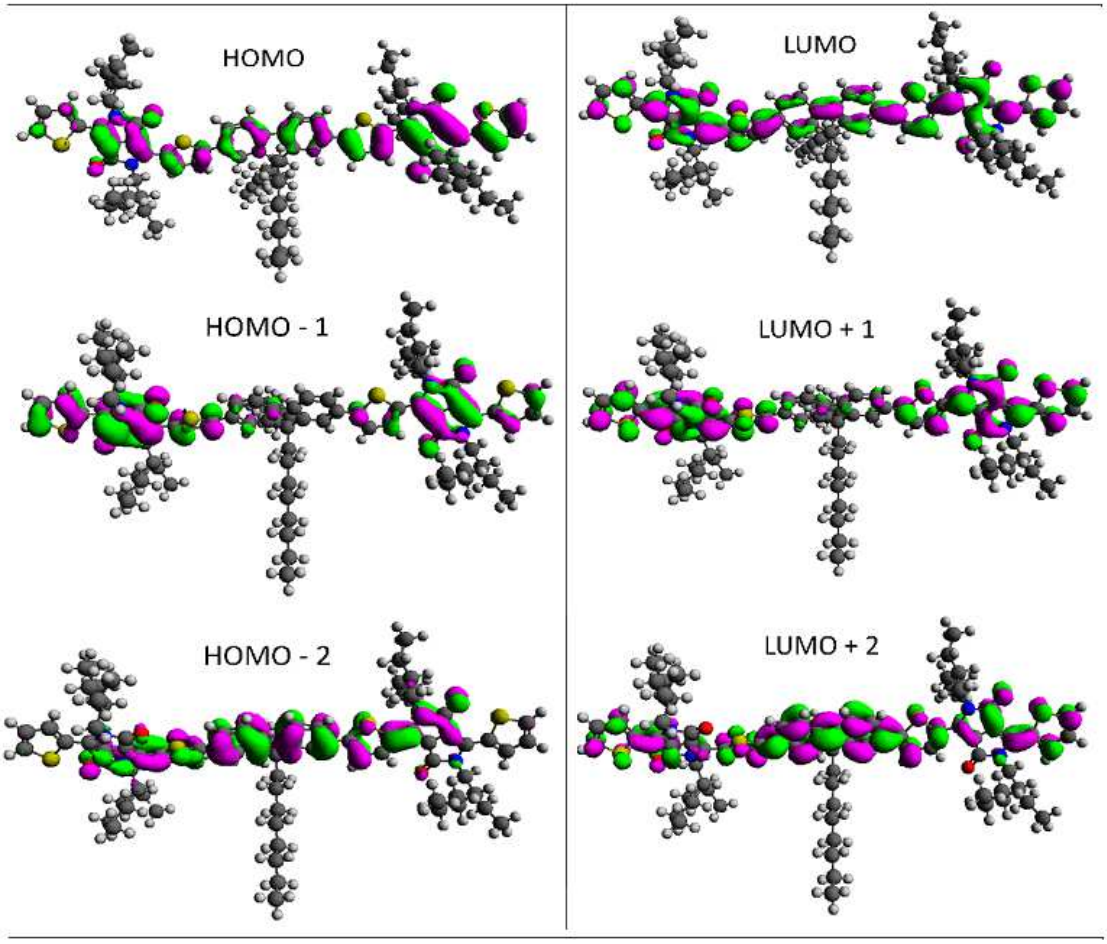

Fig. S2 Orbital density distribution for the HOMOs and LUMOs of **DPP1**. Density functional theory calculations were performed using the Gaussian 09 suite of programs and B3LYP/6-311+G(d,p)//B3LYP/6-31G(d) level of theory.

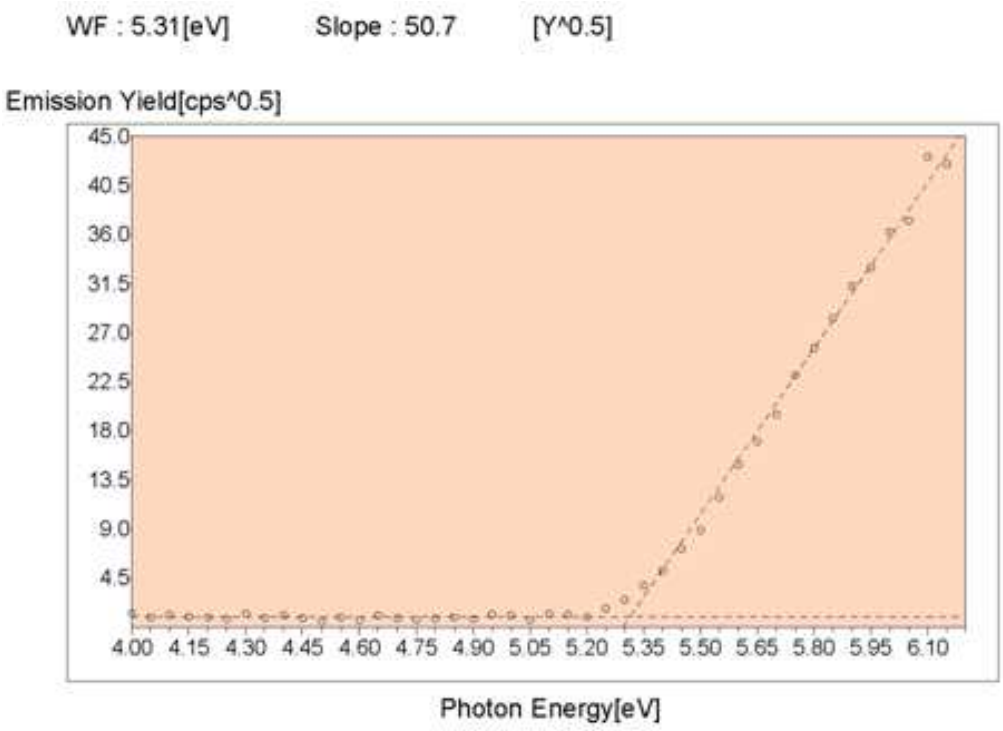

Fig. S3 PESA spectrum of thin film of **DPP1** from *o*-DCB. The dashed-lines show the fits to extract ionisation potential (-5.30eV) which corresponds to the HOMO energy level.

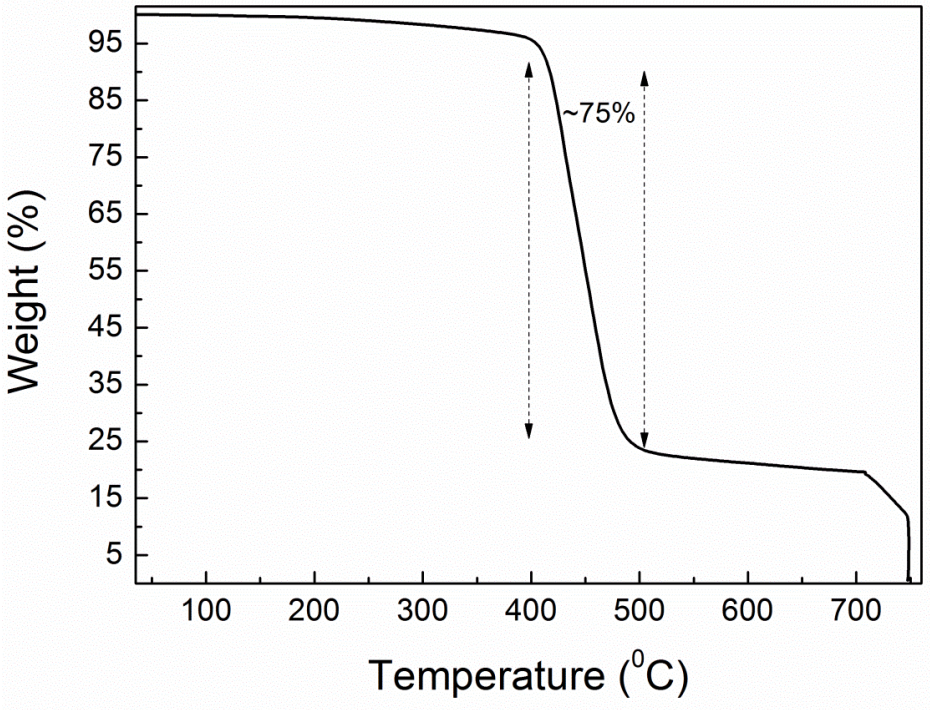

Fig. S4. TGA trace of **DPP1** under nitrogen atmosphere. Heating rate: 10 °C/min from room temperature to 800 °C.

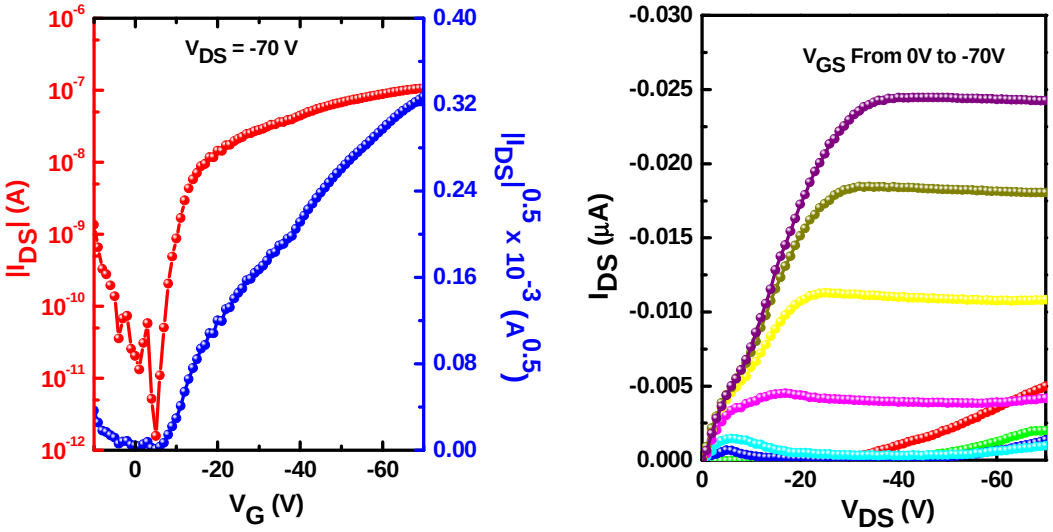

Fig. S5. Transfer (left) and output (right) characteristics of DPP1 OFET devices processed at room temperature. Device dimensions: channel length = 100 μm; channel width = 1 mm.

References

[S1] C.N. McEwen, R.G. McKay, B.S. Larsen, *Anal. Chem.* 77 (**2005**) 7826.

Chapter 3

A solution-processable electron acceptor based on diketopyrrolopyrrole and naphthalenediimide motifs for organic solar cells

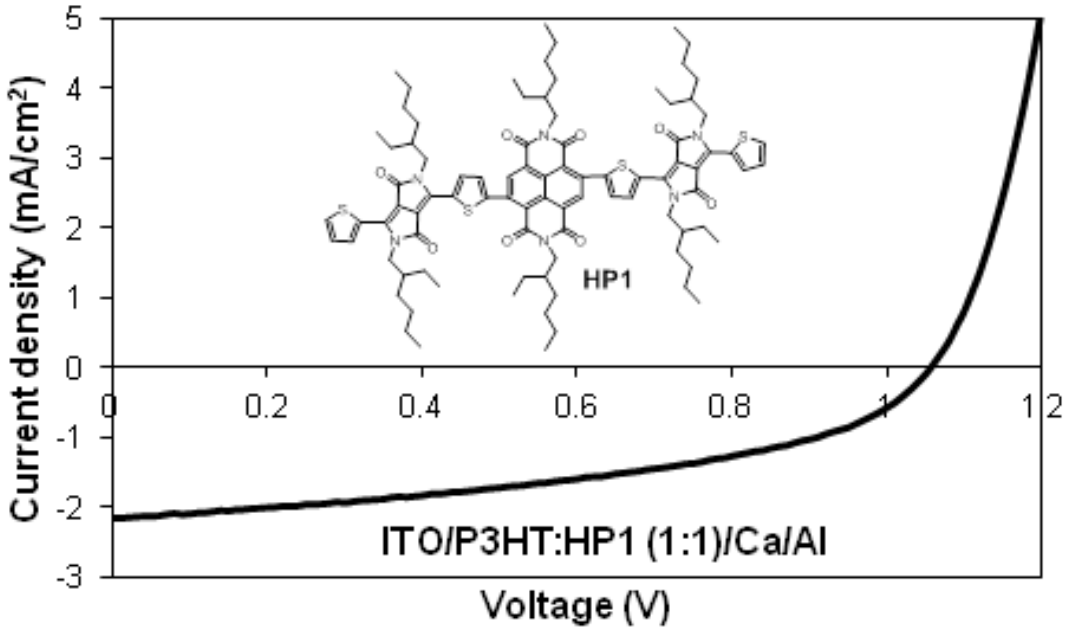

Journal article published in *Tetrahedron Letters* presented as **Chapter 3**.

Tetrahedron Letters xxx (2014) xxx–xxx

Contents lists available at ScienceDirect

Tetrahedron Letters

journal homepage: www.elsevier.com/locate/tetlet

A solution-processable electron acceptor based on diketopyrrolopyrrole and naphthalenediimide motifs for organic solar cells

Hemlata Patil [a], Akhil Gupta [a,b,*], Ante Bilic [c], Sidhanath V. Bhosale [d], Sheshanath V. Bhosale [a,*]

[a] School of Applied Sciences, RMIT University, GPO Box 2476V, Melbourne, Victoria 3001, Australia
[b] Department of Materials Engineering, Faculty of Engineering, Monash University, Wellington Road, Clayton, Victoria 3800, Australia
[c] CSIRO Computational Informatics, Private Bag 33, Clayton, South Victoria 3169, Australia
[d] Polymers and Functional Material Division, CSIR-Indian Institute of Chemical Technology, Hyderabad 50060, AP, India

ARTICLE INFO

Article history:
Received 7 February 2014
Revised 20 May 2014
Accepted 5 June 2014
Available online xxxx

Keywords:
Diketopyrrolopyrrole
Naphthalenediimide
Bulk-heterojunction solar cells
Lypophilic alkyl chains

ABSTRACT

A novel, solution-processable small molecular electron acceptor (**HP1**) based on diketopyrrolopyrrole and naphthalenediimide fragments was designed and synthesized via a Stille coupling reaction, characterized by spectroscopic means, and exhibited excellent solubility and thermal stability. **HP1** exerted strong and very broad absorption tailing into the near infra-red region, with appropriate energy levels matching with the archetypal electron donor, poly(3-hexylthiophene) (P3HT), and afforded 1.02% power conversion efficiency with a high open-circuit voltage (1.05 V) when tested in solution-processable bulk-heterojunction devices.

Over the past decade, bulk-heterojunction (BHJ) solar cells have been studied with immense interest in view of their potential for the fabrication of low-cost, lightweight and flexible photovoltaic devices.[1] One of the key challenges in BHJ research is the development of efficient photoactive and low band gap materials that can be produced at low cost, show good solubility in common organic solvents and that are thermally stable. Due to the excellent performance, superior electron affinity and good electron mobility of fullerene-based acceptor materials,[2] efforts to discover new non-fullerene acceptors for BHJ devices are limited by comparison.[3] A few chromophores have been reported as non-fullerene electron acceptors[4] and power conversion efficiencies (PCEs) approaching or exceeding 2% have been achieved.[5] Although this progress is encouraging, considerable scope still exists to develop new non-fullerene acceptors that possess strong optical absorption, good photochemical stability, adequate solubility, high charge carrier mobility and appropriate energy levels. Another strong incentive to develop new electron acceptors comes from the affliction of a number of potential disadvantages associated with the fullerene. These may include, but are not limited to, weak absorption in the visible spectrum, restricted electronic tuning and large electron affinity that can result in low open-circuit voltages (V_{oc}).[6] Therefore it is not surprising that there is growing interest in the development of small molecule non-fullerene acceptors for solution-processable BHJ devices.

Recently, a diketopyrrolopyrrole (DPP) building block was reported as a potential electron-deficient fragment for the development of non-fullerene acceptor chromophores.[5b] The naphthalenediimide (NDI) unit has interesting physical and electronic properties, and chromophores based on the NDI framework have been used as active components for field-effect transistors, two-photon absorbing materials and as electron-acceptor semiconductors.[7] Also, the NDI functionality possesses a planar conjugated structure and strong electron-withdrawing properties. A potential advantage of DPP and NDI accepting units is the possibility to incorporate alkyl chains on the nitrogen atoms that help to improve the solubility of the target materials. These alkyl chains not only enhance the solubility, but also help with excellent film formation without crystallization. Due to these reasons, we have investigated new non-fullerene electron acceptors based on NDI and DPP functionalities. This work is in continuation of our efforts on the development of small molecular chromophores for organic solar cells.[8]

Herein we report the design, synthesis and characterization of a novel non-fullerene electron acceptor based on DPP and NDI functionalities, where NDI was chosen as the central core with DPP terminal units (**HP1**, Fig. 1). **HP1** has been applied in

* Corresponding authors. Tel.: +61 3 9925 2680; fax: + 61 3 9925 3747 (S.V.B.).
E-mail addresses: akhil.gupta@monash.edu (A. Gupta), sheshanath.bhosale@rmit.edu.au (S.V. Bhosale).

http://dx.doi.org/10.1016/j.tetlet.2014.06.017
0040-4039/

Please cite this article in press as: Patil, H.; et al. *Tetrahedron Lett.* (2014), http://dx.doi.org/10.1016/j.tetlet.2014.06.017

solution-processable BHJ devices along with the classical electron donor, poly(3-hexylthiophene) (P3HT). **HP1** exhibited excellent thermal stability, broad optical absorption and appropriate energy levels matching with P3HT. This is the first time that NDI and DPP functionalities have been used in combination to generate a new electron acceptor chromophore for BHJ devices. Solution-processed BHJ devices based on P3HT:**HP1** (1:1) showed PCEs as high as 1.02% with a high V_{oc} of 1.05 V.

Compound **HP1** was easily synthesized in one step via a Stille coupling reaction of the bis-tributylstannyl derivative of NDI, 2,7-bis(2-ethylhexyl)-4,9-bis(tributylstannyl)benzo[*lmn*][3,8]phenanthroline-1,3,6,8(2*H*,7*H*)-tetraone (**1**), at reflux in toluene with commercially available 3-(5-bromothien-2-yl)-2,5-bis(2-ethylhexyl)-6-(thien-2-yl)pyrrolo[3,4-*c*]pyrrole-1,4(2*H*,5*H*)-dione (**2**) using bis(triphenylphosphine)palladium(II) dichloride [bis(PPh_3)$PdCl_2$] as the catalyst (Scheme 1). **HP1** was purified by column chromatography and was characterized by ^{1}H and ^{13}C NMR spectroscopy, and high-resolution mass spectrometry. **HP1** was found to be highly soluble in a variety of standard laboratory solvents, such as chloroform, dichlorobenzene and toluene (for instance, >30 mg/mL in $CHCl_3$), owing to the presence of six 2-ethylhexyl lypophilic chains. High solubility of organic semiconductors is an essential feature for the fabrication of solution-processable BHJ devices and **HP1** fulfils this criterion. Thermogravimetric analysis (TGA) revealed that **HP1** exhibits excellent thermal stability and is stable up to 350 °C [Fig. S1, supplementary information (SI)], a finding that strongly supports the high temperature annealing of P3HT:**HP1** devices.

The UV–vis spectra of **HP1** measured in chloroform solution and in thin solid films are shown in Figure 2. **HP1** exhibited very strong absorption with a maximum extinction coefficient of 23.1×10^4 M^{-1} cm^{-1} at 549 nm and $\sim 9.6 \times 10^4$ M^{-1} cm^{-1} at the longest wavelength. Pristine and blend film (1:1 w/w) absorption spectra of **HP1** exerted panchromatic absorbance (400–1000 nm) and the longest wavelength was red-shifted by about 80 nm when compared with the solution spectrum, a finding that is consistent with our previous work.[8] The blend film of P3HT:**HP1** (1:1 w/w) revealed quenching of the photoluminescence [see Fig. S2, Supporting Information (SI)], a finding that is consistent with literature reported non-fullerene electron acceptors.[5c] Theoretical density functional theory (DFT) calculations using Gaussian 09[9] and the B3LYP/6-311+G(d,p)//B3LYP/6-31G(d) level of theory indicated that the HOMO and LUMO orbital densities were evenly populated over the whole molecular backbone (see Fig. S3, SI), a finding that is consistent with one of the best performing non-fullerene electron acceptor materials.[5c] The electrochemical properties of **HP1** were investigated using cyclic voltammetry (CV) on a glassy carbon working electrode in 0.1 M $[Bu_4N]^+[PF_6]^-$ dichloromethane solution. The CV was run at a potential scan rate of 50 mV s^{-1}.

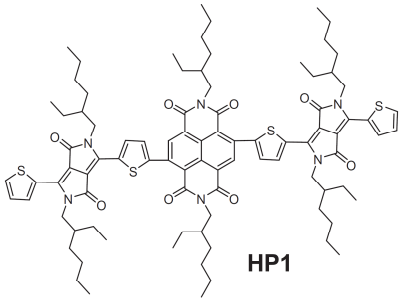

Figure 1. Molecular structure of the investigated non-fullerene electron acceptor **HP1**.

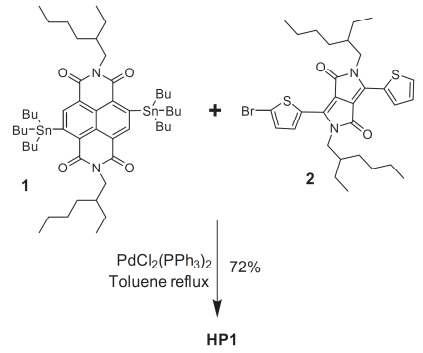

Scheme 1. Synthetic strategy for **HP1**.

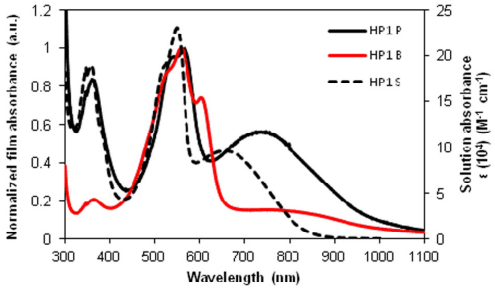

Figure 2. UV–vis absorption spectra of pristine (**HP1 P**; solid black line), 1:1 P3HT:**HP1** blend (**HP1 B**; red line), and chloroform solution (**HP1 S**; dotted line).

HP1 exhibited one reversible oxidation and two reversible reduction potentials (Fig. S4, SI). As such, the HOMO energy level (−4.92 eV) was estimated using the onset oxidation potential (0.12 eV vs F_c/F_c^+) and the LUMO energy level was calculated by adding the band gap to the HOMO value (Table S1 in SI). The difference between the LUMO of **HP1** (−3.46 eV) and the HOMO of **P3HT** (−4.76 eV from CV)[10] was as large as 1.30 eV, thus providing an incentive for high V_{oc} values of BHJ devices (Fig. S5, SI).

After establishing that **HP1** possesses promising optoelectronic properties that allow **HP1** to be considered as an electron-accepting chromophore, we fabricated solution-processable BHJ devices. The classical donor polymer P3HT was used as the *p*-type semiconducting component along with **HP1** to generate a blend solution and to cast an active layer on top of the PEDOT:PSS surface. The BHJ device architecture used was ITO/PEDOT:PSS (38 nm)/active layer/Ca (20 nm)/Al (100 nm) where the active layer was a 1:1 blend of P3HT/**HP1**, spin-cast from *o*-dichlorobenzene. It has been observed that thermal annealing of small organic molecules based on a DPP fragment has a large potential for molecular reorganization[11] and can help to achieve high V_{oc} values for BHJ devices.[12] As **HP1** is a thermally stable chromophore, we annealed our active films at 150 °C for five minutes and fabricated the devices. The BHJ devices yielded reasonable performance and the photovoltaic cell parameters, V_{oc}, short circuit current density (J_{SC}), fill factor (FF) and PCE, reached 1.05 V, 2.15 mA/cm^2, 0.45% and 1.02%, respectively. Notably, all the devices yielded very high V_{oc} values as expected. In fact, the value of V_{oc} >1 V is among the highest values reported for a single junction BHJ device. The observed high V_{oc} is in complete agreement with the large optical band gap (1.30 eV)

Please cite this article in press as: Patil, H.; et al. *Tetrahedron Lett.* (2014), http://dx.doi.org/10.1016/j.tetlet.2014.06.017

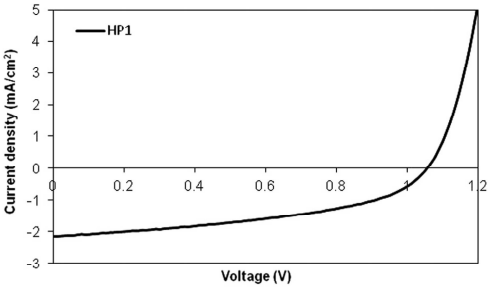

Figure 3. Current–voltage curve for the best BHJ device based on a P3HT:**HP1** blend under simulated sunlight (AM1.5, 1000 W m^{-2}).

between the LUMO and HOMO of **HP1** and P3HT, respectively. The respective current–voltage (*J*–*V*) curve is shown in Figure 3.

Incident photon-to-current conversion efficiency (IPCE) measurements indicated a broad spectrum over the whole visible range with IPCE plateaus at values of 15% at around 550 nm (Fig. S6, SI). Even though the IPCE value is moderate, the result itself is significant in view of using **HP1** in combination with low band gap conjugated donors such that charge generation could be achieved over a broad range of wavelengths. The blend film morphology was examined using atomic force microscopy (AFM) in tapping mode. The surface morphology of the blend film of P3HT:**HP1** (1:1, w/w) after annealing is shown in Figure S7 in the SI. The film exhibited crystalline grains with smaller size domains with a root-mean-square (RMS) roughness of 2.3 nm. This crystalline behaviour indicates the self-organization of P3HT that can be beneficial for charge transport in thin films.[13] The examination of field effect mobilities of charge carriers was conducted using the transistor technique (see experimental for details). No electron mobility was observed, however, the hole mobility of the blend (0.05 cm^2/Vs) suggested that the presence of **HP1** did not disrupt the hole-rich pristine P3HT, a result that is consistent with P3HT dominating the blend film microstructure.

In summary, the first non-fullerene electron acceptor, **HP1**, with NDI as a central core and DPP as terminal units was designed, synthesized, characterized and applied in solution-processable BHJ devices. **HP1** exhibited promising optoelectronic properties, excellent solubility, thermal stability and energy levels matching those of P3HT. The BHJ devices based on the P3HT:**HP1** blend after annealing at 150 °C for five minutes afforded a PCE of 1.02% and a very high V_{oc} of 1.05 V. Our results indicate that small molecules with low electron mobility and relatively deep LUMO energies (~3.5 eV) can also be studied as electron acceptors, and strongly support the excellent prospects of a simple molecule such as **HP1** for applications in organic solar cells. This work further enhances the prospects for the design and development of other electron acceptors based on the DPP functionality that should help realize significant improvements in BHJ solar cell device performance.

Acknowledgements

H.P. acknowledges the assistance of Dr Jegadesan Subbiah from Bio21 Institute, University of Melbourne VIC 3010 for providing support and guidance during the fabrication of BHJ devices. S.V.B. acknowledges financial support from the Australian Research Council, Australia under a Future Fellowship Scheme (FT110100152) and the School of Applied Sciences (RMIT University) for facilities. The RMIT University, Melbourne VIC 3001 and CSIRO Materials Science and Engineering (CMSE) Clayton is acknowledged for providing support through a visiting fellow position (A.G.). Sid. V.B. would like to thank the TAPSUN programme for financial assistance under the project NWP0054.

Supplementary data

Supplementary data (synthetic protocols, characterization, spectra, DFT calculations, and AFM images of BHJ devices) associated with this article can be found, in the online version, at http://dx.doi.org/10.1016/j.tetlet.2014.06.017.

References and notes

1. (a) Günes, S.; Neugebauer, H.; Sariciftci, N. S. *Chem. Rev.* **2007**, *107*, 1324–1338; (b) Thompson, B. C.; Frechet, J. M. J. *Angew. Chem., Int. Ed.* **2008**, *47*, 58–77.
2. (a) Brunetti, F. G.; Gong, X.; Tong, M.; Heeger, A. J.; Wudl, F. *Angew. Chem., Int. Ed.* **2010**, *49*, 532–536; (b) Brunetti, F. G.; Kumar, R.; Wudl, F. *J. Mater. Chem.* **2010**, *20*, 2934–2948; (c) Boudreault, P.-L. T.; Najari, A.; Leclerc, M. *Chem. Mater.* **2011**, *23*, 456–469; (d) Gupta, A.; Watkins, S. E.; Scully, A. D.; Singh, Th. B.; Wilson, G. J.; Rozanski, L. J.; Evans, R. A. *Synth. Met.* **2011**, *161*, 856–863; (e) Brabec, C. J.; Gowrisanker, S.; Halls, J. J. M.; Laird, D.; Jia, S.; Williams, S. P. *Adv. Mater.* **2010**, *22*, 3839–3856; (f) Walker, B.; Kim, C.; Nguyen, T.-Q. *Chem. Mater.* **2011**, *23*, 470–482; (g) Li, Y.; Guo, Q.; Li, Z.; Pei, J.; Tian, W. *Energy Environ. Sci.* **2010**, *3*, 1427–1436.
3. (a) Mishra, A.; Bäuerle, P. *Angew. Chem., Int. Ed.* **2012**, *51*, 2020–2067; (b) Dittmer, J. J.; Marseglia, E. A.; Friend, R. H. *Adv. Mater.* **2000**, *12*, 1270–1274.
4. (a) Anthony, J. E. *Chem. Mater.* **2011**, *23*, 583–590; (b) Sonar, P.; Lim, J. P. F.; Chan, K. L. *Energy Environ. Sci.* **2011**, *4*, 1558–1574.
5. (a) Bloking, J. T.; Han, X.; Higgs, A. T.; Kastrop, J. P.; Pandey, L.; Norton, J. E.; Risko, C.; Chen, C. E.; Brédas, J.-L.; McGehee, M. D.; Sellinger, A. *Chem. Mater.* **2011**, *23*, 5484–5490; (b) Lin, Y.; Li, Y.; Zhan, X. *Adv. Energy Mater.* **2013**, *3*, 724–728; (c) Winzenberg, K. N.; Kemppinen, P.; Scholes, F. H.; Collis, G. E.; Shu, Y.; Singh, Th. B.; Bilic, A.; Forsyth, C. M.; Watkins, S. E. *Chem. Commun.* **2013**, *49*, 6307–6309; (d) Woo, C. H.; Holcombe, T. W.; Unruh, D. A.; Sellinger, A.; Fréchet, J. M. J. *Chem. Mater.* **2010**, *22*, 1673–1679; (e) Zhou, Y.; Ding, L.; Shi, K.; Dai, Y.-Z.; Ai, N.; Wang, J.; Pei, J. *Adv. Mater.* **2012**, *24*, 957–961; (f) Zhou, T.; Jia, T.; Kang, B.; Li, F.; Fahlman, M.; Wang, Y. *Adv. Energy Mater.* **2011**, *1*, 431–439.
6. Shin, R. Y. C.; Sonar, P.; Siew, P. S.; Chen, Z. K.; Sellinger, A. *J. Org. Chem.* **2009**, *74*, 3293–3298.
7. (a) Bhosale, S. V.; Jani, C.; Langford, S. *Chem. Soc. Rev.* **2008**, *37*, 331–342; (b) Lin, C.-C.; Velusamy, M.; Chou, H.-H.; Lin, J. T.; Chou, P.-T. *Tetrahedron* **2010**, *66*, 8629–8634; (c) Lin, Y.; Li, Y.; Zhan, X. *Chem. Soc. Rev.* **2012**, *41*, 4245–4272.
8. (a) Gupta, A.; Ali, A.; Bilic, A.; Gao, M.; Hegedus, K.; Singh, B.; Watkins, S. E.; Wilson, G. J.; Bach, U.; Evans, R. A. *Chem. Commun.* **2012**, *48*, 1889–1891; (b) Gupta, A.; Armel, V.; Xiang, W.; Fanchini, G.; Watkins, S. E.; MacFarlane, D. R.; Bach, U.; Evans, R. A. *Tetrahedron* **2013**, *69*, 3584–3592; (c) Gupta, A.; Ali, A.; Singh, B.; Bilic, A.; Bach, U.; Evans, R. A. *Tetrahedron* **2012**, *68*, 9440–9447.
9. Frisch, M. J.; Trucks, G. W.; Schlegel, H. B.; Scuseria, G. E.; Robb, M. A.; Cheeseman, J. R.; Scalmani, G.; Barone, V.; Mennucci, B.; Petersson, G. A.; Nakatsuji, H.; Caricato, M.; Li, X.; Hratchian, H. P.; Izmaylov, A. F.; Bloino, J.; Zheng, G.; Sonnenberg, J. L.; Hada, M.; Ehara, M.; Toyota, K.; Fukuda, R.; Hasegawa, J.; Ishida, M.; Nakajima, T.; Honda, Y.; Kitao, O.; Nakai, H.; Vreven, T.; Montgomery, J. A., Jr.; Peralta, J. E.; Ogliaro, F.; Bearpark, M.; Heyd, J. J.; Brothers, E.; Kudin, K. N.; Staroverov, V. N.; Kobayashi, R.; Normand, J.; Raghavachari, K.; Rendell, A.; Burant, J. C.; Iyengar, S. S.; Tomasi, J.; Cossi, M.; Rega, N.; Millam, J. M.; Klene, M.; Knox, J. E.; Cross, J. B.; Bakken, V.; Adamo, C.; Jaramillo, J.; Gomperts, R.; Stratmann, R. E.; Yazyev, O.; Austin, A. J.; Cammi, R.; Pomelli, C.; Ochterski, J.W.; Martin, R. L.; Morokuma, K.; Zakrzewski, V. G.; Voth, G. A.; Salvador, P.; Dannenberg, J. J.; Dapprich, S.; Daniels, A. D.; Farkas, Ö.; Foresman, J. B.; Ortiz, J. V.; Cioslowski, J.; Fox, D. J. Gaussian 09 revision D.01, Gaussian Inc., Wallingford CT, 2013.
10. Hou, J.; Tan, Z.; Yan, Y.; He, Y.; Yang, C.; Li, Y. *J. Am. Chem. Soc.* **2006**, *128*, 4911–4916.
11. Mikhnenko, O. V.; Lin, J.; Shu, Y.; Anthony, J. E.; Blom, P. W. M.; Nguyen, T.-Q.; Loi, M. A. *Phys. Chem. Chem. Phys.* **2012**, *14*, 14196–14201.
12. Lin, Y.; Cheng, P.; Li, Y.; Zhan, X. *Chem. Commun.* **2012**, *48*, 4773–4775.
13. Li, G.; Shrotriya, V.; Huang, J.; Yao, Y.; Moriarty, T.; Emery, K.; Yang, Y. *Nat. Mater.* **2005**, *4*, 864–868.

Please cite this article in press as: Patil, H.; et al. *Tetrahedron Lett.* (2014), http://dx.doi.org/10.1016/j.tetlet.2014.06.017

Experimental details

1.1. *Materials*

All the reagents and chemicals used, unless otherwise specified, were purchased from Sigma-Aldrich Co. The solvents used for reactions were obtained from Merck Speciality Chemicals (Sydney, Australia) and were used as such. 3-(5-bromothiophen-2-yl)-2,5-bis(2-ethylhexyl)-6-(thiophen-2-yl)-2,5-dihydropyrrolo[3,4-c]pyrrole-1,4-dione was purchased from Luminescence Technology Corporation, Taiwan and was used as such. 2,7-bis(2-ethylhexyl)-4,9-bis(tributylstannyl)benzo[lmn][3,8]phenanthroline-1,3,6,8(2H,7H)-tetraone (**1**) was synthesized following the literature procedure.[S1]

1.2. *Instruments and characterization*

Unless otherwise specified, all ^{1}H and ^{13}C NMR spectra were recorded using a Bruker AV400 spectrometer at 400 MHz and 100.6 MHz, respectively, or a Bruker AV200 spectrometer at 200 MHz and 50 MHz, respectively. Chemical shifts (δ) are measured in parts per million (ppm). Thin Layer Chromatography (TLC) was performed using 0.25 mm thick plates precoated with Merck Kieselgel 60 F_{254} silica gel, and visualised using ultraviolet (UV) light (254 nm and 365 nm). Melting points were measured using a Gallenkamp MPD350 digital melting point apparatus and are uncorrected. High resolution mass spectra (atmospheric-pressure chemical ionization (APCI)) experiments were carried out on a Thermo Scientific Q-Exactive FTMS, ionizing by APCI from an ASAP probe.[S2]

All UV-vis absorption spectra were recorded on a Hewlett Packard HP 8453 Diode array UV-visible spectrophotometer. Thin films were spin-coated from *o*-dichlorobenzene (*o*-DCB) at a spin speed of 3000 rpm for 60 sec onto cleaned glass slides. **HP1** was spin-coated from solutions at a concentration of 30 mg/mL. P3HT: **HP1** blend solutions were prepared in the same manner as for devices, i.e. P3HT (15 mg) and **HP1** (15 mg) in a total volume of 1 mL. Films were annealed at 150 °C for 5 min. Fluorescence spectra were recorded using a Perkin-Elmer LS50B fluorimeter. Spectra were recorded of thin films spin-coated (3000 rpm/s, 60 s) onto PEDOT: PSS covered ITO glass slides from *o*-DCB.

Electrochemical measurements were carried out using a PowerLab ML160 potentiostat interfaced via a PowerLab 4/20 controller to a PC running E-Chem For Windows Ver. 1.5.2. The measurements were run in argon-purged dichloromethane with tetrabutylammonium hexafluorophosphate (0.2 M) as the supporting electrolyte. The cyclic voltammograms were recorded using a standard 3 electrode configuration with a glassy carbon (2 mm diameter) working electrode, a platinum wire counter electrode and a silver wire pseudo reference electrode. The silver wire was cleaned in concentrated nitric acid followed by concentrated hydrochloric acid and then washed with deionized water. Cyclic-voltammograms were recorded with a sweep rate of 50 mV/sec. All the potentials were referred to the $E_{1/2}$ of ferrocene/ferrocenium redox couple.

1.3 Device fabrication and characterization of photovoltaic devices, and experimental details for the preparation of thin-film transistors have been reported in our previous work.[S3]

Section 2: Synthetic Details

HP1 was synthesized as per the following procedure.

*4,9-bis(5-(2,5-bis(2-ethylhexyl)-3,6-dioxo-4-(thiophen-2-yl)-2,3,5,6-tetrahydropyrrolo[3,4-c]pyrrol-1-yl)thiophen-2-yl)-2,7-dioctylbenzo[lmn][3,8]phenanthroline-1,3,6, 8(2H,7H)-tetraone (**HP1**)*: 2,7-bis(2-ethylhexyl)-4,9-bis(tributylstannyl)benzo[lmn][3,8]phenanthroline-1,3,6,8(2H,7H)-tetraone (1) (200 mg, 0.18 mmol) was dissolved in toluene (20.0 mL) in a 100 mL round bottom flask followed by the addition of 3-(5-bromothiophen-2-yl)-2,5-bis(2-ethylhexyl)-6-(thiophen-2-yl)pyrrolo[3,4-c]pyrrole-1,4(2H,5H)-dione (2) (340 mg, 0.56 mmol) at room temperature. The resulting solution was degassed for 30 min followed by the addition of bis(triphenylphosphine)palladium(II) dichloride (351 mg, 0.50 mmol) at room temperature. The dark-coloured reaction mixture was heated to reflux overnight. Solvent was evaporated under reduced pressure and the residue was purified by silica gel chromatography (hexane: dichloromethane 10: 1) to get 200 mg (72%) of **HP1** as black powder. R_f: hexane/ dichloromethane 10/1 = 0.5; M. Pt.: 252–253 °C; IR (thin solid film, cm^{-1}): 3080, 2955, 2925, 2855, 1661, 1555, 1443, 1419, 1401, 1316, 1231, 1100, 857; ^1H NMR (400 MHz, CD_2Cl_2,

ppm): δ 8.98-8.97 (2H, m), 8.92-8.91 (2H, m), 8.79 (2H, s), 7.71-7.70 (2H, m), 7.46-7.45 (2H, m), 7.32-7.30 (2H, m), 4.10-4.01 (12H, m), 1.99-1.83 (6H, m), 1.42-1.22 (48H, m), 0.92-0.81 (36H, m); ^{13}C NMR (400 MHz, CD_2Cl_2, ppm): δ 162.43, 162.36, 161.78, 161.67, 146.12, 140.78, 139.55, 138.72, 136.30, 135.40, 135.13, 132.21, 131.09, 130.11, 129.84, 128.45, 127.96, 125.82, 123.93, 108.85, 108.26, 46.01, 45.88, 44.82, 39.34, 39.28, 37.94, 30.76, 30.31, 29.82, 29.20, 28.70, 28.53, 28.50, 24.04, 23.69, 23.63, 23.24, 23.20, 13.98, 13.95, 13.93, 10.50, 10.40, 10.35; HRMS (APCI): $[M]^+$, found 1534.7570. $C_{90}H_{114}N_6O_8{}^{32}S_4$ requires 1534.7575.

Spectra of HP1

^{1}H NMR

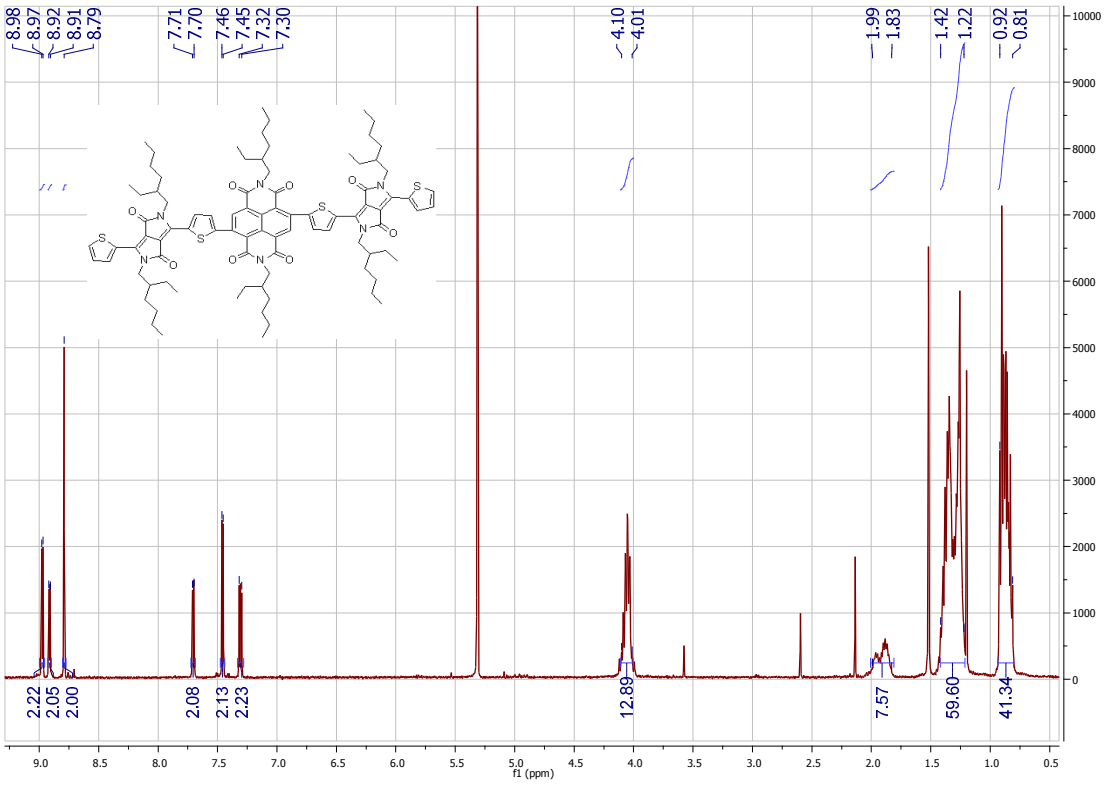

^{13}C NMR

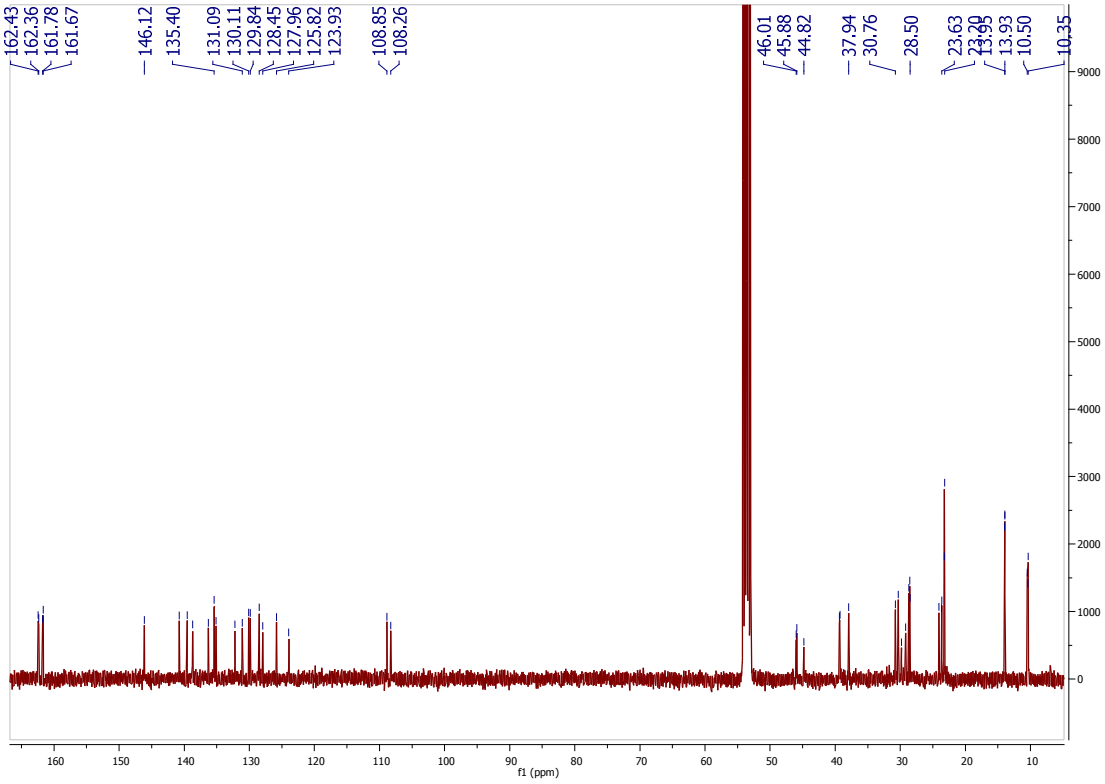
162.43
162.36
161.78
161.67
146.12
135.40
131.09
130.11
129.84
128.45
127.96
125.82
123.93
108.85
108.26
46.01
45.88
44.82
37.94
30.76
28.50
23.63
23.20
13.95
13.93
10.50
10.35
f1 (ppm)

HRMS

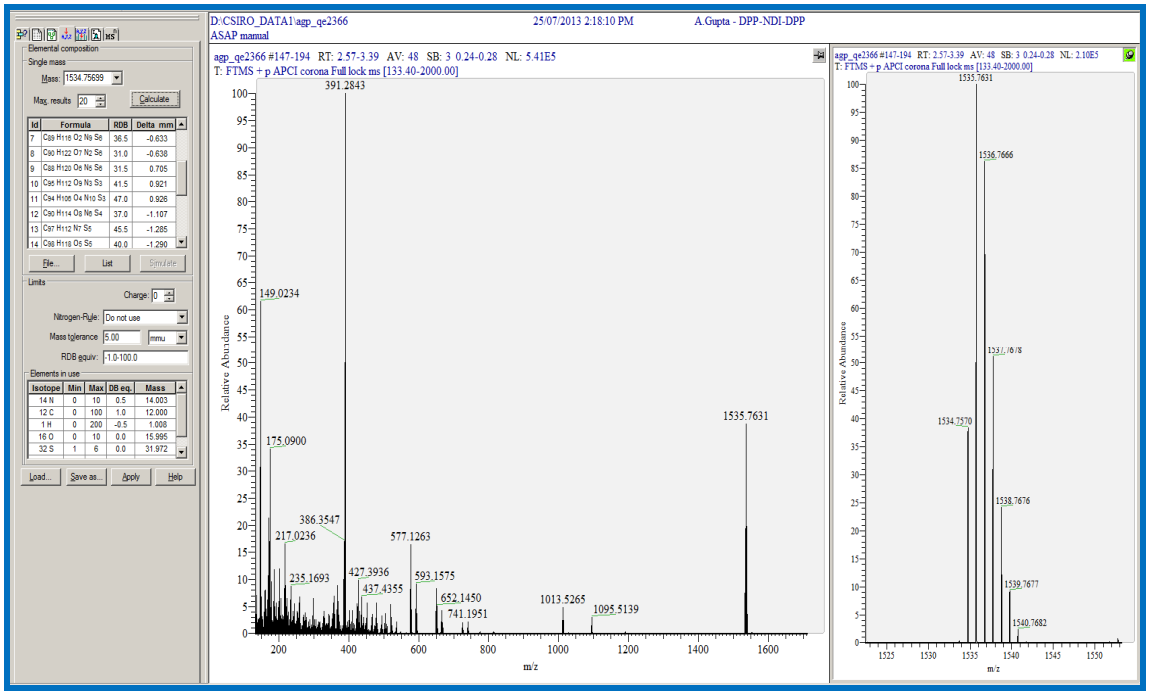

$[M]^+$

m/z	Theo. Mass	Delta (ppm)	RDB equiv.	Composition
1534.7570	1534.7571	-0.06	36.5	C89 H116 O2 N9 S6
	1534.7571	-0.06	31.0	C90 H122 O7 N2 S6
	1534.7569	0.06	28.0	C82 H118 O10 N8 S5
	1534.7569	0.08	41.0	C97 H114 O10 S3
	1534.7569	0.09	46.5	C96 H108 O5 N7 S3
	1534.7575	**-0.36**	**37.0**	**C90 H114 O8 N6 S4**
	1534.7564	0.39	40.5	C96 H116 O4 N3 S5
	1534.7577	-0.48	45.5	C97 H112 N7 S5
	1534.7577	-0.48	40.0	C98 H118 O5 S5
	1534.7562	0.51	37.5	C88 H112 O7 N9 S4
	1534.7560	0.65	47.5	C95 H104 O10 N7 S

1534.7580	-0.67	43.0	C90 H106 O9 N10 S2
1534.7582	-0.79	46.0	C98 H110 O6 N4 S3
1534.7557	0.82	31.5	C88 H120 O6 N5 S6
1534.7584	-0.93	36.0	C91 H118 O3 N6 S6
1534.7555	0.96	41.5	C95 H112 O9 N3 S3
1534.7555	0.96	47.0	C94 H106 O4 N10 S3
1534.7587	-1.09	52.0	C98 H102 O7 N8 S
1534.7589	-1.24	42.0	C91 H110 O4 N10 S4
1534.7589	-1.24	36.5	C92 H116 O9 N3 S4

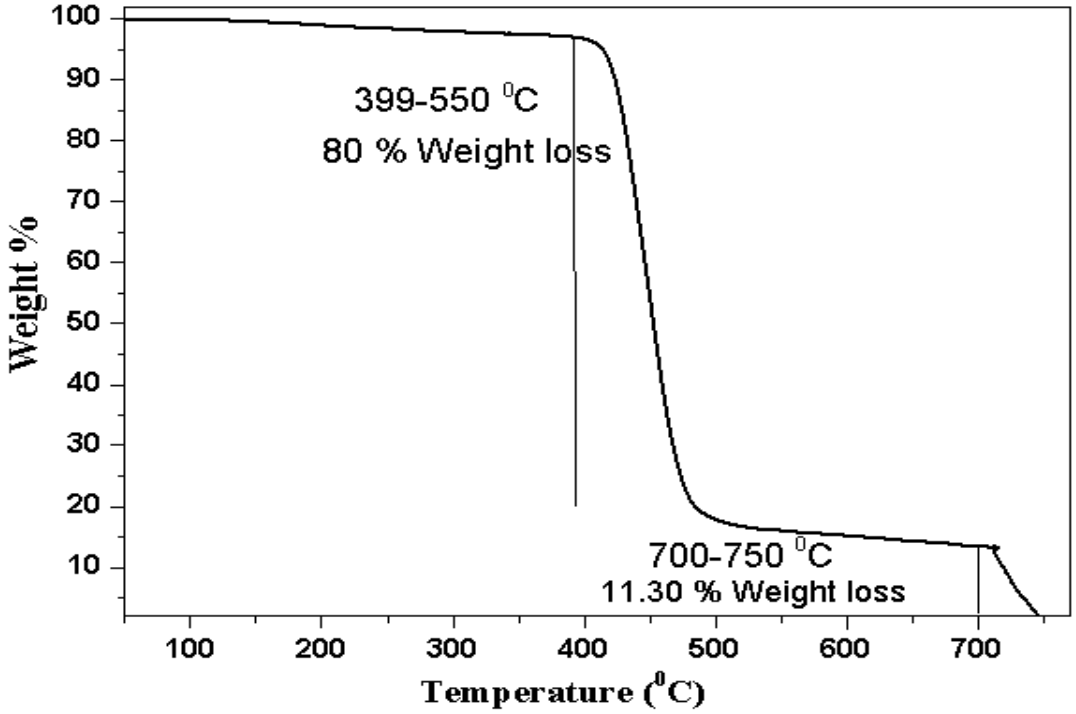

Figure S1. TGA trace of **HP1** under nitrogen atmosphere. Heating rate: 10 °C/min from room temperature to 750 °C.

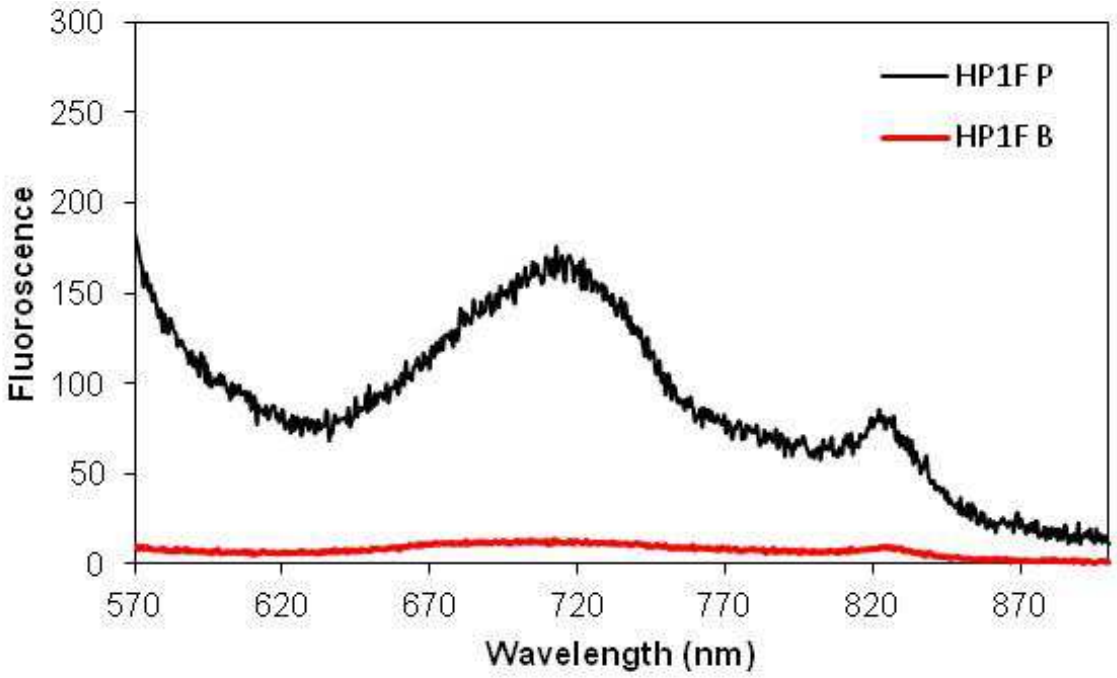

Figure S2. Fluorescence spectra of pristine film of **HP1** (black curve; HP1F P) along with its blend with P3HT [as-cast (red curve; HP1F B), spin-coated from *o*-dichlorobenzene (λ_{exc} = 600 nm).

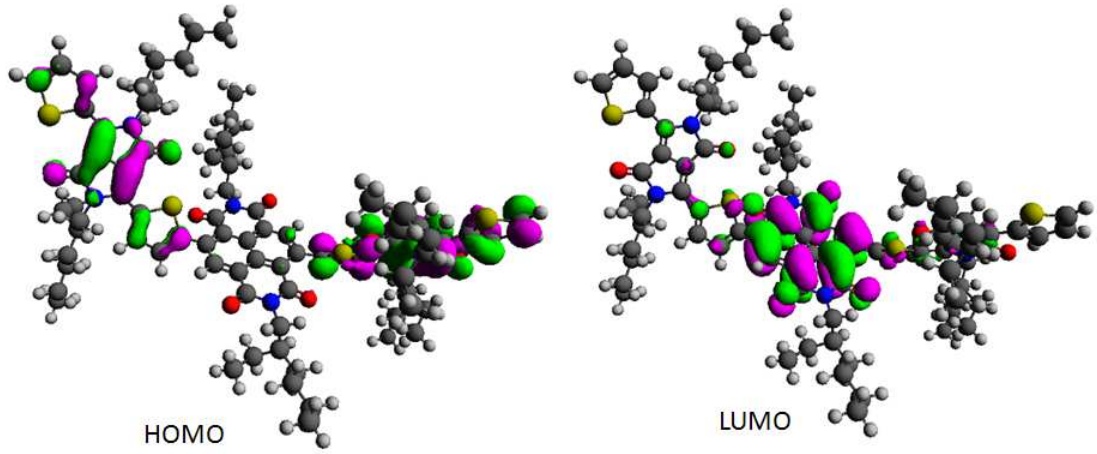

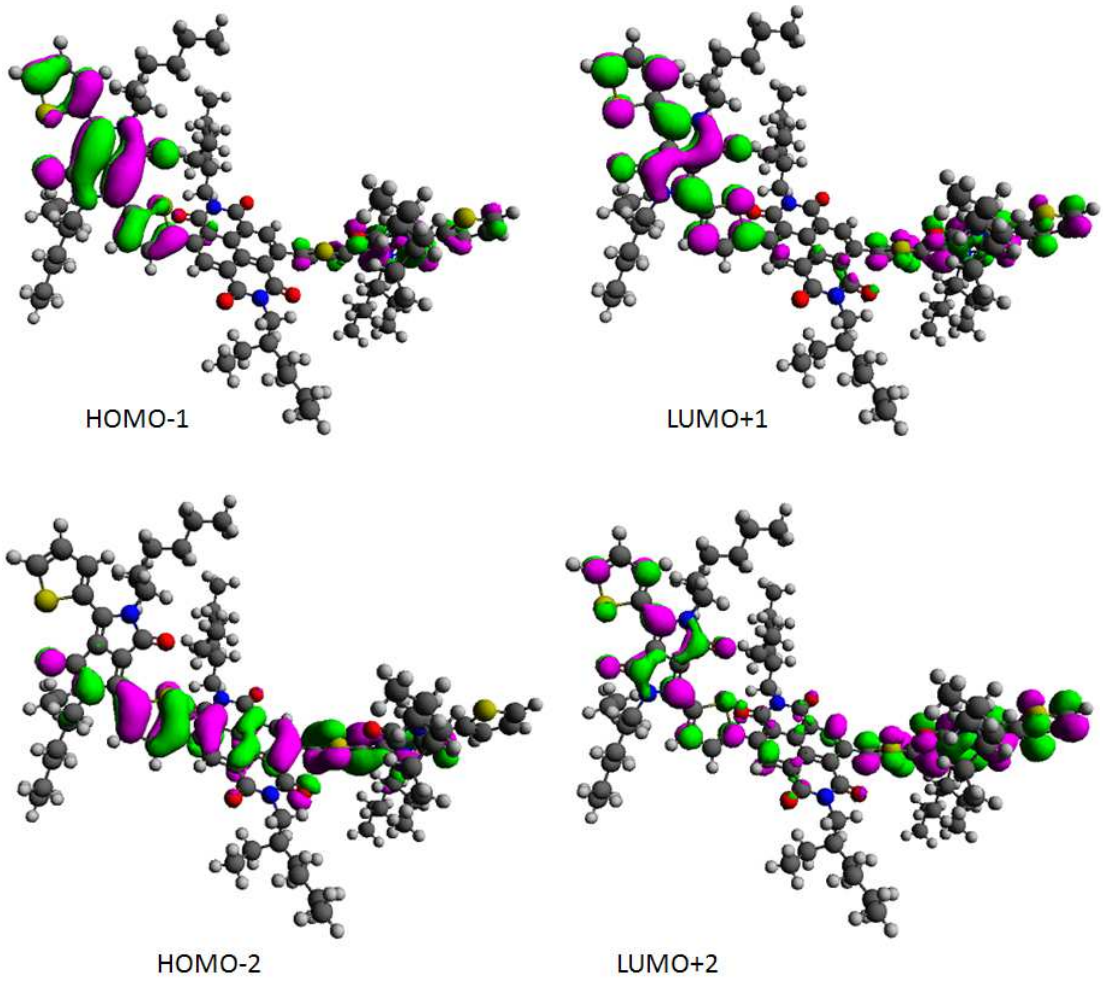

Figure S3. Orbital density distribution for frontier molecular orbitals of **HP1**. Density functional theory calculations were performed using the Gaussian 09 suite of programs and B3LYP/6-311+G(d,p)//B3LYP/6-31G(d) level of theory.

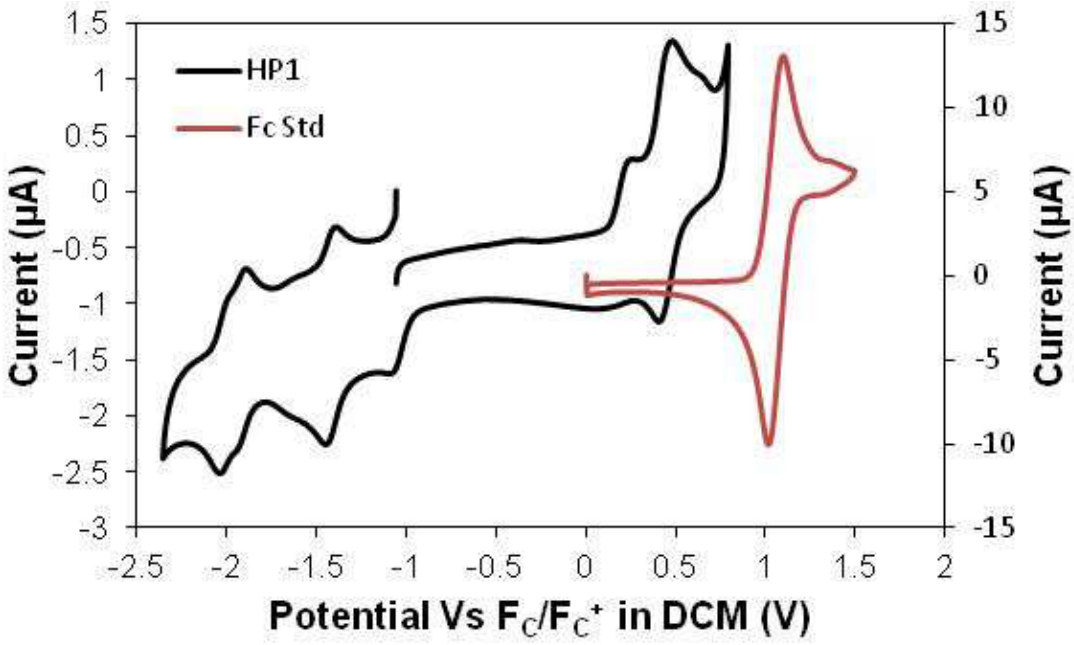

Figure S4. Cyclic-voltammogram of **HP1**, run in dichloromethane at a sweep rate of 50 mV sec^{-1}, shows reversible oxidation and reduction waves.

Table S1. Optical and electrochemical properties of **HP1**

Dye	Absorption (solution) λ_{max}[a]/onset/nm [ε/($M^{-1}cm^{-1}$)]	Absorption (film) λ_{max}[b]/onset/nm	E_{HOMO} eV[c]	$E_{bandgap}$ eV[d]	E_{LUMO} eV[e]
HP1	658/850 658 [95980] 549 [231,160] 360 [189,040]	737/1010 567 367	-4.92	1.46	-3.46

a Absorption spectrum was measured in chloroform solution. b

Absorption spectra of thin solid film spin-casted (solution spun at 2000 rpm (10 mg/mL) for 1 minute) from chloroform solution. c HOMO energy level of **HP1** was measured using CV method run in dichloromethane at a scan speed of 50 mV/sec. d Energy band-gap was estimated from the tangent of the edge of longest wavelength in solution spectrum. e LUMO energy level was calculated from the optical band-gap (solution) and HOMO energy level ($E_{LUMO} = E_{bandgap} + E_{HOMO}$).

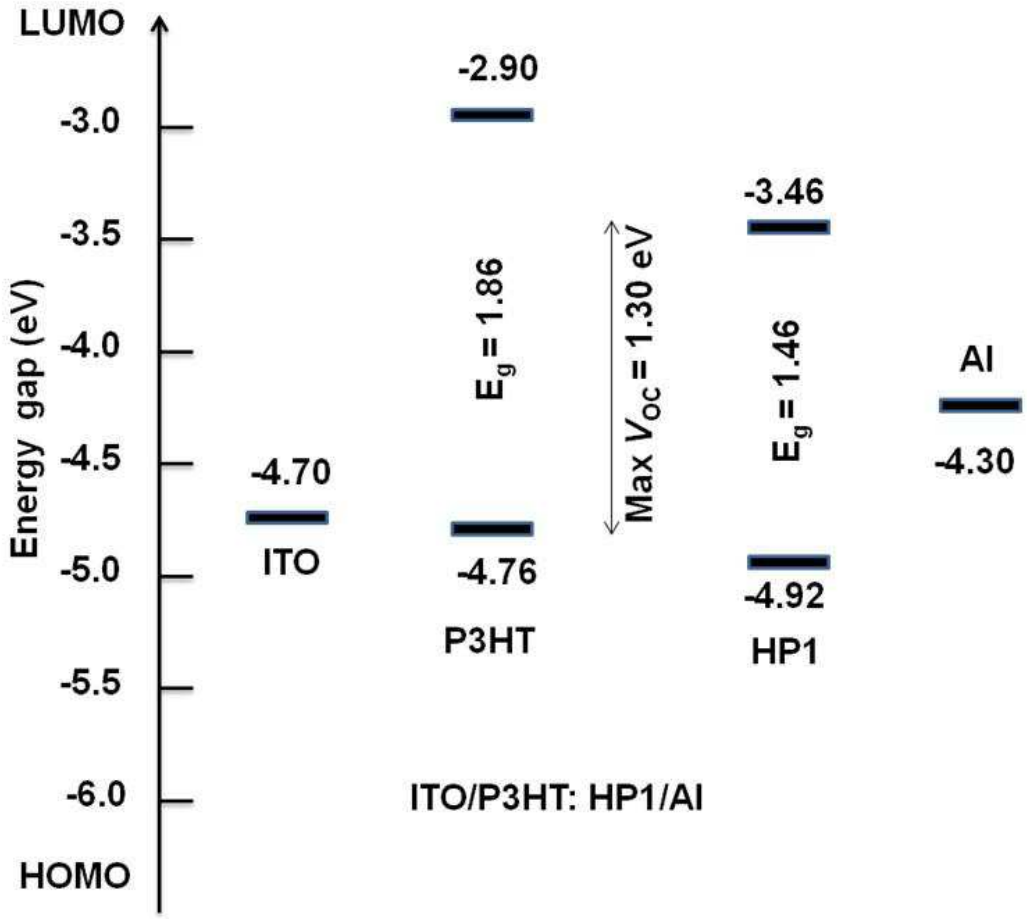

Figure S5. Energy level diagram showing alignments of various components of BHJ device architecture.

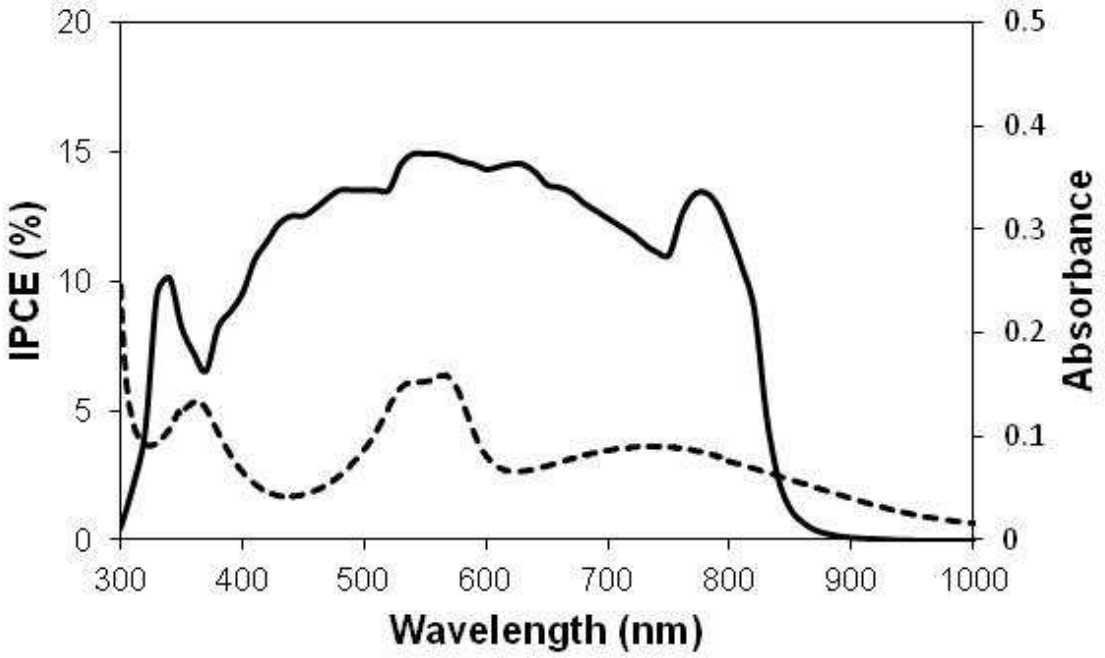

Figure S6. IPCE spectrum of the best performing device described in Figure 3.

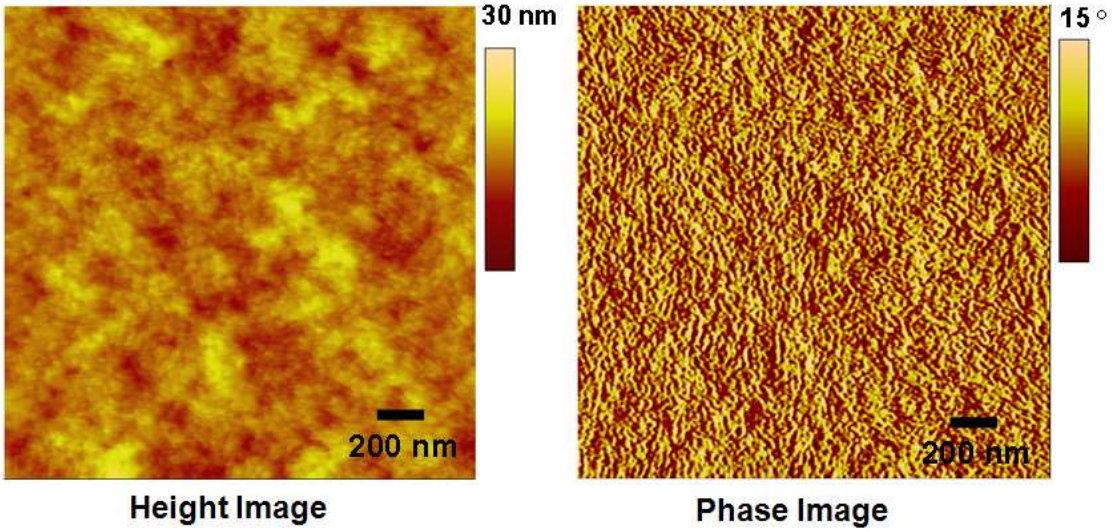

Figure S7. AFM image for thin film of P3HT: **HP1** blend annealed at 150 °C for 5 min (15 mg P3HT, 15 mg **HP1** in 1 mL *o*-DCB, 3000 rpm/s for 1 min).

References

S1 Polander, L. E.; Romanov, A. S.; Barlow, S.; Hwang, D. K.; Kippelen, B.; Timofeeva, T. V.; Marder, S. R. *Org. Lett.* **2012**, *14*, 918.

S2 McEwen, C. N.; McKay, R. G.; Larsen, B. S. *Anal. Chem.* **2005**, *77*, 7826.

S3 Gupta, A.; Armel, V.; Xiang, W.; Fanchini, G.; Watkins, S. E.; MacFarlane, D. R.; Bach, U.; Evans, R. A. *Tetrahedron* **2013**, *69*, 3584.

Chapter 4

Donor-acceptor-donor modular small organic molecules based on naphthalene diimide acceptor unit for solution processable photovoltaic devices

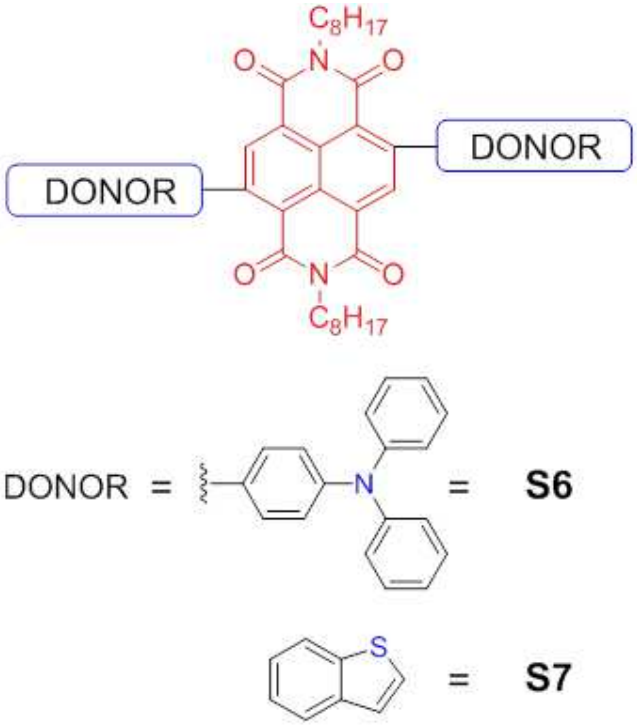

Journal article published in *Journal of Electronics Material* presented as Chapter 4

Journal of ELECTRONIC MATERIALS, Vol. 43, No. 9, 2014
DOI: 10.1007/s11664-014-3243-x

Donor–Acceptor–Donor Modular Small Organic Molecules Based on the Naphthalene Diimide Acceptor Unit for Solution-Processable Photovoltaic Devices

HEMLATA PATIL,[1] AKHIL GUPTA,[2,4] ANTE BILIC,[3] SAM LESLIE JACKSON,[1] KAY LATHAM,[1] and SHESHANATH V. BHOSALE[1,5,6]

1.—School of Applied Sciences, RMIT University, GPO Box 2476V, Melbourne, VIC 3001, Australia. 2.—Department of Materials Engineering, Faculty of Engineering, Monash University, Wellington Road, Clayton, VIC 3800, Australia. 3.—CSIRO Computational Informatics, Private Bag 33, Clayton South, VIC 3169, Australia. 4.—e-mail: akhil.gupta@monash.edu. 5.—e-mail: bsheshanath@gmail.com. 6.—e-mail: sheshanath.bhosale@rmit.edu.au

Two novel solution-processable small organic molecules, 4,9-bis(4-(diphenylamino)phenyl)-2,7-dioctylbenzo[3,8]phenanthroline-1,3,6,8(2*H*,7*H*)-tetraone (**S6**) and 4,9-bis(benzo[*b*]thiophen-2-yl)-2,7-dioctylbenzo[3,8]phenanthroline-1,3,6,8(2*H*,7*H*)-tetraone (**S7**), have been successfully designed, synthesized, characterized, and applied in solution-processable photovoltaic devices. **S6** and **S7** contain a common electron-accepting moiety, naphthalene diimide (NDI), with different electron-donating moieties, triphenylamine (**S6**) and benzothiophene (**S7**), and are based on a donor–acceptor–donor structure. **S7** was isolated as black, rod-shaped crystals. Its triclinic structure was determined by single crystal x-ray diffraction (XRD): space group $P\bar{1}$, $Z = 2$, $a = 9.434(5)$ Å, $b = 14.460(7)$ Å, $c = 15.359(8)$ Å, $\alpha = 67.256(9)$ degrees, $\beta = 80.356(11)$ degrees, $\gamma = 76.618(10)$ degrees, at 150 Kelvin (K), $R = 0.073$. Ultraviolet–visible absorption spectra revealed that use of triphenylamine donor functionality with the NDI acceptor unit resulted in an enhanced intramolecular charge transfer (ICT) transition and reduction of the optical band gap compared with the benzothiophene analogue. Solution-processable inverted bulk heterojunction devices with the structure indium tin oxide/zinc oxide (30 nm)/active layer/molybdenum trioxide (10 nm)/silver (100 nm) were fabricated with **S6** and **S7** as donors and (6,6)-phenyl C_{70}-butyric acid methyl ester ($PC_{70}BM$) as acceptor. Power conversion efficiencies of 0.22% for **S6**/$PC_{70}BM$ and 0.10% for **S7**/$PC_{70}BM$ were achieved for the preliminary photovoltaic devices under simulated AM 1.5 illumination (100 mW cm^{-2}). This paper reports donor–acceptor–donor modular small organic molecules, with NDI as central accepting unit, that have been screened for use in solution-processable inverted photovoltaic devices.

Key words: Donor–acceptor–donor, naphthalene diimide, solution-processable, bulk heterojunction solar cells

INTRODUCTION

Over the past two decades, research into organic-based heterojunction solar cells[1,2] has gained considerable momentum because of their potential to replace traditional inorganic photovoltaic (OPV) devices. Tang reported the very first bilayer heterojunction organic solar cell, in which a copper phthalocyanine (CuPc) was used as donor and a perylene-based small molecule as acceptor.[3] Traditionally, semiconducting polymers, for example poly(3-hexylthiophene) (P3HT) as electron-donor

(Received January 24, 2014; accepted May 6, 2014; published online June 3, 2014)

material and soluble fullerene derivatives, for example [6,6]-phenyl-C_{61}-butyric acid methyl ester (PCBM), as electron-acceptor material have been used.[4–8] However, recent reports of improved bulk heterojunction (BHJ) device performance as a result of using small molecules have attracted much attention.[9–15] Solution-processable small molecules have several advantages over polymers, for example high absorption coefficients, well-defined structures, and easy synthetic isolation and purification strategies, thus enabling the fabrication of very thin OPV devices with low material consumption. Development and investigation of new organic molecules from different structural classes is, thus, a challenge, and a significant topic of research.

In common with polymeric structures, the design requirements of small molecules include a preference for a low band gap, a broad absorption profile, high charge carrier mobility, and appropriate highest occupied molecular orbital (HOMO) and lowest unoccupied molecular orbital (LUMO) energy levels. It has been established that low band gap materials can be generated by incorporating an electron donor (D), a π-conjugating unit (π), and an electron acceptor (A) unit within a structure.[16,17] Reports of OPV or BHJ devices using small organic molecules as donor components have recently emerged, and a review by Mishra and Bäuerle[12] provides a strong incentive for this. Although progress is encouraging, there is still much scope for development of new light-harvesting materials with broad and efficient optical absorption, deep HOMO energy levels (−5.0 eV to −5.5 eV) and adequate solubility for thin film formation. One successful strategy is the investigation of the D–A structure. Such structures enable ICT transitions that broaden the absorption spectrum and narrow the optical band gap. It is, therefore, not surprising there is growing interest in the development of small organic molecules based on a variety of D–A combinations. D–A combinations can be generated in several ways, for example A–D–A,[18] D–A,[19–23] and D–A–D,[24,25] to enhance intermolecular associations, which can assist with charge transport. The D–A–D modular design, in particular, reported by Tamayo et al.[24] and Walker et al.[25] is a successful example, and is based on a diketopyrrolopyrrole (DPP) acceptor unit. Other examples of acceptor functionality within a D–A–D structure include use of 2-pyran-4-ylidenemalononitrile and thiazolothiazole, reported by Li et al.[26] and Shi et al.,[27] respectively.

In our own studies of small molecule chromophores and charge-transport materials based on a variety of D–A combinations, we have developed successful examples for organic electronic applications, in particular OPV.[20,21,23] We are also interested in focusing on the design and advancement of new chromophores based on D–A–D modules and the push–pull chromophores used in nonlinear optics.[28–30] Naphthalene diimide (NDI), in particular, is a synthon of current research interest because of its interesting physical and electronic properties; it has been used as an active component for field-effect transistors, because of its two-photon absorbing properties, and in electron-acceptor semiconductors.[31–33] NDI has a planar conjugated structure and strong electron-withdrawing properties. A potential advantage of the NDI accepting unit is its amenability to incorporation of alkyl chains on the nitrogen atoms. These alkyl chains not only enhance the solubility of the target materials but also aid excellent film formation without crystallization. For these reasons, we have focused on the use of NDI as an electron-deficient unit.

To generate new push–pull chromophores, we have combined highly electron-rich donor groups with NDI core units in a D–A–D structure. In this paper we report facile synthesis and characterization of the optical and electrochemical properties of two new molecules, 4,9-bis(4-(diphenylamino)phenyl)-2,7-dioctylbenzo[3,8]phenanthroline-1,3,6,8(2*H*,7*H*)-tetraone (**S6**) and 4,9-bis(benzo[*b*]thiophen-2-yl)-2,7-dioctylbenzo[3,8]phenanthroline-1,3,6,8(2*H*,7*H*)-tetraone (**S7**), shown in Fig. 1. We have fabricated inverted BHJ devices comprising a fullerene acceptor and either **S6** or **S7** as donor component. To the best of our knowledge, this is the first time NDI has been used in conjunction with different donor functionality to generate new organic chromophores based on a D–A–D module and which have been fabricated in solution-processable inverted BHJ devices. Initial screening of the BHJ devices revealed greater power-conversion efficiency (PCE) was achieved for **S6** (0.22% for **S6** compared with 0.10% for **S7**), as confirmed by the increased open circuit voltage (0.76 V for **S6** and 0.58 V for **S7**) and short-circuit current (0.90 mA cm^{-2} for **S6** and 0.40 mA cm^{-2} for **S7**) under simulated AM 1.5 illumination (100 mW cm^{-2}).

EXPERIMENTAL PROCEDURES

Instruments and Characterization

Unless otherwise specified, all ^{1}H and ^{13}C NMR spectra were recorded using a Bruker AV400 spectrometer at 400 MHz and 100.6 MHz, respectively, or a Bruker AV200 Spectrometer at 200 MHz and 50 MHz, respectively. Chemical shifts (δ) are measured in parts per million (ppm). Thin-layer chromatography (TLC) was performed on plates precoated with 0.25 mm layers of silica gel (Merck Kieselgel 60 F_{254}); chromatograms were visualized by use of ultraviolet (UV) light (254 nm and 365 nm). Melting points were measured using a Gallenkamp MPD350 digital melting point apparatus and are uncorrected. High-resolution mass spectra (atmospheric-pressure chemical ionization (APCI)) experiments were performed with a thermo scientific q-exactive Fourier-transform mass spectrometer, ionizing by APCI from an atmospheric solids analysis probe.[34] Ultraviolet–visible (UV–Vis) absorption spectra were recorded using a Hewlett Packard HP 8453 diode-array spectrometer.

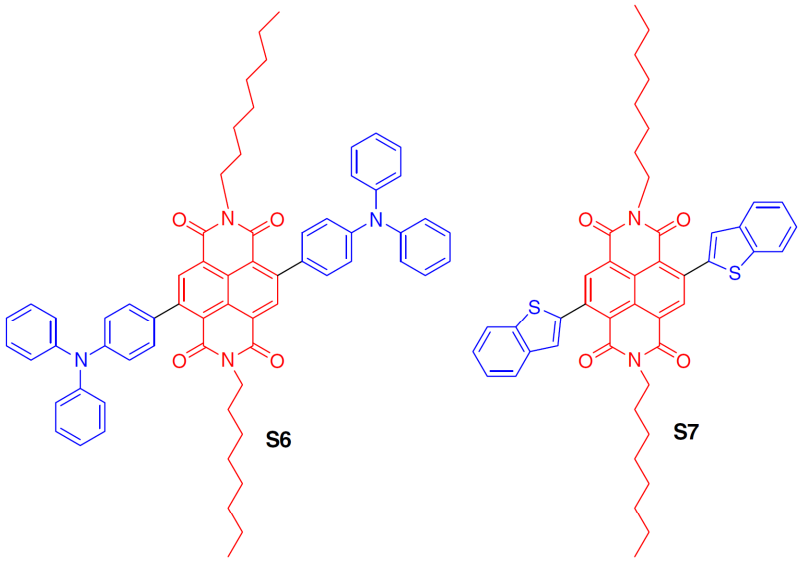

Fig. 1. Molecular structures of the organic chromophores investigated, **S6** and **S7**.

Fluorescence spectra were acquired by use of a Perkin Elmer LS50B fluorimeter. Photo electron spectroscopy in air (PESA) was performed with a Riken Keiki AC-2 PESA spectrometer with a power setting of 5 nW and a power number of 0.5. Samples for PESA were prepared on cleaned glass substrates.

A doped ($N \sim 3 \times 10^{17}$ cm^{-3}) silicon (Si) wafer was used as a substrate and as gate electrode. Discrete bottom contact organic field-effect transistors (OFETs) were fabricated on thermally grown smooth silicon dioxide (SiO_2) (230 nm). Interdigitated source and drain electrodes were photo-lithographically patterned from a 50-nm sputtered gold layer. Channel length, L, of the devices was 20 μm and the channel width, W, was 2 mm. The SiO_2 layer was first cleaned with acetone, then with 2-propanol, and finally treated with UV ozone. Device fabrication was completed by spin coating the organic semiconductor layers at 1500 rpm in a glove box from solutions in chloroform. The active layers consisted of pristine compounds. Without any further treatment, completed devices were transferred (under air-free conditions) to another glove box equipped to probe the devices by use of a probe station. Electrical measurements were obtained by use of a Keithley 2612 dual-channel SMU. The reproducibility of the OFET preparation procedure was high; for the values presented in this paper, the confidence interval for the extracted mobility was ±15%. The carrier mobility values presented in this work were usually averages from measurements on at least four devices on the same substrate.

Unit cell and intensity data for complex **S7** were obtained by use of a Bruker APEX II CCD area detector system. Single crystals were mounted on a glass loop and coated with liquid paraffin. Data were then collected at 150 Kelvin (K) using Mo Kα radiation (λ = 0.71073 Å) from a fine-focus sealed tube source fitted with a graphite monochromator. The structure was solved by direct methods in the triclinic space group $P\bar{1}$ using SHELXS-97,[35] and was refined by use of SHELXL-97.[35] A mixed strategy was used for refinement of the hydrogen atoms. Hydrogen atoms attached to carbon atoms were placed in calculated positions with a C–H bond length of 0.93 Å, whereas hydrogen atoms attached to oxygen atoms were located from difference Fourier maps and were refined without constraint. Molecular graphics were performed using SHELXTL[36] and Mercury[37] software. Selected crystal data for **S7** are presented in Tables S1 to S3 (see supporting information). Further details of the crystal structure investigation may be obtained, free of charge, from the Cambridge Crystallographic Data Centre (CCDC; no. 950394).

Fabrication and Characterization of Photovoltaic Devices

Inverted solar cells were processed on pre-patterned indium tin oxide (ITO)-coated glass substrates with a sheet resistance of 15 ohms (Ω) per square. First, a thin layer of zinc oxide (ZnO) nanoparticles was deposited on a cleaned ITO substrate by spin-coating (3000 rpm) to form a 30-nm ZnO layer, followed by backing on a hot plate at 140°C for 5 min. An active layer of the device was deposited by spin coating a chlorobenzene solution containing 8 mg of **S6** or **S7** with 16 mg of $PC_{70}BM$. The thickness of the active layer was measured as

75–80 nm. Molybdenum trioxide (MoO_3) (10 nm) and silver (Ag) (100 nm) were thermally evaporated at a vacuum of $\sim 10^{-7}$ mbar on the top of active layer as an anode. The area of the devices was 0.1 cm^2. Film thickness was determined by use of a Veeco Dektak 150 surface profiler. Current density–voltage measurements for the devices were obtained by use of a 1 kW Oriel solar simulator with an AM 1.5G filter as the light source in conjunction with a Keithley 2400 source measurement unit. Solar measurements were conducted under 1000 W/m^2 AM 1.5G illumination conditions. For accurate measurement, the light intensity was calibrated using a reference silicon solar cell (PV Measurements) certified by the national renewable energy laboratory (NREL). Device fabrication and characterization were performed in an ambient environment without any encapsulation. OPV device data were determined as an average from eight cells.

Materials and Reaction Strategy

All the reagents and chemicals used, unless otherwise specified, were purchased from Sigma–Aldrich. The solvents used for reactions were obtained from Merck speciality chemicals (Sydney, Australia) and were used as received. 4,9-Dibromo-2,7-dioctylbenzo[3,8]phenanthroline-1,3,6,8(2*H*,7*H*)-tetraone (abbreviated to "NDI" throughout this manuscript) was synthesized in accordance with a literature report.[38] ZnO nano-particles (NP) were synthesized by a sol–gel method, using zinc acetate dihydrate ($Zn(CH_3COO)_2{\cdot}2H_2O$) and tetramethylammonium hydroxide (TMAH, $(CH_3)_4NOH$) as precursors.[39] In a typical process, 0.4 M TMAH in ethanol was added dropwise to the solution of 0.1 M $Zn(CH_3COO)_2{\cdot}2H_2O$ in dimethyl sulfoxide (DMSO). The resulting ZnO NP were washed and dispersed in ethanol at 25 mg/mL.

The reaction strategy used for synthesis of **S6** and **S7** is depicted in Fig. 2.

*4,9-Bis(4-(diphenylamino)phenyl)-2,7-dioctylbenzo[3,8]phenanthroline-1,3,6,8(2H,7H)-tetraone (**S6**)*

4,9-Dibromo-2,7-dioctylbenzo[3,8]phenanthroline-1,3,6,8(2*H*,7*H*)-tetraone (0.20 g, 0.31 mmol) and (4-(diphenylamino)phenyl)boronic acid (0.19 g, 0.67 mmol) were mixed in dioxane (18 mL) in a 100-mL round-bottomed flask at room temperature and the reaction mixture was stirred for 15 min followed by addition of aqueous 2 M potassium carbonate (K_2CO_3) (6 mL). The resulting suspension was degassed for 10 min by purging with argon, and tetrakis(triphenylphosphine)palladium(0) ($Pd(PPh_3)_4$) catalyst (0.10 g) was added to the reaction mixture. The reaction mixture was heated at 90°C in an oil bath for 12 h in the absence of light and the progress of the reaction was followed by TLC, which indicated consumption of the starting dibromo derivative. The reaction mixture was cooled to room temperature, diluted with water (50 mL), and the product was extracted in chloroform. The organic layer was washed with water then brine, dried over anhydrous $MgSO_4$, and the crude solid obtained by evaporation of the solvent was purified by column chromatography on silica gel (dichloromethane–hexane 2:1 as eluent) to afford **S6** (0.25 g, yield 84%) as a bluish-black solid. m.p. 219–222°C. IR (thin solid film, cm^{-1}) 3035, 2955, 2925, 2854, 1705, 1668, 1590, 1509, 1492, 1439, 1314, 1280, 1183, 830, 753. ^{1}H NMR (400 MHz, CD_2Cl_2) δ = 8.62 (s, 2H), 7.36–7.29 (m, 12H), 7.22–7.19 (m, 8H), 7.14–7.07 (m, 8H), 4.09–4.05 (m, 4H), 1.69–1.62 (m, 4H), 1.41–1.21 (m, 20H), 0.87–0.83 (m, 6H) ppm. ^{13}C NMR (400 MHz, CD_2Cl_2) δ = 162.70, 148.10, 147.56, 146.96, 136.03, 134.02, 129.86, 129.56, 127.41, 125.61, 125.26, 123.69, 122.61, 121.92, 40.97, 31.93, 29.44, 29.37, 28.12, 27.25, 22.77, 13.99 ppm. HRMS (APCI): *m/z* (%): $[M + H]^+$ calculated for $C_{66}H_{65}N_4O_4$: 977.5000; found 977.4995. Elemental analysis (calculated): C, 81.12; H, 6.60; N, 5.73; found: C, 81.08; H, 6.58; N, 5.70.

*4,9-Bis(benzo[b]thiophen-2-yl)-2,7-dioctylbenzo[3,8]phenanthroline-1,3,6,8(2H,7H)-tetraone (**S7**)*

Synthesis and reaction work up of **S7** were the same as for **S6**, except that a different reagent, benzo[*b*]thiophen-2-ylboronic acid (0.12 g, 0.67 mmol), was used. Column purification on silica gel (dichloromethane–hexane 2:1 as eluent) afforded **S7** (0.18 g, yield 77%) as a reddish-brown solid. m.p. 232–234°C; IR (thin solid film, cm^{-1}) 2953, 2926, 2851, 1708, 1673, 1582, 1441, 1313, 1245, 1185. ^{1}H NMR (400 MHz, CD_2Cl_2) δ = 8.84 (s, 2H), 7.98–7.93 (m, 4H), 7.51–7.44 (m, 6H), 4.13–4.09 (m, 4H), 1.74–1.65 (m, 4H), 1.43–1.23 (m, 20H), 0.94–0.85 (m, 6H) ppm. ^{13}C NMR (400 MHz, CD_2Cl_2) δ = 161.99, 161.65, 141.60, 140.78, 140.07, 139.72, 136.00, 127.56, 125.61, 124.90, 124.66, 124.34, 123.98, 123.92, 122.15, 41.03, 31.76, 29.26, 29.20, 27.91, 27.07, 22.61, 13.82 ppm. HRMS (APCI): *m/z* (%): $[M + H]^+$ calculated for $C_{46}H_{47}N_2O_4^{32}S_2$, 755.2972; found 755.2969. Elemental analysis (calculated): C, 73.18; H, 6.14; N, 3.71; found: C, 73.15; H, 6.10; N, 3.68. Black, rod-shaped crystals, suitable for single-crystal-ray diffraction analysis, were prepared by diffusion of methanol into a dichloromethane solution of **S7**, over approximately over a week.

RESULTS AND DISCUSSION

Design Concept, Synthesis, and Solubility of S6 and S7

Both **S6** and **S7** were developed on the basis of the D–A–D module and the central acceptor moiety was directly linked to the donor functionality to create a conjugated structure. The development of these target materials incorporates use of two identical donor units on each side of the central core, resulting in "symmetrical chromophores". In **S6**, the triphenylamine (TPA) group was selected for its

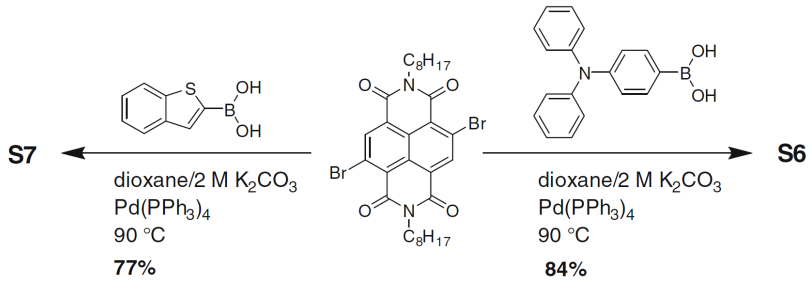

Fig. 2. Reaction schemes for the synthesis of **S6** and **S7**.

believed ability to act as an energy antenna, which may be responsible for the overall bathochromic absorption[40] compared with **S7**, for which a benzothiophene (BT) donor unit was used. **S6** and **S7** were synthesized by reacting the bis-bromoNDI precursor, 4,9-dibromo-2,7-dioctylbenzo[3,8]phenanthroline-1,3,6,8(2*H*,7*H*)-tetraone, at reflux, with 4-(diphenylamino)phenyl)boronic acid or benzo[*b*]thiophen-2-ylboronic acid, respectively, in 7:3 (*v*/*v*) dioxane–water as solvent in the presence of K_2CO_3 as base. Both of the materials were purified by column chromatography. The chemical structures of **S6** and **S7** were confirmed by ^{1}H NMR spectroscopy and mass spectrometry, and, where possible (**S7** only), by single crystal XRD. For **S7**, single rod-shaped black crystals were isolated; no crystal growth was observed for **S6**. The crystals of **S7** were subsequently analyzed by single crystal XRD; the results are discussed the section "Structure Geometry and Crystal Chemistry". Both new materials were obtained in moderate to high yield and were highly soluble in a variety of conventional organic solvents, for example chlorobenzene, chloroform, and toluene. The solubility of organic *p*-type materials is an important feature required for fabrication of solution processable OPV devices.

Structure Geometry and Crystal Chemistry

The detailed single-crystal x-ray investigation of **S7** provided conclusive confirmation of the chemical composition and a "symmetric" structure shown in Fig. 1. The oak ridge thermal ellipsoid plot (ORTEP) diagram of **S7** in Fig. 3 shows the coordination environments and numbering schemes used in the tables (for details, see Tables S1 to S3 in the supporting information). The crystal data and data collection conditions are given in Table S1, and selected bond distances and angles are listed in Tables S2 and S3. The NDI core and the aromatic donor rings of **S7** have high coplanarity within themselves, as illustrated by the torsion angles in Table S3. However, there is significant deviation from coplanarity between the NDI core and the donor rings. For example, the torsion angles C3–C9–C15–S2 and C7–C14–C19–S1a are 78.0(1) and 63.6(0) degrees (deg), respectively. The geometry (approximately trigonal), bond lengths, and angles about the branching *n*-octyl and BT substituents at N1 and N2, and at C14 and C9, respectively, are similar, but with greater symmetry observed at N2 (e.g. C1–N2–C27 = C2–N2–C27 = 117.2(3) deg, whereas C12–N1–C35 ≠ C13–N1–C35 (Table S2)). The most key feature is the structural disorder of the BT rings. This disorder is observed more strongly in the S1–C20 ring, with "flipping" of the positions of S1 to S1a and C20 to C20a (occupancies 0.655(4) and 0.345(4), respectively, in both cases). The S2–C16 ring has similar disorder, but with lower occupancy. Indeed, the occupancy is sufficiently low to render further refinement redundant, but the disorder is still apparent in the ADP max/min ratios for C20 and C16.

Intermolecular Interactions and Crystal Packing

Neighboring molecules are connected in a chain-like manner through H-bonding interactions, which occur between the *n*-octyl chains and the NDI core (O4···H32A″–C32″ = 3.605 Å (D–A)/3.637 Å (D–H–A), 163.09 deg; O4···H40B′–C40′ = 3.348 Å (D–A)/3.639 Å (D–H–A), 127.80 deg) (Fig. 4a). Medium to weak hydrogen-bonding interaction[41,42] are also present between the BT rings (C26–H26···C45′ = 3.646 Å (D–A)/3.816 Å (D–H–A), 140.01 deg), and the BT rings and the NDI core (C45–H45···O1′ = 3.372 Å (D–A)/3.396 Å (D–H–A), 164.60 deg; C16–H16···O33′ = 3.263 Å (D–A)/3.485 Å (D–H–A), 133.63 deg; S2···H6′–C6′ = 3.562 Å (D–A)/3.833 Å (D–H–A), 129.35 deg). Additional 3D connectivity of the chains is achieved through perfectly parallel offset-face-to-face (OFF) π–π stacking interactions of the NDI core along the *a*-axis (centroid NDI—plane NDI′ = 3.355 Å (Fig. 4b)), together with edge-to-face (EF) π–π stacking interactions of the benzothiophene substituents (angle between planes: S2–C15–C16–C17–C18–C23–C24–C25–C26 and S1′–C19′–C20′–C21′–C22′–C46′–C45′–C44′–C43′ = 44.26 deg, closest approach between H26–C45′ = 2.866 Å). The overall packing of **S7** can be seen in Fig. S1.

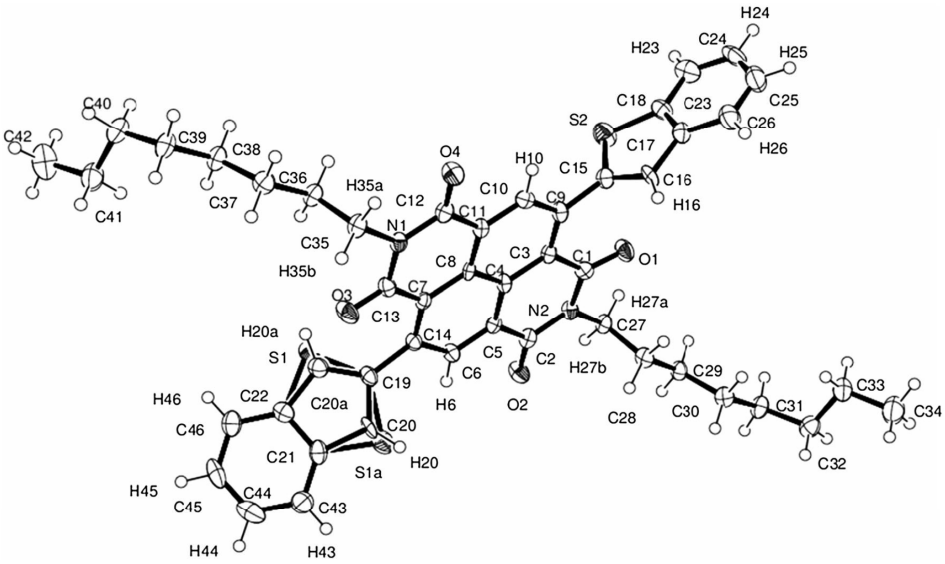

Fig. 3. ORTEP diagram of **S7** showing atom labels (some H atom labels of *n*-octyl chains omitted for clarity), and disorder in the S1–C20 benzothiophene ring.

Optical Properties

The UV–Vis spectral absorptivity of both of the new materials, **S6** and **S7**, were measured in chloroform solution (Fig. 5). Absorption maximum at 618 nm (ε = 8883 M^{-1} cm^{-1}) for **S6** and 487 nm (ε = 7007 M^{-1} cm^{-1}) for **S7** were recorded. A red-shift of the longest wavelength absorption maximum (λ_{max}) and enhancement of the respective extinction coefficient were observed for **S6** in which the TPA donor unit was used. This was in agreement with design principle that the TPA donor unit can act as an energy antenna that is helpful for stronger bathochromic shift, compared with other donor functionality, for example BT. We observed ~26% enhancement of the peak molar absorptivity of **S6** compared with **S7**.

Absorption spectra of **S6** and **S7** in pristine films were also measured by spin-casting their films from chloroform solution (equimolar solutions of **S6** and **S7** spun at 2000 rpm for 1 min) (Fig. 6). Generally, the absorption spectrum of a thin film is bathochromically shifted compared with the solution spectrum of same compound, and we found the same observation for both the materials reported in this study. The spectra of **S6** and **S7** were red shifted by approx. 27 nm and 45 nm compared with the respective solution spectra. It was observed that use of the TPA donor can help to enhance the film absorption profile of a given chromophore that can lead to greater light harvesting on its surface during the process of photo-excitation.

Energy Levels

Theoretical density functional theory (DFT) calculations by use of the Gaussian 09 software suite[43] and the B3LYP/6-311 + G(d,p)//B3LYP/6-31G(d) level of theory indicated that HOMO → LUMO excitation moves the orbital density distribution from the donor functionality to the NDI core unit (Fig. 7). The HOMO densities of **S6** and **S7** resided typically over the donor functionality. It was further realized that use of a TPA energy antenna in **S6** improves the electron-donating ability. LUMO orbital densities received a sizable contribution from the NDI core unit. This spatially directed separation of HOMO and LUMO densities is an ideal condition for ICT between donor and acceptor structures.

Experimentally, HOMO energies of **S6** and **S7** were estimated by use of PESA, and LUMO energies were calculated by adding the optical band gap (band gaps were estimated from the tangent of the edge of longest wavelength in thin solid films) to the HOMO values. PESA measurement of these materials was performed on thin solid films (the same films that were used to measure the absorption spectra) to measure their work functions corresponding to the HOMO levels. On the basis of PESA measurement and UV–Vis spectrometry, it was evident that use of a TPA unit helped to reduce the band gap of **S6** compared with **S7**. The energy band gaps of **S6** and **S7** were all in the range required of donor materials for BHJ devices (the energy level

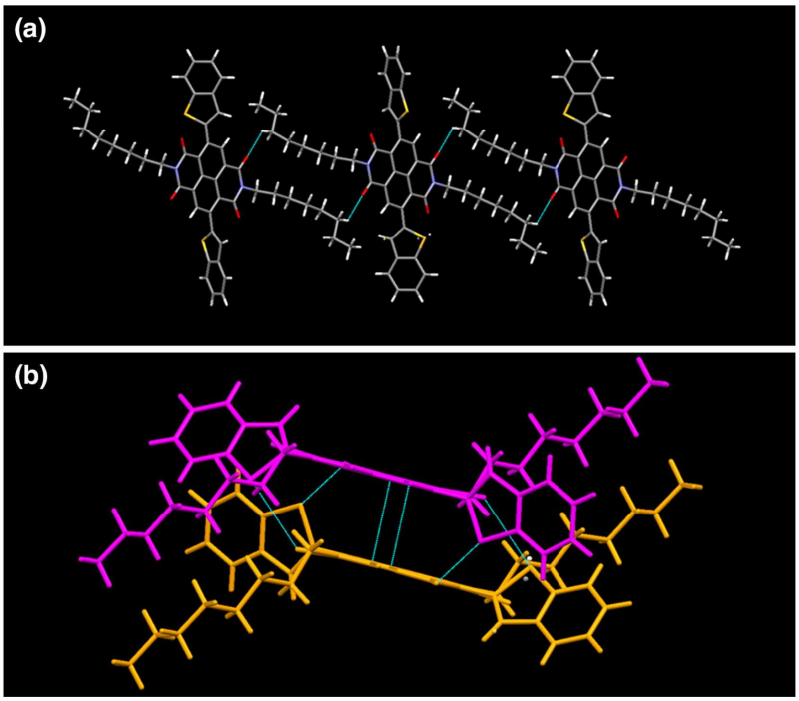

Fig. 4. (a) H-bonding interactions between the *n*-octyl substituents and the NDI core of adjacent **S7** molecules to form a chain along the *b*-axis; (b) OFF π–π interactions between the NDI core of adjacent **S7** molecules.

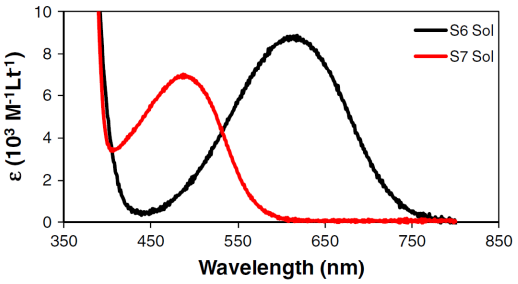

Fig. 5. Molar absorptivity of newly synthesized **S6** and **S7** in chloroform solutions.

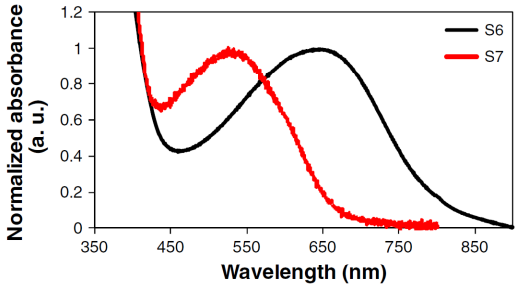

Fig. 6. Normalized UV–Vis absorption spectra of **S6** and **S7** in thin solid films, spin-cast from their chloroform solutions (equimolar solutions of **S6** and **S7** spun at 2000 rpm for 1 min).

diagram is given in Fig. 8). The LUMO of **S7** was less negative as a result of a wider band-gap. The optical and electrochemical properties of all the materials are summarized in Table I.

Photovoltaic Properties

One obvious strategy used to increase conversion efficiency is to narrow the optical band gap of semiconducting materials,[44] to enable absorption of more of the solar spectrum. The energy level diagram (Fig. 8) indicated that **S6** and **S7** have appropriate energy levels, thus making them potential candidates for BHJ devices. Both compounds were used as *p*-type semiconducting components with *n*-type $PC_{70}BM$ in solution processable BHJ devices. BHJ architecture typically delivers higher device power conversion efficiencies by maximizing the surface area of the interface between the donor and acceptor materials in the active layer. We adopted inverted device architecture in our solar

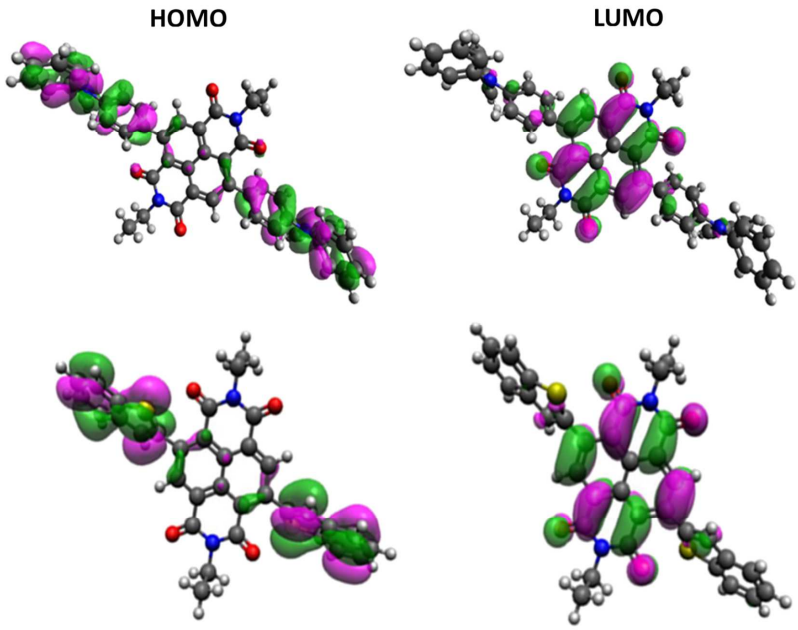

Fig. 7. Orbital density distribution for the HOMOs and LUMOs of **S6** (upper) and **S7** (lower). DFT calculations were performed on all the materials by use of the Gaussian 09 software suite and the B3LYP/6-311 + G(d,p)//B3LYP/6-31G(d) level of theory. (*NOTE:* long alkyl chains present on the NDI unit have been trimmed for DFT calculations because they do not contribute to the molecular electronics but are still an additional burden on the calculating software).

cells, using metal oxide interlayers, for example ZnO and MoO_3, to improve the stability and performance of photovoltaic devices. This device architecture rules out the use of hole-transporting poly(3,4-ethylenedioxythiophene):poly(styrenesulfonate) (PEDOT:PSS), which can be detrimental to the ITO surface because of its strong acidity.

For each individual dye, a series of inverted BHJ devices, with the general structure ITO/ZnO (30 nm)/active layer/MoO_3 (10 nm)/Ag (100 nm), were fabricated by varying the D:A ratio; a suitable ratio was found to be 1:2. In these unoptimized devices, the active layers were fabricated by spin coating the chlorobenzene blend solutions and dried in glove box at room temperature. The film thicknesses were in the approximate range 65–85 nm. Initial screening of the inverted devices, based on **S6**: $PC_{70}BM$, revealed device performance with an open-circuit voltage (V_{oc}) of 0.76 V, a fill factor (FF) of 32%, and a short-circuit current (J_{sc}) of 0.90 mA/cm^2, which resulted in a PCE value of 0.22%. Devices with **S7**: $PC_{70}BM$ as the active layer had a lower V_{oc} of 0.58 V, J_{sc} of 0.40 mA/cm^2, and an overall PCE of 0.10%. A schematic diagram of the BHJ cell with inverted device architecture, and the respective current–voltage (J–V) curves, is shown in Fig. 9. Devices based on compound **S6** had a higher photocurrent than **S7**, a finding that is consistent with the observed red shift in the thin film absorbance for **S6** compared with **S7**. In these initial devices, we used $PC_{70}BM$, because it can enhance absorption in the thin blend film. We envisaged use of a high-boiling solvent, chlorobenzene, to limit the formation of large crystals, which could be a problem in the manufacture of small molecular semiconductors.

We also investigated the blend film morphology by use of atomic force microscopy (AFM) in its tapping mode. Figure 10 shows the topographic and phase images of 1:2 blends of **S6** and **S7**. AFM images of the active layers of devices based on **S6** and **S7** show film surfaces are fairly smooth, with root mean square surface roughness of ~0.33 nm and ~0.35 nm respectively. This homogenous morphology with minimum phase separation may account for the observed low conversion efficiencies and suggests poor formation of interpenetrating networks of donor and acceptor blend.[45] In addition, relatively low values of the fill factors suggests that insufficient hole mobility may be involved in the limited conversion efficiency of the cells. To gain insight into the effective charge carrier mobilities in active blends, we examined the field effect mobility, $\mu_{e,h}$, of charge carriers in devices fabricated, by use of **S6** and **S7**, from their corresponding OFETs (details are given in the section "Experimental Procedures"). We were unable to measure either of the blend mobility, being $\leq 10^{-7}$ cm^2/Vs. We only found the hole mobilities of the order of $\sim 10^{-6}$ cm^2/Vs for both **S6** and **S7** in their pristine states. These

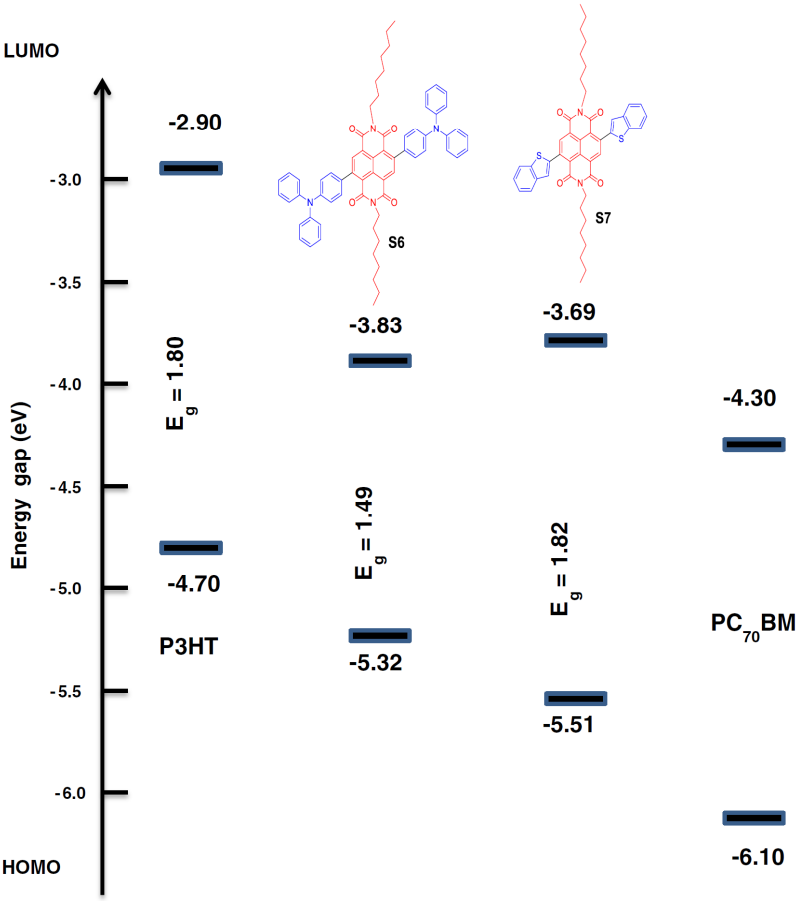

Fig. 8. Energy level diagram depicting the band gaps of **S6** and **S7** in comparison with P3HT.

Table I. Comparative optical and electrochemical properties of S6 and S7

Material	Absorption (solution) λ^{a}_{max}/ onset/nm [ε/($M^{-1}cm^{-1}$)]	Absorption (film) λ^{b}_{max}/ onset/nm	E_{HOMO} (eV[c])	$E_{bandgap}$ (eV[d])	E_{LUMO} (eV[e])
S6	618/750 [8883]	645/830	−5.32	1.49	−3.83
S7	487/570 [7007]	532/680	−5.51	1.82	−3.69

[a]Absorption spectra were measured in chloroform solution.[b]Absorption spectra of thin solid film spin-cast (equimolar solutions of S6 and S7 were spun at 2000 rpm for 1 min) from chloroform solutions.[c]HOMO levels of the *p*-type materials were measured using PESA on thin solid films on glass.[d]Energy band gaps were estimated from the tangent of the edge of longest wavelength in thin solid films.[e]LUMO levels were calculated from the optical band gaps (film) and HOMO levels ($E_{LUMO} = E_{bandgap} + E_{HOMO}$).

observed values of $\leq 10^{-6}$ cm^2/Vs confirm the limited charge transport properties of these donor materials.

Taken as a whole, this study revealed that PCE can be seen as one aspect of the designed molecular structure. The optoelectronic properties of these new D–A–D modular "symmetrical" organic molecules are quite different, depending on donor functionality. Although the materials reported in this study achieved moderate conversion efficiencies,

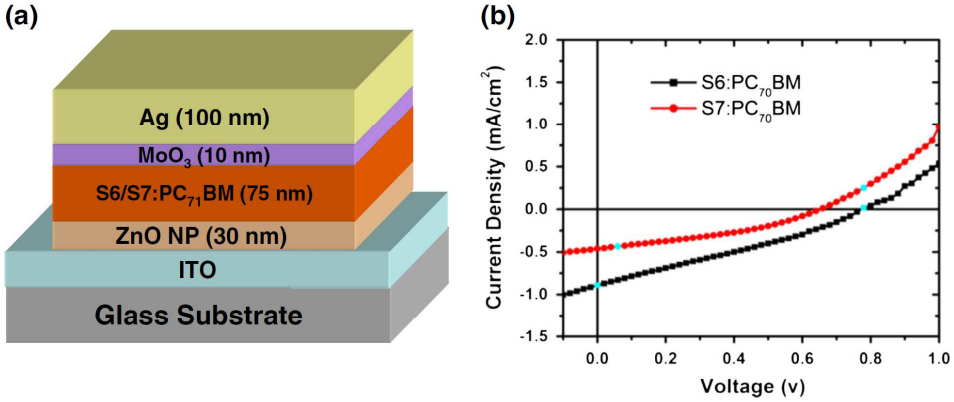

Fig. 9. (a) Schematic diagram of BHJ cell with inverted device architecture; (b) J_{sc}–V_{oc} curves of **S6**/**S7**: $PC_{70}BM$-based BHJ solar cells.

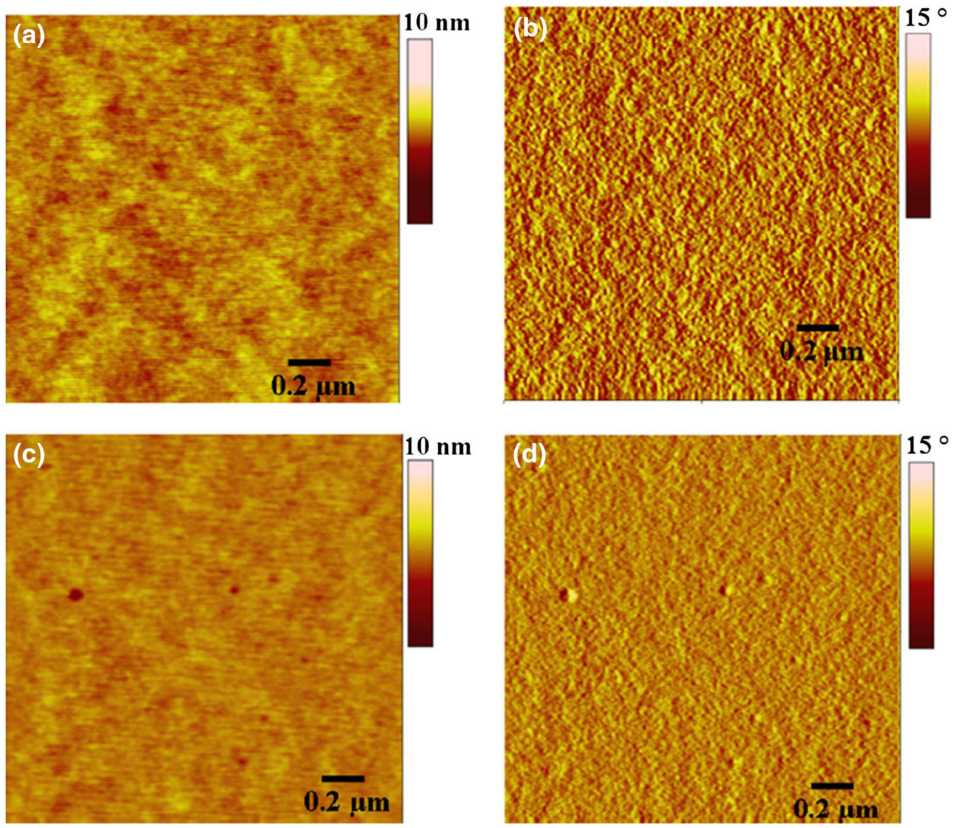

Fig. 10. AFM images of 1:2 blend films of **S6** and **S7** with $PC_{70}BM$ as spun-cast from chlorobenzene solution. Topographic images: (a) as-cast, RMS ~0.33 nm of **S6** and (c) as-cast, RMS ~0.35 nm of **S7**. Phase images: (b) as-cast for **S6** and (d) as-cast for **S7**.

the discovery of such materials with promising optoelectronic properties might lead to the development of such structures based on the central NDI functionality and to the use of such materials for other organic electronic applications, for example light-emitting diodes and field-effective transistors.

CONCLUSIONS

In conclusion, we have demonstrated the use of NDI accepting functionality to generate new D–A–D modular small organic molecules that contain a common NDI core unit and different donor functionality. We have shown that use of a D–A–D structure with the NDI central core can furnish a material with suitable optoelectronic properties that are viable for BHJ device architecture. The new materials **S6** and **S7** were synthesized, found to be highly soluble in a variety of organic solvents, and used as *p*-type semiconducting components with *n*-type $PC_{70}BM$ in solution-processable inverted BHJ photovoltaic devices. Use of a TPA donor unit helped to achieve a substantial red-shift of the absorption maximum in the visible region and, in devices, resulted in a higher photocurrent compared with devices based on a BT unit. Devices based on **S6**, in which a TPA donor unit was used, were more efficient than devices based on **S7**, in which a BT donor unit was used. These preliminary results strongly suggest that use of an NDI acceptor unit with different donor units might lead to new materials based on the D–A–D structure. Work is in progress to further improve device performance; future studies will focus on use of "unsymmetrical" donor functionality and incorporation of π-spacers between donor and acceptor functionality. Our results suggest that changing the design structure can be of crucial importance in achieving new organic materials for OPV devices. Further research is needed to develop the D–A–D module with the NDI acceptor core to furnish high-performing materials for OPV and OFET applications.

ACKNOWLEDGEMENTS

H.P. acknowledges the assistance of Dr. Jegadesan Subbiah from Bio21 Institute, University of Melbourne, VIC 3010, for providing support and guidance during the fabrication of OPV devices. S.V.B. acknowledges financial support from the Australian Research Council under a Future Fellowship Scheme (FT110100152) and the School of Applied Sciences (RMIT University) for the facilities. The CSIRO Materials Science and Engineering (CMSE) is acknowledged for providing support through a visiting fellow position (A.G.). A.B. thanks CSIRO for support through the Julius Career Award. Use of the NCI National Facility supercomputers at the ANU is gratefully acknowledged.

ELECTRONIC SUPPLEMENTARY MATERIAL

The online version of this article (doi:10.1007/s11664-014-3243-x) contains supplementary material, which is available to authorized users.

REFERENCES

1. S. Günes, H. Neugebauer, and N.S. Sariciftci, *Chem. Rev.* 107, 1324 (2007).
2. B.C. Thompson and J.M.J. Frechet, *Angew. Chem. Int. Ed.* 47, 58 (2008).
3. C.W. Tang, *Appl. Phys. Lett.* 48, 183 (1986).
4. A. Facchetti, *Chem. Mater.* 23, 733 (2011).
5. P.-L.T. Boudreault, A. Najari, and M. Leclerc, *Chem. Mater.* 23, 456 (2011).
6. A. Gupta, S.E. Watkins, A.D. Scully, ThB Singh, G.J. Wilson, L.J. Rozanski, and R.A. Evans, *Synth. Met.* 161, 856 (2011).
7. C.J. Brabec, S. Gowrisanker, J.J.M. Halls, D. Laird, S. Jia, and S.P. Williams, *Adv. Mater.* 22, 3839 (2010).
8. D. Gendron and M. Leclerc, *Energy Environ. Sci.* 4, 1225 (2011).
9. B. Walker, C. Kim, and T.-Q. Nguyen, *Chem. Mater.* 23, 470 (2011).
10. Y. Li, Q. Guo, Z. Li, J. Pei, and W. Tian, *Energy Environ. Sci.* 3, 1427 (2010).
11. J.E. Anthony, *Chem. Mater.* 23, 583 (2011).
12. A. Mishra and P. Bäuerle, *Angew. Chem. Int. Ed.* 51, 2020 (2012).
13. J. Huang, C. Zhan, X. Zhang, Y. Zhao, Z. Lu, H. Jia, B. Jiang, J. Ye, S. Zhang, A. Tang, Y. Liu, Q. Pei, and J. Yao, *ACS Appl. Mater. Interfaces* 5, 2033 (2013).
14. S. Zhang, B. Jiang, C. Zhan, J. Huang, X. Zhang, H. Jia, A. Tang, L. Chen, and J. Yao, *Chem. Asian J.* 8, 2407 (2013).
15. A. Tang, L. Li, Z. Lu, J. Huang, H. Jia, C. Zhan, Z. Tan, Y. Li, and J. Yao, *J. Mater. Chem. A* 1, 5747 (2013).
16. J. Chen and Y. Cao, *Acc. Chem. Res.* 42, 1709 (2009).
17. Y.-J. Cheng, S.-H. Yang, and C.-S. Hsu, *Chem. Rev.* 109, 5868 (2009).
18. J. Zhou, X. Wan, Y. Liu, Y. Zuo, Z. Li, G. He, G. Long, W. Ni, C. Li, X. Su, and Y. Chen, *J. Am. Chem. Soc.* 134, 16345 (2012).
19. N.M. Kronenberg, M. Deppisch, F. Wurthner, H.W.A. Lademann, K. Deing, and K. Meerholz, *Chem. Commun.* 48, 6489 (2008).
20. A. Gupta, A. Ali, A. Bilic, M. Gao, K. Hegedus, B. Singh, S.E. Watkins, G.J. Wilson, U. Bach, and R.A. Evans, *Chem. Commun.* 48, 1889 (2012).
21. A. Gupta, V. Armel, W. Xiang, G. Fanchini, S.E. Watkins, D.R. MacFarlane, U. Bach, and R.A. Evans, *Tetrahedron* 69, 3584 (2013).
22. A. Gupta, A. Ali, B. Singh, A. Bilic, U. Bach, and R.A. Evans, *Tetrahedron* 38, 9440 (2012).
23. R.J. Kumar, Q.I. Churches, J. Subbiah, A. Gupta, A. Ali, R.A. Evans, and A.B. Holmes, *Chem. Commun.* 49, 6552 (2013).
24. A.B. Tamayo, X.-D. Dang, B. Walker, J. Seo, T. Kent, and T.-Q. Nguyen, *Appl. Phys. Lett.* 94, 103301 (2009).
25. B. Walker, A.B. Tamayo, X.-D. Dang, P. Zalar, J.H. Seo, A. Garcia, M. Tantiwiwat, and T.-Q. Nguyen, *Adv. Funct. Mater.* 19, 1 (2009).
26. Z. Li, Q. Dong, Y. Li, B. Xu, M. Deng, J. Pei, J. Zhang, F. Chen, S. Wen, Y. Gao, and W. Tian, *J. Mater. Chem.* 21, 2159 (2011).
27. Q. Shi, P. Cheng, Y. Li, and X. Zhan, *Adv. Energy Mater.* 2, 63 (2012).
28. P.V. Bedworth, Y. Cai, A. Jen, and S.R. Marder, *J. Org. Chem.* 61, 2242 (1996).
29. N. Tirelli, S. Amabile, C. Cellai, A. Pucci, L. Regoli, G. Ruggeri, and F. Ciardelli, *Macromolecules* 34, 2129 (2001).
30. P.F. Xia, X.J. Feng, J. Lu, S.-W. Tsang, R. Movileanu, Y. Tao, and M.S. Wong, *Adv. Mater.* 20, 4810 (2008).
31. S.V. Bhosale, C. Jani, and S. Langford, *Chem. Soc. Rev.* 37, 331 (2008).
32. C.-C. Lin, M. Velusamy, H.-H. Chou, J.T. Lin, and P.-T. Chou, *Tetrahedron* 66, 8629 (2010).
33. Y. Lin, Y. Li, and X. Zhan, *Chem. Soc. Rev.* 41, 4245 (2012).
34. C.N. McEwen, R.G. McKay, and B.S. Larsen, *Anal. Chem.* 77, 7826 (2005).

35. SHELXS97 and SHELXL97, Programs for the Refinement of Crystal Structures, University of Göttingen, Göttingen, Germany, 1997.
36. SHELXTL, Version 6.12, Bruker AXS Inc., Madison, Wisconsin, 2001.
37. I.J. Bruno, J.C. Cole, P.R. Edgington, M.K. Kessler, C.F. Macrae, P. McCabe, J. Pearson, and R. Taylor, *Acta Crystallogr. Sect. B* 58, 389 (2002).
38. S.V. Bhosale, M.B. Kalyankar, S.V. Bhosale, S.J. Langford, E.F. Reid, and C.F. Hogan, *New J. Chem.* 33, 2409 (2009).
39. G. Sarasqueta, K.R. Choudhury, J. Subbiah, and F. So, *Adv. Funct. Mater.* 21, 167 (2003).
40. H. Tian, X. Yang, J. Cong, R. Chen, J. Liu, Y. Hao, A. Hagfeldt, and L. Sun, *Chem. Commun.* 41, 6288 (2009).
41. G.A. Jeffrey, *An Introduction to Hydrogen Bonding* (New York: Oxford University, 1997).
42. G.R. Desiraju and T. Steiner, *The Weak Hydrogen Bond* (In Structural Chemistry and Biology: Oxford University, Chichester, 1999).
43. M.J. Frisch, G.W. Trucks, H.B. Schlegel, G.E. Scuseria, M.A. Robb, J.R. Cheeseman, G. Scalmani, V. Barone, B. Mennucci, G.A. Petersson, H. Nakatsuji, M. Caricato, X. Li, H.P. Hratchian, A.F. Izmaylov, J. Bloino, G. Zheng, J.L. Sonnenberg, M. Hada, M. Ehara, K. Toyota, R. Fukuda, J. Hasegawa, M. Ishida, T. Nakajima, Y. Honda, O. Kitao, H. Nakai, T. Vreven, J.A. Montgomery Jr., J.E. Peralta, F. Ogliaro, M. Bearpark, J.J. Heyd, E. Brothers, K.N. Kudin, V.N. Staroverov, R. Kobayashi, J. Normand, K. Raghavachari, A. Rendell, J.C. Burant, S.S. Iyengar, J. Tomasi, M. Cossi, N. Rega, J.M. Millam, M. Klene, J.E. Knox, J.B. Cross, V. Bakken, C. Adamo, J. Jaramillo, R. Gomperts, R.E. Stratmann, O. Yazyev, A.J. Austin, R. Cammi, C. Pomelli, J.W. Ochterski, R.L. Martin, K. Morokuma, V.G. Zakrzewski, G.A. Voth, P. Salvador, J.J. Dannenberg, S. Dapprich, A.D. Daniels, Ö Farkas, J.B. Foresman, J.V. Ortiz, J. Cioslowski, and D.J. Fox, *Gaussian 09*, *Revision D.01* (Wallingford, CT: Gaussian Inc., 2013).
44. F. Padinger, R.S. Rittberger, and N.S. Sariciftci, *Adv. Funct. Mater.* 13, 85 (2003).
45. J. Subbiah, K.R. Choudhury, S. Ellinger, J.R. Reynolds, and F. So, *IEEE J. Sel. Top. Quantum Electron.* 16, 1792 (2010).

Experimental Part

XRD data of S7

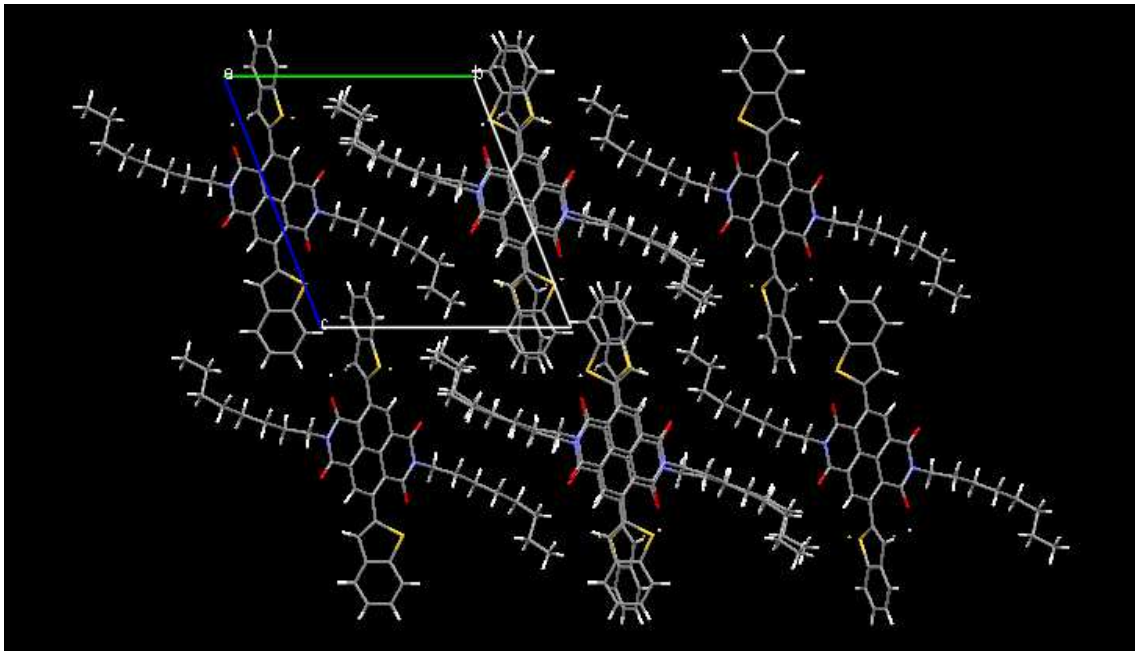

Fig. S1. Packing of **S7** viewed along *a*-axis: 2-D H-bonded molecular chains, connected in 3-D to form layers as a result of π-π stacking interactions.

Table S1. Crystallographic data, experimental details and results of structure refinement for **S7**.

Chemical formula	C46 H46 N2 O4 S2
Formula Mass	754.97
Crystal system	Triclinic
Space group	*P*-1
No. of formula units per unit cell, *Z*	2
a / Å	9.434(5)
b / Å	14.460(7)
c / Å	15.359(8)

α / °	67.256(9)
β / °	80.356(11)
γ / °	76.618(10)
Unit cell volume / Å	1872.7(17)
D_x [g sm^{-3}]	1.339
Temperature / K	150(2)
Crystal description	rod, black
Sample size [mm]	0.404 x 0.057 x 0.049
Diffractometer	Bruker APEX II CCD
Scan mode	ϕ and ω
Radiation type, λ / Å	MoKα, 0.71073 (graphite monochromators)
Correction for absorption	On the crystal shape
Absorption coefficient, μ/mm	0.191
T_{max}, T_{min}	0.991, 0.987
θ max [°]	23.8826
h, k, l ranges	-11 ≤ *h* ≥ 10 -18 ≤ *k* ≥ 18 -19 ≤ *l* ≥ 19
No. of reflections measured	23181
No. of independent reflections	7953
R_{int}	0.1328
Final R_1 values ($I > 2sigma(I)$)	0.0730
Final $wR(F^2)$ values ($I > 2sigma(I)$)	0.1420
Final R_1 values (all data)	0.2009
Final $wR(F^2)$ values (all data)	0.1881
Goodness of fit on F^2	

	0.961

Table S2. Selected bond lengths and angles for **S7**.

	Bond Length (Å)		**Bond Angle (°)**
N1 - C12	1.389(5)	C13 - N1 - C35	116.6(3)
N1 - C13	1.390(5)	C12 - N1 - C35	118.9(3)
N1 - C35	1.475(5)	C12 - N1 - C13	124.5(4)
N2 - C2	1.388(5)	C1 - N2 - C27	117.2(3)
N2 - C1	1.394(5)	C2 - N2 - C27	117.2(3)
N2 - C27	1.475(5)	C2 - N2 - C1	125.4(4)
C6 - C14	1.420(6)	C7 - C14 - C6	117.3(4)
C7 - C14	1.395(6)	C6 - C14 - C19	115.9(4)
C14 - C19	1.473(5)	C7 - C14 - C19	126.8(4)
C3 - C9	1.379(6)	C3 - C9 - C10	117.8(4)
C10 - C9	1.408(6)	C10 - C9 - C15	115.6(4)
C9 - C15	1.481(6)	C3 - C9 - C15	126.6(4)
S2 - C18	1.720(5)	S2 - C15 - C9	118.8(3)
S2 - C15	1.739(4)	C18 - S2 - C15	91.3(2)
S1 - C19	1.764(3)	C14 - C19 - S1	120.0(2)
S1 - C22	1.702(4)	C22 - S1 - C19	89.0(2)
S1A - C19	1.764(3)	C14 - C19 - S1A	115.8(3)
S1A - C21	1.701(4)	C21 - S1A - C19	86.9(2)

Spectra of S6

FTIR

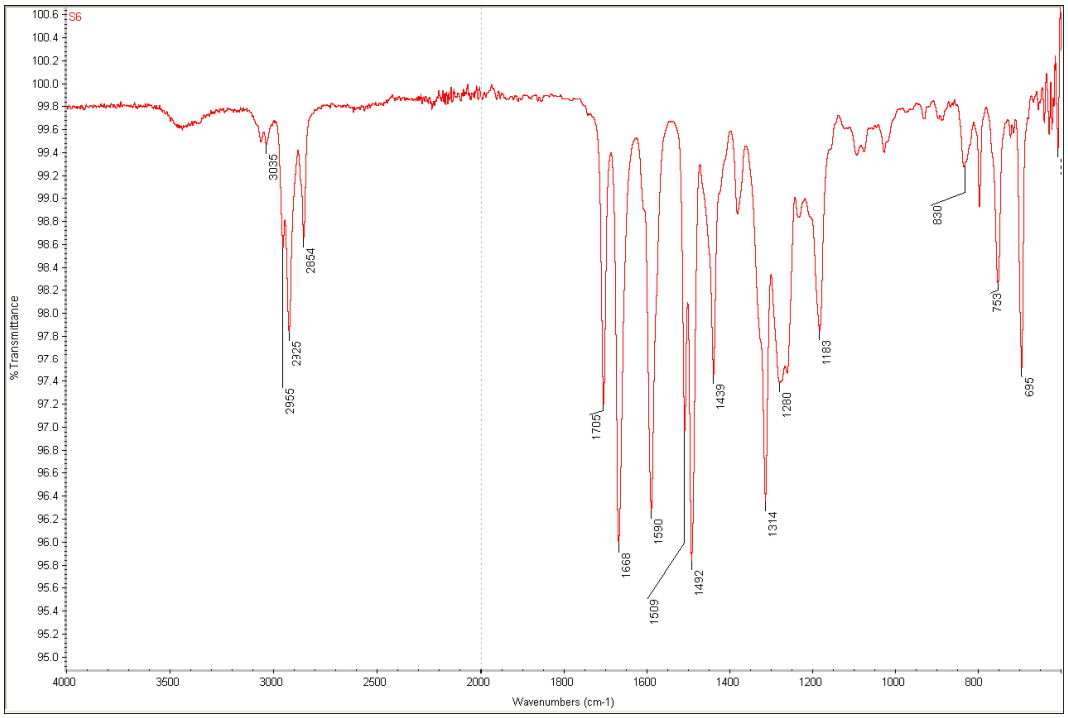

^{1}H NMR

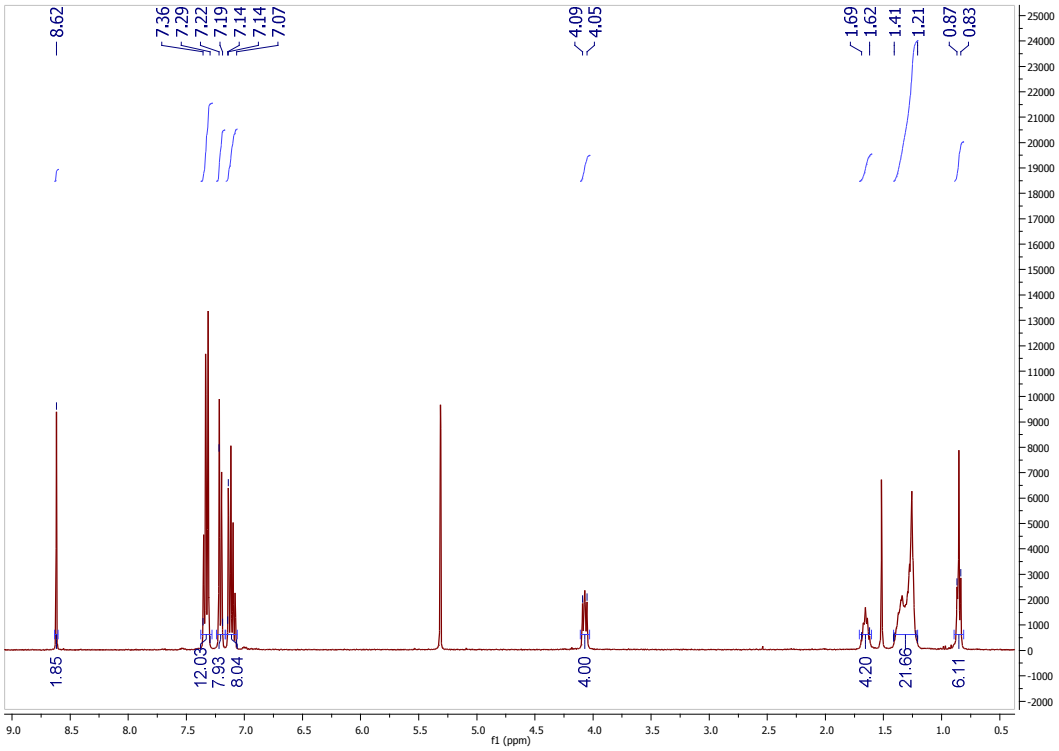
8.62
7.36
7.29
7.22
7.19
7.14
7.14
7.07
4.09
4.05
1.69
1.62
1.41
1.21
0.87
0.83
1.85
12.03
7.93
8.04
4.00
4.20
21.66
6.11
f1 (ppm)

^{13}C NMR

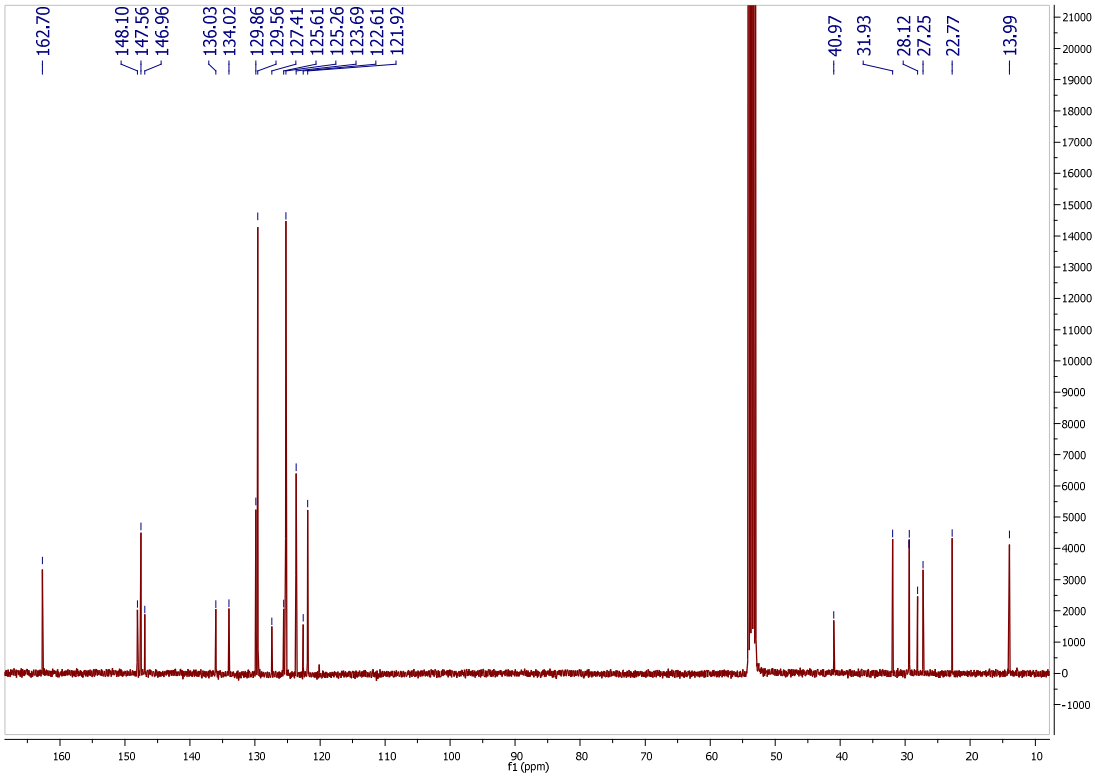
162.70
148.10
147.56
146.96
136.03
134.02
129.86
129.56
127.41
125.61
125.26
123.69
122.61
121.92
40.97
31.93
28.12
27.25
22.77
13.99
f1 (ppm)

HRMS

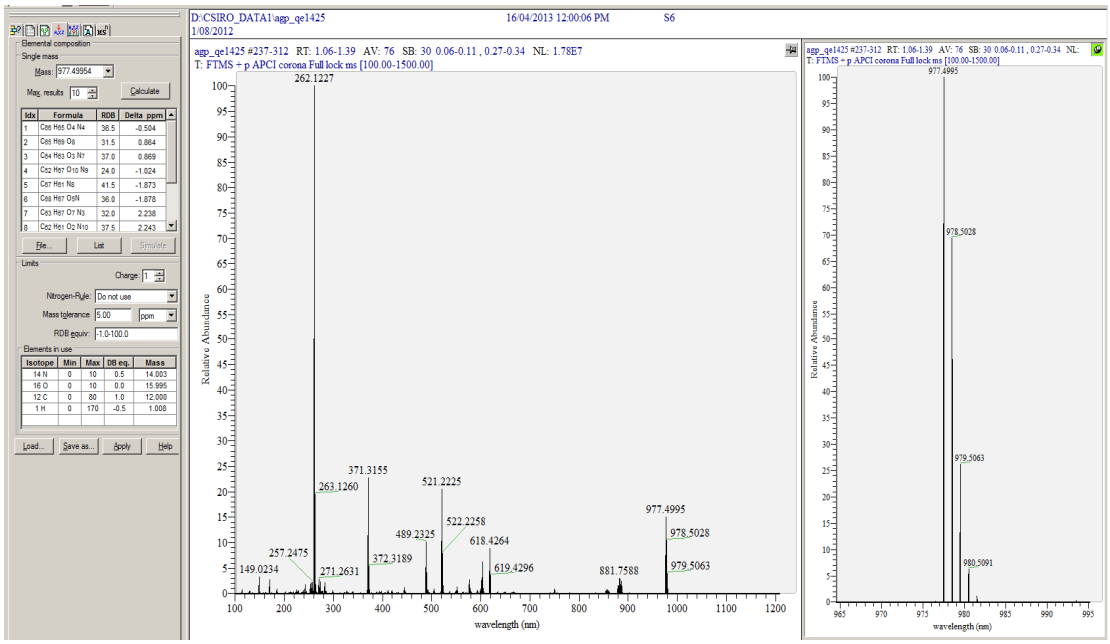

$[M+H]^+$

m/z	Theo. Mass	Delta (ppm)	Composition
977.4995	**977.5000**	**-0.50**	**C66 H65 O4 N4**
	977.4987	0.86	C65 H69 O8
	977.4987	0.87	C64 H63 O3 N7
	977.5005	-1.02	C52 H67 O10 N9
	977.5014	-1.87	C67 H61 N8
	977.5014	-1.88	C68 H67 O5 N
	977.4974	2.24	C63 H67 O7 N3
	977.4973	2.24	C62 H61 O2 N10
	977.5027	-3.25	C69 H63 O N5
	977.4960	3.61	C61 H65 O6 N6

Spectra of S7

FTIR

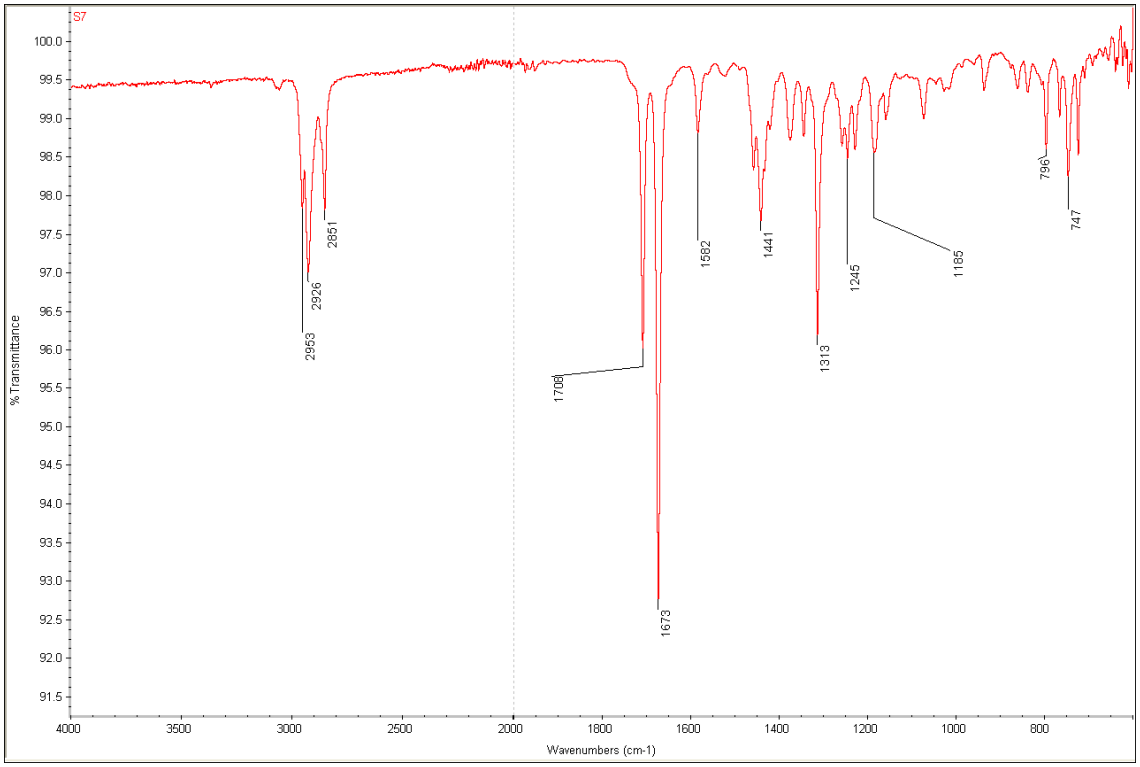

^{1}H NMR

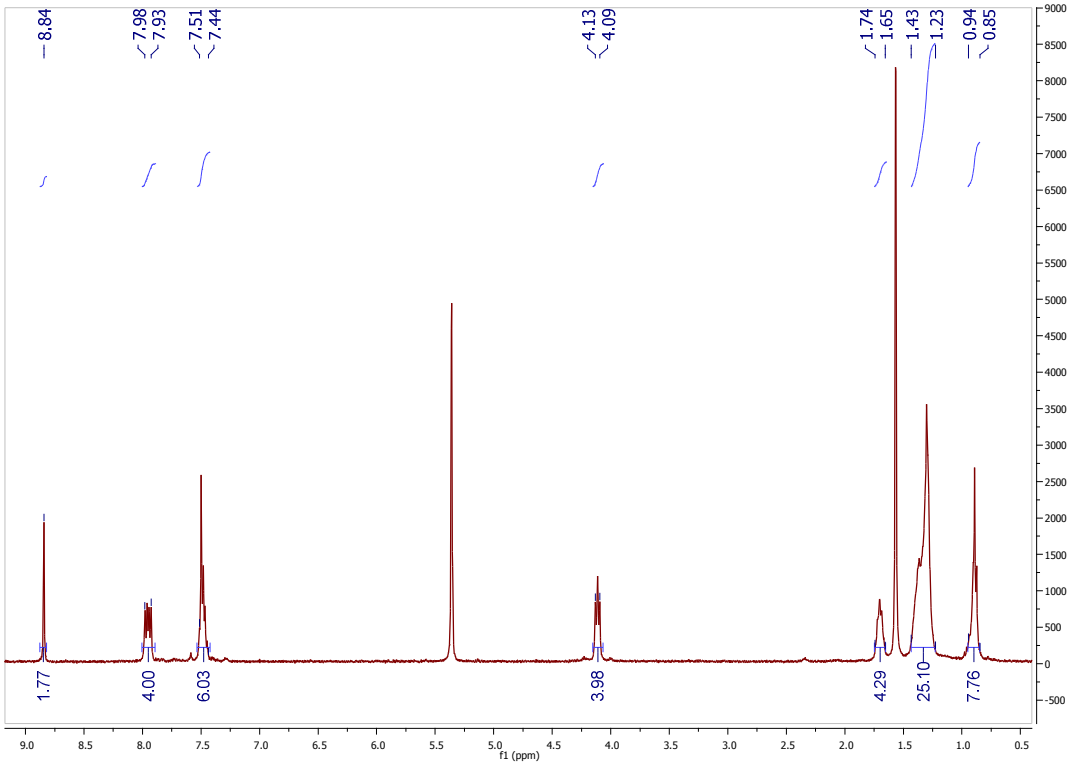
8.84
7.98
7.93
7.51
7.44
4.13
4.09
1.74
1.65
1.43
1.23
0.94
0.85
1.77
4.00
6.03
3.98
4.29
25.10
7.76
f1 (ppm)

^{13}C NMR

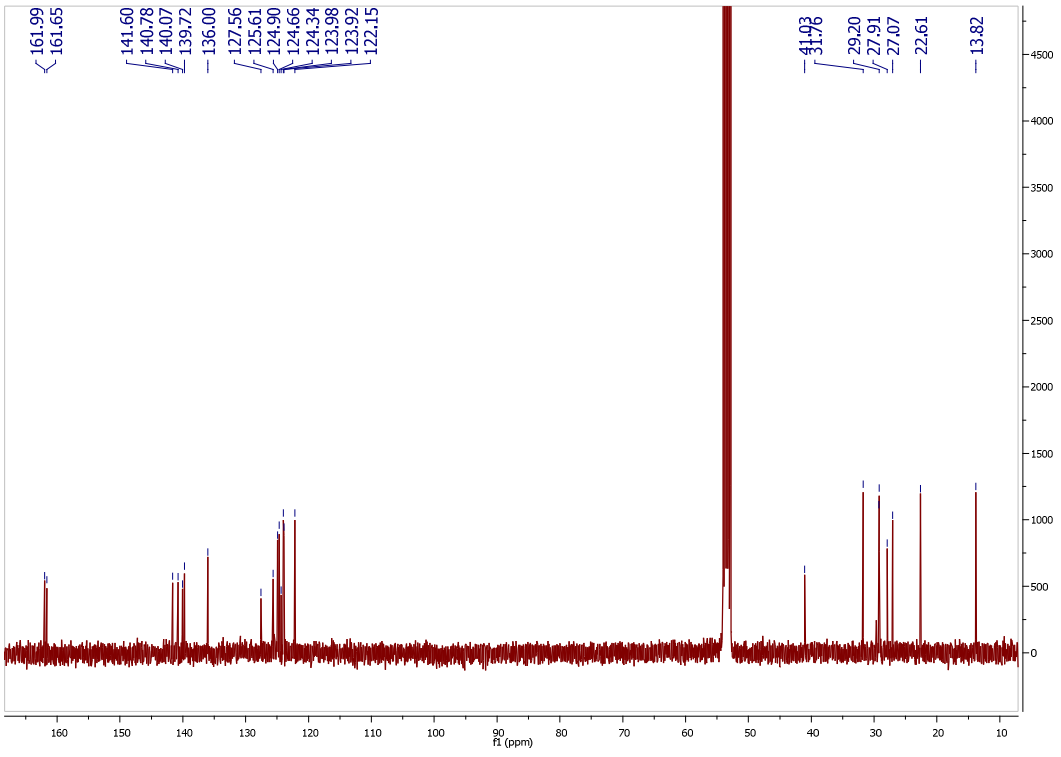
161.99
161.65
141.60
140.78
140.07
139.72
136.00
127.56
125.61
124.90
124.66
124.34
123.98
123.92
122.15
41.03
31.76
29.20
27.91
27.07
22.61
13.82
f1 (ppm)

HRMS

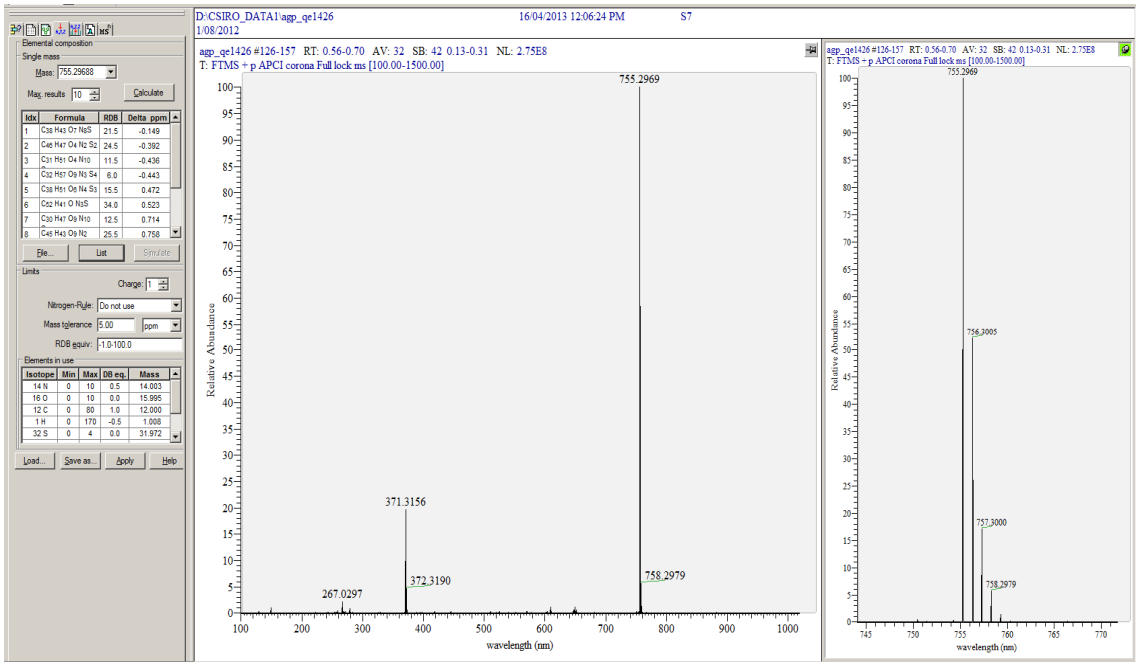

$[M+H]^+$

m/z	Theo. Mass	Delta (ppm)	Composition
755.2969	755.2970	-0.15	C38 H43 O7 N8 S
	755.2972	**-0.39**	**C46 H47 O4 N2 S2**
	755.2972	-0.44	C31 H51 O4 N10 S4
	755.2972	-0.44	C32 H57 O9 N3 S4
	755.2965	0.47	C38 H51 O6 N4 S3
	755.2965	0.52	C52 H41 O N3 S
	755.2963	0.71	C30 H47 O9 N10 S2
	755.2963	0.76	C45 H43 O9 N2
	755.2963	0.77	C44 H37 O4 N9
	755.2976	-1.01	C46 H39 O5 N6

Chapter 5

Conjoint use of dibenzosilole and indan-1, 3-dione functionalities to prepare an efficient non-fullerene acceptor for solution-processable bulk-heterojunction devices

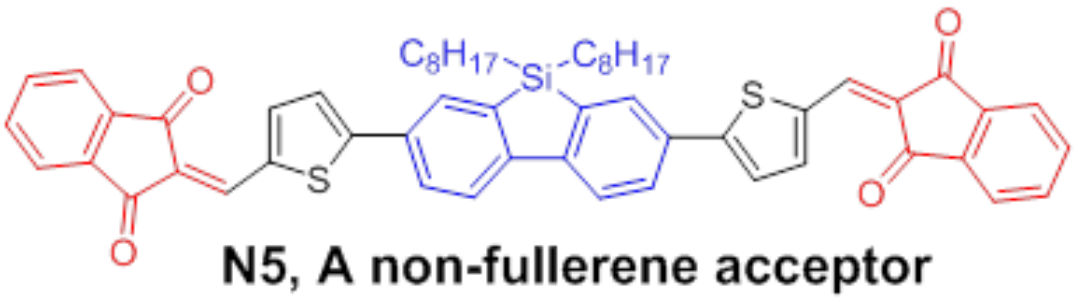

N5, A non-fullerene acceptor

ITO/P3HT:N5 (1:1)/Ca/Al
PCE: 2.76%

Journal article accepted for publication in *Asian J. Org. Chem.* presented as **Chapter 5**

ASIAN JOURNAL
OF ORGANIC CHEMISTRY

Accepted Article

Title: Conjoint use of dibenzosilole and indan-1,3-dione functionalities to prepare an efficient non-fullerene acceptor for solution-processable bulk-heterojunction devices

Authors: Sheshanath V. Bhosale; Hemlata Patil; Akhil Gupta; Ben Alford; Di Ma; Steven H Privér; Ante Bilic; Prashant Sonar

To be cited as: Asian J. Org. Chem. 10.1002/ajoc.201500207

Link to VoR: http://dx.doi.org/10.1002/ajoc.201500207

Supported by:

ChemPubSoc Europe

WILEY-VCH

An ACES journal

ACES

DOI: 10.1002/ajoc.201500207

ASIAN JOURNAL OF ORGANIC CHEMISTRY
Full Paper

Non-Fullerene Organic Solar Cells

Conjoint use of Dibenzosilole and Indan-1,3-dione Functionalities to Prepare an Efficient Non-Fullerene Acceptor for Solution-Processable Bulk-Heterojunction Solar Cells

Hemlata Patil,[a] Akhil Gupta,*[a] Ben Alford,[a] Di Ma,[b] Steven H. Privér,[a] Ante Bilic,[c] Prashant Sonar,[d] and Sheshanath V. Bhosale*[a]

Abstract: A solution-processable, non-fullerene electron acceptor, 2,2′-(((5,5-dioctyl-5*H*-dibenzo[*b*,*d*]silole-3,7-diyl)bis-(thiophene-5,2-diyl))bis(methanylylidene))bis(1*H*-indene-1,3(2*H*)-dione) (called **N5**) comprised of dibenzosilole and 1,3-indanedione building blocks was designed, synthesized, and fully characterized. **N5** is highly soluble in various organic solvents, has high thermal stability, and has energy levels matching those of archetypal donor poly(3-hexylthiophene). Solution-processable, bulk-heterojunction solar cells afforded promising power conversion efficiency of 2.76% when **N5** was used as a non-fullerene electron acceptor along with the conventional donor polymer poly(3-hexylthiophene). As per our knowledge, the material reported herein is the first example in the literature where synchronous use of such building blocks is demonstrated in the design an efficient, non-fullerene acceptor.

Introduction

There is significant attention towards the design and development of new organic semiconductors for organic photovoltaic (OPV) devices. OPV devices are divided into two major types; one is bilayer and the other is bulk-heterojunction (BHJ) device type. In the bilayer devices, two distinct electron donor and acceptor layers are deposited on top of each other between the electrodes, whereas in BHJ devices, an active photon absorbing layer is a bicontinuous, interpenetrating network of an electron donor and an electron acceptor.[1] The most examined and widely accepted BHJ system is a blend of donor polymer poly(3-hexylthiophene) (P3HT) and solubilized fullerene derivative [6,6]-phenyl C_{61} butyric acid methyl ester ($PC_{61}BM$) as an acceptor. From the materials perspective, considerable research has been done on the design and development of polymeric as well as small-molecule donors,[2–6] but for electron acceptors, there is limited number of materials reported in the literature.

Power conversion efficiencies (PCEs) have surpassed the 10% mark because of the development of donors and fullerene acceptors;[7] however, PCEs linger around 3% for non-fullerene acceptors,[8–22] albeit reports from Holliday et al., Zhao et al., and Lin et al. displayed over 4% and 6% PCEs with the use of P3HT and non-P3HT donors.[23–26] Although the PCEs of devices based on non-fullerene acceptors are moving upwards and various research groups are trying to achieve big numbers, it is vital to mention that, in order to make these acceptors viable for practical applications, one must consider their foremost suitability with easily synthesizable and commercially available donors such as P3HT. This requirement is a great challenge for an organic chemist to investigate new building blocks which can potentially be used for the design and development of non-fullerene acceptors. In this paper, we describe a small-molecule electron acceptor and demonstrate that union of carefully selected building blocks can be used to generate promising, non-fullerene, electron-accepting chromophores.

With regard to conventional photoactive acceptors, $PC_{61}BM$ or $PC_{71}BM$ are the acceptors of choice mainly due to their inherent properties, such as high electron affinity, high electron mobility, good solubility, ability to form a favorable nanoscale network with donor materials, and isotropy of charge transport.[27] However, these high-performing and versatile acceptors are afflicted with a number of shortcomings, such as the lack of electronic tuning via structural modification, weak absorption in the visible spectrum, and high electron affinity that can result in low open-circuit voltage (V_{oc}) of BHJ devices.[28] To

[a] H. Patil, Dr. A. Gupta, Dr. B. Alford, Dr. S. H. Privér, Dr. S. V. Bhosale
School of Applied Sciences
RMIT University
GPO Box 2476, Melbourne Victoria 3001 (Australia)
E-mail: sheshanath.bhosale@rmit.edu.au
akhilgk15@gmail.com

[b] Dr. D. Ma
College of Material Science and Engineering
Beijing University of Chemical Technology
Beijing 100029 (China)

[c] Dr. A. Bilic
CSIRO Manufacturing, Virtual Nanoscience Lab
Parkville Victoria 3052 (Australia)

[d] Dr. P. Sonar
School of Chemistry, Physics and Mechanical Engineering
Queensland University of Technology
GPO Box 2434, Brisbane QLD 4001 (Australia)

Supporting information for this article is available on the WWW under http://dx.doi.org/10.1002/ajoc.201500207.

understand and solve these problems, electron acceptor materials should be designed by considering crucial factors, such as strong and broad absorption, adequate solubility, and appropriate energy levels. Recently, non-fullerene electron acceptors have been explored, and reviews by Sonar et al. and Lin and Zhan highlight the key examples of their development.[29,30]

Even though the advancement of non-fullerene acceptors is noteworthy, incentives remain to develop materials which will not only have better properties than fullerenes, but will also have imperative characteristics such as solubility and matching energy levels with donors. One strategy to design such materials is the conjoint use of donor and acceptor functionalities that can be arranged in a meaningful manner to generate an elongated conjugated system. Inspired by the recent use of versatile donor and acceptor building blocks,[9,13,14,16,23,31,32] functionalities such as dibenzosilole (DBS) and 1,3-indanedione (IDO) were identified as potentially suitable electron-donor and electron-deficient templates in order to generate a target chromophore that can have elongated conjugation, thermal and photochemical stability, and high solubility.

Herein we report the design, synthesis, and characterization of the optoelectronic and photovoltaic properties of a small-molecule, non-fullerene electron acceptor, 2,2′-(((5,5-dioctyl-5*H*-dibenzo[*b*,*d*]silole-3,7-diyl)bis(thiophene-5,2-diyl))bis(methanylylidene))bis(1*H*-indene-1,3(2*H*)-dione) (**N5**; Figure 1), based

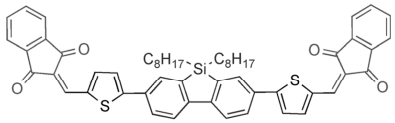

N5

Figure 1. Molecular structure of the newly designed, synthesized, and characterized non-fullerene electron acceptor **N5**.

on DBS and IDO building blocks. Replacement of carbon with silicon, that is, from fluorene to DBS, is an interesting chemical modification that has been studied with keenness, as silole derivatives can also have electron-transporting properties.[33] The DBS unit in particular is a kind of silole-containing fused ring that has been used in DBS-based polymers, and such polymers have shown promising performance in organic electronic devices such as light-emitting diodes,[34] field-effect transistors,[35] and solar cells.[36] However, to our knowledge, there are very limited reports on DBS-based materials as non-fullerene acceptors.[9] This state of affairs inspired us and provided an opportunity to investigate the use of DBS-based chromophores, and we were able to envision **N5**.

By designing and developing **N5** we were able to demonstrate that **N5**, when blended with P3HT in solution-processable BHJ solar cells, can deliver promising PCE that approaches 3%, and that the BHJ devices based on the combination of DBS/IDO building blocks perform better than devices based on the combination of fluorine/IDO blocks. To our knowledge, there are no reports on the conjoint use of DBS and IDO building blocks to generate a non-fullerene electron acceptor for solution-processable BHJ devices. The present work is a continuation of our efforts on the design and development of small-molecule chromophores for organic electronic devices.[37–40]

Result and Discussion

Synthesis

Compound **N5** was successfully synthesized via Suzuki coupling of 9,9-dioctyl-9*H*-9-silafluorene-2,7-bis(boronic acid pinacol ester) with 5-bromothiophene-2-aldehyde followed by a Knoevenagel condensation reaction with 2,3-dihydro-1*H*-indene-1,3-dione (Scheme 1). **N5** was obtained as a red crystal-

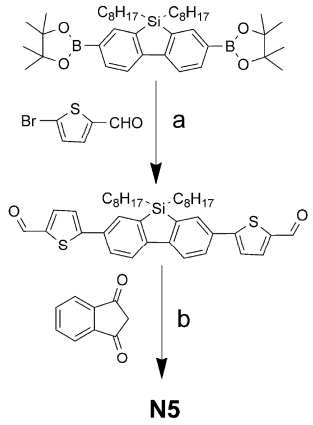

N5

Scheme 1. Synthetic route to **N5**. Reagents and conditions: a) $Pd(PPh_3)_4$, dimethoxyethane, 2 M Na_2CO_3, N_2, RT, 12 h, 73%; b) *t*BuOH/piperidine, reflux, 12 h, 72%.

line material in 72% yield, and the synthetic route to **N5** was simple, facile, and viable for generating >5 g of product. **N5** was fully characterized by high-resolution mass spectrometry, ^1H and ^{13}C NMR spectroscopy, and X-ray crystallography. The molecular structure of **N5**, obtained as a dichloromethane solvate, is shown in Figure 2 (see also Figure S1 and Table S1 in the Supporting Information). In general, the measured parameters for **N5** are comparable to those of the closely related structure in which the silicon atom was replaced by carbon.[32] As expected, the Si–C bonds in **N5** are ca. 1.2 times longer than the corresponding C–C in the C-analogue and the geometry about the silicon atom is distorted tetrahedral. Notably, the C1-Si1-C21 angle is significantly smaller (91.00(11)°) than the corresponding angle in the C-analogue (99.8(2)°), presumably to accommodate the larger silicon atom, while the C1-Si1-C41 angle is significantly larger (117.25(12)° vs 110.5(2)°). In the solid state, stacking of the indan-1,3-dione moieties with neighboring molecules takes place, the intermolecular separation being about 3.4 Å; the C-analogue also behaves similarly.

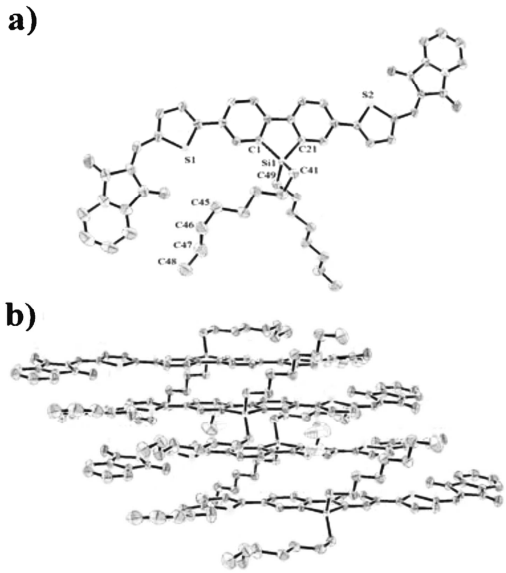

Figure 2. (a) Molecular structure of $C_{56}H_{54}O_2S_2Si{\cdot}CH_2Cl_2$ (**N5**·CH_2Cl_2). Ellipsoids show 50% probability levels. Hydrogen atoms and disordered dichloromethane of solvation have been omitted for clarity. The alkyl chain at C45–C48 was disordered over two positions and only the major orientation (0.8342) is shown. (b) Molecular packing in the crystal of **N5**. CCDC 1048201 (**N5**) contains the supplementary crystallographic data for this paper. These data are provided free of charge by The Cambridge Crystallographic Data Centre

N5 was found to be highly soluble in a variety of common organic solvents, such as dichlorobenzene, toluene, and chloroform (for instance, $>20\ mg\,mL^{-1}$ in *o*-dichlorobenzene). High solubility is a vital feature required for the fabrication of small-molecule organic semiconductors, and **N5** being adequately soluble fulfils this criterion. Thermogravimetric analysis (TGA) and differential scanning calorimetry (DSC) analyses revealed that the thermal stability of **N5** is excellent (decomposition temperature ca. 393 °C from DSC analysis), a finding that is supported by the fact that P3HT:**N5** devices can be thermally annealed (for TGA and DSC curves, please see Figure S2 in the Supporting Information).

The UV/vis spectra of **N5** measured in chloroform solution and in thin solid films are shown in Figure 3. In solution, the longest wavelength absorption maximum (λ_{max}) of **N5** was at 492 nm with an absorbance onset at around 560 nm. Film spectra were measured on cleaned glass substrates. Generally, for a given compound, the thin film absorption spectrum will be bathochromically shifted compared with its solution spectrum. In this study, the film spectrum of **N5** was also bathochromically shifted, and this result is in good agreement with the literature reported materials.[37,40] The λ_{max} was red-shifted in the pristine state and the spectrum was broadened over the visible range. The latter was also true for the absorption of a blend P3HT:**N5**.

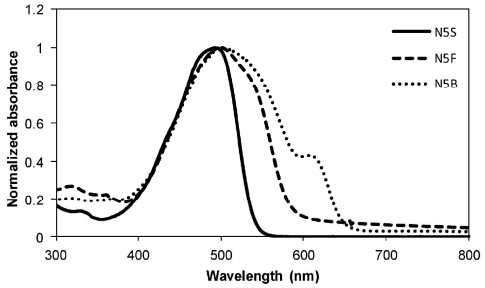

Figure 3. UV/vis absorption spectra of **N5** in chloroform solution (**N5** S; solid curve), as-casted pristine film (**N5** F; dashed curve) and 1:1 blend with P3HT (**N5** B; dotted curve).

The fluorescence quenching ability of **N5** blended with P3HT was investigated to measure its potential utility as an electron acceptor for photovoltaic application. The fluorescence quenching measurement can provide valuable insight about the ability of donor-acceptor interface to dissociate excitons. The blend film of P3HT:**N5** (1:1 w/w) quenched fluorescence (Figure S3 in the Supporting Information), a finding that is in agreement with the literature reported non-fullerene acceptors.[14]

Density functional theory (DFT) calculations using the Gaussian 09 suite of programs[41] and B3LYP/6-311+G(d,p)//B3LYP/6-31G(d) level of theory indicated that orbital densities are evenly distributed over the whole molecular backbone, a result that is quite usual with small-molecule non-fullerene acceptors (see Figure 4).[14,32] Based on the DFT calculations it was further realized that the torsional angle between the two wings (from thiophene to the end) and the central DBS block was as large as 23.7°. These two wings were mutually parallel, as shown in Figure S4 in the Supporting Information, giving the molecule a non-planar structure overall, which matched with the crystallographic data.

Holliday et al.[23] have shown that structures with a hint of non-planarity can perform better than their planar counterparts. As such, the highest occupied molecular orbital (HOMO) and lowest unoccupied molecular orbital (LUMO) energy levels

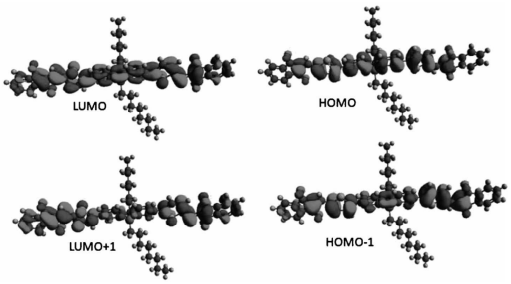

Figure 4. Orbital density distribution for the HOMOs and LUMOs of **N5**. DFT calculations were performed using the Gaussian 09 suite of programs and B3LYP/6-311+G(d,p)//B3LYP/6-31G(d) level of theory.

were estimated using a combination of photoelectron spectroscopy in air (PESA) and UV/vis spectroscopy on thin films. The HOMO energy level was estimated as −5.71 eV and the LUMO energy level was calculated using the onset of UV/vis absorbance (600 nm) of **N5**. The HOMO value of **N5** was low mainly due to the presence of two electron-withdrawing IDO groups at the terminals. The LUMO energy level of **N5** is around −3.64 eV, which indicates its apparent suitability to be an electron acceptor in conjunction with a P3HT donor (for energy level diagram and PESA curve, please see Figure 5 and Figure S5 in the Supporting Information, respectively). The LUMO level of **N5** is higher than the literature reported fluorene analogue (−3.75 eV),[32] which is beneficial for achieving high V_{oc}.

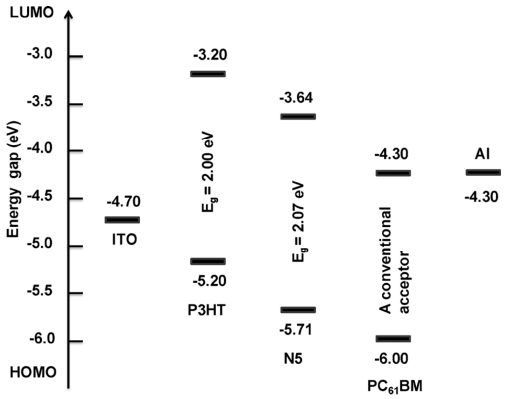

Figure 5. Energy level diagram depicting the band gaps of **N5** compared with P3HT and a conventional $PC_{61}BM$ acceptor.

As **N5** had promising optical and electrochemical properties, we decided to fabricate solution-processable BHJ devices using **N5** as an acceptor. The BHJ devices were fabricated using the classical donor polymer P3HT as it has the potential to be generated via low cost and high throughput methods.[42] For comparison, we also fabricated P3HT:$PC_{61}BM$ devices under similar conditions. Simple device architecture was chosen due to stability, reproducibility, ease of fabrication, and solution processability. The BHJ device architecture used was indium-tin oxide (ITO)/poly(3,4-ethylenedioxythiophene) polystyrene sulfonate (PEDOT:PSS, 38 nm)/active layer (58 nm)/Ca (20 nm)/Al (100 nm) where the active layer was a 1:1 blend of P3HT:**N5**, spin-cast from *o*-dichlorobenzene on top of the PEDOT:PSS surface.

Kim et al.,[31] Lin et al.,[15] and Patil et al.[10] have shown that thermal annealing of devices incorporating small-molecule non-fullerene acceptors and use of high boiling solvents, such as *o*-dichlorobenzene, during the fabrication of photovoltaic devices is beneficial for higher current density and optimal cell performance. Keeping such conditions in mind, we used *o*-dichlorobenzene as the processing solvent and annealed our blend films at 110 °C for 5 min. The performance of the preliminary BHJ devices based on the blends of P3HT:**N5** was promising and photovoltaic cell parameters; V_{oc}, short circuit current density (J_{sc}), fill factor (FF), and PCE, reached 0.78 V, 7.61 mA cm^{-2}, 0.46, and 2.76%, respectively. In contrast, the maximum PCE, V_{oc}, and J_{sc} reached 2.85%, 0.61 V and 7.91 mA cm^{-2}, respectively, for a device based on P3HT:$PC_{61}BM$ when fabricated under similar conditions, thus suggesting the reliability of our device strategy (Figure S6 in the Supporting Information). The **N5** fabricated devices (a total of six devices were made) yielded high V_{oc}, a finding that is in agreement with the measured optical band gap between the LUMO of **N5** and the HOMO of P3HT. The obtained V_{oc} was higher than the literature reported fluorene-IDO-based devices,[32] hence, this confirms the better positioning of HOMO and LUMO of **N5** and supports the use of the DBS/IDO combination.

It was also shown that annealing of active films at higher temperatures, for example at 120 °C, resulted in minor cracks to film surfaces and poor photovoltaic performance. The former was particularly true when low boiling solvent, such as chloroform, was used, hence justifying the literature recommendation of using high boiling solvent.[14,31] The use of high-boiling solvent is further preferable from a processing point of view. It is also notable that all the devices afforded PCE > 2.5% and the reported results are for the best photovoltaic device. It is worth mentioning that even though the PCEs with the use of non-fullerene acceptors are surging,[23–26] the DBS-based acceptors still straggle in design, development, and efficiency.[30] Having said that, the design and development of **N5** provided a PCE among the top values reported in the literature for DBS-based chromophores,[28,29] thus advocating the conjoint use of electron-donating and electron-accepting building blocks, of which DBS and IDO are favorable examples, in order to generate a highly conjugated chromophore as an interesting structural concept for the design and development of non-fullerene acceptors. A representative current-voltage (*J-V*) curve is shown in Figure 6.

Incident-photon-to-current conversion efficiency (IPCE) measurement of the blend film with a donor-acceptor weight ratio of 1:1 is shown in Figure S7 in the Supporting Information. Broad spectrum IPCE over the whole visible region indicated

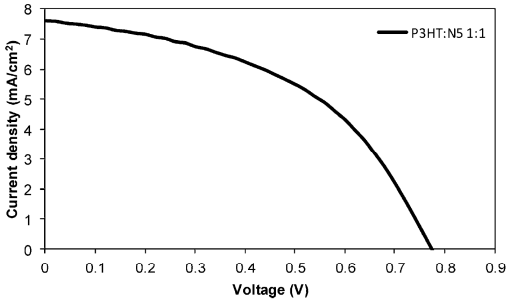

Figure 6. Current-voltage curve for the best device based on an **N5** and P3HT blend (1:1 w/w) under simulated sunlight (AM1.5, 1000 W m^{-2}). Device structure was ITO/PEDOT:PSS (38 nm)/active layer (58 nm)/Ca (20 nm)/Al (100 nm).

that both donor and acceptor components in the BHJ blend have participated for drawing out the IPCE and J_{sc}. The IPCE value for P3HT:**N5** device reached a maximum of approximately 25% at around 550 nm. We also observed that the IPCE of **N5** active device was slightly red-shifted compared with its absorption spectrum. This slight bathochromic shift can be attributed to either uneven surface morphology or film thickness at an incident point on the blend surface. Such divergent variations in solution-processable thin film devices are also common in similar types of photochemical cells where multiple conducting surfaces are coated on top of each other.[43] However, in view of this broad IPCE, good optical profile, and appropriately positioned energy levels, it is anticipated that **N5** can also be a suitable acceptor for other electron-donating, low-band gap, conjugated polymers and small-molecule solids.

Microstructure analysis of the P3HT:**N5** blend surface deposited on ITO coated glass was examined by conventional atomic force microscopy (AFM) in tapping mode. The actual surface morphology of the blend film of P3HT:**N5** (1:1 w/w) is shown in Figure 7. The blend appears to have crystalline grains

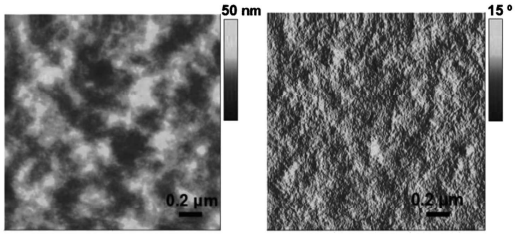

Figure 7. AFM image for the blend film of P3HT:**N5** annealed at 110 °C for 5 min (10 mg P3HT, 10 mg **N5** in 1 mL *o*-dichlorobenzene, 2000 rpm).

with a root-mean-square (RMS) roughness of 1.2 nm. Though the crystalline grains may be a result of P3HT self-organization, a finding that is beneficial to ordered structure formation and charge transport in thin film,[44] an interpenetrating network of donor-acceptor components was observed which can be beneficial to exciton dissociation and charge-carrier transport, and can result in enhanced efficiency of the photovoltaic devices. This network of the conventional donor (P3HT) and acceptor ($PC_{61}BM$) components was found to be superior than **N5**, hence the device current and PCE were better (for the AFM image of P3HT:$PC_{61}BM$ device, please see Figure S8 in the Supporting Information). Although the efficiency of our best performing device is among the top values reported in literature for the DBS-based, non-fullerene chromophores, we achieved lower values of FF. The lower value of FF can be attributed to the imbalance of hole and electron mobilities of donor and acceptor components used in the blend. The hole and electron mobilities were measured using transistor devices and the values for electron and hole were measured in the range of 10^{-6} and 10^{-4} respectively. Higher hole mobility indicated that the presence of **N5** does not disrupt the hole-rich P3HT, a result consistent with blend film absorption (strong shoulder peak over 600 nm).

Despite the fact that research for non-fullerene electron acceptors is surging, this work clearly demonstrates the possibility of achieving promising PCE in terms of design, chemistry, and efficacy. Not only does it demonstrate that careful selection of versatile building blocks and their union is vital for the development of non-fullerene acceptors, but it also advocates the advantages of simple and smart chemistry that is achievable by rational design.

Conclusions

In summary, a solution-processable, highly conjugated chromophore, **N5**, was designed and developed as an electron acceptor for organic solar cells. The thermal stability of **N5** is excellent, the absorption strong and broad, the energy levels appropriate for matching with those of the classical donor polymer P3HT. The blend film of P3HT:**N5** is a good nanoscale interpenetrating network with a broad spectrum IPCE over the visible range and PCE as high as 2.76%, which is among the highest values reported so far for the solution-processable BHJ devices using DBS-based non-fullerene acceptors. Lastly, the P3HT:**N5** device is well-suited to the simple device architecture with no special treatment, which offers advantages over complex device strategies. Evidently, this work demonstrates that small-molecule acceptors, such as **N5**, with promising optoelectronic properties have a bright prospect to be at the leading edge of non-fullerene acceptor research, and bridges the gap between the research fields of donor and acceptor semiconducting materials.

Experimental Section

Chemistry

Materials: All the reagents and chemicals used, unless otherwise specified, were purchased from Sigma–Aldrich Co. The solvents used for reactions were obtained from Merck Specialty Chemicals (Sydney, Australia) and were used as received. 9,9-Dioctyl-9*H*-9-silafluorene-2,7-bis(boronic acid pinacol ester) was purchased from Luminescence Technology Corporation, Taiwan, and was used as received.

Instruments and characterization: Unless otherwise specified, all the NMR spectra were recorded on a Bruker Avance III 300 MHz spectrometer where the residual solvent peaks from the deuterated solvents ($CDCl_3$ ^1H $\delta = 7.26$ ppm, ^{13}C $\delta = 77.0$ ppm) were used as the reference. Chemical shifts (δ) were measured in parts per million (ppm). Thin layer chromatography (TLC) was performed on 0.25 mm thick plates precoated with Merck Kieselgel 60 F254 silica gel, and visualized using UV light (254 nm and 365 nm). Melting points were recorded on a Stuart SMP10 melting point apparatus and are uncorrected. High-resolution mass spectra (HRMS) spectra were recorded on Thermo Scientific Q Exactive FTMS, employing an ASAP probe. All UV/vis absorption spectra were recorded on a Hewlett Packard HP 8453 diode array UV/vis spectrophotometer. Thin films were spin-coated from *o*-dichlorobenzene (*o*-DCB) at a spin speed of 2000 rpm for 1 min onto cleaned glass slides. Fluorescence spectra were recorded on a PerkinElmer LS50B fluorime-

ter. Photoelectron Spectroscopy in air (PESA) measurements were recorded on a Riken Keiki AC-2 PESA spectrometer with a power setting of 5 nW and a power number of 0.5. Samples for PESA were prepared on clean glass substrates.

Device fabrication and characterization of photovoltaic devices, and experimental details for the preparation of thin-film transistors have been reported previously.[37,38] Crystals suitable for single-crystal X-ray diffraction were obtained by layering a CH_2Cl_2 solution of the complex with hexane. X-ray diffraction data were collected on a D8 Bruker diffractometer with an APEX2 area detector using graphite monochromated $Mo_{K\alpha}$ radiation ($\lambda = 0.71073$ Å) from a 1 μS microsource. Geometric and intensity data were collected using SMART software.[45] The data were processed using SAINT[46] and corrections for absorption were applied using SADABS.[47] The structures were solved using direct methods and refined with full-matrix least-squares methods on F^2 using the SHELX-TL package.[48] Selected crystal data and details of data collection and structure refinement are listed in Table S1 in the Supporting Information. In the structure of **N5**, the CH_2Cl_2 molecule of crystallization was disordered over two positions (0.59145) and the displacement ellipsoids and CCl bond lengths were restrained to be equal.

5,5′-(5,5-Dioctyl-5*H*-dibenzo[*b*,*d*]silole-3,7-diyl)bis(thiophene-2-carbaldehyde): To a solution of 2-bromo-5-formylthiophene (0.36 g, 1.90 mmol) in 1,2-dimethoxyethane (25.0 mL) and 1 M sodium carbonate (Na_2CO_3) (25.0 mL) was added 9,9-dioctyl-9*H*-9-silafluorene-2,7-bis(boronic acid pinacol ester) (0.41 g, 0.61 mmol). The mixture was then degassed for 30 min by purging with N_2 before tetrakis(triphenylphosphine)palladium(0) ($Pd(PPh_3)_4$, 55 mg, 0.05 mmol) was added, and the reaction mixture was heated to reflux for 4 h. Upon the consumption of substrates (TLC, 1% MeOH/$CHCl_3$) the yellow solution was allowed to cool to room temperature and water (100 mL) was added. The mixture was then extracted with $CHCl_3$ (3×30 mL) and the combined organic layers were washed with H_2O followed by brine, dried over $MgSO_4$, filtered through a thin pad of $MgSO_4/SiO_2$, and evaporated to yield an oily, yellow residue. The crude product was then crystallized from CH_2Cl_2/*i*PrOH to yield **1** (0.28 g, 73%) as fine yellow crystals; m.p 100–101 °C; ^{1}H NMR (300 MHz, $CDCl_3$): $\delta = 0.84$ (6H, t, $J = 13.6$, 6.8 Hz, 2×CH_3), 1.03 (4H, m, 2×CH_2), 1.30 (24H, m, 2×Si-$(CH_2)_6$), 7.48 (2H, d, $J = 4.0$ Hz, ArH), 7.78 (4H, m, ArH), 7.90 (4H, m, ArH), 9.92 ppm (2H, s, 2×CHO); ^{13}C NMR (75 MHz, $CDCl_3$): $\delta = 12.1$, 14.0, 22.6, 24.0, 29.0, 29.2, 31.8, 33.2, 121.8, 124.0, 128.4, 131.1, 132.2, 137.4, 139.6, 142.3, 148.6, 154.3, 182.7 ppm; IR (neat): $\tilde{\nu} = 2922$ (w), 2851 (w), 1662 (s), 1468 (w), 1433 (w), 1402 (w), 1378 (w), 1224 (m), 1057 (w), 1224 (m), 798 cm^{-1} (s); HRMS (FTMS-ASAP): *m*/*z*: calcd for $C_{38}H_{46}O_2S_2Si$: 626.2703 $[M]^+$; found: 626.2704.

2,2′-(((5,5-Dioctyl-5*H*-dibenzo[*b*,*d*]silole-3,7-diyl)bis(thiophene-5,2-diyl))bis(methanylylidene))bis(1*H*-indene-1,3(2*H*)-dione) (N5): To a solution of 5,5′-(5,5-dioctyl-5*H*-dibenzo[*b*,*d*]silole-3,7-diyl)bis(thiophene-2-carbaldehyde) (0.256 g, 0.41 mmol) in *t*BuOH (50 mL) was added 1,3-indandione (0.176 g, 1.21 mmol) followed by the addition of piperidine (1 mL). The reaction mixture was refluxed for 6 h under a stream of N_2. The dark red solution was then cooled to 50 °C before ethanol (50 mL) was added and the flask was placed in the refrigerator overnight. The crude product was filtered, washed with ethanol, and crystallized from a hot solution of CH_2Cl_2/*i*PrOH to afford **N5** (0.254 g, 72%) as fine, dark red to purple crystals; m.p. 200–201 °C; ^{1}H NMR (300 MHz, $CDCl_3$): $\delta = 0.82$ (6H, t, $J = 13.6$, 6.4 Hz, 2×CH_3), 1.09 (4H, m, 2×CH_2), 1.30 (24H, m, Si-$(CH_2)_6$), 7.56 (2H, d, $J = 4.2$ Hz, ArH), 7.81 (4H, m, ArH), 7.91 (4H, m, ArH), 8.01 (7H, m, ArH), 8.05 ppm (2H, m, 2×methylidene-CH); ^{13}C NMR (75 MHz, $CDCl_3$): $\delta = 12.2$, 14.0, 22.6, 25.3, 29.1, 29.2, 31.8, 33.3, 121.8, 122.7, 123.0, 124.7, 128.5, 131.1, 132.4, 134.8, 135.0, 136.1, 136.6, 139.6, 140.5, 142.0, 143.6, 148.8, 157.3, 189.7, 190.2 ppm; IR (neat): $\tilde{\nu} = 2920$ (w), 2851 (w) 1720 (w), 1676 (s), 1598 (m), 1580 (s), 1564 (s), 1432 (s), 1400 (m), 1372 (w), 1331 (w), 1205 (s), 992 (m), 801 (s), 728 cm^{-1} (s); HRMS (FTMS-ASAP): *m*/*z*: calcd for $C_{56}H_{54}O_4S_2Si$: 882.3227 $[M]^+$; found: 882.3223.

Acknowledgements

S.V.B. (RMIT) acknowledges financial support from the Australian Research Council (ARC), Australia, under a Future Fellowship Scheme (FT110100152). The CSIRO Division of Materials Science and Engineering, Clayton, Victoria, is acknowledged for providing support through a visiting fellow position for A.G.. P.S. is thankful to the ARC Future Fellowship Scheme (FT130101337) at Queensland University of Technology, Brisbane, Queensland.

Keywords: 1,3-indanedione · bulk-heterojunction devices · dibenzosiloles · non-fullerene acceptors · solution processing

[1] C. J. Brabec, S. Gowrisanker, J. J. M. Halls, D. Laird, S. Jia, S. P. Williams, *Adv. Mater.* **2010**, *22*, 3839–3856.
[2] Y. Lin, Y. Li, X. Zhan, *Chem. Soc. Rev.* **2012**, *41*, 4089–4380.
[3] A. Mishra, P. Bäuerle, *Angew. Chem. Int. Ed.* **2012**, *51*, 2020–2067; *Angew. Chem.* **2012**, *124*, 2060–2109.
[4] A. Facchetti, *Chem. Mater.* **2011**, *23*, 733–758.
[5] L. Bian, E. Zhu, J. Tang, W. Tang, F. Zhang, *Prog. Polym. Sci.* **2012**, *37*, 1292–1331.
[6] H. Zhou, L. Yang, W. You, *Macromolecules* **2012**, *45*, 607–632.
[7] J. B. You, L. T. Dou, K. Yoshimura, T. Kato, K. Ohya, T. Moriarty, K. Emery, C. C. Chen, J. Gao, G. Li, Y. Yang, *Nat. Commun.* **2013**, *4*, 1446–1455.
[8] J. T. Bloking, X. Han, A. T. Higgs, J. P. Kastrop, L. Pandey, J. E. Norton, C. Risko, C. E. Chen, J.-L. Brèdas, M. D. McGehee, A. Sellinger, *Chem. Mater.* **2011**, *23*, 5484–5490.
[9] Y. Lin, Y. Li, X. Zhan, *Adv. Energy Mater.* **2013**, *3*, 724–728.
[10] H. Patil, A. Gupta, A. Bilic, S. V. Bhosale, S. V. Bhosale, *Tetrahedron Lett.* **2014**, *55*, 4430–4432.
[11] Y. Lin, Y. Wang, J. Wang, J. Hou, Y. Li, D. Zhu, X. Zhan, *Adv. Mater.* **2014**, *26*, 5137–5142.
[12] P. Cheng, L. Ye, X. Zhao, J. Hou, Y. Li, X. Zhan, *Energy Environ. Sci.* **2014**, *7*, 1351–1356.
[13] H. Patil, W. X. Zu, A. Gupta, V. Chellappan, A. Bilic, P. Sonar, A. Ranana-ware, S. V. Bhosale, S. V. Bhosale, *Phys. Chem. Chem. Phys.* **2014**, *16*, 23837–23842.
[14] A. M. Raynor, A. Gupta, H. Patil, A. Bilic, S. V. Bhosale, *RSC Adv.* **2014**, *4*, 57635–57638.
[15] Y. Lin, P. Cheng, Y. Li, X. Zhan, *Chem. Commun.* **2012**, *48*, 4773–4775.
[16] X. Zhang, Z. Lu, L. Ye, C. Zhan, J. Hou, S. Zhang, B. Jiang, Y. Zhao, J. Huang, S. Zhang, Y. Liu, Q. Shi, Y. Liu, J. Yao, *Adv. Mater.* **2013**, *25*, 5791–5797.
[17] W. Chen, X. Yang, G. Long, X. Wan, Y. Chen, Q. Zhang, *J. Mater. Chem. C* **2015**, *3*, 4698–4705.
[18] W. Chen, T. Salim, H. Fan, Y. M. Lam, Q. Zhang, *RSC Adv.* **2014**, *4*, 25291–25301.
[19] Q. Zhang, J. Xiao, Z. Yin, H. M. Duong, F. Qiao, F. Boey, X. Hu, H. Zhang, F. Wudl, *Chem. Asian J.* **2011**, *6*, 856–862.
[20] Y. Lin, J. Wang, S. Dai, Y. Li, D. Zhu, X. Zhan, *Adv. Energy Mater.* **2014**, *4*, 400420.
[21] H. Bai, Y. Wang, P. Cheng, J. Wang, Y. Wu, J. Hou, X. Zhan, *J. Mater. Chem. A* **2015**, *3*, 1910–1914.
[22] X. Zhan, Z. Tan, B. Domercq, Z. An, X. Zhang, S. Barlow, Y. Li, D. Zhu, B. Kippelen, S. R. Marder, *J. Am. Chem. Soc.* **2007**, *129*, 7246–7247.
[23] S. Holliday, R. S. Ashraf, C. B. Nielsen, M. Kirkus, J. A. Röhr, C.-H. Tan, E. C. Fregoso, A.-C. Knall, J. R. Durrant, J. Nelson, I. McCulloch, *J. Am. Chem. Soc.* **2015**, *137*, 898–904.

[24] J. Zhao, Y. Li, H. Lin, Y. Liu, K. Jiang, C. Mu, T. Ma, J. Y. L. Lai, H. Hu, D. Yu, H. Yan, *Energy Environ. Sci.* **2015**, *8*, 520 – 525.
[25] Y. Lin, Z.-G. Zhang, H. Bai, Y. Yao, Y. Li, D. Zhu, X. Zhan, *Energy Environ. Sci.* **2015**, *8*, 610 – 616.
[26] Y. Lin, Z.-G. Zhang, H. Bai, Y. Li, D. Zhu, X. Zhan, *Adv. Mater.* **2015**, *27*, 1170 – 1174.
[27] Y. He, Y. Li, *Phys. Chem. Chem. Phys.* **2011**, *13*, 1970 – 1983.
[28] R. Y. C. Shin, P. Sonar, P. S. Siew, Z. K. Chen, A. Sellinger, *J. Org. Chem.* **2009**, *74*, 3293 – 3298.
[29] P. Sonar, J. P. F. Lim, K. L. Chan, *Energy Environ. Sci.* **2011**, *4*, 1558 – 1574.
[30] Y. Lin, X. Zhan, *Mater. Horiz.* **2014**, *1*, 470 – 488.
[31] Y. Kim, C. E. Song, S.-J. Moon, E. Lim, *Chem. Commun.* **2014**, *50*, 8235 – 8237.
[32] K. N. Winzenberg, P. Kemppinen, F. H. Scholes, G. E. Collis, Y. Shu, Th. B. Singh, A. Bilic, C. M. Forsyth, S. E. Watkins, *Chem. Commun.* **2013**, *49*, 6307 – 6309.
[33] K. Tamao, M. Uchida, T. Izumizawa, K. Furukawa, S. Yamaguchi, *J. Am. Chem. Soc.* **1996**, *118*, 11974 – 11975.
[34] K. L. Chan, M. J. McKiernan, C. R. Towns, A. B. Holmes, *J. Am. Chem. Soc.* **2005**, *127*, 7662 – 7663.
[35] H. Usta, G. Lu, A. Facchetti, T. J. Marks, *J. Am. Chem. Soc.* **2006**, *128*, 9034 – 9035.
[36] E. Wang, L. Wang, L. Lan, C. Luo, W. Zhuang, J. Peng, Y. Cao, *Appl. Phys. Lett.* **2008**, *92*, 033307.
[37] A. Gupta, A. Ali, A. Bilic, M. Gao, K. Hegedus, B. Singh, S. E. Watkins, G. J. Wilson, U. Bach, R. A. Evans, *Chem. Commun.* **2012**, *48*, 1889 – 1891.
[38] A. Gupta, V. Armel, W. Xiang, G. Fanchini, S. E. Watkins, D. R. MacFarlane, U. Bach, R. A. Evans, *Tetrahedron* **2013**, *69*, 3584 – 3592.
[39] R. J. Kumar, Q. I. Churches, J. Subbiah, A. Gupta, A. Ali, R. A. Evans, A. B. Holmes, *Chem. Commun.* **2013**, *49*, 6552 – 6554.
[40] A. Gupta, A. Ali, T. B. Singh, A. Bilic, U. Bach, R. A. Evans, *Tetrahedron* **2012**, *68*, 9440 – 9447.
[41] Gaussian 09, Revision D.01, M. J. Frisch, G. W. Trucks, H. B. Schlegel, G. E. Scuseria, M. A. Robb, J. R. Cheeseman, G. Scalmani, V. Barone, B. Mennucci, G. A. Petersson, H. Nakatsuji, M. Caricato, X. Li, H. P. Hratchian, A. F. Izmaylov, J. Bloino, G. Zheng, J. L. Sonnenberg, M. Hada, M. Ehara, K. Toyota, R. Fukuda, J. Hasegawa, M. Ishida, T. Nakajima, Y. Honda, O. Kitao, H. Nakai, T. Vreven, J. A. Montgomery, Jr., J. E. Peralta, F. Ogliaro, M. Bearpark, J. J. Heyd, E. Brothers, K. N. Kudin, V. N. Staroverov, R. Kobayashi, J. Normand, K. Raghavachari, A. Rendell, J. C. Burant, S. S. Iyengar, J. Tomasi, M. Cossi, N. Rega, J. M. Millam, M. Klene, J. E. Knox, J. B. Cross, V. Bakken, C. Adamo, J. Jaramillo, R. Gomperts, R. E. Stratmann, O. Yazyev, A. J. Austin, R. Cammi, C. Pomelli, J. W. Ochterski, R. L. Martin, K. Morokuma, V. G. Zakrzewski, G. A. Voth, P. Salvador, J. J. Dannenberg, S. Dapprich, A. D. Daniels, . Farkas, J. B. Foresman, J. V. Ortiz, J. Cioslowski, D. J. Fox, Gaussian, Inc., Wallingford CT, **2013**.
[42] J. H. Bannock, S. H. Krishnadasan, A. M. Nightingale, C. P. Yau, K. Khaw, D. Burkitt, J. J. M. Halls, M. Heeney, J. C. de Mello, *Adv. Funct. Mater.* **2013**, *23*, 2123 – 2129.
[43] W. Xiang, A. Gupta, M. K. Kashif, N. Duffy, A. Bilic, R. A. Evans, L. Spiccia, U. Bach, *ChemSusChem* **2013**, *6*, 256 – 260.
[44] G. Li, V. Shrotriya, J. Huang, Y. Yao, T. Moriarty, K. Emery, Y. Yang, *Nat. Mater.* **2005**, *4*, 864 – 868.
[45] SMART version 5.625 software for the CCD Detector System, Bruker AXS Inc., Madison, WI, **2001**.
[46] SAINTPLUS version 6.22 software for the CCD Detector System, Bruker AXS Inc., Madison, WI, **2001**.
[47] SADABS program for absorption correction using SMART CCD data based on the method of Blessing: R. H. Blessing, *Acta Crystallogr. Sect. A* **1995**, *51*, 33.
[48] G. M. Sheldrick, SHELXTL, version 6.10, University of Göttingen, Germany, **1994**.

Manuscript received: June 3, 2015
Accepted article published: July 25, 2015
Final article published: ■■ ▮▮, 0000

Experimental Part

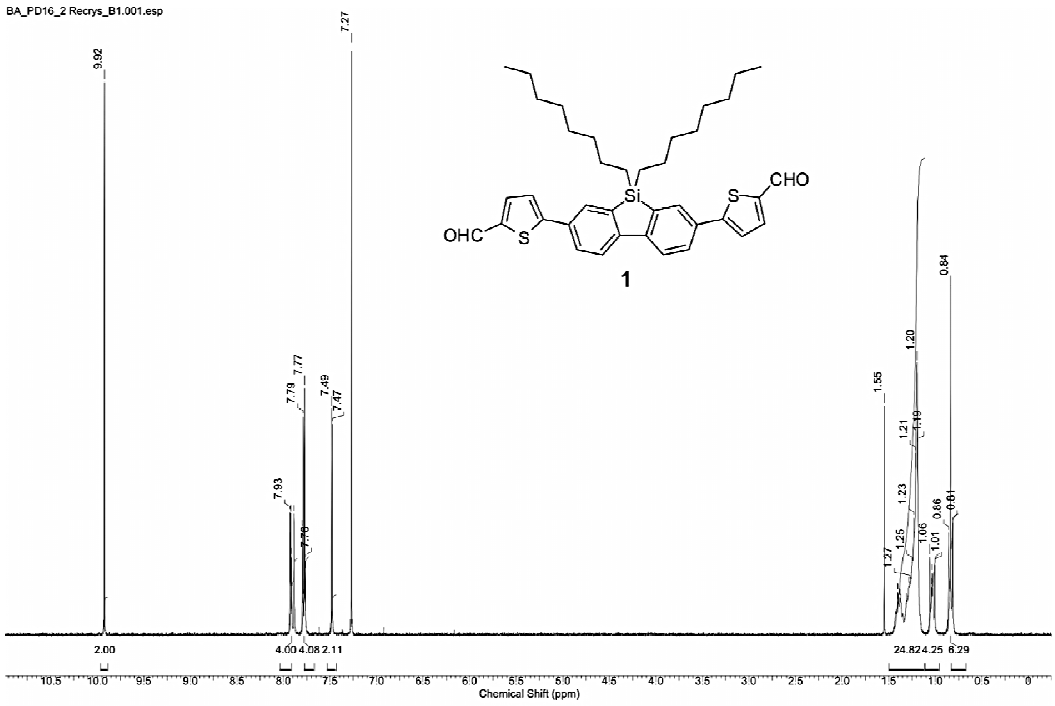

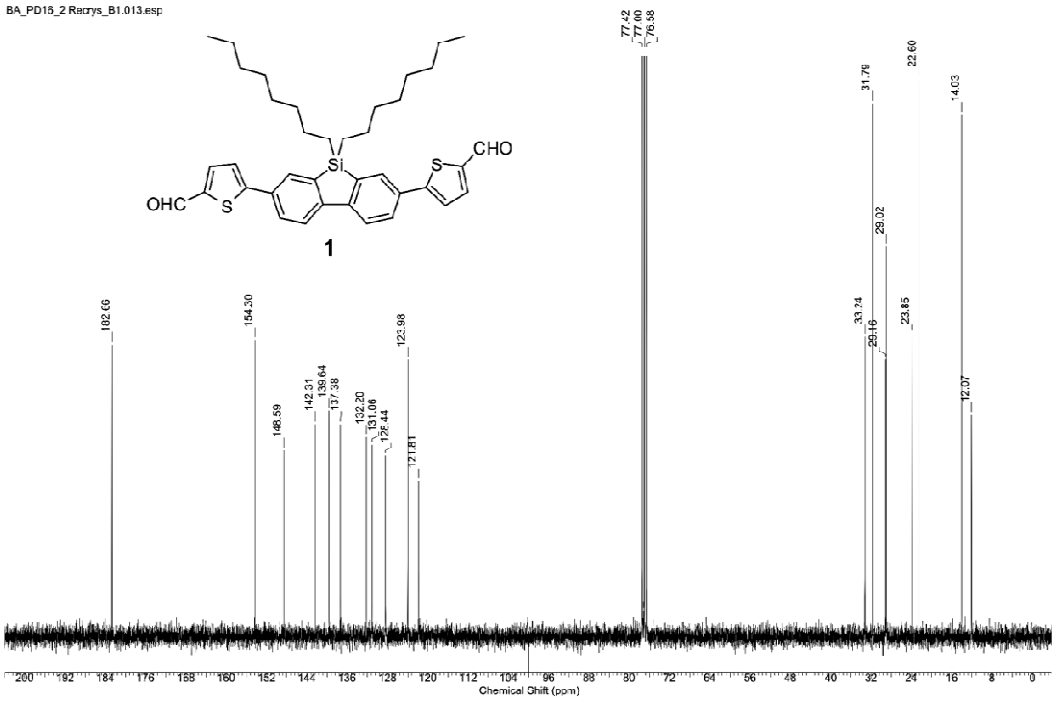

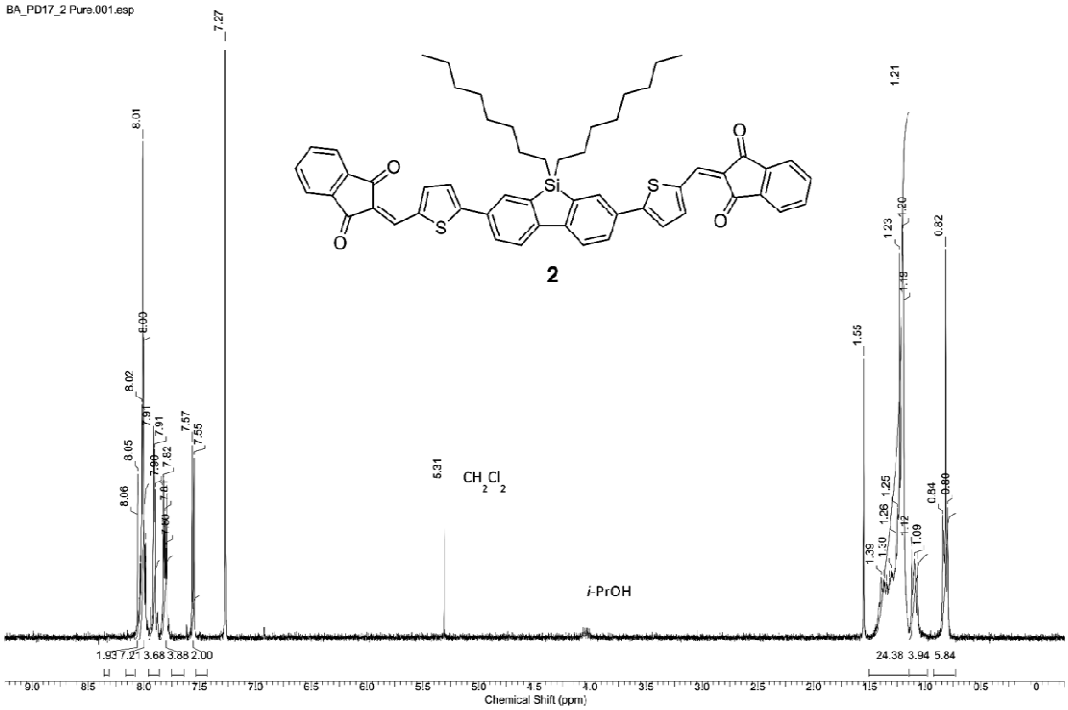
BA_PD17_2 Pure.001.esp
2
CH2Cl2
i-PrOH
Chemical Shift (ppm)

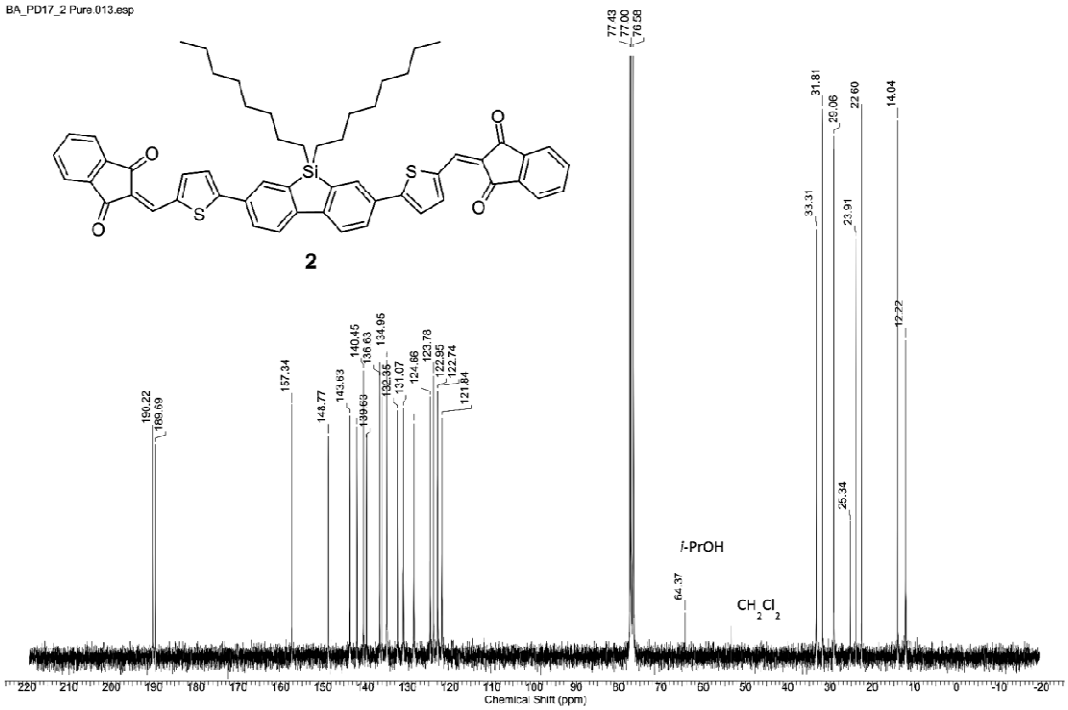
BA_PD17_2 Pure.013.esp
2
i-PrOH
CH2Cl2
Chemical Shift (ppm)

Supporting Figures

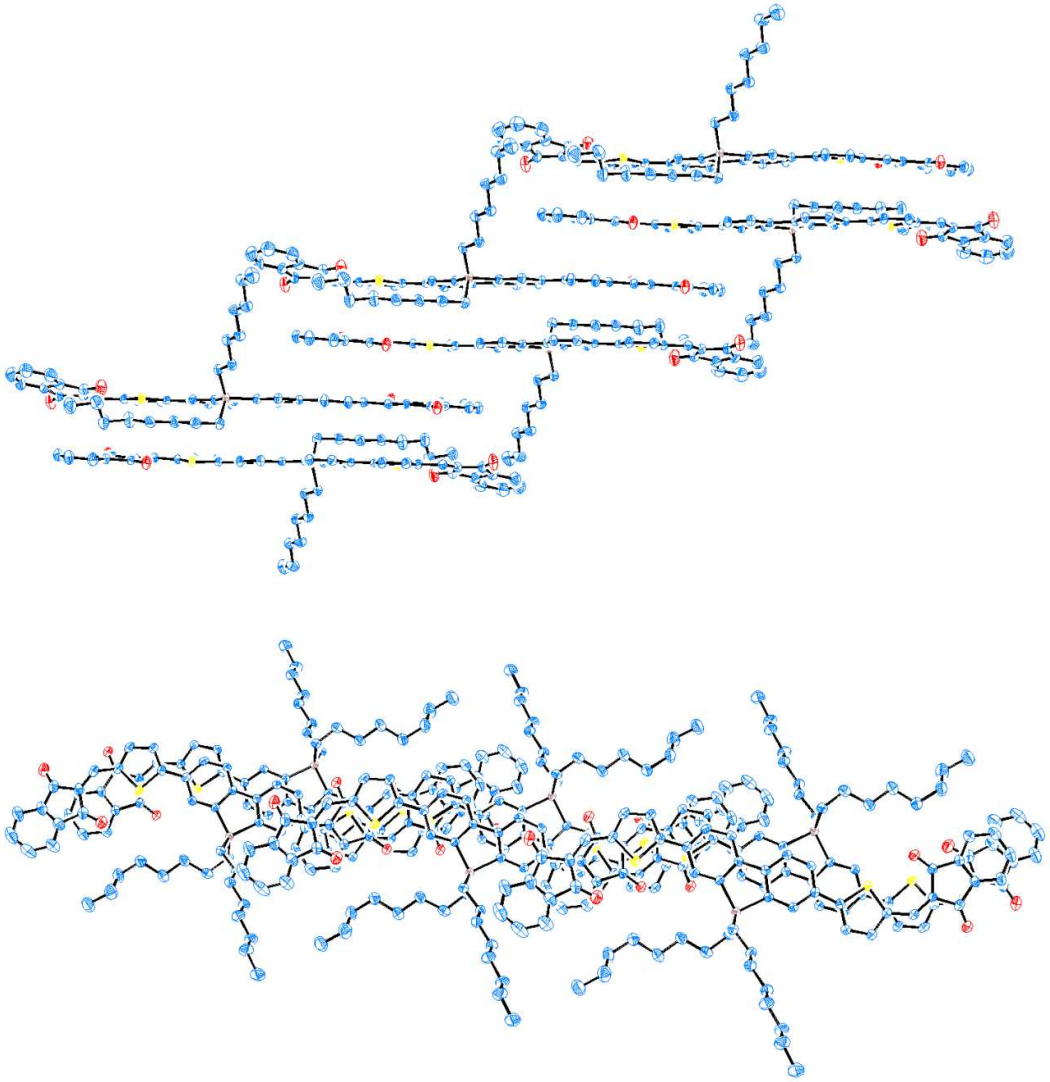

Figure S1. Molecular packing in the crystal of **N5** from the side and top

Table S1: Crystal and refinement data for **N5**

Formula	$C_{56}H_{54}O_2S_2Si \cdot CH_2Cl_2$
F. Wt.	968.13
crystal system	monoclinic
space group	$P2_1/n$
a, Å	8.471(3)

b, Å	37.690(11)
c, Å	15.660(5)
β, deg	97.816(7)
V, $Å^3$	4954(3)
Z	4
T (K)	200(2)
colour, habit	red, plate
cryst dimens (mm^{-3})	$0.11 \times 0.07 \times 0.0.$
D_{calc} (g cm^{-3})	1.298
μ (mm^{-1})	0.287
no. indep. reflns (R_{int})	8662 (0.0495)
no. of obsd. reflns [$I > 2\sigma(I)$]	5905
no. params refined	630
R (F^2)	0.0494
R_w (F^2)	0.1098
ρ_{max}/ρ_{min} (e $Å^{-3}$)	0.409/-0.366

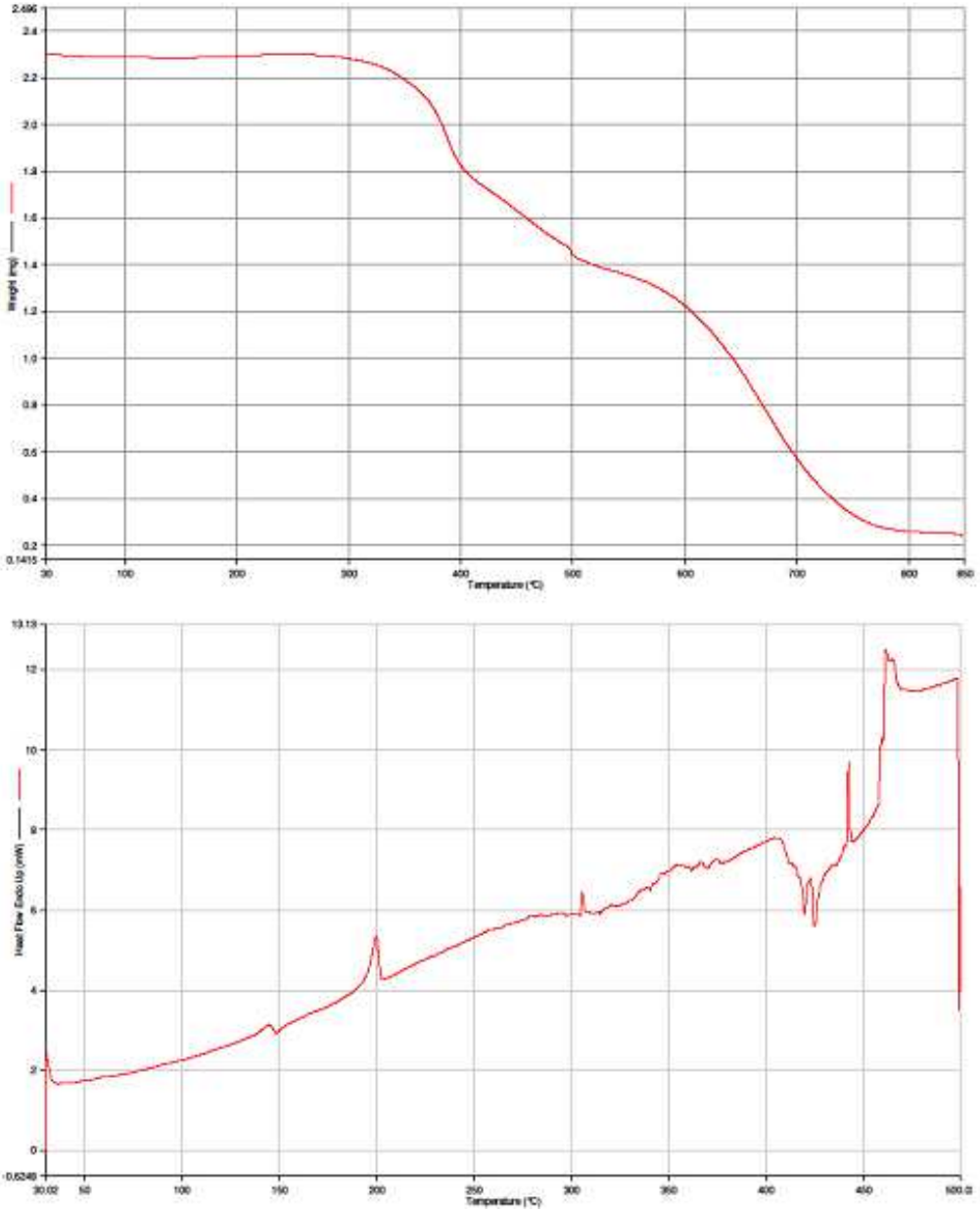

Figure S2. TGA (above) and DSC (below) curves of **N5** showing its thermal stability

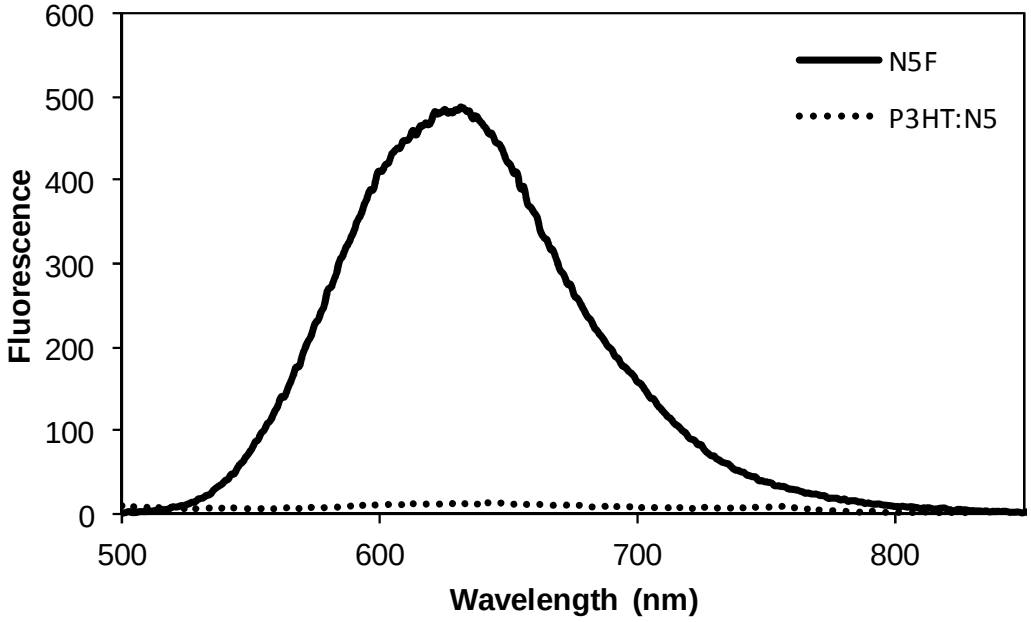

Figure S3. Fluorescence spectra of pristine film of **N5** (solid curve; **N5F**) along with its blend with P3HT [1:1; as-cast (square dotted black curve; P3HT:**N5**)], spin-coated from *o*-dichlorobenzene (excitation wavelength = 480 nm).

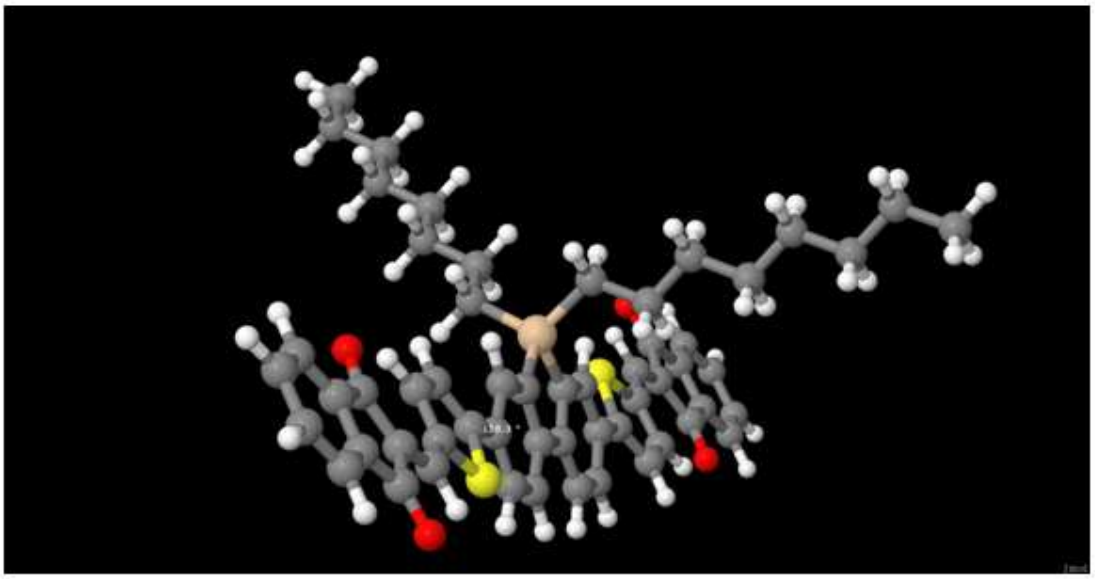

Figure S4. Torsional angle of 156.3° or 23.7° between the two wings (from thiophene to the end) and the central DBS block of N5 from the minimum energy conformations calculated using the Gaussian 09 suite of programs and B3LYP/6-311+G(d,p)//B3LYP/6-31G(d) level of theory.

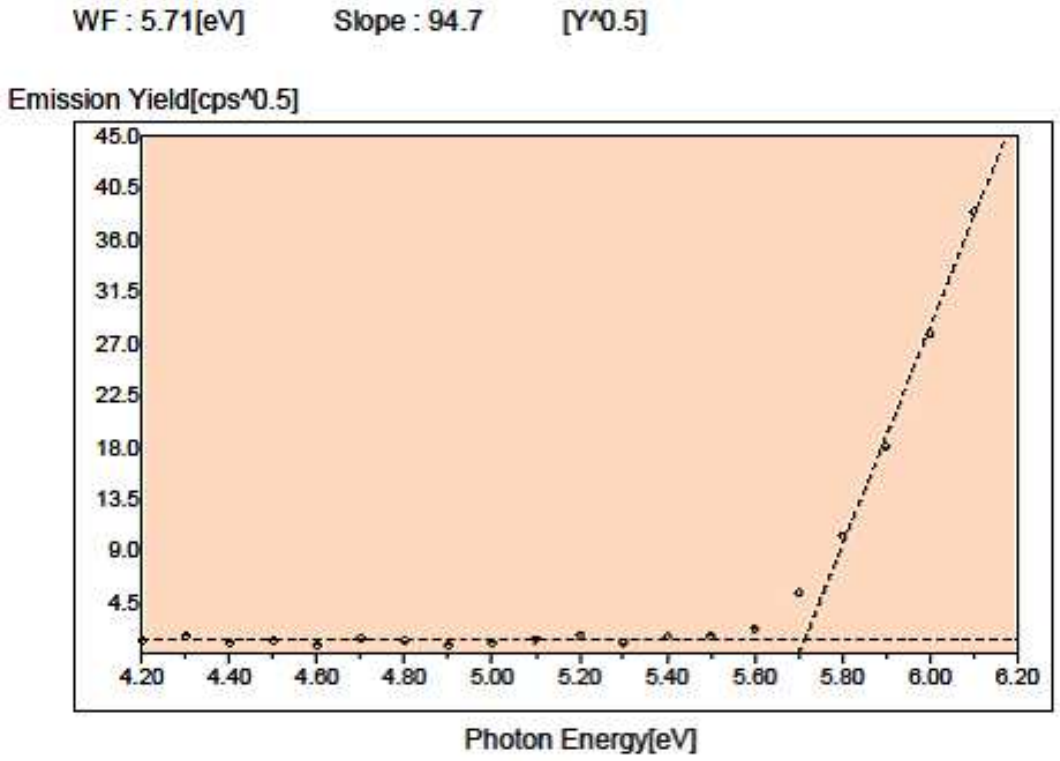

Figure S5. PESA spectrum of thin film (same film which was used for measuring the optical absorption) of **N5** on plain glass substrate. The dashed-lines show the fits to extract ionisation potentials which correspond to the HOMO energy levels.

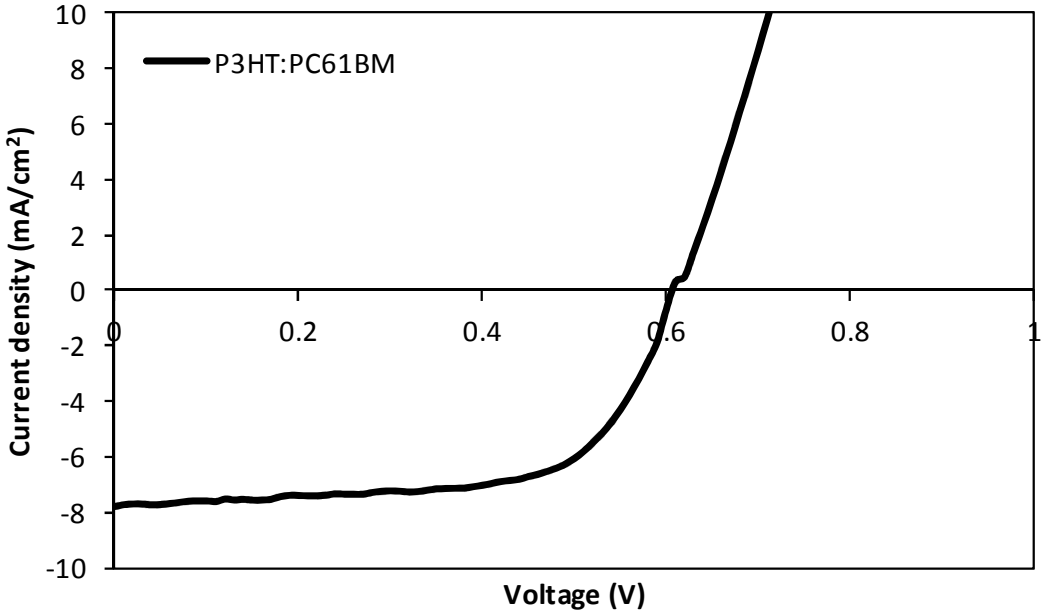

Figure S6. Current–voltage curve for the BHJ device based on P3HT:$PC_{61}BM$ blend under similar conditions reported for **N5**.

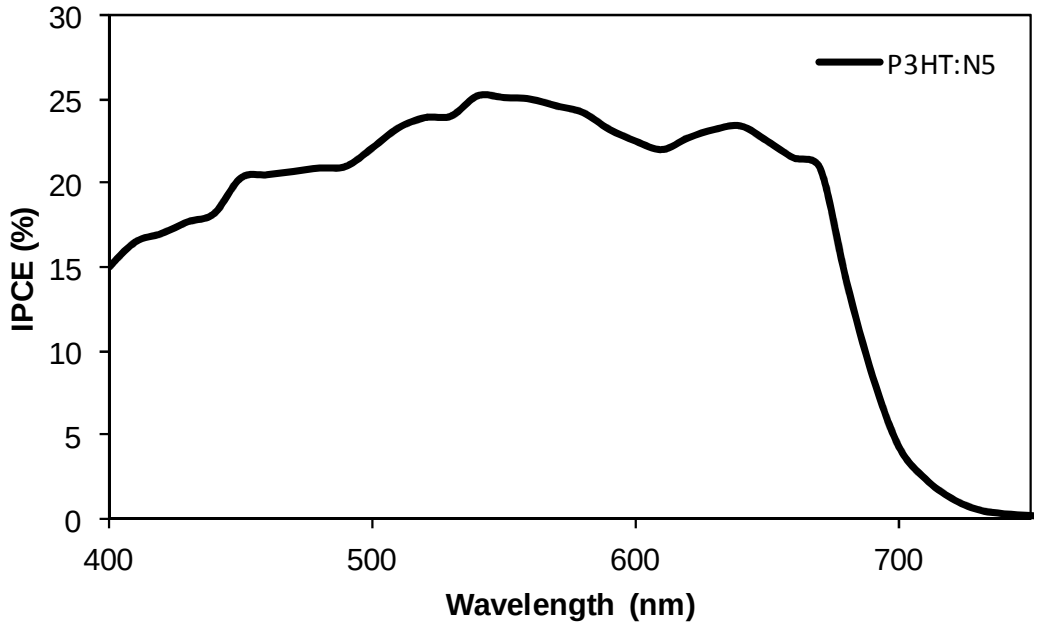

Figure S7. IPCE curve of the best BHJ device based on a blend of P3H

Chapter 6

Isoindigo-based small molecules with varied donor components for solution-processable organic field effect transistor devices

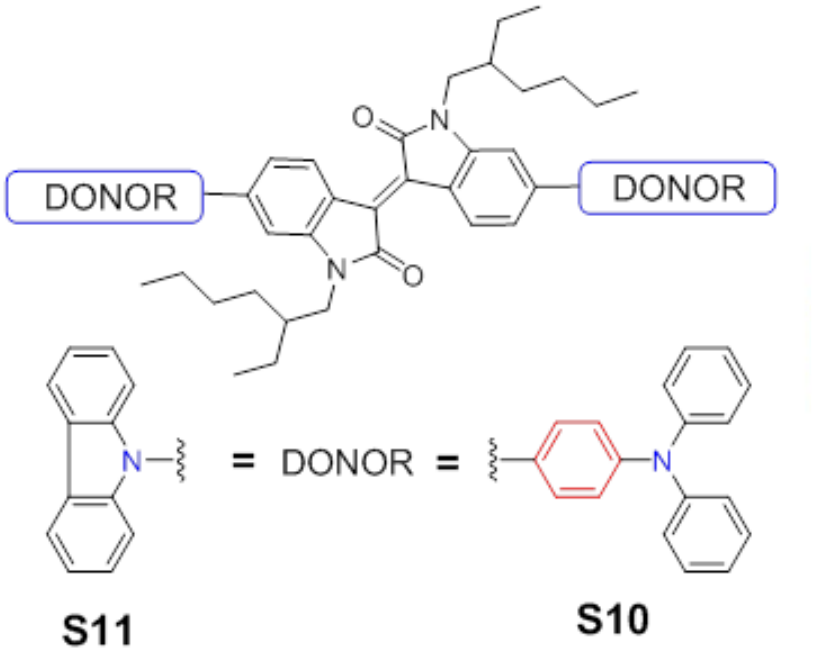

Journal article submitted for publications in *Physical Chemistry Chemical Physics* and as presented as **Chapter 6**.

Molecules **2015**, *20*, 1-x manuscripts; doi:10.3390/molecules200x0000x

OPEN ACCESS

molecules

ISSN 1420-3049

www.mdpi.com/journal/molecules

Type of the Paper (Article)

Isoindigo-based small molecules with varied donor components for solution-processable organic field effect transistor devices

Hemlata Patil,[1] Jingjing Chang,[2] Akhil Gupta,*[1,3] Ante Bilic,[4] Jishan Wu,[2] Prashant Sonar,*[5] and Sheshanath V. Bhosale*[1]

[1] School of Applied Sciences, RMIT University, GPO Box 2476, Melbourne Victoria 3001 Australia; Tel: +61 3 99252680; E-mail: sheshanath.bhosale@rmit.edu.au

[2] Institute of Materials Research and Engineering (IMRE), A*STAR (Agency for Science, Technology and Research), 3, Research Link, Singapore 117602

[3] Medicinal Chemistry, Monash Institute of Pharmaceutical Sciences, Monash University, Parkville Victoria 3052 Australia; E-mail: akhil.gupta@monash.edu

[4] CSIRO Manufacturing, Virtual Nanoscience Lab, Parkville Victoria 3052 Australia

[5] School of Chemistry, Physics and Mechanical Engineering, Queensland University of Technology, GPO Box 2434, Brisbane QLD 4001 Australia; E-mail: sonar.prashant@qut.edu.au

* Author to whom correspondence should be addressed; E-Mail: sheshanath.bhosale@rmit.edu.au; Tel.: +61-3-9925-2680 (ext. 123); Fax: +61-3-9925-2680.

Academic Editor:

Received: / Accepted: / Published:

Abstract: Two novel, solution-processable small organic molecules, (*E*)-6,6'-bis(4-(diphenylamino)phenyl)-1,1'-bis(2-ethylhexyl)-[3,3'-biindolinylidene]-2,2'-dione (coded as **S10**) and (*E*)-6,6'-di(9*H*-carbazol-9-yl)-1,1'-bis(2-ethylhexyl)-[3,3'-biindolinylidene]-2,2'-dione (coded as **S11**) were successfully designed, synthesized and fully characterized. **S10** and **S11** are based on a donor-acceptor-donor structural motif and contain a common electron accepting moiety, isoindigo, along with different electron donating functionalities, triphenylamine and carbazole, respectively. Ultraviolet-visible absorption spectra revealed that the use of triphenylamine donor functionality resulted in an enhanced intramolecular charge transfer transition and reduction of optical band gap, when compared with its carbazole analogue. Both of these materials were designed to be donor semiconducting components, exerted excellent solubility in common organic solvents, showed excellent thermal stability, and their promising optoelectronic properties encouraged us to scrutinize charge-carrier mobilities using solution-processable organic field effect transistors. Hole

mobilities of the order of 2.2×10^{-4} cm^2/Vs and 7.8×10^{-3} cm^2/Vs were measured using **S10** and **S11** as active materials respectively.

Keywords: Isoindigo; solution-processable; organic field effective transistors; donor-acceptor-donor; carbazole; triphenylamine

1. Introduction

Over the past two decades, the design and development of new organic semiconductors has been a subject of increasing research interest since these materials are widely used as active components for electronic devices such as light emitting diodes [1], field effect transistors [2], photodiodes [3], and photovoltaic cells [4–8]. Such vast and industrial applications place high demands on both the electronic and chemical properties of materials, including chemical and thermal stability, broad absorption profile, appropriately tuned energy levels, solution processability and charge carriers mobility. The fulfilment of such properties constitutes a challenge for synthetic organic chemists who generally use a "structural strategy" in which blocks of distinctive electronic properties are assembled together in one chromophore through appropriate chemical coupling reactions [9].

Prior to their use as active materials for organic electronic devices, semiconductor materials were also used for optical data storage or optical switching [10–11]. Such materials/structures are typically based on a "push–pull" modular design that combines electron-rich (donor) and electron-deficient (acceptor) units connected via a π-conjugated linker [8,12]. Such designs have turned out to be highly successful in view of generating new semiconducting materials, controlling highest occupied molecular orbital (HOMO) and lowest unoccupied molecular orbital (LUMO) energy levels of target chromophores and tuning optoelectronic and redox properties. This approach has also been successful to tune the solubility of target materials which is an essential requirement for the fabrication of organic electronic devices. These push–pull or donor–acceptor (D–A) modules allow intramolecular charge transfer (ICT) transition that is beneficial for broadening absorption spectrum and narrowing optical band gap. Most studied designs with various D–A combinations include, but are not limited to, D–A, D–A–D, A–D–A and A–D–A–D–A. Because of the vast majority of structural blocks and advances in organic chemistry, it is not surprising that there is tremendous interest in the development of such designs by varying D–A combinations with the goals of achieving panchromatic absorbance, appropriate energy levels and solution processability. Exploration of such designs is possible with polymeric entities as well as small organic molecules. However, small molecular semiconductors can offer advantages over polymeric counterparts in terms of ease of synthesis, introduction of structural variation, purification, less batch to batch variations and less end-group contamination. It has been realized that in order to take full advantage of the properties of small organic molecules, engineering of chemical structure as well as incorporation of appropriate D and/or A functionalities are highly desirable [13–14]. We are decidedly interested in exploring small organic molecules for their potential applications in organic electronics. In our efforts to design and develop versatile and novel materials for organic electronic applications [15–18], we are interested to explore D–A–D module in particular. We [19] and others [20–23] have demonstrated that such modules facilitate the favourable π–π

interactions in the film, leading to an enhanced charge transport between adjacent molecules. Few examples of acceptor functionalities within a D–A–D structural motif include diketopyrrolopyrrole (DPP), 2-pyran-4-ylidenemalononitrile, thiazolothiazole, naphthalene diimide (NDI) and isoindigo [20–27]. The use of isoindigo has been widely reported to develop polymeric entities for organic electronics [28–29], however, progress on small molecular semiconductors is finitely reported [8]. Material development programme based on isoindigo functionality has trailed behind than other emerging accepting functionalities.

In this study we report the design, synthesis and characterization of the optoelectronic properties of two novel materials, (*E*)-6,6'-bis(4-(diphenylamino)phenyl)-1,1'-bis(2-ethylhexyl)-[3,3'-biindolinylidene]-2,2'-dione (**S10**) and (*E*)-6,6'-di(9*H*-carbazol-9-yl)-1,1'-bis(2-ethylhexyl)-[3,3'-biindolinylidene]-2,2'-dione (**S11**), which are based on isoindigo functionality and are represented in Fig. 1. The chemical structures of both the materials, **S10** and **S11**, were confirmed by ^{1}H and ^{13}C NMR spectroscopies and high resolution mass spectrometry. The target materials prepared in this work were found to be highly soluble in a variety of common organic solvents, such as dichloromethane, chloroform, chlorobenzene and toluene, which is a feature that is essential for the fabrication of solution-processed organic semiconductor devices. In fact **S10** exerted greater solubility than **S11** by an order of magnitude of 1.5. We have fabricated the solution-processable organic field effective transistors (OFETs) using **S10** and **S11**. Hole mobilities of the order of 2.2×10^{-4} and 7.8×10^{-3} cm^2/Vs were measured using **S10** and **S11** respectively. This study builds upon our search for the versatile and efficient organic materials by exploring D–A–D module and is a comparative study of the effect of different donors [triphenylamine (**S10**) and carbazole (**S11**)] whilst keeping the acceptor part (isoindigo) constant.

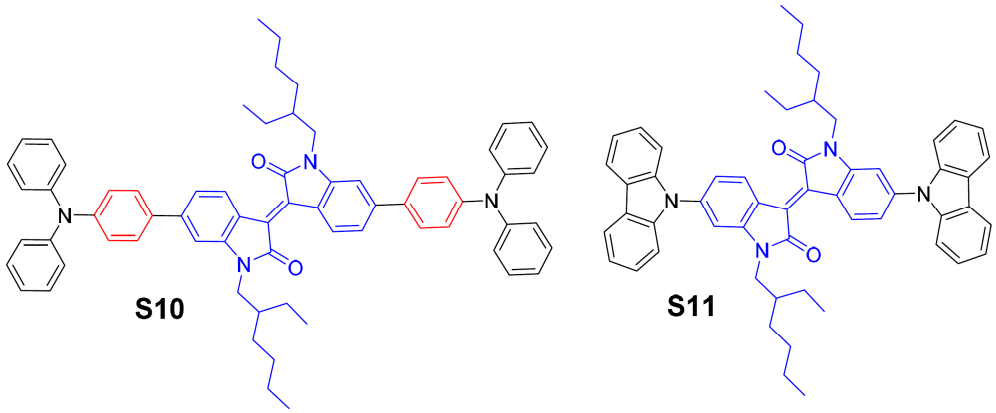

Figure 1. Molecular structures of the new organic materials investigated in this work.

2. Results and Discussion

2.1. Design strategy, synthesis and characterization

Both materials, **S10** and **S11**, were developed based on the D–A–D module and the central acceptor moiety was directly linked to the donor functionalities to create a highly conjugated backbone. The

development of such structures involves the use of two identical donor units placed on either side of the central core, thus resulting in a symmetrical chromophore. In **S10**, triphenylamine (TPA) group was selected for its believed ability to act as an energy antenna [31], which may be responsible for an overall bathochromic absorption when compared with **S11** for which carbazole functionality was used. Both **S10** and **S11** were synthesized as per reaction Scheme 1 (For their spectra, please see Figures S1 to S6 in Supplementary Information (SI)). The use of isoindigo functionality for enhancing the solubility of target materials is paramount as it allows an incorporation of lypophilic chains on its core nitrogen atoms. These alkyl chains facilitate the deposition of target materials as films or layers on appropriate substrates by relatively simple fabricating techniques.

2.1. Optoelectronic properties

The optical properties of **S10** and **S11** were investigated by measuring their UV–Vis absorption spectra in chloroform solution and in pristine as-casted films (Fig. 2). The longest wavelength absorption maximum (λ_{max}) exhibited by **S10** was at 572 nm with an absorption onset at 710 nm. **S11** exhibited its λ_{max} at 560 nm with an onset at 670 nm. Both the absorption maximum and extinction coefficient increased with the use of TPA donor unit. This is in agreement with the design principle that the use of TPA donor unit can indeed act as an energy antenna that is helpful for stronger bathochromic shift when compared with other donor functionalities, such as carbazole. This is consistent with the idea that greater ICT can be achieved with increasing donating strength. Absorption spectra of **S10** and **S11** in pristine films were also measured by spin-casting their films from chloroform solutions (equimolar solutions of **S10** and **S11** spun at 2500 rpm for 1 min). Thin film absorption spectra exhibited bathochromic shifts when compared with solution spectra, a finding that is consistent with literature reported materials [15–16]. The use of TPA donor unit in **S10** provided an augmentation of λ_{max} by 20 nm when compared to the carbazole unit in **S11**. Evidently, the use of such a strong donor can be helpful (1) to enhance the absorption profile of a given chromophore that can lead to greater light harvesting on its surface during the process of photo-excitation and (2) to intensify the π-conjugation within the molecular backbone.

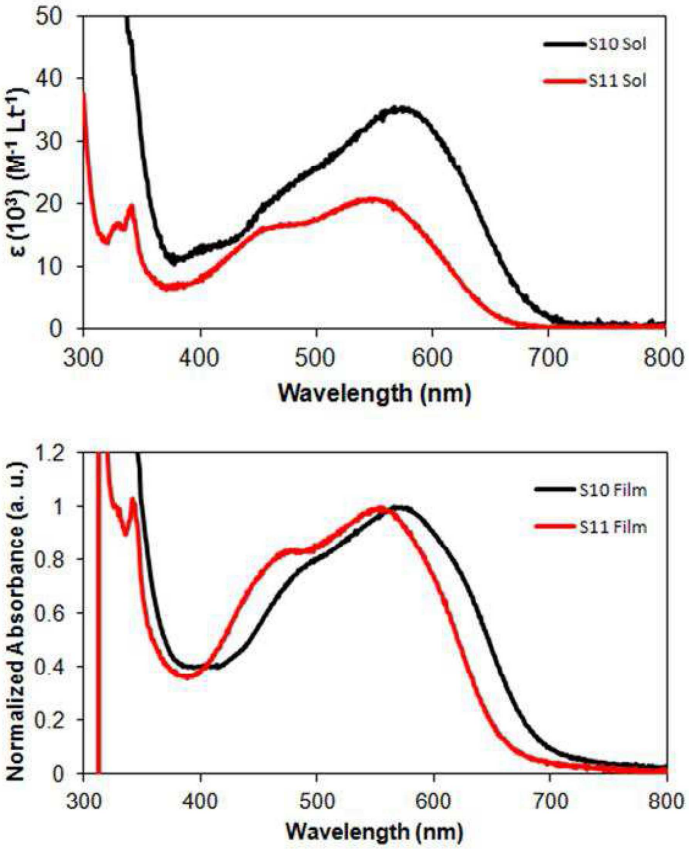

Figure 1. Molar absorptivity of newly synthesized materials **S10** and **S11** in chloroform solutions (above) and normalized UV–Vis absorption spectra of **S10** and **S11** in thin solid films (below) , spin-cast from their chloroform solutions (equimolar solutions of **S10** and **S11** spun at 2500 rpm for 1 min).

We performed density functional theory (DFT) calculations on both the materials using the Gaussian 09 suite of programs [32] and B3LYP/6-311+G(d,p)//B3LYP/6-31G(d) level of theory. DFT investigation indicated that HOMO to LUMO excitation moves the orbital density distribution from the donor functionalities to the isoindigo core unit. The HOMO densities of **S10** and **S11** have spread across the whole molecular backbone with major dwelling over the donor functionalities. The LUMO orbital densities were delocalized over the central part of molecule and received a sizable contribution from the isoindigo core unit (see Fig. 3). This type of density distribution may be advantageous for ICT transition between donor and acceptor components. It was further observed that the use of a TPA unit as an energy antenna in **S10** improves the electron-donating ability and the theoretical optical band-gap was reduced as a result of using TPA [2.26 eV (**S10**)] against carbazole functionality [2.39 eV (**S11**)]. Experimentally, the HOMO energies of **S10** and **S11** were estimated using PESA and the

LUMO energies were calculated by adding the band gap determined by the onset of thin film UV-Vis absorption to the HOMO values.

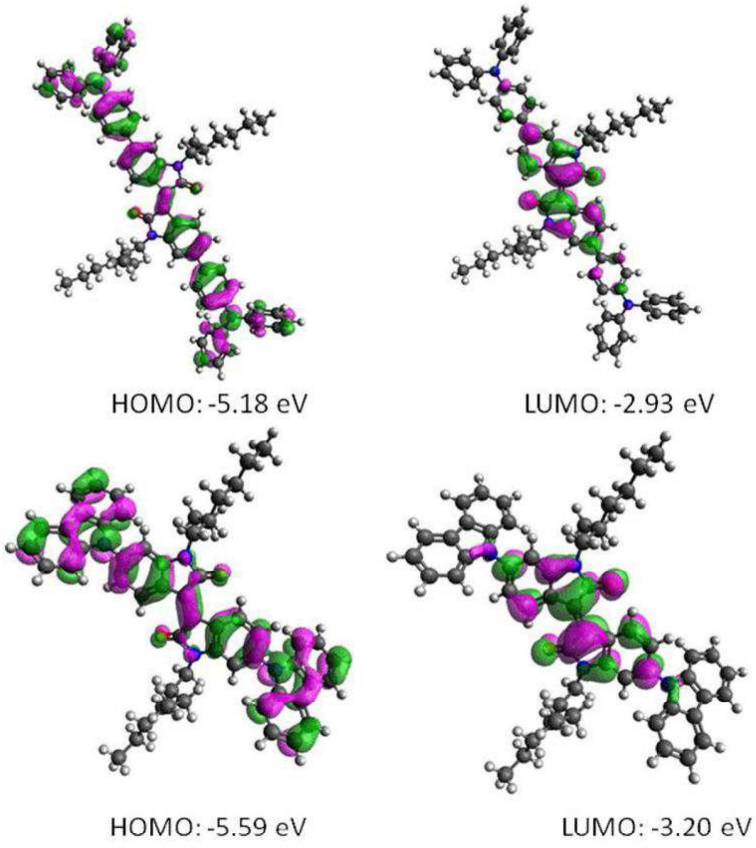

Figure 3. Orbital density distribution for the HOMOs and LUMOs of **S10** (upper) and **S11** (lower). DFT calculations on both the materials were performed using the Gaussian 09 software suite and the B3LYP/6-311 + G(d,p)//B3LYP/6-31G(d) level of theory.

These PESA measurements were performed on thin solid as-casted films (same films that were used to measure the absorption spectra) to measure work functions corresponding to their HOMO levels. The HOMO energy level of **S10** was reduced by 0.07 eV in comparison to the HOMO level of **S11**. The band gap was reduced by 0.11 eV with the use of a TPA donor in **S10**. These experimental findings (1) followed the theoretical calculations trend which indicated that with the use of a strong donor, of which TPA is an example, band gap reduces and (2) that both the target chromophores are electron donating semiconducting components (see energy level diagram, Fig. 4).

Apart from PESA measurement, we also conducted the cyclic-voltammetry (CV) experiments in order to observe the solution behaviour of these materials, and to look out for reversible oxidation potentials (one or multiple) which might suggest the suitability of these materials to be used as donor semiconducting components. We conducted the CV experiments on a glassy carbon electrode. The cyclic voltammograms are included in Fig. 5. Both the compounds exhibit a chemically reversible first cathodic process, thus indicating that the species formed by acceptance of an electron is stable on the voltammetry timescale. Direct connection of TPA donor to the diimide core of **S10** pushes the first reduction process to a more cathodic potential relative to **S11**, resulting in a higher LUMO of -3.47 eV for **S10** (calculated by the onset potential method relative to ferrocene) compared to **S11**, which has the LUMO energy of -3.55 eV. This suggests that the direct bond of tertiary nitrogen atom to the central π-system in **S11** reduces the electron density of electro-active centre of **S11** compared to **S10**. Reversible oxidation potential in **S10** indicates the strong donating capacity of TPA donor, an observation that verifies the design principle, absorption behaviour as well as literature reports [15].

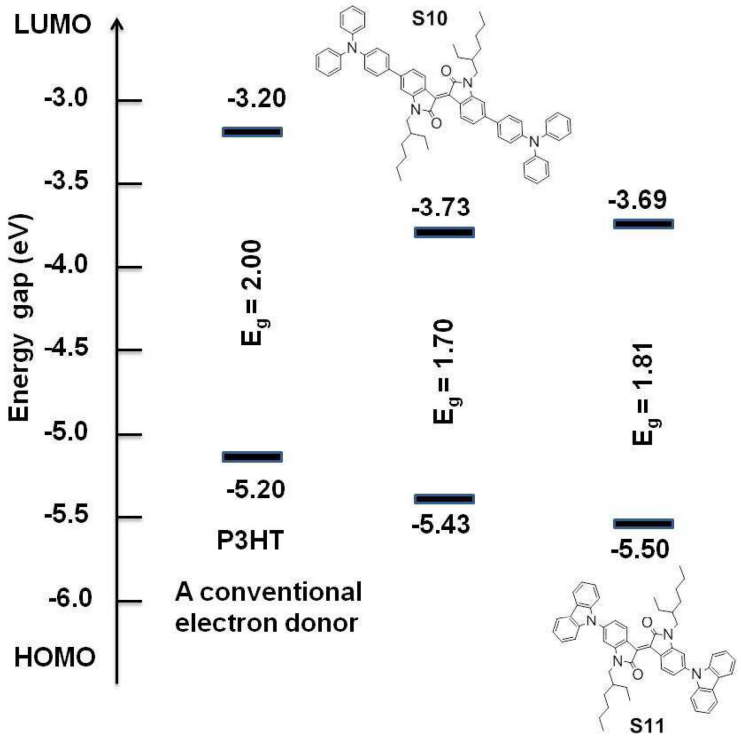

Figure 4. Energy level diagram depicting HOMOs LUMOs of **S10** and **S11**, where HOMO levels were measured using PESA on thin solid films and LUMO levels were calculated from the optical band gaps and HOMO levels ($E_{LUMO}=E_{bandgap}+E_{HOMO}$).

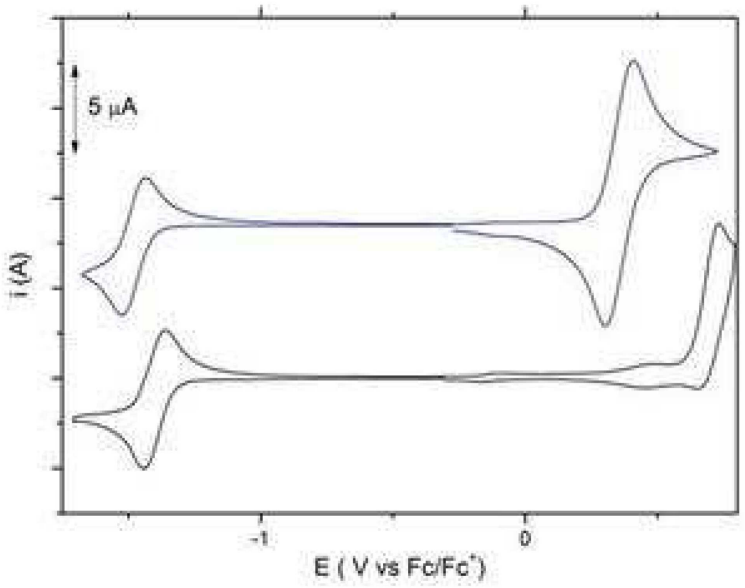

Figure 5. Cyclic-voltammograms of **S10** (upper) and **S11** (lower), run in freshly distilled dichloromethane at a sweep rate of 50 mV sec^{-1}, showing reversible reduction potential waves (both **S10** and **S11**) and reversible oxidation potential wave (**S10**).

It was further realized that despite the presence of intriguing and advantageous optoelectronic properties, organic semiconducting materials must possess thermal stability so that they can sustain rigid device fabricating conditions, such as device annealing at a higher temperature. In-line with this requirement, we conducted TGA and DSC analyses. TGA curves of **S10** and **S11** were run at a heating rate of 10 °C min^{-1} under the protection of nitrogen. TGA indicated that both **S10** and **S11** are thermally stable up to 350 °C (Fig. 6), a finding that supports high temperature annealing of as-casted organic electronic devices and corroborates DSC analysis (Fig. S7, SI).

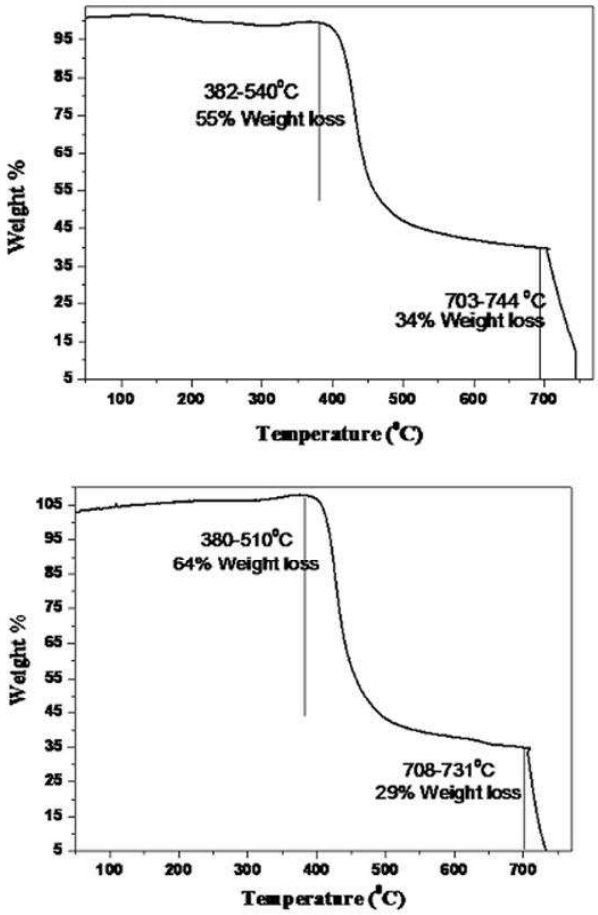

Figure 6. TGA traces of **S10** (upper) and **S11** (lower) under nitrogen atmosphere. Heating rate: 10 °C/min from room temperature to 800 °C.

The electrical properties of **S10** and **S11** as an active channel semiconductor in OFET devices were characterized using a bottom-gate, top-contact geometry. Heavily n-doped conductive silicon wafer with a layer of ~200 nm SiO_2 on the surface was used as the substrate. The SiO_2 functions as the gate insulator and the doped Si as the gate. The active **S10** and **S11** thin films (~40 nm) were spin coated on top of an HMDS modified SiO_2 surface using **S10** and **S11** $CHCl_3$ solution (0.5 wt%). On top of **S10** and **S11** thin films, gold was deposited as source and drain electrode via shadow mask. The OFET schematic of the complete device fabrication has shown in Fig. 7a. The small molecule thin films were selectively annealed at 100 °C, 120 °C, for 10 min on a hot plate in nitrogen atmosphere. OFET devices exhibit typical p-type electrical characteristics. The hole mobility was calculated from the saturation regime of transfer curve. The **S10** and **S11** thin film annealed at 120 °C exhibited hole mobility of 2.2×10^{-4} and 7.8×10^{-3} cm^2/Vs respectively (Table 1). The output and transfer characteristics of 120 °C annealed **S10** and **S11** based OFET devices are shown in Figures 7b, 7c and

7d, 7e respectively. The on/off ratios for all of the devices were calculated around 10^4 to 10^5 whereas the threshold voltage was observed in the range of -21 V to -16 V with respect to annealing. To our knowledge, there are very few reports which explore isoindigo-based small molecules and their applications in OFET devices. The obtained hole mobility values for **S10** and **S11** are in good agreement with some of the previously reported small molecules based on isoindigo core [33].

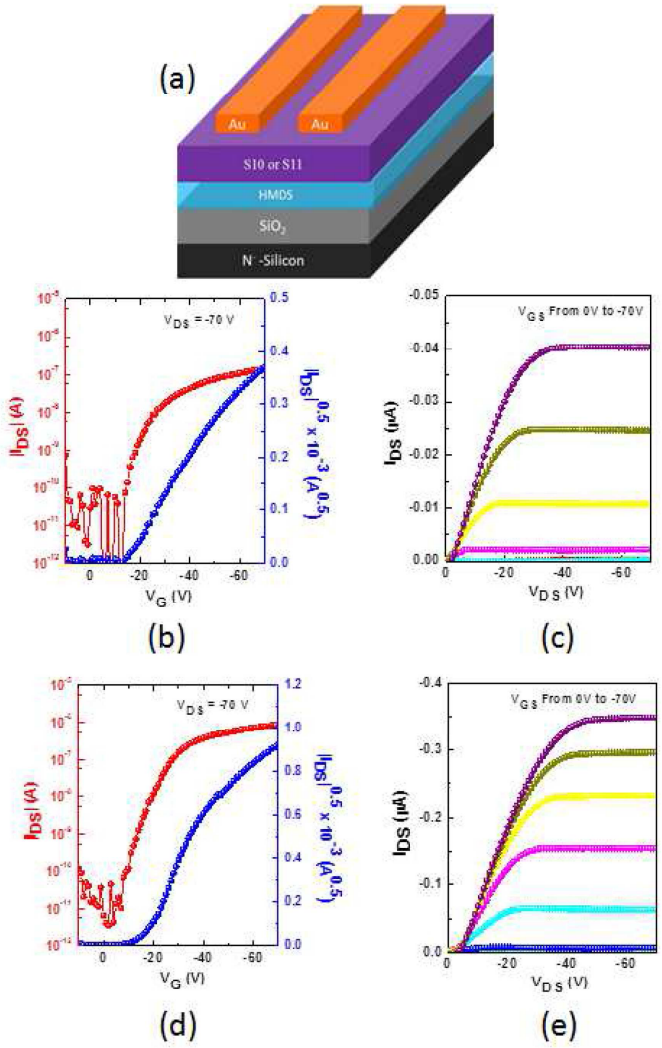

Figure 7. (a) Organic field effect transistor (OFETs) device geometry. Output and transfer characteristics of **S10** (b, c) and **S11** (d, e) based p-channel OFET annealed at 120°C on HMDS treated n+-Si/SiO2 substrate. The hole transfer curves were derived at drain voltages (V_D) of -70 V.

Table 1. OFET device performance of **S10** and **S11** thin films annealed at 120°C on HMDS treated n+-Si/SiO2 substrates using bottom-gate, top-contact (BGTC) device architecture.

Annealing temperature [°C]		μ[$cm^2V^{-1}s^{-1}$]	V_T [V]	On/off ratio
S10	120	2.2×10^{-4}	-16 – -20	1.1×10^{4}
S11	120	7.8×10^{-3}	-17 – -21	1.3×10^{5}

The surface morphologies of **S10** and **S11** thin films were studied by atomic force microscopy (AFM) in the tapping mode and are shown in Fig. 8. The spin coated films exhibited amorphous domains for both the materials. For **S10**, upon thermal annealing at 120 °C, the thin films become discontinuous due to strong aggregation, which deteriorate the charge transport properties. Compared to **S10**, **S11** exhibited interconnected network, which is beneficial for charge carrier transport. Two dimensional X-ray diffraction measurements of these two films were further investigated to study the crystallinity and microstructure of these films (see Fig. S8, SI). It can be seen that both thin films exhibited week diffraction peaks indicating amorphous nature of these two films. These results are consistent with the surface morphologies results, as well as the slightly low charge transport properties.

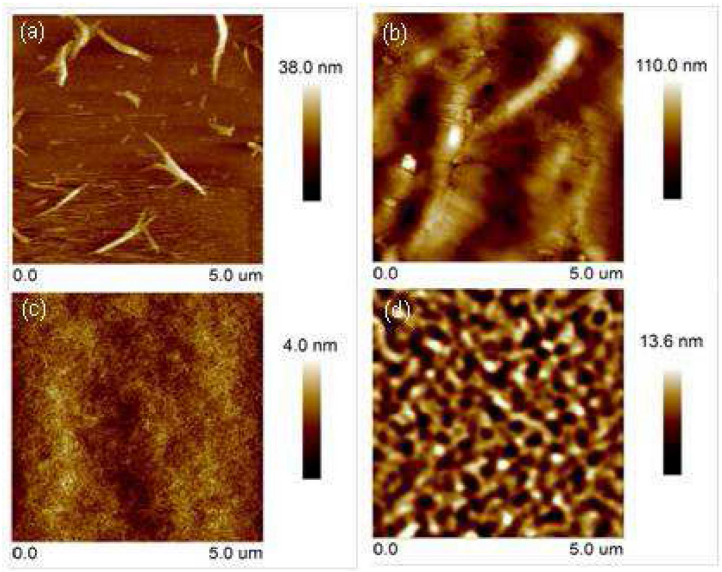

Figure 8. The AFM images of **S10** (a, b) and **S11** (c, d) for as-cast and thermally annealed films.

3. Experimental Section

3.1 Materials and instruments

All the reagents and chemicals used, unless otherwise specified, were purchased from Sigma-Aldrich Co. The solvents used for reactions were obtained from Merck Speciality Chemicals (Sydney, Australia) and were used as such. (*E*)-6,6'-dibromo-1,1'-bis(2-ethylhexyl)-[3,3'-biindolinylidene]-2,2'-dione was purchased from Luminescence Technology Corporation (LTC), Taiwan and was used as such. Unless otherwise specified, all ^{1}H and ^{13}C NMR spectra were recorded using a Bruker AV400 spectrometer at 400 MHz and 100.6 MHz, respectively. Chemical shifts (δ) are measured in parts per million (ppm). Thin layer chromatography (TLC) was performed using 0.25 mm thick plates precoated with Merck Kieselgel 60 F_{254} silica gel, and visualised using ultraviolet (UV) light (254 nm and 365 nm). Melting points were measured using a Gallenkamp MPD350 digital melting point apparatus and are uncorrected. High-resolution mass spectra (atmospheric-pressure chemical ionization (APCI)) experiments were performed with a thermo scientific Q *E*xactive Fourier-transform mass spectrometer, ionizing by APCI from an atmospheric solids analysis probe (ASAP) [30]. Ultraviolet–visible (UV–Vis) absorption spectra were recorded using a Hewlett Packard HP 8453 diode-array UV–Vis spectrometer. Work functions of all the materials were estimated using photoelectron spectroscopy in air (PESA). PESA measurements were recorded using a Riken Keiki AC-2 PESA spectrometer with a power setting of 5 nW and a power number of 0.5. Samples for PESA were prepared on cleaned glass substrates. The thermal stability of **S10** and **S11** was investigated by thermogravimetric analysis (TGA) and differential scanning calorimetry (DSC).

3.2 Cyclic-voltammetry

Cyclic-voltammetry was carried out in freshly distilled dichloromethane (over calcium hydride), with a supporting electrolyte of 0.1 M tetrabutylammoniumhexafluorophosphate (Bu_4NPF_6, Electrochemical grade, Aldrich), which was twice recrystallized from ethanol before use. A Glassy carbon electrode was used as a working electrode (ALS, Japan), which was polished with 0.05 μM alumina on a felt pad, washed with distilled water followed by ethanol and dried under a N_2 stream before use. A platinum wire was used as a counter electrode and a silver wire was used as a pseudo reference electrode. Ferrocene was used as an internal reference, by doping all solutions with an approximately equimolar amount of ferrocene. Reported voltammograms were recorded at a scan rate of 50 mV sec^{-1}. Redox potentials ($E_{1/2}$ values) were taken as a half-way point between forward and reverse peaks for each reversible redox process.

3.3 Device preparation for thin film transistors

Top contact/bottom gate OFET devices fabricated using n+-Si/SiO_2 substrates where n+-Si and SiO_2 work as gate electrode and gate dielectric, respectively. The thickness of thermally grown silicon oxide layer is around ~200 nm with a capacitance of about 17 nF/cm^2. The SiO_2/Si substrate was cleaned with acetone followed by isopropyl alcohol. It was then immersed in a piranha solution ($V(H_2SO_4)$: $V(H_2O_2)$ = 2:1) for 20 minutes, followed by rinsing with deionized water, and then

immersed in a 0.1M solution of hexamethyldisilazane (HMDS) in anhydrous toluene at 60 °C for 30 minutes. It was then rinsed with toluene followed by drying under nitrogen stream. Device fabrication was completed by deposition of **S10** and **S11** by spin coating $CHCl_3$ solution (0.5 wt%) at 3000 rpm for 1 min. Subsequently, on top of the **S10** and **S11** active layer, a 100 nm thick Gold (Au) thin film was deposited for source (S) and drain (D) electrodes through a shadow mask. For a typical OFET device reported here, the source-drain channel length (L) and channel width (W) was 100 μm and 1 mm, respectively. The device characteristics of the OFETs were measured at room temperature under nitrogen with a Keithley 4200 source meter. The field effect mobility (μ) was calculated from the saturation regime of transfer characteristics. Estimation of the carrier mobility was done using the standard transistor equation (1) in saturation mode:

$$\mu = \frac{2L}{WC_i}\left(\frac{\delta\sqrt{I_D}}{\delta V_G}\right)^2 \qquad (1) \qquad (1)$$

where μ is the field effect mobility, L is channel length, W is channel width, C_i is the gate insulator capacitance.

3.4 Synthesis and characterisation of target molecules

Both the materials, **S10** and **S11**, were synthesized by reacting the bis-bromoisoindigo precursor, (*E*)-6,6'-dibromo-1,1'-bis(2-ethylhexyl)-[3,3'-biindolinylidene]-2,2'-dione, at reflux, with 4-(diphenylamino)phenyl)boronic acid and carbazole in dimethoxyethane and toluene solvents, respectively. The reaction strategy is depicted in scheme 1. Both the materials were purified through conventional column chromatography on silica and their chemical structures were confirmed via spectroscopic analyses.

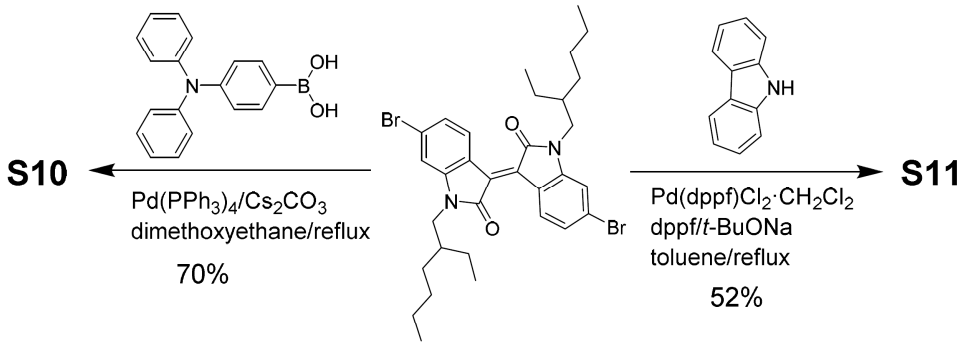

Scheme 1. Reaction scheme for the synthesis of **S10** and **S11**

(*E*)-6,6'-bis(4-(diphenylamino)phenyl)-1-(2-ethylheptyl)-1'-(2-ethylhexyl)-[3,3'-biindolinylidene]-2,2'-dione (S10). (*E*)-6,6'-dibromo-1,1'-bis(2-ethylhexyl)-[3,3'-biindolinylidene]-2,2'-dione (0.25 g, 0.38 mmol) and (4-(diphenylamino)phenyl)boronic acid (0.27 g, 0.95 mmol) were

mixed in dimethoxyethane (25 mL) in a 100 mL round-bottomed flask at room temperature and the reaction mixture was stirred for 15 min followed by the addition of cesium carbonate (Cs_2CO_3) (0.37 g, 1.14 mmol). The resulting suspension was degassed for 10 min by purging with argon, and tetrakis(triphenylphosphine)palladium(0) ($Pd(PPh_3)_4$) catalyst (0.10 g) was added to the reaction mixture. The reaction mixture was refluxed in an oil bath for 12 h in the absence of light and the progress of reaction was followed by thin layer chromatography, which indicated the consumption of starting dibromo derivative. The reaction mixture was cooled to room temperature, diluted with water (50 mL), and the product was extracted in chloroform. The organic layer was washed with water followed by brine, dried over anhydrous $MgSO_4$, and recovered to get crude solid which was purified by column chromatography on silica (hexane: ethyl acetate 9:1 as eluent) to afford **S10** (0.26 g, 70%) as a bluish-black solid. IR (thin solid film, cm^{-1}): 3034, 2957, 2928, 2858, 1693, 1608, 1591, 1518, 1493, 1455, 1357, 1330, 1281, 1179, 1109, 818, 754; ^1H NMR (400 MHz, CD_2Cl_2, TMS): δ (ppm) 9.22-9.19 (2H, m), 7.58-7.56 (4H, m), 7.32-7.25 (10H, m), 7.15-7.05 (16H, m), 7.04-7.00 (2H, m), 3.78-3.67 (4H, m), 1.97-1.86 (2H, m), 1.46-1.26 (16H, m), 0.97-0.93 (6H, m), 0.90-0.86 (6H, m); ^{13}C NMR (400 MHz, CD_2Cl_2, TMS): δ (ppm) 168.63, 148.13, 147.39, 145.87, 144.06, 133.71, 131.93, 129.95, 129.31, 127.56, 124.76, 123.55, 123.07, 120.53, 119.60, 105.78, 44.00, 37.69, 30.71, 28.72, 24.09, 23.05, 13.79, 10.47; HRMS (APCI): $[M]^+$, found 972.5338. $C_{68}H_{68}N_4O_2$ requires 972.5337.

(*E*)-6,6'-di(9*H*-carbazol-9-yl)-1-(2-ethylheptyl)-1'-(2-ethylhexyl)-[3,3'-biindolinylidene]-2,2'-dione (S11). (*E*)-6,6'-dibromo-1,1'-bis(2-ethylhexyl)-[3,3'-biindolinylidene]-2,2'-dione (0.25 g, 0.38 mmol) was added to the mixture of carbazole (0.15 g, 0.87 mmol), sodium *t*-butoxide (0.11 g, 1.14 mmol), and [1,1′-bis(diphenylphosphino)ferrocene]dichloropalladium(II), complex with dichloromethane [$Pd(dppf)Cl_2.CH_2Cl_2$] (0.081 g, 0.1 mmol) in toluene (25 mL) followed by the addition of 1,1′-bis(diphenylphosphino)ferrocene (0.22 g, 0.4 mmol) at room temperature, and the resulting suspension was refluxed overnight. The reaction mixture was cooled to room temperature, filtered through Celite bed and the solvent was evaporated off to get crude solid, which was subjected to column chromatography on silica (10% ethyl acetate/hexane) to afford title compound **S11** (0.161 g, 52%) as a black solid. IR (thin solid film, cm^{-1}): 3057, 2958, 2928, 2872, 1694, 1610, 1501, 1447, 1384, 1334, 1224, 1112, 1099, 736; 1H NMR (400 MHz, CD_2Cl_2, TMS): δ (ppm) 9.50-9.48 (2H, m), 8.18-8.16 (4H, m), 7.63-7.61 (4H, m), 7.49-7.45 (4H, m), 7.35-7.31 (6H, m), 7.10-7.09 (2H, m), 3.80-3.66 (4H, m), 1.97-1.87 (2H, m), 1.48-1.22 (16H, m), 0.96-0.92 (6H, m), 0.86-0.82 (6H, m); ^{13}C NMR (400 MHz, CD_2Cl_2, TMS): δ (ppm) 168.50, 146.88, 141.07, 140.21, 132.19, 131.23, 126.17, 123.76, 120.48, 120.31, 120.21, 119.28, 110.20, 106.12, 44.38, 37.81, 30.74, 28.74, 24.04, 23.00, 13.74, 10.41; HRMS (APCI): $[M]^+$, found 816.4397. $C_{56}H_{56}N_4O_2$ requires 816.4398.

4. Conclusions

In conclusion, we have demonstrated the use of isoindigo accepting functionality to generate new D–A–D modular small organic molecules, **S10** and **S11**, which contain a common isoindigo core unit and varied donor functionalities. The new materials, **S10** and **S11**, were synthesized, found to be highly soluble in a variety of common organic solvents, and were thermally stable. Use of a TPA unit as an energy antenna helped to achieve a substantial red-shift of the absorption maximum in the visible

region, improved the solubility of target material and helped to reduce optical band-gap. Upon testing these materials as active layers in OFET devices, hole mobilities of the order of 2.2×10^{-4} cm^2/Vs and 7.8×10^{-3} cm^2/Vs were achieved for **S10** and **S11** respectively. There are several reports on isoindigo-based polymers but not much work has been done so far on the design and development of small molecules. The reported charge-carrier mobility values for **S10** and **S11** are promising and through further novel designing, high mobility values can be achieved. Our results on the effect of donor types on electronic properties of D–A–D modular organic materials can indeed inform the design of futuristic materials for organic electronic applications. Future studies will focus on the use of unsymmetrical donor units and incorporation of π-spacers between donor and acceptor functionalities.

Acknowledgments

S.V.B. (RMIT) acknowledges financial support from the Australian Research Council (ARC), Australia, under a Future Fellowship Scheme (FT110100152). The CSIRO Division of Materials Science and Engineering, Clayton, Victoria is acknowledged for providing support through a visiting fellow position (A.G.). P.S. is thankful to the ARC Future Fellowship Scheme (FT130101337) at Queensland University of Technology, Brisbane, Queensland.

Author Contributions

H. P. synthesis and fabricated devices, J. C., A. G., J. W., and P. S. measure mobility of devices, A. B. performed DFT calculation and S.V. B. design, supervise and analysis data. All the authors contributed for manuscript preparation.

Conflicts of Interest

The authors declare no conflict of interest.

References and Notes

1. Wu, H.; Ying, L., Yang, W.; Cao, Y. Progress and perspective of polymer white light-emitting devices and materials. *Chem. Soc. Rev.,* **2009**, *38*, 3391–400.
2. Pron, A.; Gawrys, P.; Zagorska, M.; Djurado, D.; Demadrille, R.; Electroactive materials for organic electronics: preparation strategies, structural aspects and characterization techniques. *Chem. Soc. Rev.,* **2010**, *39*, 2577–2632.
3. Hadfield, R.H. Single-photon detectors for optical quantum information applications. *Nat. Photon.,* **2009**, *3*, 696–705.
4. Cheng, Y. J.; Yang, S. H.; Hsu, C. S.; Synthesis of conjugated polymers for organic solar cell
5. applications. *Chem. Rev.,* **2009**, *109*, 5868–923.
6. Gupta, A.; Watkins, S. E.; Scully, A. D.; Singh, Th. B.; Wilson, G. J.; Rozanski, L. J.; Evans, R. A. Band- gap tuning of pendant polymers for organic light-emitting devices and photovoltaic applications. *Synthetic Met*., **2011**, *161*, 856–863.
7. Helgesen, M.; Søndergaard, R.; Krebs, F. C. Advanced materials and processes for polymer solar cell devices. *J. Mater. Chem*., **2012**, *20*, 36–60.

8. Li, Y.; Guo, Q.; Li, Z.; Pei, J.; Tian, W. Solution processable D–A small molecules for bulk-heterojunction solar cells. *Energ. Environ. Sci*., **2010**, *3*, 1427–1436.
9. Mishra, A.; Bäuerle, P. Small molecule organic semiconductors on the move: promises for
10. future solar energy technology. *Angew. Chem. Inter. Ed*., **2012**, *51*, 2020–2067.
11. Rybakiewicz, R.; Djurado, D.; Cybulski, H.; Dobrzynska, E.; Kulszewicz-Bajer, I.; Boudinet, D.; Verilhac, J.-M.; Zagorska, M.; Pron, A. Arylene bisimides with triarylamine N-substituents as new solution processable organic semiconductors: Synthesis, spectroscopic, electrochemical and electronic properties. *Synthetic Met*., **2011**, *161*, 1600–1610.
12. Marks, T. J.; Ratner, M. A. Design, synthesis, and properties of molecule-based assemblies with large second-order optical nonlinearities. *Angew. Chem. Int. Ed. Engl*., **1995**, *34*, 155–173.
13. Marder, S. R.; Kippelen, B.; Jen, A. K. Y.; Peyghambarian, N. Design and synthesis of chromophores and polymers for electro-optic and photorefractive applications. *Nature*, **1997**, *388*, 845–851.
14. Facchetti, A. π-Conjugated polymers for organic electronics and photovoltaic cell applications. *Chem. Mater*., **2011**, *23*, 733–758.
15. Günes, S.; Neugebauer, H.; Sariciftci, N. S. Conjugated polymer-based organic solar cells. *Chem. Rev*., **2007**, *107*, 1324–1338.
16. Lin, Y.; Li, Y.; Zhan, X. Small molecule semiconductors for high-efficiency organic photovoltaics. *Chem. Soc. Rev*., **2012**, *41*, 4245–4272.
17. Gupta, A.; Ali, A.; Bilic, A.; Gao, M.; Hegedus, K.; Singh, Th. B.; Watkins, S. E.; Wilson, G. J.; Bach, U.; Evans, R. A. Absorption enhancement of oligothiophene dyes through the use of a cyanopyridone acceptor group in solution-processed organic solar cells. *Chem. Commun*., **2012**, *48*, 1889–1891.
18. Gupta, A.; Ali, A.; Singh, B.; Bilic, A.; Bach, U.; Evans, R. A. Molecular engineering for panchromatic absorbing oligothiophene donor–π–acceptor organic semiconductors. *Tetrahedron*, **2012**, *68*, 9440–9447.
19. Gupta, A.; Armel, V.; Xiang, W.; Fanchini, G.; Watkins, S. E.; MacFarlane, D. R.; Bach, U.; Evans, R. A. The effect of direct amine substituted push–pull oligothiophene chromophores on dye-sensitized and bulk heterojunction solar cells performance. *Tetrahedron*, **2013**, *69*, 3584–3592.
20. Kumar, R. J.; Churches, Q. I.; Subbiah, J.; Gupta, A.; Ali, A.; Evans, R. A.; Holmes, A. B. Enhanced photovoltaic efficiency via light-triggered self-assembly. *Chem. Commun*., **2013**, *49*, 6552–6554.
21. Patil, H.; Gupta, A.; Bilic, A.; Jackson, S. L.; Latham, K.; Bhosale, S. V. Donor–acceptor–donor modular small organic molecules based on the naphthalenediimide acceptor unit for solution-processable photovoltaic devices. *J. Electron. Mater*., **2014**, *43*, 3243–3254.
22. Tamayo, A. B.; Dang, X.-D.; Walker, B.; Seo, J.; Kent, T.; Nguyen, T.-Q. A low band gap, solution processable oligothiophene with a dialkylated diketopyrrolopyrrole chromophore for use in bulk heterojunction solar cells. *Appl. Phys. Lett*., **2009**, *94*, 103301-1–103301-3.
23. Walker, B.; Tamayo, A. B.; Dang, X.-D.; Zalar, P.; Seo, J. H.; Garcia, A, Tantiwiwat, M.; Nguyen, T.-Q. Nanoscale phase separation and high photovoltaic efficiency in solution-processed, small-molecule bulk heterojunction solar cells. *Adv. Funct. Mater*., **2009**, *19*, 3063–3069.

24. Li, Z.; Dong, Q.; Li, Y.; Xu, B.; Deng, M.; Pei, J.; Zhang, J.; Chen, F.; Wen, S.; Gao, Y.; Tian, W. Design and synthesis of solution processable small molecules towards high photovoltaic performance. *J. Mater. Chem*., **2011**, *21*, 2159–2168.
25. Shi, Q.; Cheng, P.; Li, Y.; Zhan, X. A solution processable D-A-D molecule based on thiazolothiazole for high performance organic solar cells. *Adv. Energy. Mater*., **2012**, *2*, 63–67.
26. Stalder, R.; Mei, J.; Reynolds, J. R. Isoindigo-based donor-acceptor conjugated polymers. *Macromolecules*, **2010**, *43*, 8348–52.
27. Zhang, G.; Fu, Y.; Xie, Z.; Zhang, Q. Synthesis and photovoltaic properties of new low bandgap isoindigo-based conjugated polymers. *Macromolecules*, **2011**, *44*, 1414–1420.
28. Lei, T.; Cao, Y.; Fan, Y.; Liu, C.-J.; Yuan, S.-C.; Pei, J. High-performance air-stable organic field-effect transistors: isoindigo-based conjugated polymers. *J. Am. Chem. Soc*., **2011**, *133*, 6099–6101.
29. Stalder, R.; Mei, J.; Graham, K. R.; Estrada, L. A.; Reynolds, J. R. Isoindigo, a versatile electron-deficient unit for high performance organic electronics. *Chem. Mater*., **2014**, *26*, 664–678.
30. Deng, P.; Zhang, Q. Recent developments on isoindigo-based conjugated polymers. *Polym. Chem*., **2014**, *5*, 3298–3305.
31. Lei, T.; Wang, J.-Y.; Pei, J. Design, synthesis, and structure-property relationships of isoindigo-based conjugated polymers. *Acc. Chem. Res*., **2014**, *47*, 1117−1126.
32. McEwen, C. N.; McKay, R. G.; Larsen, B. S. Analysis of solids, liquids, and biological tissues using solids probe introduction at atmospheric pressure on commercial LC/MS instruments. *Anal. Chem*., **2007**, *77*, 7826–31.
33. Tian, H.; Yang, X.; Cong, J.; Chen, R.; Liu, J.; Hao, Y.; Hagfeldt, A.; Sun, L. Tuning of phenoxazine chromophores for efficient organic dye-sensitized solar cells. *Chem. Commun*., **2009**, *41*, 6288–6290.
34. Frisch, M. J.; Trucks, G. W.; Schlegel, H. B.; Scuseria, G. E.; Robb, M. A.; Cheeseman J. R. *et al.* Gaussian 09, revision D.01. Wallingford CT: Gaussian Incorporation; **2013**.
35. Dasari, R. R.; Dindar, A.; Lo, C. K.; Wang, C.-Y.; Quinton, C.; Singh, S.; Barlow, S.; Fuentes-Hernandez, C.; Reynolds, J. R.; Kippelen, B.; Marder, S. R. Tetracyano isoindigo small molecules and their use in n-channel organic field-effect transistors. *Phys. Chem. Chem. Phys.*, **2014**, *16*, 19345–19350.

Sample Availability: Samples of the compounds **S10** and **S11** are available from the authors.

Experimental Part

S10 Spectra

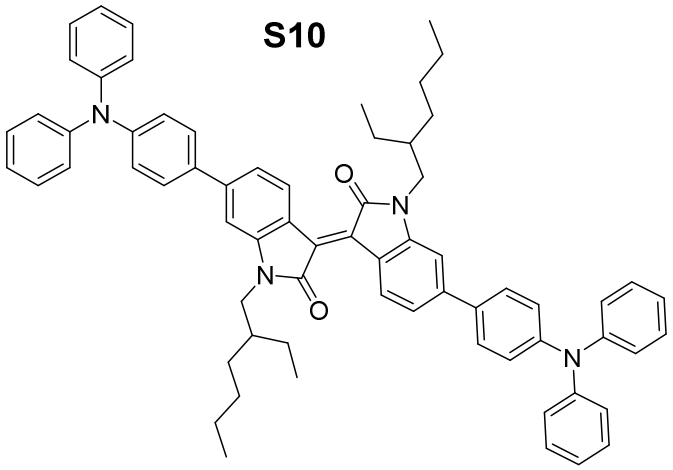

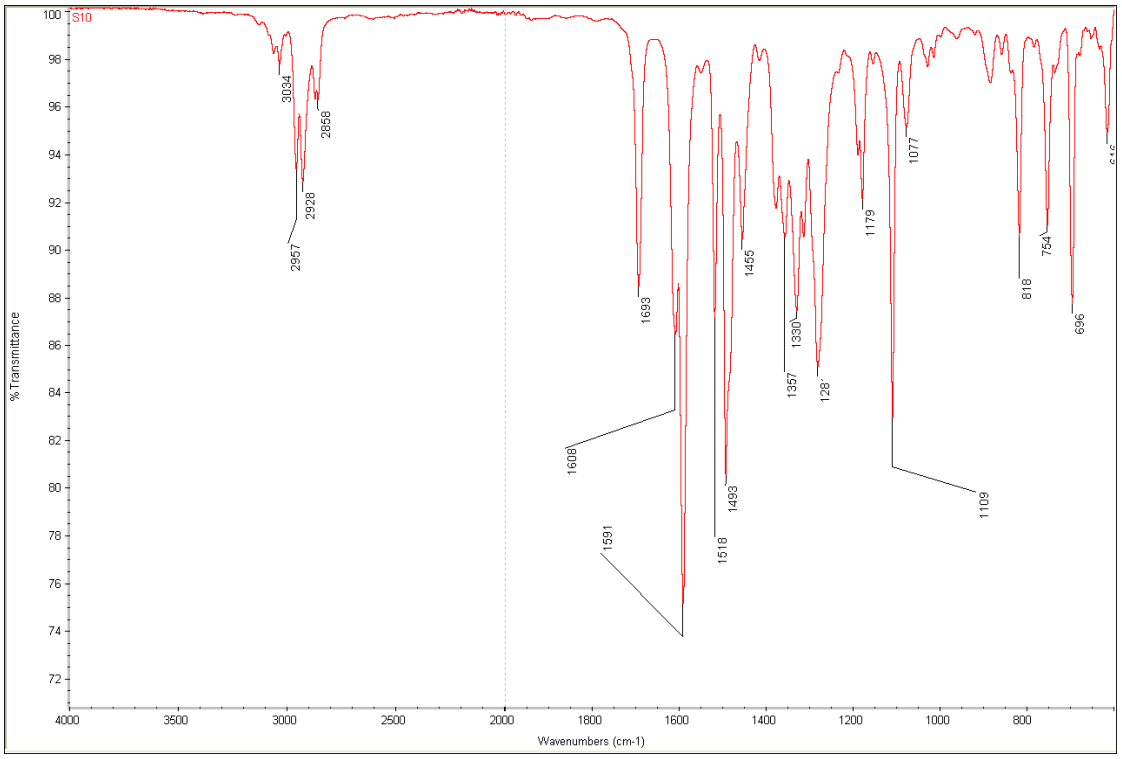

Figure S1. Infrared (IR) spectrum of **S10**.

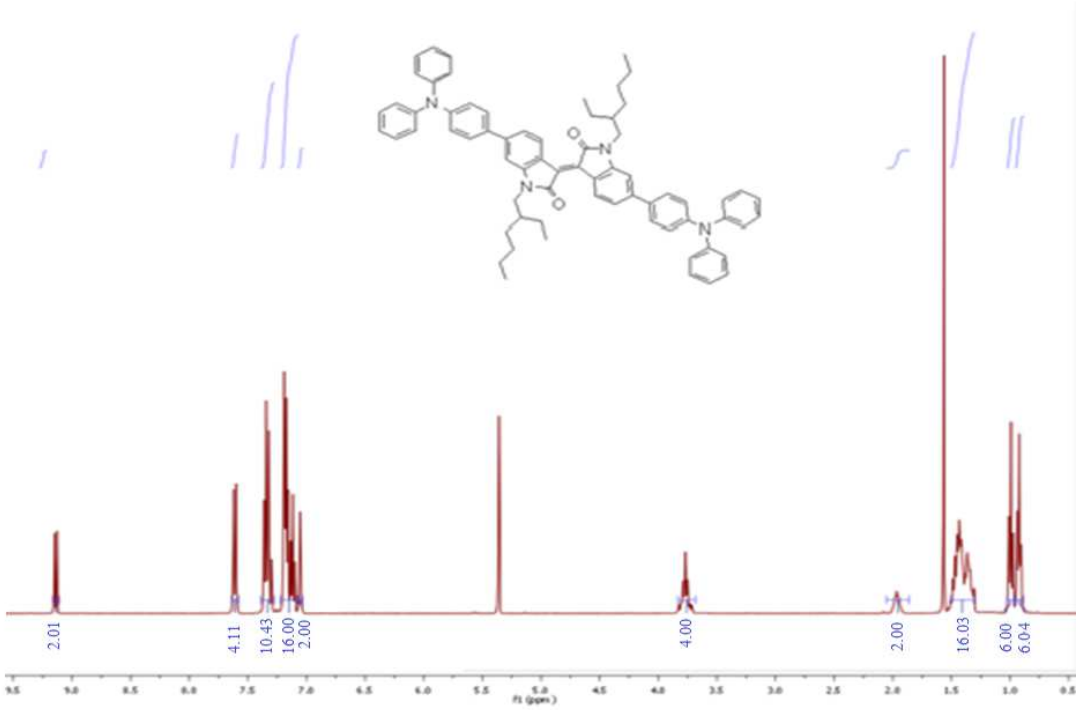

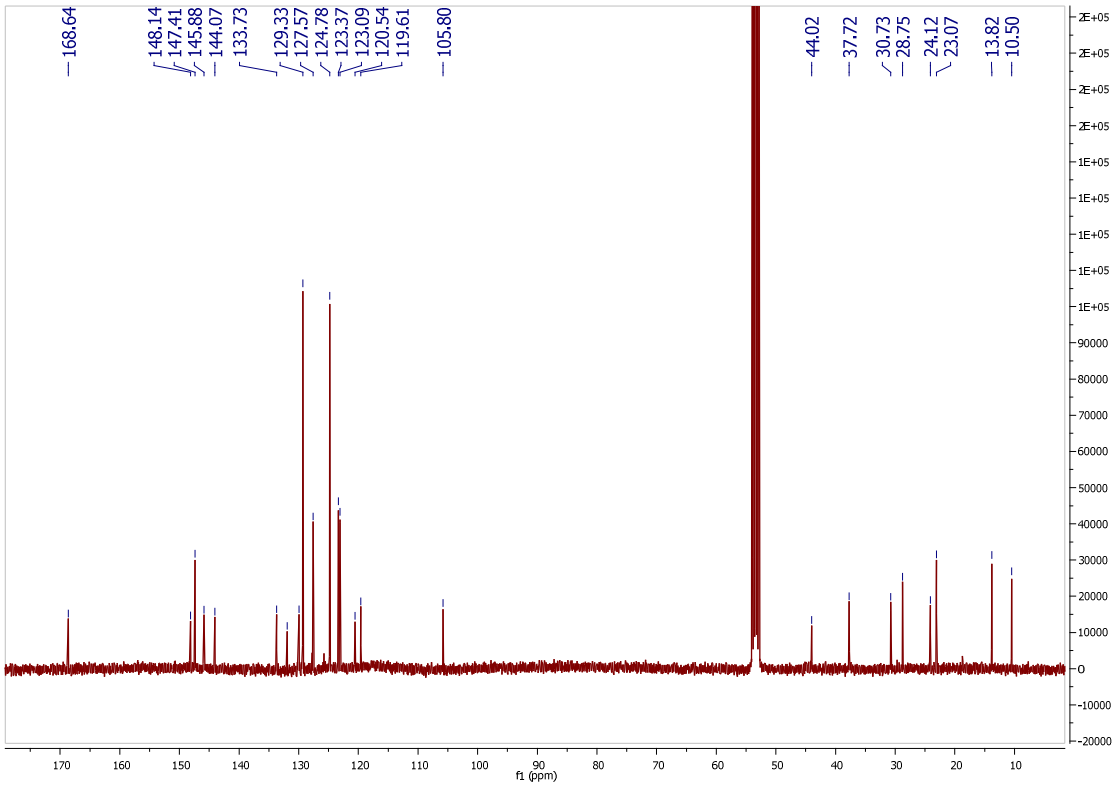

Figure S2. IH NMR (above) and 13C NMR (below) spectra of **S10**.

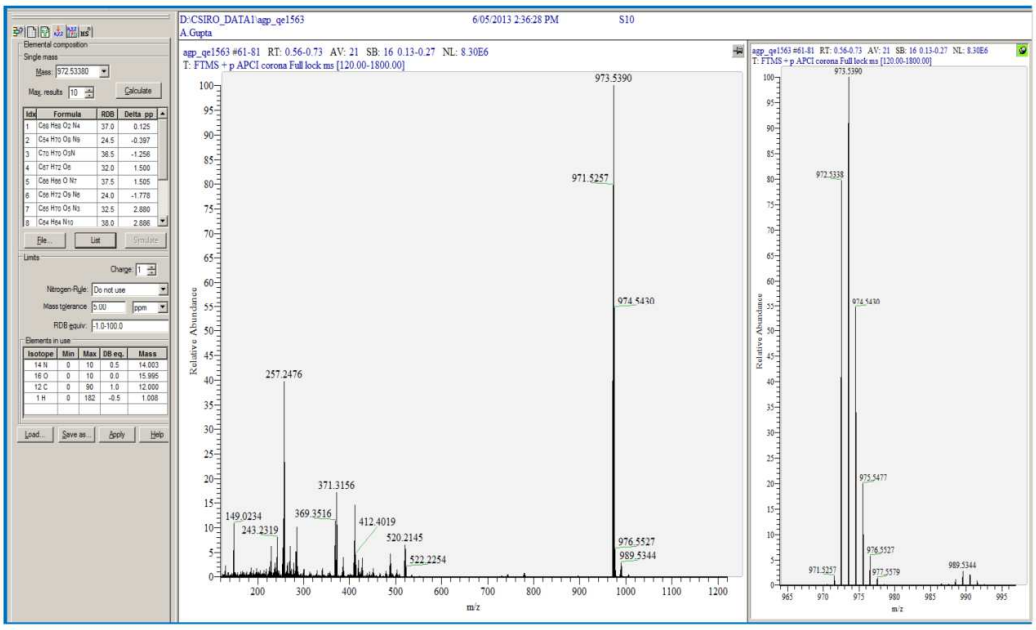

All experiments were carried out on a Thermo Scientific Q Exactive FTMS, employing ASAP probe.

CSIRO Material Science & Engineering
A.Gupta

QExactive ASAP Probe Accurate Mass Report
S10

m/z	Theo. Mass	Delta (ppm)	Composition
972.5338	972.5337	0.12	C68 H68 O2 N4
	972.5342	-0.40	C54 H70 O8 N9
	972.5350	-1.26	C70 H70 O3 N
	972.5323	1.50	C67 H72 O6
	972.5323	1.51	C66 H66 O N7
	972.5355	-1.78	C56 H72 O9 N6
	972.5310	2.88	C65 H70 O5 N3
	972.5310	2.89	C64 H64 N10
	972.5369	-3.15	C57 H68 O5 N10
	972.5369	-3.16	C58 H74 O10 N3

All experiments were carried out on a Thermo Scientific Q Exactive FTMS, employing ASAP probe.

Figure S3. HRMS spectrum of **S10**.

S11 Spectra

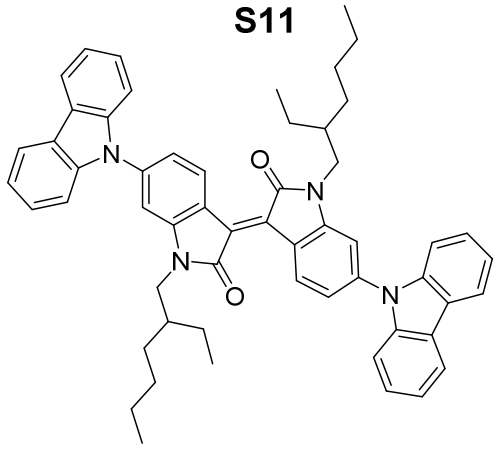

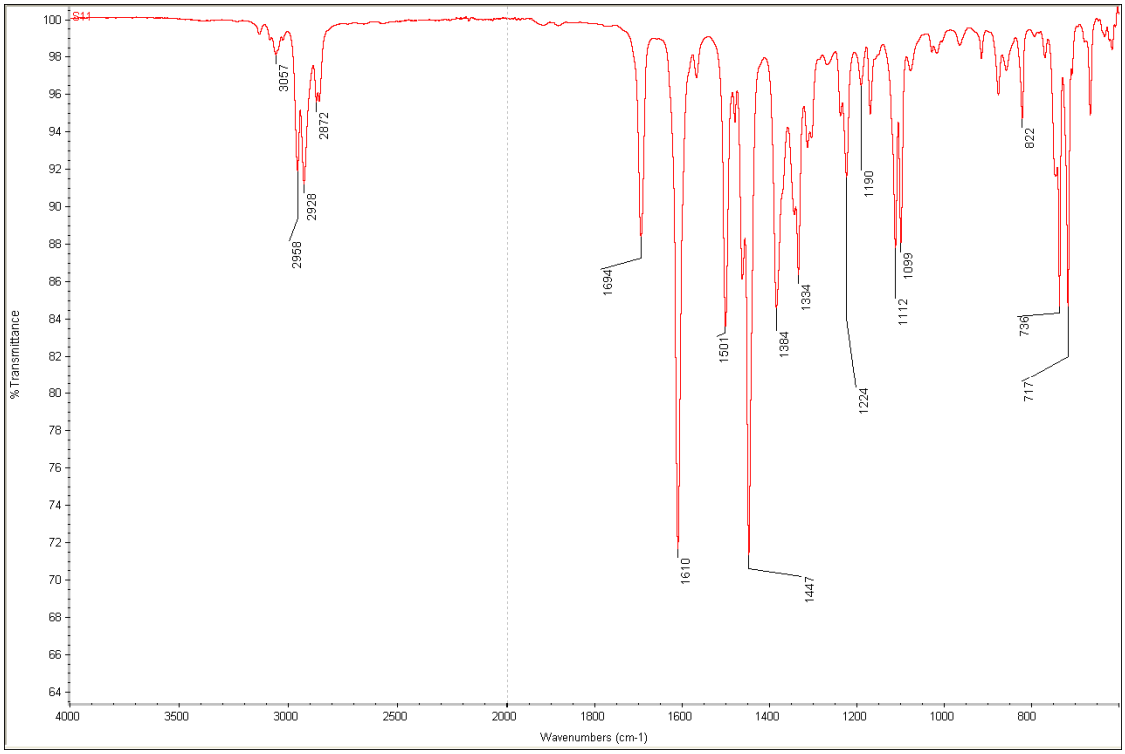

Figure S4. IR spectrum of **S11**.

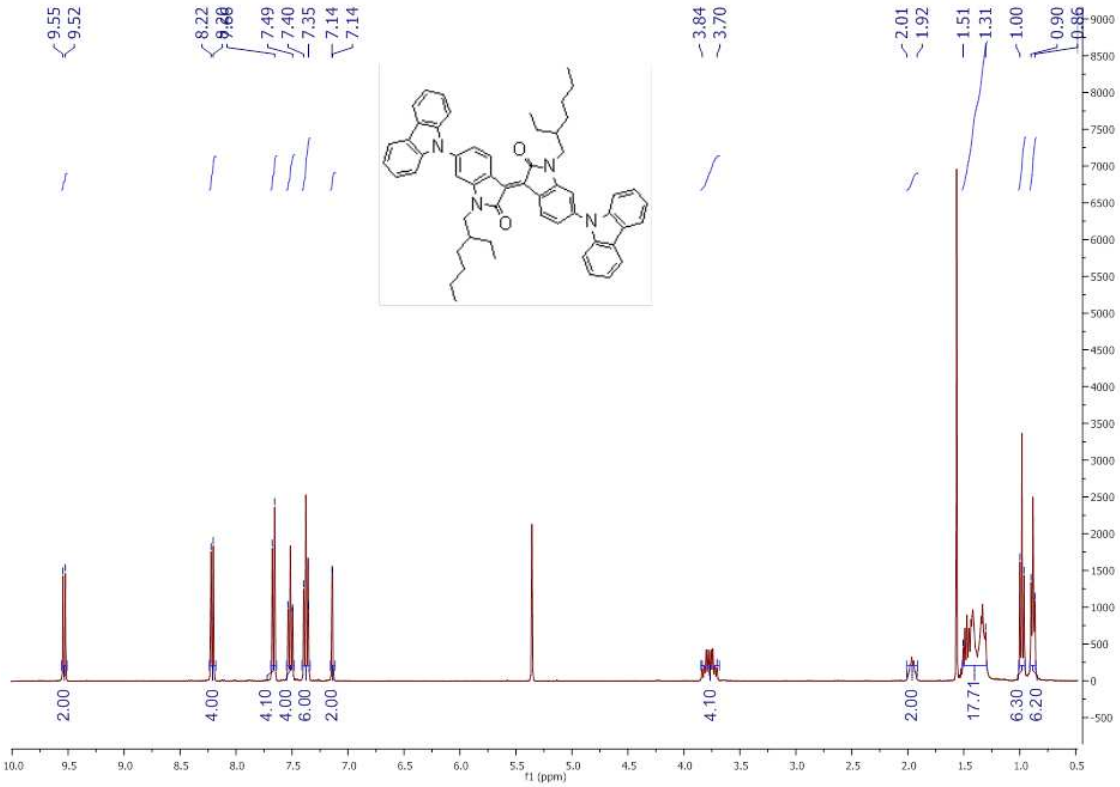
9.55
9.52
8.22
7.49
7.40
7.35
7.14
7.14
3.84
3.70
2.01
1.92
1.51
1.31
1.00
0.90
0.86
2.00
4.00
4.10
4.00
6.00
2.00
4.10
2.00
17.71
6.30
6.20
f1 (ppm)

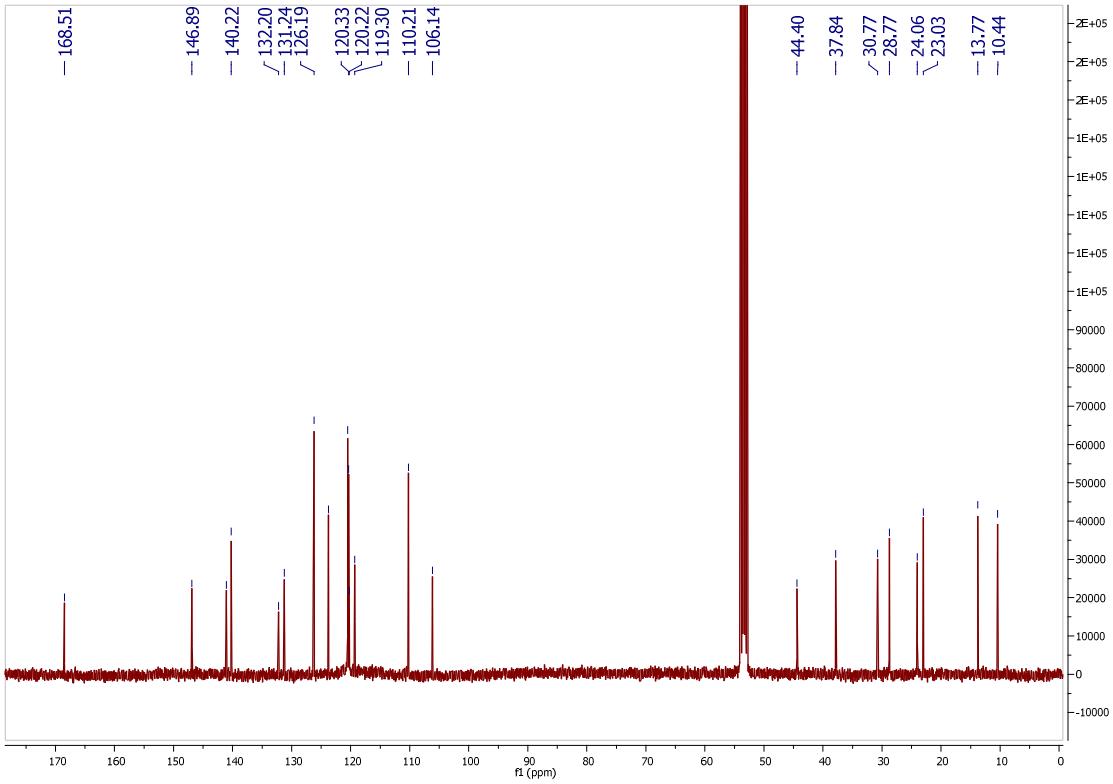
168.51
146.89
140.22
132.20
131.24
126.19
120.33
120.22
119.30
110.21
106.14
44.40
37.84
30.77
28.77
24.06
23.03
13.77
10.44
f1 (ppm)

Figure S5. ^{1}H and ^{13}C NMR spectra of **S11**.

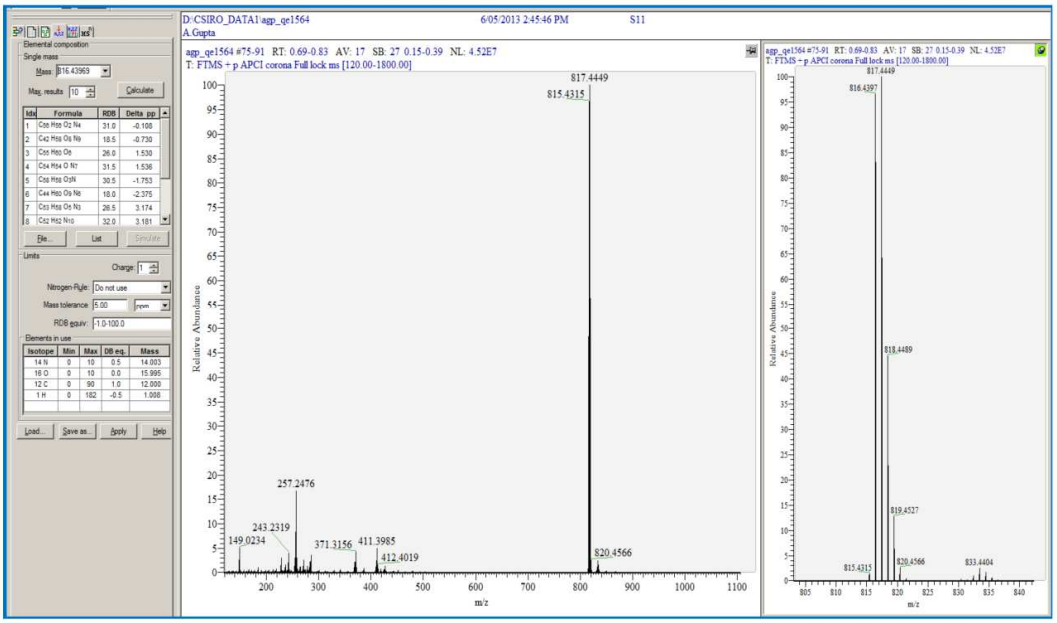

CSIRO Material Science & Engineering
A.Gupta
QExactive ASAP Probe Accurate Mass Report
S11

m/z	Theo. Mass	Delta (ppm)	Composition
816.4397	816.4398	-0.11	C56 H56 O2 N4
	816.4403	-0.73	C42 H58 O8 N9
	816.4384	1.53	C55 H60 O6
	816.4384	1.54	C54 H54 O N7
	816.4411	-1.75	C58 H58 O3 N
	816.4416	-2.37	C44 H60 O9 N6
	816.4371	3.17	C53 H58 O5 N3
	816.4371	3.18	C52 H52 N10
	816.4430	-4.01	C45 H56 O5 N10
	816.4430	-4.02	C46 H62 O10 N3

All experiments were carried out on a Thermo Scientific Q Exactive FTMS, employing ASAP probe.

Figure S6. HRMS spectrum of **S11**.

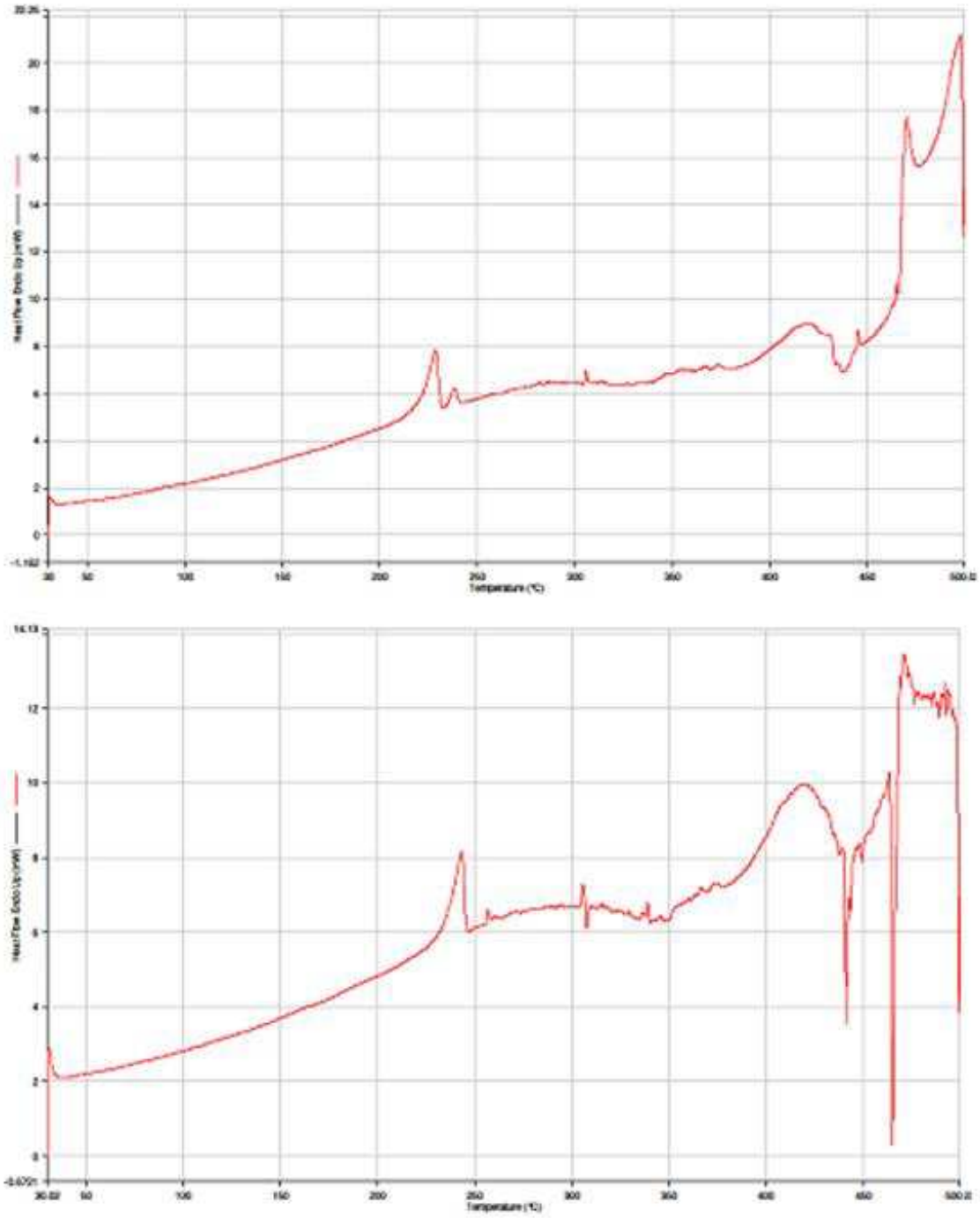

Figure S7. DSC curves of **S10** (above) and **S11** (below).

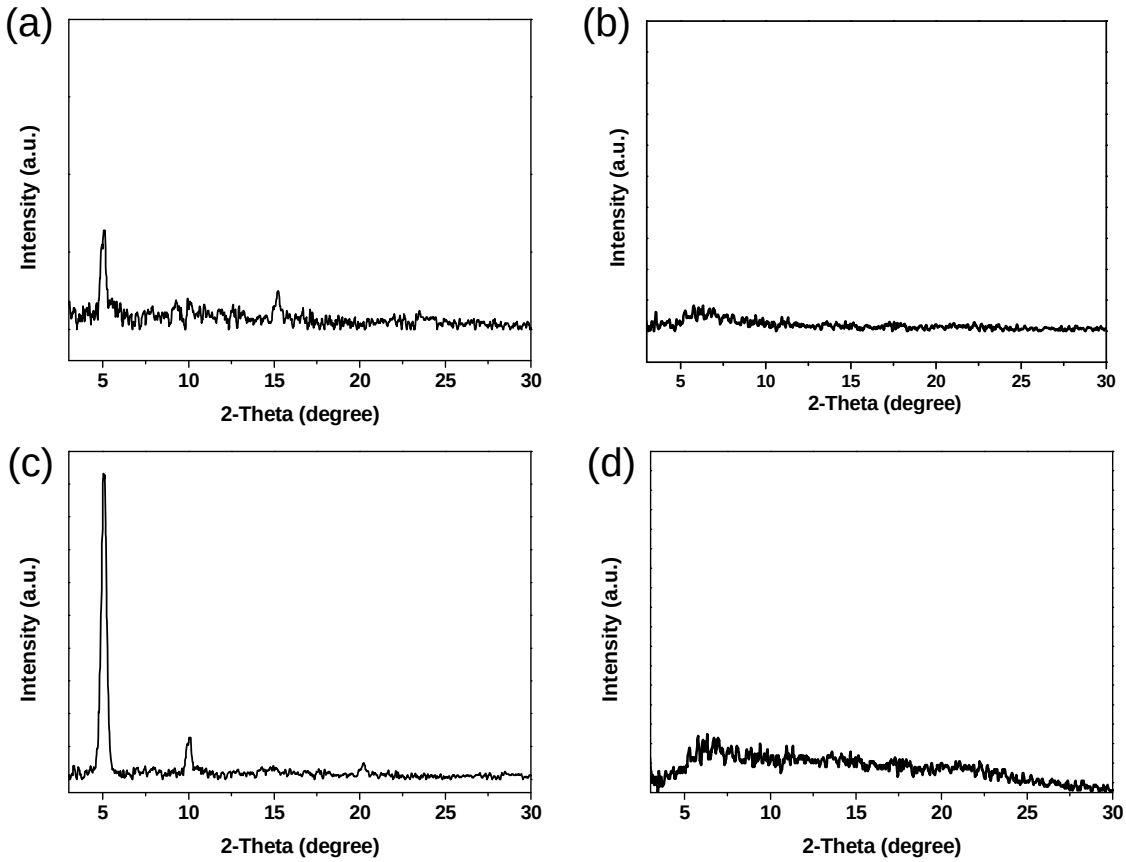

Figure S8. The XRD spectra of **S10-** (a, c) and **S11-**based (b, d) thin films under as-spun (a, b) and thermal annealing at 120 °C (c, d) conditions.

Chapter 7: General Discussion, Summary of research results, Overview, and Future directions

7.1 General Discussion

Natural photosynthetic systems harvest solar energy *via* converting sunlight into a usable form of chemical energy, and to produce a synthetic version is an attractive and challenging goal. If large arrays of light harvesters could be produced economically enough, so as to offset the comparative loss of initial efficiency in light collection, organic solar cells could be of critical importance to a long-term and sustainable future. The rationale for supporting research in this area is based on diminishing fuel reserves, the increased reliance on foreign fuel suppliers and the unsustainability of the current energy supply.[1] The development of effective systems for solar energy conversion and storage requires a fundamental understanding of the natural processes of photon absorption, charge separation, transport and storage. This was recognized by Ciamicin[1] a century ago, followed by recent advances in the development of catalytic systems that use sunlight to generate molecular hydrogen and oxygen.[2] From the work by Grätzel in dye-sensitized solar cells (DSSC)[3], there remains the need for the

investigation of artificial photosynthesis across all scientific disciplines. In essence, this thesis focuses on bio-inspired disciplines, aimed at utilising Nature's concepts in the laboratory. There is considerable interest in the development of macromolecular chemical systems forming long-lived, charge-separated states for technological advances in solar energy conversion, molecular-based optoelectronics, and other applications. Although many biomimetic and supramolecular compounds have been devised to collect photons, the output of these systems often consists of photons of lower energy. The outstanding challenge is to devise schemes in which acceptor chromophores can transfer the charge carrier (electron or hole) to generate a chemical product (for example, H_2 or O_2) before relaxation to the initial state occurs.

Photovoltaic solar cells, which convert sunlight to electricity, are a mature technology.[4-9] Inorganic solar cells are the dominant photovoltaic (PV) technology and are based on crystalline silicon. The commercial silicon cells typically achieve module efficiencies of about 15–18%[10], but their wide-spread application is hampered by their high cost. However, there has been interest in the development of novel types of low-cost solar cells to replace inorganic silicon. Among the alternative technologies, organic photovoltaic (OPV) solar cells are a promising, cost effective alternative to conventional silicon

based solar cells. The main potential advantages include easy solution processing, roll-to-roll processability for large area devices, mechanical flexibility and versatility of chemical structures.[11] However, some of the current disadvantages include their moderate efficiencies and lower stability compared to conventional silicon based solar cells. But there are ongoing extensive research efforts to solve these issues with OPV solar cells.[12] OPV solar cells are defined as those cells which include at least one organic component or an organic material, such as small organic molecule or polymer, in their fabrication. This area of research gained significant momentum in the 1980's when Tang's group developed a single heterojunction OPV cell and reported a power conversion efficiency of about 1%.[13] From late 80's to early 90's, high-purity conjugated polymers allowed the fabrication of OPV cells and these cells were called polymeric solar cells.[14] From the mid 90's was the development of bulk-heterojunction (BHJ) solar cells, which is where donor functionality and acceptor functionality were processed from the same solution and an active thin film was spin-cast on the metal oxide surface.[15] Since then, OPV solar cells are commonly called BHJ solar cells and a variety of polymeric entities have been used in the past two decades.[16]

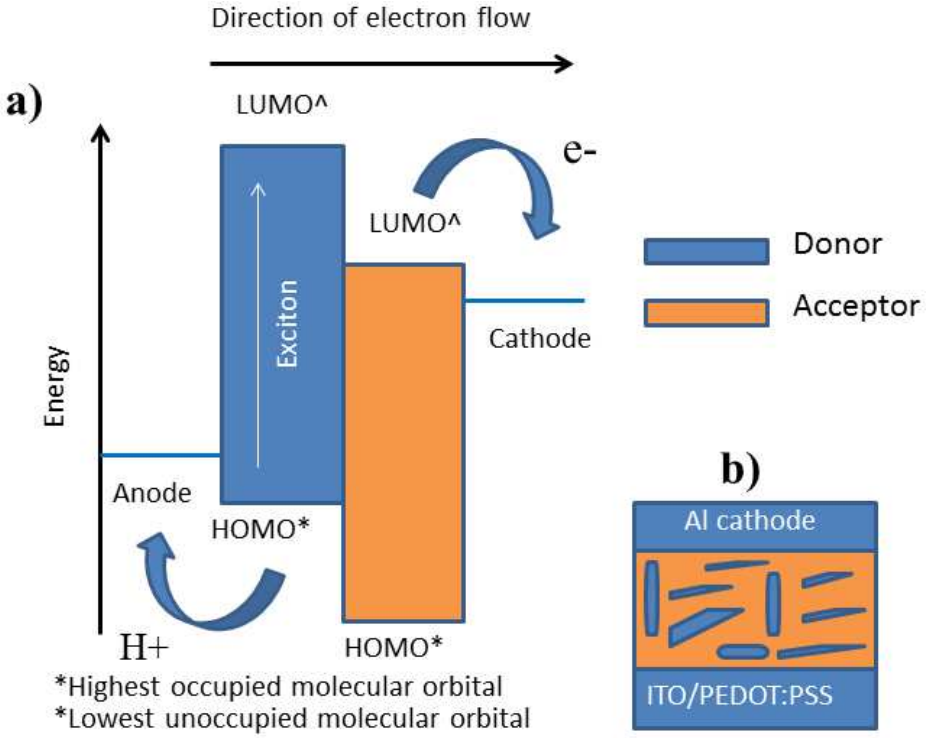

Fig. 1: Operational depiction of a heterojunction solar cell**:** (a) the energy diagram of a heterojunction solar cell with an exciton generation in the electron donor (polymeric entity or small molecular solid) phase; (b) BHJ device architecture in which active layers are spin-casted from a blend solution of donor and an electron acceptor material (typically fullerene (C_{60}) or its derivatives) and form a bi-continuous interpenetrating network. Till date, this is the most successful architecture for the development of OPV solar cells.

Figure 1, represents the operational depiction of a typical heterojunction solar cell with the concept of BHJ solar cell. Although most of the research in the field of BHJ solar cells has been focused on the use of *p*-type conducting polymers as donors and fullerene-based acceptors, recent research in the field of small organic molecules has demonstrated the viability of solution-processed BHJ devices composed entirely of these molecular solids. From a synthetic point of view, small molecules offer potential advantages over polymeric materials

in terms of ease of synthesis and purification and suffer less from batch to batch variations and end group contamination.

These small organic molecules act as donor components and are based on various structural motifs. Some of the common motifs are donor-acceptor (D-A), D-A-D and A-D-A. These D-A motifs could be directly attached to each other or through a conjugated π-spacer. Most of the donor functionalities that have been studied within these D-A designs include triphenylamine or its subsequent derivatives, indoline, benzothiophene and oligothiophenes for their potential use in the development of target donor material.[17] The development of such modular designs pose a challenge for an organic chemist to generate a material which is:

- Highly soluble in common organic solvents, such as dichloromethane, chloroform and toluene, as the BHJ solar cells are processed from solution.
- Developing new molecules capable of broad band solar harvesting which are stable at high temperature and easily processable.
- Able to absorb in visible to near infra-red region and should possess a narrow energy band-gap.

Therefore it is not surprising that there is such growing interest in the development of small organic molecules based on various D-A combinations with the goal of achieving novel donor

materials for their practical applications in Bulk heterojunction (BHJ) solar cells.

It is important to note that, fullerene and their derivatives have been used as an electron acceptor for fabrication of BHJ devices.

However, fullerenes suffer from a number of disadvantages, such as high cost, weak absorption in the visible range spectrum, restricted electronic tuning *via* synthesis and cumbersome purification. Also, the large electron affinity of C_{60}-derivatives can yield a low open circuit voltage (V_{oc}) for the photovoltaic devices.

7.2 Summary of research results

This project aimed to investigate and develop new materials and device architectures in order to improve the conversion efficiency of next generation organic solar cells. In particular, the focus of this research was on developing innovative and cutting-edge molecular devices and synthesising novel heterocyclic derivatives.

The main aim of this research was the design, synthesis and characterization of chromophores with donor-acceptor geometry for applications in BHJs. Examination of new acceptors, central π-conjugating functionalities, extended π-spacers, phenyl replacement with thiophene functionality and a common

synthon for the development of BHJ materials was carried out. **A total of seven new BHJ materials are reported in this research.** The three building blocks of D-π-A materials were systematically varied and their performance was benchmarked against the standard building blocks.

To further explore this idea of small aromatic π-conjugated molecules, cNDI was chosen as one of the counter components in A-D-A (acceptor-donor-acceptor), A-A-A (acceptor-acceptor-acceptor) and D-A-D (donor-acceptor-donor) solution-based BHJs. As NDI is a compact, planar, aromatic and fascinating π-conjugated compound, it has been widely studied. Subsequently it has found use in organic electronics because it has excellent n-type conductivity and stability (Chapter 1, ref. 93; *Nature*, **2000**, *404*, 478-481). Thus, diketopyrrolopyrrole (DPP) and core-substituted naphthalene diimides (cNDIs) were chosen to construct organic photovoltaic (OPV) solar cell devices by strengthening π–π-stacking within the three types of systems (A-D-A, D-A-D and A-A-A). These small organic molecules act as donor components and are based on various structural motifs. These designs could be directly attached to each other or through a conjugated π-spacer.

In recent years, DPP based derivative functionalised with electron withdrawing end capping i.e. trifluoromethylphenyl) has been investigated for solution processable device fabrication. The best power conversion efficiency (PCE) using 1:2 donor-acceptor, (poly(3-hexylthiophene) i.e. P3HT:DPP) by weight mixture, was 1%. A star-shaped molecule based on triphenyl-amine functionalization, terminating with three DPP, improves efficiency to 1.2 %.[18-22] In other examples, DPP derivatives have shown to have very good electron mobility and hole mobility, under vacuum as well as in air. Reported examples shows DPP functionality is suitable as an acceptor for solution processable BHJ.

On the other hand, literature examples also show that core-substituted naphthalene diimides (cNDIs) will have very good mobility under vacuum, as well as in air.[23-27] Despite these results, there is no report of utilising cNDIs in BHJ solar cell device fabrication.

These results suggest that the DPP and cNDI core functionality will be good candidates for solution processable, low bandgap, n-type organic semiconductors for organic solar cell application.

Recently, non-fullerene electron acceptors have been developed[30] and PCEs exceeding 2-4% have been achieved using P3HT and non-P3HT donors.[31] Even though this progress is encouraging, considerable scope still exists to develop new

non-fullerene acceptors which possess strong optical absorption and good stability.

To achieve such derivatives, we have designed a new acceptor having strong absorption, adequate solubility, and high charge carrier mobility along with appropriate energy levels.

In this work I have demonstrated for the first time that a common D-A-D, A-D-A and A-A-A synthon can be used to produce BHJ materials in a single synthetic step. A total of eight of these intermediates were used as common synthons for BHJ materials.

7.3 Key Findings

Chapter 2

This chapter illustrates the synthesis of **DPP1**, based on A-D-A design, which is a novel non-fullerene electron acceptor in which fluorene (FL) is a central core and has two **DPP** units as the terminal substituents on both side of the FL, *via* Suzuki coupling. **DPP1** shows excellent solubility and thermal stability, strong and broad absorption and matching energy levels with P3HT. The BHJ devices based on a P3HT: **DPP1** blend (1:1), after annealing at 150 ^{o}C for 5 min, yielded a notable PCE of 1.20% and a very high V_{oc} of 1.10 V. The electron mobility of

DPP1 was ~8x10^{-6} cm^2 V^{-1} s^{-1}, measured using the time of flight photoconductivity (TOF-PC) method.

Chapter 3

In this chapter, an A-A-A based system (**HP1**) was designed and synthesised *via* a Stille coupling reaction, bearing cNDI as a central core and DPP as terminal units. **HP1** exhibited promising optoelectronic properties, excellent solubility, thermal stability and energy levels matching those of P3HT. The BHJ devices based on the P3HT: **HP1** blend, after annealing at 150 ^{o}C for five minutes, afforded a PCE of 1.02% and a very high V_{oc} of 1.05 V. Our results indicate that small molecules with low electron mobility and relatively deep LUMO energies (~3.5 eV) can also be studied as electron acceptors, and strongly support the excellent prospects of a simple molecule such as **HP1** for applications in organic solar cells.

Chapter 4

This chapter demonstrates the use of a cNDI accepting functionality to generate new D–A–D modular small organic molecules. In this design, cNDI as a core unit and two different donor functionalities, namely triphenylamine (**S6**) and benzothiophene (**S7**) are attached to the core of the NDIs. Results demonstrate that the D–A–D structure with the cNDI

central core can furnish a material with suitable optoelectronic properties that are viable for BHJ device architecture. The new materials **S6** and **S7** were soluble in a variety of organic solvents and used as *p*-type semiconducting components, with *n*-type $PC_{70}BM$ in solution-processable inverted BHJ photovoltaic devices. Use of a triphenylamine donor unit helped achieve a substantial red shift of the absorption maximum in the visible region and, in devices, resulted in higher photocurrent compared with devices based on a benzothiophene unit. Devices based on **S6** were found to be more efficient than devices based on **S7**, in which a benzothiophene donor unit was used. These preliminary results strongly suggest that use of an NDI acceptor unit with different donor units might lead new materials, based on the D–A–D structure.

Chapter 5

This chapter demonstrates the use of a novel, solution-processable, highly conjugated chromophore **N5** as an electron acceptor for organic solar cells. **N5** has good thermal stability, strong and broad absorption and appropriate energy levels matching with those of classical donor polymer P3HT. The blend film of P3HT:**N5** exhibited a good nanoscale

interpenetrating network, broad spectrum IPCE over the visible range and PCE as high as 2.76%, which is among the highest values reported so far for solution-processed BHJ devices using DBS-based non-fullerene acceptors. Lastly, the P3HT:**N5** device is well-suited to simple device architecture with no special treatment, which offers advantages over more complex device strategies. This work demonstrates that small molecule acceptors with promising optoelectronic properties, such as **N5**, have bright prospects to be at the leading edge of non-fullerene acceptor research, and bridges the gap between the research fields of donor and acceptor semiconducting materials.

Chapter 6

This chapter describes the use of the isoindigo accepting functionality to generate new D–A–D modular small organic molecules, **S10** and **S11**, which contain a common isoindigo core unit and varied donor functionalities. The new materials, **S10** and **S11**, were synthesized, found to be highly soluble in a variety of common organic solvents, and were thermally stable. Use of a triphenyl amine (TPA) unit as an energy antenna helped to achieve a substantial red-shift of the absorption maximum in the visible region, improved the solubility of target material and helped to reduce the optical band-gap. Upon testing these materials as active layers in OFET devices, hole mobilities of the order of 2.2×10^{-4} cm^2/Vs and 7.8×10^{-3} cm^2/Vs were

achieved for **S10** and **S11,** respectively. The reported charge-carrier mobility values for **S10** and **S11** are promising and through further novel design developments, high mobility values may be achieved. These results on the effect of donor types on electronic properties of D–A–D modular organic materials can indeed inform the design of futuristic materials for organic electronic applications.

This chapter also demonstrated the use of a common synthon to generate D-A-D, A-A-A and D-A-D materials for BHJ applications. We observed that BHJ materials based on the common synthon showed superior light-harvesting properties and enhanced solubility but also showed relatively low efficiencies against the parent design incorporating a phenyl linking group.

7.4 Directions for future work

The exploration of the above materials **(chapter 2-6)** which display promising optoelectronic and photovoltaic properties

opens up the way to develop novel motifs based on terminal cNDI and DPP functionalities.

The focus of this research was the development of D-π-A materials for BHJ applications. The maximum conversion efficiency of ~2.14% reported for D-π-A materials in this work is lower than that for other molecular architectures, such as A-D-A, D-A-D-A-D and D-A-D, reported recently in the literature. The overall performance of BHJ solar cells based on small molecules is dependent on a number of factors. Two key parameters are their nanomorphology and the charge mobility in the respective phases. In the field of D-π-A materials, only very limited work has been undertaken to characterize or optimize these two properties. This raises the question of whether the higher efficiencies recently reported for some molecular architectures, such as A-D-A, D-A-D-A-D and D-A-D are related to their *inherent* superiority, or related to film formation and mobility, or whether further optimization work can help to put these new D-π-A materials on par with their peers.

Further systematic studies into the effects of film morphology and charge transport properties of small molecule materials for BHJ solar cells could help to help to answer this question.

Another important aspect to be considered for future work is the implementation of various acceptor synthons and π-spacers, which have been examined for the D-A architecture, to the higher performing architectures, such as A-D-A. This work has shown that acceptor synthons such as cyanopyridone and central π-spacers such as bridged thiophenes are ideal candidates for new architectures. Some possible examples for future study include:

Future BHJ materials:

1. It would be worthwhile to study the scope of new aromatisable and non-aromatisable acceptors based on a D-π-A architecture.

The design can be elaborated as:

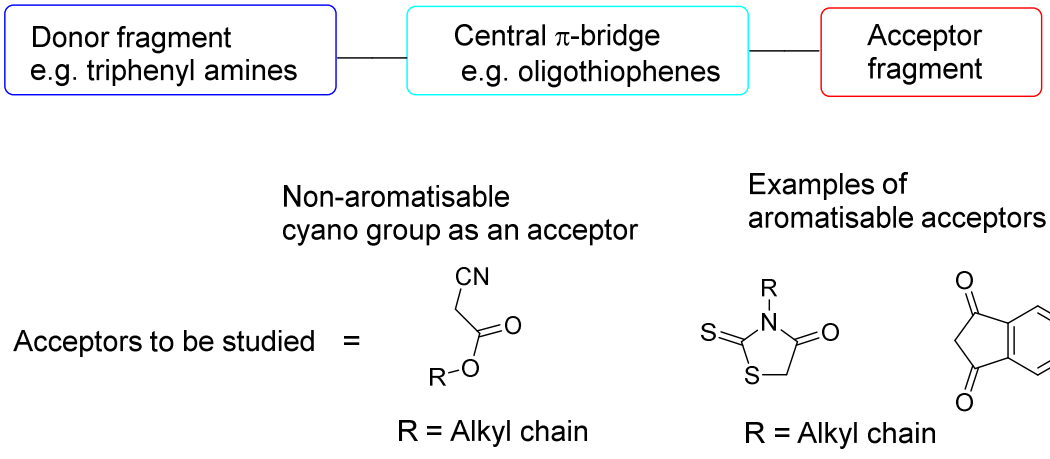

2. It would be worthwhile to explore the possibilities of using a variety of π-spacers that have been reported for efficient polymeric BHJ solar cells. These π-spacers can help to improve light-harvesting, stability, solubility and charge carrier motilities of the target small molecular D-π-A solids. Some examples of central π-spacers are:

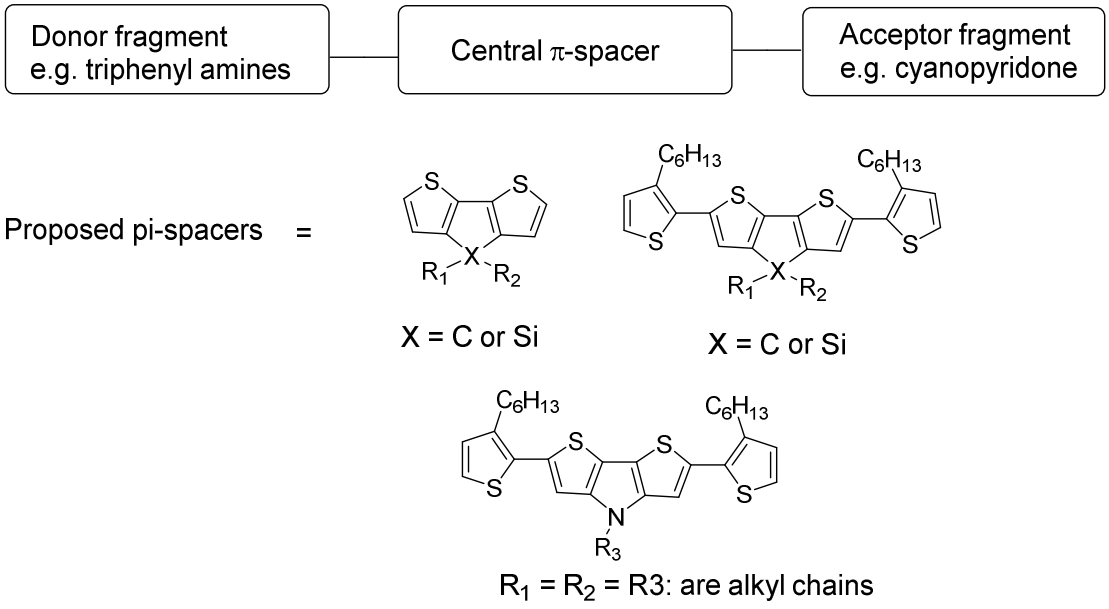

Proposed future work includes investigation of film blends in a variety of solvents, the study of film blend morphologies using atomic force microscopy (AFM) and transmission electron microscopy (TEM), and the use of varieties of additives in the blend solutions. Future studies should also be focused on the use of unsymmetrical donor units and incorporation of π-spacers between donor and acceptor functionalities.

Conclusions

This work enhances the prospects for the design and development of other electron acceptors based on the **DPP** and cNDI functionality that should help realize significant improvements in BHJ solar cell device performance. Our finding also reveals that changing the design structure can be of crucial importance in achieving new organic materials for OPV devices such as the small molecule **N5**, which possesses promising optoelectronics properties and has a bright future at the leading edge of non-fullerene acceptor research by bridging the gap between the research fields of donor and acceptor semiconducting materials.

Based on my PhD thesis work, it is clear that cNDI and DPP based systems are likely to contribute to a new generation of bio-inspired materials in *biotechnology and nanotechnology*, including high throughput identification screening systems, and new energy transduction systems. The importance of cNDI functionalised systems can be gauged by their recent use in solar energy conversion that requires application of multilayers and distance and time dependent study of electron transfer.

Development of cNDI and DPP with the appropriate spacers for charge separation will aid the development of molecular systems and supramolecular arrays, which are capable of solar energy conversion and other photonic applications. Future research on these systems may also contribute to major efforts in basic research on smart optoelectric nanomaterials that is, according to pertinent reports, needed today to meet tomorrow's energy demands in a sustainable way.[32]

7.5 References

1 Ciamician, G. *Science*, **2012**, *36*, 385.

2 (a) Steinberg-Yfrach, G. P. A. *et al*. *Nature*, **1997**, *385*, 239. (b) Gust, D. *et al*., Acc. *Chem. Res.,* **2001**, *34*, 40. (c) Bhosale, S. *et al*., *Science*, **2006**, *313*, 84.

3 Yum, J.-H., Chen, P. M., Gratzel, M. K. Nazeruddin, *ChemSusChem* **2008**, *1*, 699.

4 Cubasch, U., Meehl, G. A. Climate Change 2001: The Scientific Basis, Eds J. T. Houghton *et al*., Cambridge Univ. Press, Cambridge, **2001**, Chapter 9: Projections of future climate change, pp. 525–582.

5 Wigley, T. M. L., Raper, S. C. B. *Science*, **2001**, 293, 451.

6 2012 Key World Energy Statistics, International Energy Agency, Paris France;

http://www.iea.org/publications/freepublications/ Publication/ kwes.pdf.

7 http://www.worldcoal.org/resources/coal-statistics/.

8 (a) BP Statistical Review of World Energy, June 2012; bp.com/statisticalreview. (b) Bentley R. W., Global oil & gas depletion: an overview, *Energy Policy*, **2002**, *30*, 189.

9 World Energy Council-**2010** survey of energy resources; http://www.worldenergy.org/documents/ser2010exsumsept 8.pdf

10 Zhou, Y. F., Eckab, M., Kruger, M., *Energy Environ. Sci.*, **2010**, *3*, 1851.

11 Brabec, C. J., *Solar Energy Mater. Solar Cells*, **2004**, *83*, 273.

12 Dennler, G., Scharber, M. C., Brabec, C. J., *Adv. Mater.*, **2009**, *21*, 1323.

13 Tang, C. W., *Appl. Phys. Lett.*, **1986**, *48*, 183.

14 Mayer, A. C. *et al*., *Materials Today*, **2007**, *10*, 28. 15 Yu, G. et. al., *Science*, **1995**, 270, 1789.

15 (a) Brabec, C. J. *et al*., *Adv. Mater.*, **2010**, *22*, 3839; (b) Helgesen, M. *et al.*, *J. Mater. Chem.*, **2010**, *20*, 36; (c) Grätzel, M. *Acc. Chem. Res*., **2009**, *42*, 1788;

16 Lu, H. P. *et al. J. Phys. Chem. C*, **2009**, *113*, 20990.

17 Mishra, A., Bäuerle, P., *Angew. Chem. Int. Ed.*, **2012**, *51*, 2020.

18 Suraru, S.-L., Zschiescang, U., Klauk, H., Wurthner, F. *Chem Commun.* **2011**, *47*, 1767.

19 Qiao, Y. Guo, Y. Yu, C. Zhang, F., Xu, W. Liu, Y., Zhu, D. *J. Am. Chem. Soc.* **2012**, *134*, 4084.

20 Zhong, H., Smith, J., Rossbauer, S., White, A. J. P., Anthopoulos, T. D., Heeney, M. *Adv. Mater.* **2012**, *24*, 3205.

21 Sonar, P. *J. Mater. Chem.* **2010**, *20*, 3626

22 Lin, Y., Cheng, P., Li, Y., Zhan, X. *Chem. Commun.* **2012**, *48*, 4773.

23 Hu, J.-Y., Nakano, M., Osaka, I Takimiya, K. *J. Mater. Chem. C,* **2015**, *3*, 4244

24 *Zhang, F., Zang, Y., Huang, D., Di, C., Gao, X., Sirringhaus, H., Zhu, D. Adv. Funct. Mater.* **2015**, *25*, 3004

25 *Liu, Y. Zhang, L., Lee, H., Wang, H.-W., Santala, A., Liu, F. Diao, Y., Briseno, A. L., Russell, T. P. Adv. Energy Mater.* **2015**, 1500195

26 L. Tan, Y. Guo, G. Zhang, Y. Yang, D. Zhang, G. Yu, W. Xu and Y. Liu, *J. Mater. Chem.*, **2011**, *21*, 18042.

27 Y. Fukutomi, M. Nakano, J.-Y. Hu, I. Osaka and K. Takimiya, *J. Am. Chem. Soc.*, **2013**, *135*, 11445.

28 L. E. Polander, S. P. Tiwari, L. Pandey, B. M. Seifried, Q. Zhang, S. Barlow, C. Risko, J.-L. Bredas, B. Kippelen and S. R. Marder, *Chem. Mater.*, **2011**, *23*, 3408.

29 D. K. Hwang, R. R. Dasari, M. Fenoll, V. Alain-Rizzo, A. Dindar, J. W. Shim, N. Deb, C. Fuentes-Hernandez, S. Barlow, D. G. Bucknall, P. Audebert, S. R. Marder and B. Kippelen, *Adv. Mater.*, **2012**, *24*, 4445.

30 Sonar, P. *et al. Energy Environ. Sci.*, **2011**, *4*, 1558.

31 Lin, Y. *et al. Adv. Energy Mayt.*, **2013**, *3*, 724.

32 G. Hess, *Chem. Eng. News* **2005,** *83*, 12.